# UNIVERSIDAD NACIONAL AUTÓNOMA DE MÉXICO

PROGRAMA DE MAESTRÍA Y DOCTORADO EN INGENIERÍA
INGENIERÍA CIVIL – HIDRÁULICA

## ANÁLISIS DE LA VULNERABILIDAD COSTERA DE LAS COSTAS NO DE MÉXICO Y SE DE AUSTRALIA BAJO EXPANSIÓN TÉRMICA TROPICAL POR EFECTOS DE CAMBIO CLIMÁTICO

TESIS
QUE PARA OPTAR POR EL GRADO DE:
DOCTOR EN INGENIERÍA

PRESENTA:
ITXASO ODÉRIZ MARTÍNEZ

TUTORES PRINCIPALES
DR. RODOLFO SILVA CASARÍN, INSTITUTO DE INGENIERÍA UNAM
DR. THOMAS R. MORTLOCK, RISK FRONTIERS Y MACQUARIE UNIVERSITY

COMITÉ TUTOR
DR. EDGAR G. MENDOZA BALDWIN, INSTITUTO DE INGENIERÍA UNAM
DR. JESÚS GRACIA SÁNCHEZ, INSTITUTO DE INGENIERÍA UNAM
DR. OSCAR A. FUENTES MARILES, INSTITUTO DE INGENIERÍA UNAM

CIUDAD DE MÉXICO, JUNIO 2021

**JURADO ASIGNADO:**

| | |
|---|---|
| Presidente: | Dr. Jesús Gracia Sánchez |
| Secretario: | Dr. Oscar Arturo Fuentes Mariles |
| 1 er. Vocal: | Dr. Rodolfo Silva Casarín |
| 2 do. Vocal: | Dr. Edgar Gerardo Mendoza Baldwin |
| 3 er. Vocal: | Dr. Thomas R. Mortlock |

Posgrado en ingeniería civil, UNAM, Ciudad de México, México

**TUTORES DE TESIS:**

| | |
|---|---|
| Dr. Rodolfo Silva Casarín | Dr. Thomas R. Mortlock |
|  |  |
| --- | --- |
| **FIRMA** | **FIRMA** |

Este trabajo fue posible gracias al Fondo CONACYT-SENER/Sustentabilidad Energética a través del Centro Mexicano de Innovación en Energías del Océano (CEMIE-Océano), número 249795; y DPRI *research funds*, JSPS KAKENHI e *Integrated Research Program for Advancing Climate Models* (TOUGOU Program: JPMXD0717935498) apoyado por el MEXT de Japan.

# Agradecimientos

Me gustaría destacar el compromiso de CEMIE-Océano con la educación, el medio ambiente y la investigación como futuro para una sociedad mejor y el desarrollo socioeconómico de México.

Al Instituto de Ingeniería de la UNAM por su eficiencia, ser ejemplo de organización y por proporcionar todos los medios para el desarrollo de los proyectos de investigación. Hago mención especial a la Secretaría de Telecomunicaciones e Informática y a la administración por seguir proveyendo todos los medios y servicios en este año de pandemia.

A mis compañeros del Grupo de Ingeniería de Costas y Puertos de todas estas etapas, los que siguen, los que se fueron a emprender otros caminos y los que ya no están. En mi corazón siempre Regina, Erika y Maday.

A Erick por hacer de todo algo divertido.

Quiero mencionar de manera especial a mi familia. A mi padre, por enseñarme la constancia en el trabajo y, aunque de esto me he dado cuenta tarde, por enseñarme la cultura del campo y el medio ambiente, las historias de tu pueblo y esa sabiduría terrenal que espero no la perdamos en las próximas generaciones. A mi hermano, que eres ejemplo de liderazgo, creatividad, y que nuestros debates sobre procesos creativos me han motivado y enseñado a realizar esta tesis. A mi madre, por tu valentía, que sabes mejor que nadie lo que es importante en la vida y esa manera tan tuya de disfrutarla, todavía tengo mucho que aprender de ti.

A Elena, por traer alegría, curiosidad e inocencia al mundo.

Este trabajo me ha llevado a explorar nuevos temas junto al apoyo de muchas personas. Agradezco a todos los que disfrutaron del proyecto, se adentraron en el tema y germinaron ideas que fueron esenciales para el desarrollo de esta tesis. A David K. Adams, por presentarme el mundo de la atmósfera y su disponibilidad para apoyarme en todo momento. Thanks to Stipo Sentic for your generosity and all your support with the Hadley cells. A Sofía Villers, por enseñarme que los datos dicen mucho más de lo que uno imagina. A Roberto Padilla, por ser como es, tener la paciencia conmigo y sus enseñanzas sobre el oleaje. Thanks to Adrean Webb and Tomoya Shimura for your support with the climate change analysis. A Edgar Mendoza, por sus siempre acertadas indicaciones.

Gracias a todos los que han hecho una revisión del inglés de esta tesis, Tom, Edgar, Carmina, Rodolfo y Erick. Especial mención a Jill, gracias infinitas por tu tiempo, inmensa paciencia y por enseñarme el “menos es más”.

Al Posgrado de Ingeniería de la UNAM y al comité de esta tesis por su compromiso con ella, Dr. Rodolfo Silva, Dr. Thomas R. Mortlock, Dr. Edgar G. Mendoza, Dr. Jesús Gracia y Dr. Oscar A. Fuentes.

Thanks to Nobuhito for supporting this work from the beginning; for improving it by proposing great ideas, data, and for giving me the possibility of doing an internship. In the end, you couldn't be part of this thesis committee, but you deserve it. Thanks to all the lab for the warm welcome and for taking care of me.
ありがとうございます

Por su puesto, a mis tutores que en equipo hemos hecho crecer este proyecto. Cuesta creer cómo empezamos y lo que hemos construido. Ojalá sólo sea el comienzo y mucho más esté por venir.

Tom, muchísimas gracias por proponer esta colaboración, por estar en todo momento apoyándome, por tus ganas de siempre hacerme crecer y tu disposición a llegar más lejos con este trabajo. Por esas grandes conversaciones, que tristemente fueron vía email y videoconferencia. Quedan pendientes las conversaciones en persona.

Qué decir Rodolfo, eternamente agradecida por siempre darme la oportunidad y creer en mí. Sin ti no habría llegado a donde ahora estoy. Gracias por ser ejemplo de trabajo y enseñarme que las oportunidades llegan cuando se buscan. Por no dudar, por apostar y creer en las nuevas generaciones, por esquivar vientos y mareas en estos años y por adentrarte en la locura de liderar el CEMIE- Océano del que tanto te debemos.

A todos, gracias de corazón.

*A mi madre*

# List of contents

# Lise of figures

# List of tables

## List of the acronyms and abbreviations

AAO: Antarctic Oscillation

AO: Arctic Oscillation

CFSR: Climate Forecast System Reanalysis

DJF: December, January, February

ECMWF: European Centre for Medium-Range Weather Forecasts

ENSO: El Niño-Southern Oscillation

EOFs: Empirical Orthogonal Functions

ERA 5: fifth generation ECMWF atmospheric reanalysis of the global climate

ETIs: Expanding Tropics indices

GCMs: Global Climate Models

GHG: Greenhouse Gas Emissions

IPCC: Intergovernmental Panel on Climate Change

ITCZ: Inter Tropical Convergence Zone

JJA: June, July, and August

JRA-55: Japanese 55-year Reanalysis

LECZ: Low-Elevation Coastal Zones

MAM: March, April, and May

MEI: Multivariate ENSO Index

MERRA: Modern-Era Retrospective analysis for Research and Applications

NCEP: National Centres for Environmental Prediction

ONI: Oceanic Nino Index

PAC: Principal Components Analysis

PDO: Pacific Decadal Oscillation

SAM: Southern Annular Mode

RCP: Representative Concentration Pathways

SLP: Sea Level Pressure

SOI: Southern Oscillation Index

SON: September, October, and November

SST: Sea Surface Temperature

WECs: Wave Energy Converters

WCT: Wave Climate Type

# RESUMEN

El oleaje es esencial en los procesos e industrias costeras, por ello, una evaluación integral del riesgo costero debe incluir y considerar el análisis de sus condiciones históricas y proyectadas para el futuro cercano y lejano. Es por ello que esta tesis evalúa las fluctuaciones a largo plazo inducidas por variabilidad natural y cambio climático en las características del clima global del oleaje, incluyendo potencia y dirección media.

Primero, se estudió en detalle *El Niño-Southern Oscillation* (ENSO), que ha sido ampliamente identificado como el principal impulsor de variabilidad interanual del oleaje a escala global. Los resultados mostraron que durante EL Niño (fase positiva del ENSO), el clima de oleaje en las regiones extratropicales es el más afectado con señales más intensas presentadas a lo largo de las costas este del Pacífico y océano Índico.

Sin embargo, actualmente uno de los mayores desafíos de la ciencia es diferenciar entre las fluctuaciones inherentes forzadas por la variabilidad natural (interna) de aquellas inducidas por el calentamiento global. Para analizar mejor ambos fenómenos en las características históricas del oleaje, se propuso un marco climático que consistió en una clasificación del oleaje en tipos, generados por los sistemas de vientos planetarios. Para cada tipo de clima, las tendencias a largo plazo relacionadas con la temperatura superficial del mar, un indicador del calentamiento global, fueron comparadas con aquellas variaciones inducidas por los patrones climáticos. Específicamente, se analizaron las fases de ENSO y ENSO cuando ocurre simultáneamente con *Southern Annular Mode* y *Pacific Decadal Oscillation*. Los resultados indicaron que una señal de calentamiento ya ha emergido y excedido el umbral de la variabilidad natural en el oleaje en el océano Índico y en las regiones tropicales del Atlántico y Pacífico. Mientras que, en el Pacífico sur, todavía la señal gobernante es la variabilidad natural, cuando ocurren simultáneamente el *Southern Annular Mode* y el ENSO. Este trabajo es valioso para identificar áreas prioritarias, regiones que ya necesitan medidas de adaptación y regiones que requieren más monitoreo, y tiempos para planificar la adaptación costera en un futuro cercano.

La expansión de los trópicos es una señal de cambio climático y un impulsor de variación del oleaje. Se examinó el impacto de las tendencias y fluctuaciones de la expansión tropical en el oleaje global y se demostró que el desplazamiento hacia los polos de las regiones tropicales influencia significativamente las características del oleaje, con mayor impacto en la dirección que en la potencia.

Para el futuro lejano (2075-2099), el clima de oleaje fue examinado bajo diferentes escenarios de cambio climático, RCP 2.6 (emisiones bajas) y RCP 8.5 (emisiones altas). Se concluyó que los oleajes provenientes del sur y este predominarán más en futuros escenarios de calentamiento global con implicaciones en los ambientes costeros. Se identificaron las regiones de transición de los climas de oleaje que deberán ser áreas prioritarias para la adaptación costera. Además, por primera vez, se presentan las proyecciones de oleaje en las costas circumpolares donde podrían emerger nuevas regiones marinas debido al deshilo.

Con estos resultados, se propusieron tres atlas para las costas del mundo que fueron clasificadas de acuerdo con la respuesta del oleaje a la variabilidad natural, al calentamiento global, y a las regiones donde se detectaron cambios en la frecuencia de climas de oleaje para el escenario RCP 8.5. Con ello, se pueden establecer bases para la adaptación costera a niveles nacionales y transnacionales. Finalmente, todos estos análisis y datos generados fueron aplicados al caso de México para evaluar detalladamente el cambio a largo plazo del oleaje a escala nacional.

# ABSTRACT

Ocean waves are essential for coastal environments and industries; thereby, a comprehensive coastal risk management should include historical and projected wave climate analysis for near and far future scenarios. In this vein, this doctoral research evaluates the long-term fluctuations induced by natural variability and climate change on global wave characteristics, including wave power and mean wave direction.

First, we studied in detail El Niño-Southern Oscillation (ENSO), as it has been widely identified as the principal climate driver of interannual variability in global ocean wave climate. Results showed that, during El Niño (positive phase of ENSO), the wave climate of the extratropical regions is the most affected with the strongest signals detected along the East coast of the Pacific and the Indian Ocean.

However, one of the great challenges in present-day climate science is to differentiate between the inherent fluctuations forced by natural (internal) climate variability from those forced by global warming. To better analyse both phenomena on historical wave characteristics, a climate framework was proposed that consisted of a wave climate classification into types that are driven by the planetary wind systems. For each wave climate type, the long-term trends related to the sea surface temperature, an indicator of global warming, were compared with those variations induced by climate patterns. Specifically, we analysed the phases of ENSO and ENSO coupled with the Southern Annular Mode and the Pacific Decadal Oscillation. Results indicated that a signal of ocean warming has already emerged and exceeded the threshold of natural variability in the wave climate of the Indian Ocean, the tropical Atlantic, and the tropical Pacific. Meanwhile, in the South Pacific, natural variability is still the governing signal, forced by the climate patterns Southern Annular Mode and ENSO. This work is valuable for identifying priority areas, regions that already need adaptation measurements and regions that require ongoing monitoring, and timing for planning coastal adaptation in the near future.

The expansion of the tropics is a sign of climate change and a wave climate driver. The impact of trends and fluctuations of the tropical expansion on global wave conditions was examined. We demonstrated that the poleward displacement of the tropical regions significantly influences wave characteristics, with the most impact seen on wave direction rather than wave power.

For the far future (2075-2099), the wave climate was examined under different climate change scenarios, RCP 2.6 (low emissions) and RCP 8.5 (high emissions). We concluded that waves coming from the south and east will become more prevalent under global warming with implications for coastal environments. We identified the transitional wave climate regions that should be priority areas for climate change adaptation. Furthermore, for the first time, our analysis depicts wave climate projections of the coasts at the circumpolar scale, where new marine regions may emerge.

From these results, we propose three coastal atlases that classify the coasts according to the wave climate response to natural variability, global warming signal, and those regions that will suffer changes in the frequency of the prevailing wave climate under the RCP 8.5 scenario. From this, some bases can establish to plan coastal adaptation at national and transnational scales. Finally, all of the datasets and analysis developed in this thesis were applied to the case of Mexico to assess in detail long-term changes in wave climate at the national scale.

# CHAPTER 1

# Introduction

This chapter discusses the context, motivation and fundamental background behind this thesis.

## 1.1 Context and motivation

Low-Elevation Coastal Zones (LECZ) around the world are especially vulnerable to climate-related drivers (Toimil et al., 2020) and climate change (Vousdoukas et al., 2020). Furthermore, it is expected that the population of these regions will increase in the next century (Neumann et al., 2015). In recent years, the signs of climate change observed in ocean basins have already passed the point of no return. On the other hand, the slow response of governments to reduce greenhouse gas emissions (GHG), has shown that coastal adaptation is fundamental (COP-21). The risk to LECZ is due to the combination of vulnerability, exposure, and hazards. Adaptation measures involve reducing coastal risk by implementing changes in the factors of exposure and vulnerability of social-ecological systems in response to the impacts expected, induced by climate change and natural variability along with local and global changes (Moser and Ekstrom, 2010; IPCC-AR5), see Figure 1. 1. To develop adequate coastal adaptation strategies, we must first respond: what are the coastal hazards we have to adapt to? For this, we need to first quantify the long-term coastal hazards, if we are to successfully build healthy coastal environments (UN-SDG 14) and resilient coastal communities. The long-term variation of climate includes the climate change caused by the emissions of GHG, and the variability caused by natural anomalies in the coupled ocean-atmospheric system. Both variations impact the wave climate, which is one of the main driver of hazards. This thesis investigates the effects induced by climate change and natural variability in the wave climate, and the results could be a baseline for coastal risk analysis and for implementation of adaptation strategies for the near and far future.

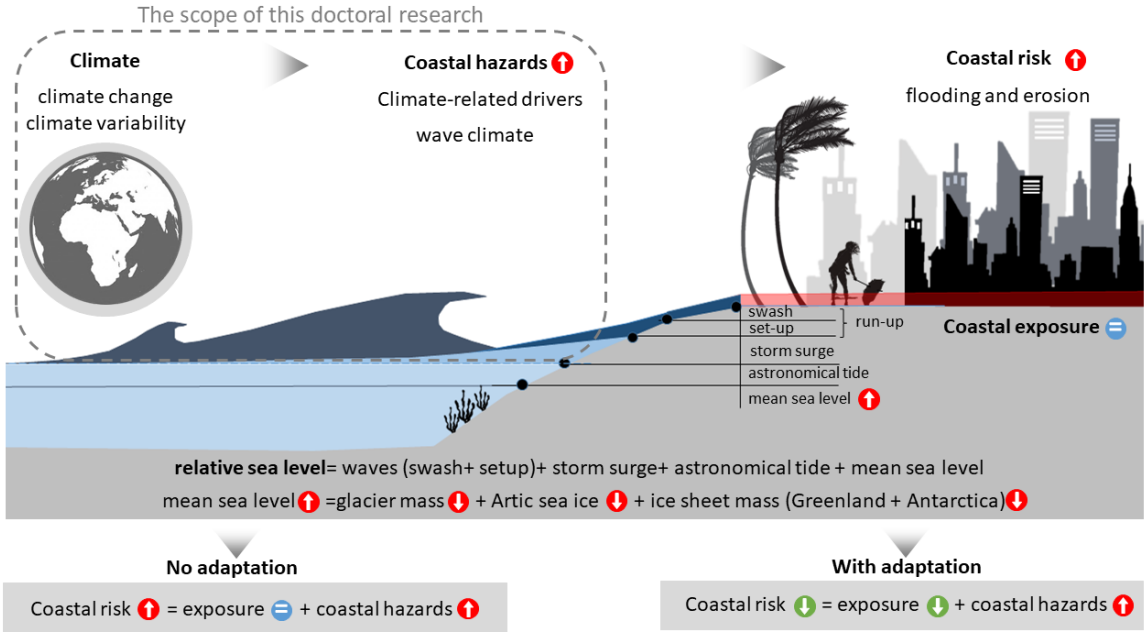


Figure 1. 1 Elements of coastal adaption to climate change, modified from AR5-Chapter 5 (IPCC, 2013) and SROCC (IPCC, 2019). The scope of this thesis is highlighted.

## 1.2 Literature review

### 1.2.1 The importance of ocean waves in coastal industries and environments

Wave climate is one of the primary driver of coastal hazards, due to the erosion (Silva *et al.*, 2016; Mendoza *et al.*, 2017; Morim *et al.*, 2019; Meucci *et al.*, 2020; Odériz, Knöchelmann, *et al.*, 2020) and flooding that it can induce (Melet *et al.*, 2018, 2020), see Figure 1.1. There are many examples of extreme events that have caused economic losses and fatalities around the world.

The lockdown of the ports of New York and New Jersey due to Storm Sandy in 2012 (Smythe, 2013), the catastrophic effects in the Philippines of Typhoon Haiyan in 2014 (Mori *et al.*, 2014), in 2005 Hurricane Wilma in the Mexican Caribbean (Mendoza *et al.*, 2015), large swells on the west coast of Latin America in 2015 (Godwyn-Paulson *et al.*, 2020), the destruction of houses in Australia in both 2016 (Harley *et al.*, 2017) and 2020 (in press), as well as the extreme hurricane season in the Atlantic in 2020.

Wave climate also impacts a wide range of coastal industries, such as ports (Camus *et al.*, 2019; Izaguirre *et al.*, 2020), wave energy generation (Fairley *et al.*, 2020) and the sun-and-sand tourism industry. Furthermore, the role of wave climate is fundamental in ecosystem biodiversity (Gillis *et al.*, 2017; Odériz, Gómez, *et al.*, 2020; Silva *et al.*, 2020), blue carbon sequestration (Li, S. and Babanin, 2021) and water quality (Huizer *et al.*, 2019).

Wave climate influences so many of these different factors that it is essential for us to plan adaptation measures to respond to global climate change. The long-term variability of wave climate must be analysed before we can decipher all the effects of coastal hydrodynamics, as well as the complicated interrelations this has with local factors, such as sea-bed interactions, sediment supply, river mouths, coastal structures and ecosystems (Toimil *et al.*, 2020).

### 1.2.2 Natural variability and wave climate

Natural variability, from interannual to multidecadal scales, modifies the seasonal characteristics of the wave climate (Wahl and Plant, 2015). These long-term variations are forced by climate patterns, as is the case in the North Atlantic, where the inter-annual variability of waves is highly correlated with the North Atlantic Oscillation (Bauer, 2001). Similarly, extreme waves in the North Pacific increase with positive events of the El Niño-Southern Oscillation (ENSO) (Bromirski *et al.*, 2013; Gibbs *et al.*, 2014), and with the Pacific/North American pattern (Menéndez *et al.*, 2008).

Of all the climate patterns, ENSO has been identified as the primary driver of interannual wave climate variability (Stopa and Cheung, 2014). In previous works, it has been demonstrated that the vulnerability of Pacific coasts is governed by ENSO (Barnard *et al.,* 2015; Goodwin, 2005; Ruiz de Alegría-Arzaburu and Vidal-Ruiz, 2018; Silva *et al.,* 2017). Some studies have been carried out to identify the wave climate response to ENSO at a global scale (Semedo *et al.,* 2010; Stopa and Cheung, 2014; Reguero *et al.,* 2015, 2019; Mori *et al.,* 2018), but more work is needed, particularly for data-poor locations. The ENSO impacts are amplified when they occur with multidecadal climate patterns, such as the Pacific Decadal Oscillation (PDO) or Southern Annular Mode (SAM). The PDO shows an ENSO-like pattern and is also marked in the North Pacific. The SAM causes variations in the low pressure belt of the southern polar atmospheric circulation, and is also the governing large-scale pattern in the Southern Ocean (Wang & Cai, 2013).

The identification of inherent natural variability is also essential in order to reduce uncertainties in wave climate projections under global warming for four main reasons (Wong *et al.*, 2014). First, natural variability can mask a global warming signal in areas with a high level of natural fluctuation (Tebaldi, Arblaster and Knutti, 2011; Deser *et al.*, 2012; Clem *et al.*, 2020). Second, natural variability can delay the restoration and climate change adaptability of natural and human systems (Moser and Ekstrom, 2010; Duarte *et al.*, 2020). Third, natural variability can dampen, or amplify, the hazards associated with global warming (Deser *et al.*, 2012). And finally, climate change will potentially amplify the phases of the climate patterns (Cai *et al.*, 2015).

### 1.2.3 Climate change and wave climate

**The expanding tropics**

The poleward widening of the Hadley cells, is one of the main consequences of climate change in the atmospheric circulation (Reichler, 2009), and is associated with the increase of greenhouse gases (Lu, Chen and Frierson, 2008), ozone depletion (Kang *et al.*, 2011; Polvani *et al.*, 2011), and anthropogenic aerosols (Lucas, Timbal and Nguyen, 2014). Since 1979, the latitude of the tropical belt has expanded 1 to 3° in both hemispheres, extending more in the Northern Hemisphere. This is projected to continue throughout this century, between 1 and 2° (Lucas, Timbal and Nguyen, 2014). The widening and strengthening of the Hadley cells have implications for the surrounding climatic zones in the context of a changing climate (Seidel *et al.*, 2008; Reichler, 2009). The expanding tropics have worldwide effects, but will be especially critical in regions of transitional climate, where the prevailing conditions (temperature, precipitation, wind, pressure, and waves) could mean it has a new type of climate (e.g. subtropical could become tropical climate). The effect of this climate driver on other climate variables, such as precipitation, have been addressed elsewhere, but the implications on global wave climate have not yet been examined, although some works has been done at a regional scale (Wandres *et al.*, 2016; Mortlock *et al.*, 2020).

**Wave climate projections**

To a large extent, the climate of the next century depends on the agreements by all nations to reduce their levels of $CO_2$ emissions. In the Sixth Assessment Report (AR6, 2021), the Intergovernmental Panel on Climate Change (IPCC) proposed four scenarios to describe future climate, considering distinct Representative Concentration Pathways (RCP), RCP 2.6, RCP 4.5, RCP 6.0 and RCP 8.5. They represent the $CO_2$ emission levels for the next century (see Figure 1.2).

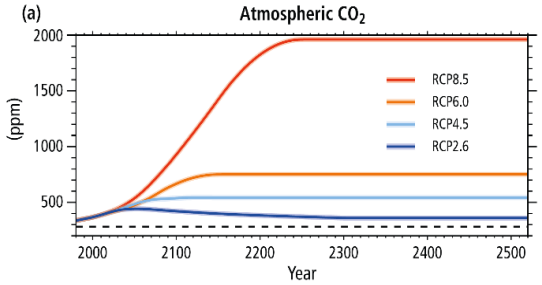


Figure 1. 2 Future baselines of carbon dioxide emissions for the four RCPs, up to 2300. The Fifth Assessment Report (AR5) IPCC (2013).

Until relatively recently, research on projected coastal hazards, has focussed on sea level rise. The Fifth Assessment Report (AR5) IPCC (2013), related to the wave climate, concluded that, overall, wave projections were of low confidence in the IPCC scale. This is linked to low confidence in wind projections, natural variability, and extreme waves (Wong *et al.*, 2014), and the uncertainties associated with GHG projections, Global Climate Models (GCMs), and wave models (Morim *et al.*, 2019). However, the predictions are of high confidence in the IPCC scale for the Southern Ocean (Morim *et al.*, 2019; Meucci *et al.*, 2020); wave heights will increase and wave directions will shift clockwise in the tropics and anticlockwise in the rest of the ocean areas (Morim *et al.*, 2019).

Existing work also concentrates on significant wave height (Meucci *et al.*, 2020; Lobeto, Menendez and Losada, 2021), and very little research focuses on the wave period and direction (Morim *et al.*, 2019). Moreover, other wave parameters are also needed for effective coastal

management strategies, regarding natural systems and industries. For example, the mean wave direction is a critical component in coastal sediment transport (Barnard et al., 2015; Hemer et al., 2010), and port operability (Camus *et al.*, 2019), while wave power determines the wave energy flux, and is a key parameter in coastline stability (Ranasinghe, 2016), coastal structures and wave energy extraction (Reguero et al., 2015). Moreover, previous studies have shown that sea surface temperature (SST) and global wave power are strongly linked (Shimura *et al.*, 2020) and the latter may be a good indicator of global warming signal inherent in wave climate (Reguero et al., 2019). More investigation on these variables will help to adopt more optimal solutions for a wide range of coastal activities and industries.

From the above, this thesis is based on following statements:

1. Wave climate is essential in coastal processes that influences coastal environments and industries. It is also a source of coastal risk. Wave climate is characterized by several parameters, such as wave power and direction, and its long-term variability is very relevant for coastal activities. It is therefore not only to examine sea level, it is also necessary to integrate wave climate into coastal adaptation strategies.
2. As natural variability drives seasonal wave climate, a fuller understanding of the impacts of climate patterns in the wave climate is needed, both when the climate patterns occur individually, and when they occur simultaneously. This knowledge should be integrated into the near-future coastal assessment.
3. The expanding tropics is a consequence of climate change that impacts the atmospheric circulation with important implications for the climate. It has not yet been studied related to wave climate, but could be a primary wave climate driver for tropical, subtropical and extratropical coastal regions.
4. Despite efforts to quantify the impacts of climate change in wave characteristics, global wave projections are still not completely understood. Discrepancies exist, as well as a lack of information regarding some wave parameters.
5. Both natural variability and climate change are essential for coastal assessment in the future. Understanding the extent to which changes in wave climate are presently driven by global warming, natural variability, or both, is pivotal to coastal risk analysis and therefore to coastal adaptation.

## 1.3 Goal and objectives

This thesis aims to quantify the long-term impacts in wave climate, which is a principal coastal hazard, induced by natural variability and climate change, to reduce the barriers in the area of coastal hazard knowledge for climate change adaptation. The work proposes a wave climate framework on which coastal risk and adaptation strategies can be based. Although the work focuses on the global wave climate, the results are applied to the case study of Mexico. Since the goal is very ambitious, intermediate objectives are addressed in different chapters as shown in Figure 1. 3.

**Objective 1 (Chapter 3):** To quantify the wave climate characteristics, wave power and mean direction, in response to ENSO. The results should identify the anomalies caused in the average wave climate induced by the different phases of ENSO (positive, negative, and neutral phase).

**Objective 2 (Chapter 4):** To generate a framework that classifies the global wave climate into types that are intrinsically linked to the atmospheric circulation responsible for their genesis. The link between planetary winds and wave climate types should give a fuller understanding of the causal mechanisms between climate patterns, global warming and wave climate, and should provide a more accurate quantification of their impacts.

**Objective 3 (Chapter 4):** To evaluate the impact of natural variability and global warming in the net long-term variation, composite anomalies and trends of each wave climate type, over the last three decades.

**Objective 4 (Chapter 5):** To identify the impacts of the expanding tropics in wave climate. The results will identify those areas that are affected by this potential climate driver and propose how to integrate it in coastal assessment.

**Objective 5 (Chapter 6):** To project the wave climate types under climate change scenarios RCP 2.6 and 8.5 in the next century, and evaluate the impacts on wave power, mean wave direction, and the area of each. From these results, the regions affected by changes in prevailing wave conditions; area covered, intensity, and wave direction, will be identified.

**Objective 6 (Chapter 7):** To classify the coastal regions based on long-term wave climate variability (impacts forced by ENSO, the prevailing wave climate types in the historical scenarios and the projected transitional wave climate regions), and to establish a general basis for coastal risk assessment and adaptation strategies.

**Objective 7 (Chapter 8):** To develop a wave climate framework for the coast of Mexico that includes the statistical analysis of wave climate, wave climate types, long-term variation and climate change projections.

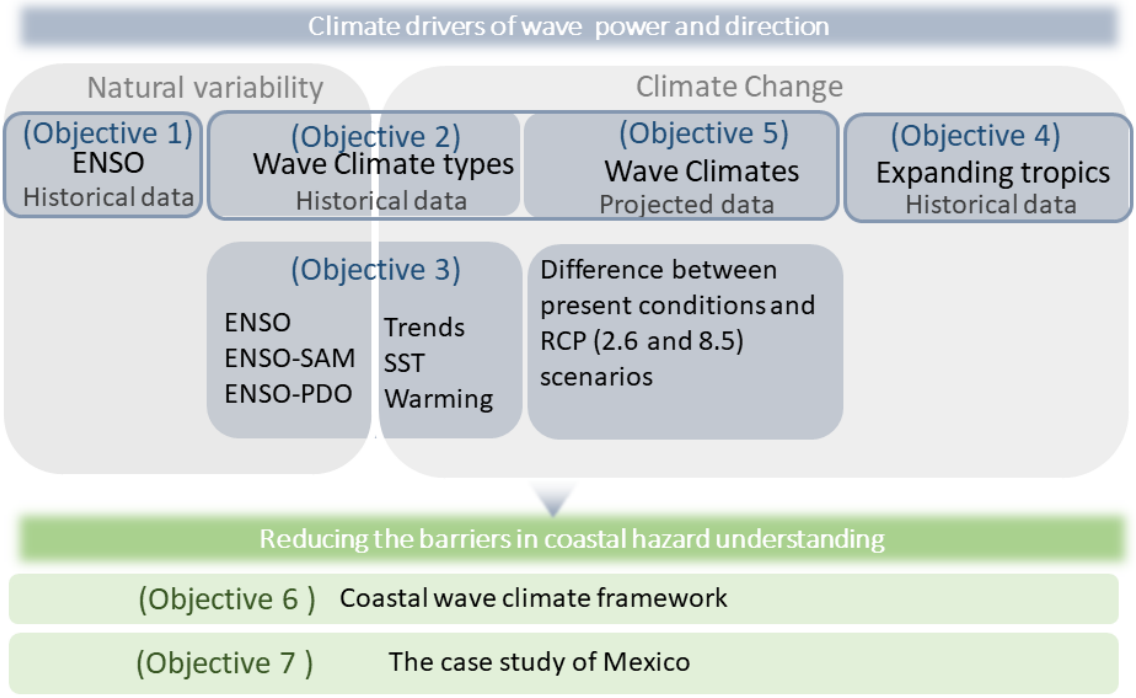


Figure 1. 3 Objectives of this thesis.

### References

Barnard, P. L. et al. (2015) 'Coastal vulnerability across the Pacific dominated by El Niño/Southern Oscillation', Nature Geoscience. Nature Publishing Group, 8, p. 801. Available at: https://doi.org/10.1038/ngeo2539.

Bauer, E. (2001) 'Interannual changes of the ocean wave variability in the North Atlantic and in the North Sea', Climate Research. Inter-Research Science Center, 18(1/2), pp. 63–69. Available at:

http://www.jstor.org/stable/24861559.

Bromirski, P. D. et al. (2013) 'Wave power variability and trends across the North Pacific', Journal of Geophysical Research: Oceans, 118(12), pp. 6329–6348. doi: 10.1002/2013JC009189.

Cai, W. et al. (2015) 'ENSO and greenhouse warming', Nature Climate Change, 5(9), pp. 849–859. doi: 10.1038/nclimate2743.

Camus, P. et al. (2019) 'Probabilistic assessment of port operation downtimes under climate change', Coastal Engineering, 147, pp. 12–24. doi: https://doi.org/10.1016/j.coastaleng.2019.01.007.

Clem, K. R. et al. (2020) 'Record warming at the South Pole during the past three decades', Nature Climate Change, 10(8), pp. 762–770. doi: 10.1038/s41558-020-0815-z.

Deser, C. et al. (2012) 'Communication of the role of natural variability in future North American climate', Nature Climate Change, 2(11), pp. 775–779. doi: 10.1038/nclimate1562.

Duarte, C. M. et al. (2020) 'Rebuilding marine life', Nature, 580(7801), pp. 39–51. doi: 10.1038/s41586-020-2146-7.

Fairley, I. et al. (2020) 'A classification system for global wave energy resources based on multivariate clustering', Applied Energy, 262, p. 114515. doi: https://doi.org/10.1016/j.apenergy.2020.114515.

Gibbs, A. et al. (2014) '17A . 3 NUMERICAL OPTIMIZATION AND VALIDATION OF THE NEARSHORE WAVE PREDICTION SYSTEM ACROSS THE TROPICAL ATLANTIC OCEAN DRIVEN BY THE OFFICIAL TROPICAL ANALYSIS AND FORECAST BRANCH / NATIONAL HURRICANE CENTER GRIDDED WIND FORECASTS', (section 5), pp. 1–12.

Gillis, L. G. et al. (2017) 'Opportunities for protecting and restoring tropical coastal ecosystems by utilizing a physical connectivity approach', Frontiers in Marine Science, 4(NOV). doi: 10.3389/fmars.2017.00374.

Godwyn-Paulson, P. et al. (2020) 'Coastline variability of several Latin American cities alongside Pacific Ocean due to the unusual "Sea Swell" events of 2015', Environmental Monitoring and Assessment, 192(8), p. 522. doi: 10.1007/s10661-020-08469-x.

Goodwin, I. D. (2005) 'A mid-shelf, mean wave direction climatology for southeastern Australia, and its relationship to the El Niño—Southern Oscillation since 1878 A.D.', International Journal of Climatology. John Wiley & Sons, Ltd, 25(13), pp. 1715–1729. doi: 10.1002/joc.1207.

Harley, M. D. et al. (2017) 'Extreme coastal erosion enhanced by anomalous extratropical storm wave direction', Scientific Reports, 7(1), p. 6033. doi: 10.1038/s41598-017-05792-1.

Hemer, M. A., Church, J. A. and Hunter, J. R. (2010) 'Variability and trends in the directional wave climate of the Southern Hemisphere', International Journal of Climatology. John Wiley & Sons, Ltd, 30(4), pp. 475–491. doi: 10.1002/joc.1900.

Huizer, S. et al. (2019) 'Global potential for the growth of fresh groundwater resources with large beach nourishments', Scientific Reports, 9(1), p. 12451. doi: 10.1038/s41598-019-48382-z.

Izaguirre, C. et al. (2020) 'Climate change risk to global port operations', Nature Climate Change. doi: 10.1038/s41558-020-00937-z.

Kang, S. M. et al. (2011) 'Impact of Polar Ozone Depletion on Subtropical Precipitation', Science, 332(6032), pp. 951 LP – 954. doi: 10.1126/science.1202131.

Li, S. and Babanin, A. (2021) 'New parameterizations of air-sea CO2 gas transfer velocity on wave breaking', in EGU General Assembly, pp. EGU21-6956, https://doi.org/10.5194/egusphere-egu2.

Lobeto, H., Menendez, M. and Losada, I. J. (2021) 'Future behavior of wind wave extremes due to climate change', Scientific Reports, 11(1), p. 7869. doi: 10.1038/s41598-021-86524-4.

Lu, J., Chen, G. and Frierson, D. M. W. (2008) 'Response of the Zonal Mean Atmospheric Circulation to El Niño

versus Global Warming', Journal of Climate. American Meteorological Society, 21(22), pp. 5835–5851. doi: 10.1175/2008JCLI2200.1.

Lucas, C., Timbal, B. and Nguyen, H. (2014) 'The expanding tropics: A critical assessment of the observational and modeling studies', Wiley Interdisciplinary Reviews: Climate Change, 5(1), pp. 89–112. doi: 10.1002/wcc.251.

Melet, A. et al. (2018) 'Under-estimated wave contribution to coastal sea-level rise', Nature Climate Change. Springer US, 8(3), pp. 234–239. doi: 10.1038/s41558-018-0088-y.

Melet, A. et al. (2020) 'Contribution of Wave Setup to Projected Coastal Sea Level Changes', Journal of Geophysical Research: Oceans. John Wiley & Sons, Ltd, 125(8), p. e2020JC016078. doi: 10.1029/2020JC016078.

Mendoza, E. et al. (2015) 'Analysis of the Hazards and Vulnerability of the Cancun Beach System', Extreme Events. (Geophysical Monograph Series), pp. 125–136. doi: doi:10.1002/9781119157052.ch10.

Mendoza, E. et al. (2017) 'Measurements and Modelling of Small Scale Processes of Vegetation Preventing Dune Erosion', Journal of Coastal Research, 2017-Sprin. doi: 10.2112/SI77-003.1.

Menéndez, M. et al. (2008) 'Variability of extreme wave heights in the northeast Pacific Ocean based on buoy measurements', Geophysical Research Letters, 35(22), pp. 1–6. doi: 10.1029/2008GL035394.

Meucci, A. et al. (2020) 'Projected 21st century changes in extreme wind-wave events', Science Advances, 6(24), p. eaaz7295. doi: 10.1126/sciadv.aaz7295.

Mori, N. et al. (2014) 'Local amplification of storm surge by Super Typhoon Haiyan in Leyte Gulf', Geophysical Research Letters. John Wiley & Sons, Ltd, 41(14), pp. 5106–5113. doi: https://doi.org/10.1002/2014GL060689.

Mori, N., Kishimoto, R. and Shimura, T. (2018) 'WAVE CLIMATE VARIABILITY AND RELATED CLIMATE INDICES', Coastal Engineering Proceedings, 1(36), p. 75. doi: 10.9753/icce.v36.risk.75.

Morim, J. et al. (2019) 'Robustness and uncertainties in global multivariate wind-wave climate projections', Nature Climate Change, 9(9), pp. 711–718. doi: 10.1038/s41558-019-0542-5.

Mortlock, T. R. et al. (2020) 'Influence of the subtropical ridge on directional wave power in the southeast Indian Ocean', International Journal of Climatology. John Wiley & Sons, Ltd, n/a(n/a). doi: 10.1002/joc.6522.

Moser, S. C. and Ekstrom, J. A. (2010) 'A framework to diagnose barriers to climate change adaptation', Proceedings of the National Academy of Sciences, 107(51), pp. 22026 LP – 22031. doi: 10.1073/pnas.1007887107.

Neumann, B. et al. (2015) 'Future Coastal Population Growth and Exposure to Sea-Level Rise and Coastal Flooding - A Global Assessment', PLOS ONE, 10(6), p. e0131375.

Odériz, I., Knöchelmann, N., et al. (2020) 'Reinforcement of vegetated and unvegetated dunes by a rocky core: A viable alternative for dissipating waves and providing protection?', Coastal Engineering, 158, p. 103675. doi: https://doi.org/10.1016/j.coastaleng.2020.103675.

Odériz, I., Gómez, I., et al. (2020) 'Understanding Drivers of Connectivity and Resilience Under Tropical Cyclones in Coastal Ecosystems at Puerto Morelos, Mexico', Journal of Coastal Research, 95(sp1), pp. 128–132. doi: 10.2112/SI95-025.1.

Polvani, L. M. et al. (2011) 'Stratospheric Ozone Depletion: The Main Driver of Twentieth-Century Atmospheric Circulation Changes in the Southern Hemisphere', Journal of Climate. Boston MA, USA: American Meteorological Society, 24(3), pp. 795–812. doi: 10.1175/2010JCLI3772.1.

Ranasinghe, R. (2016) 'Assessing climate change impacts on open sandy coasts: A review', Earth-Science Reviews, 160, pp. 320–332. doi: https://doi.org/10.1016/j.earscirev.2016.07.011.

Reguero, B. G., Losada, I. J. and Méndez, F. J. (2015) 'A global wave power resource and its seasonal, interannual and long-term variability', Applied Energy, 148, pp. 366–380. doi: https://doi.org/10.1016/j.apenergy.2015.03.114.

Reguero, B. G., Losada, I. J. and Méndez, F. J. (2019) 'A recent increase in global wave power as a consequence of oceanic warming', Nature Communications. Springer US, 10(1), pp. 1–14. doi: 10.1038/s41467-018-08066-0.

Reichler, T. (2009) 'Chapter 7 - Changes in the Atmospheric Circulation as Indicator of Climate Change', in Letcher, T. M. B. T.-C. C. (ed.). Amsterdam: Elsevier, pp. 145–164. doi: https://doi.org/10.1016/B978-0-444-53301-2.00007-5.

Ruiz de Alegría-Arzaburu, A. and Vidal-Ruiz, J. A. (2018) 'Beach recovery capabilities after El Niño 2015–2016 at Ensenada Beach, Northern Baja California', Ocean Dynamics, 68(6), pp. 749–759. doi: 10.1007/s10236-018-1164-6.

Seidel, D. J. et al. (2008) 'Widening of the tropical belt in a changing climate', Nature Geoscience, 1(1), pp. 21–24. doi: 10.1038/ngeo.2007.38.

Semedo, A. et al. (2011) 'A Global View on the Wind Sea and Swell Climate and Variability from ERA-40', Journal of Climate. American Meteorological Society, 24(5), pp. 1461–1479. doi: 10.1175/2010JCLI3718.1.

Shimura, T. et al. (2020) 'Impacts of Ocean Wave-Dependent Momentum Flux on Global Ocean Climate', Geophysical Research Letters. John Wiley & Sons, Ltd, 47(20), p. e2020GL089296. doi: https://doi.org/10.1029/2020GL089296.

Silva, R. et al. (2016) 'Response of vegetated dune-beach systems to storm conditions', Coastal Engineering, 109. doi: 10.1016/j.coastaleng.2015.12.007.

Silva, R. et al. (2017) 'Coastal risk mitigation by green infrastructure in Latin America', Proceedings of the Institution of Civil Engineers - Maritime Engineering, 170(2), pp. 39–54. doi: 10.1680/jmaen.2016.13.

Silva, R. et al. (2020) 'A Framework to Manage Coastal Squeeze', Sustainability. doi: 10.3390/su122410610.

Smythe, T. C. (2013) Assessing the impacts of Hurricane Sandy on the port of New York and New Jersey's maritime responders and response infrastructure. doi: https://doi.org/doi:10.7282/T30R9MMM.

Stopa, J. E. and Cheung, K. F. (2014) 'Periodicity and patterns of ocean wind and wave climate', Journal of Geophysical Research: Oceans. John Wiley & Sons, Ltd, 119(8), pp. 5563–5584. doi: 10.1002/2013JC009729.

Tebaldi, C., Arblaster, J. M. and Knutti, R. (2011) 'Mapping model agreement on future climate projections', Geophysical Research Letters. John Wiley & Sons, Ltd, 38(23). doi: https://doi.org/10.1029/2011GL049863.

Toimil, A. et al. (2020) 'Climate change-driven coastal erosion modelling in temperate sandy beaches: Methods and uncertainty treatment', Earth-Science Reviews, 202, p. 103110. doi: https://doi.org/10.1016/j.earscirev.2020.103110.

Vousdoukas, M. I. et al. (2020) 'Sandy coastlines under threat of erosion', Nature Climate Change, 10(3), pp. 260–263. doi: 10.1038/s41558-020-0697-0.

Wahl, T. and Plant, N. G. (2015) 'Changes in erosion and flooding risk due to long-term and cyclic oceanographic trends', Geophysical Research Letters, 42(8), pp. 2943–2950. doi: 10.1002/2015GL063876.

Wandres, M. et al. (2016) 'The Influence of the Subtropical High-Pressure Ridge on the Western Australian Wave Climate', Journal of Coastal Research, 75(sp1), pp. 567–571. doi: 10.2112/SI75-114.1.

Wang, G. and Cai, W. (2013) 'Climate-change impact on the 20th-century relationship between the Southern Annular Mode and global mean temperature', Scientific Reports, 3(1), p. 2039. doi: 10.1038/srep02039.

Wong, P. P. et al. (2014) 'Coastal systems and low-lying areas', in Field, C. B. et al. (eds) Climate Change 2014: Impacts, Adaptation, and Vulnerability. Part A: Global and Sectoral Aspects. Contribution of Working Group II to the Fifth Assessment Report of the Intergovernmental Panel of Climate Change. Cambridge, United Kingdom and New York, NY, USA: Cambridge University Press, pp. 361–409.

# CHAPTER 2

# Methodology

This Chapter describes the data and methods used in this thesis.

## 2.1 Methodological framework

The methodology employed for each objective is addressed in individual sections of this chapter. The subsequent chapters address the results for each intermediate objective and are written to be read independently, as shown in Figure 2. 1.

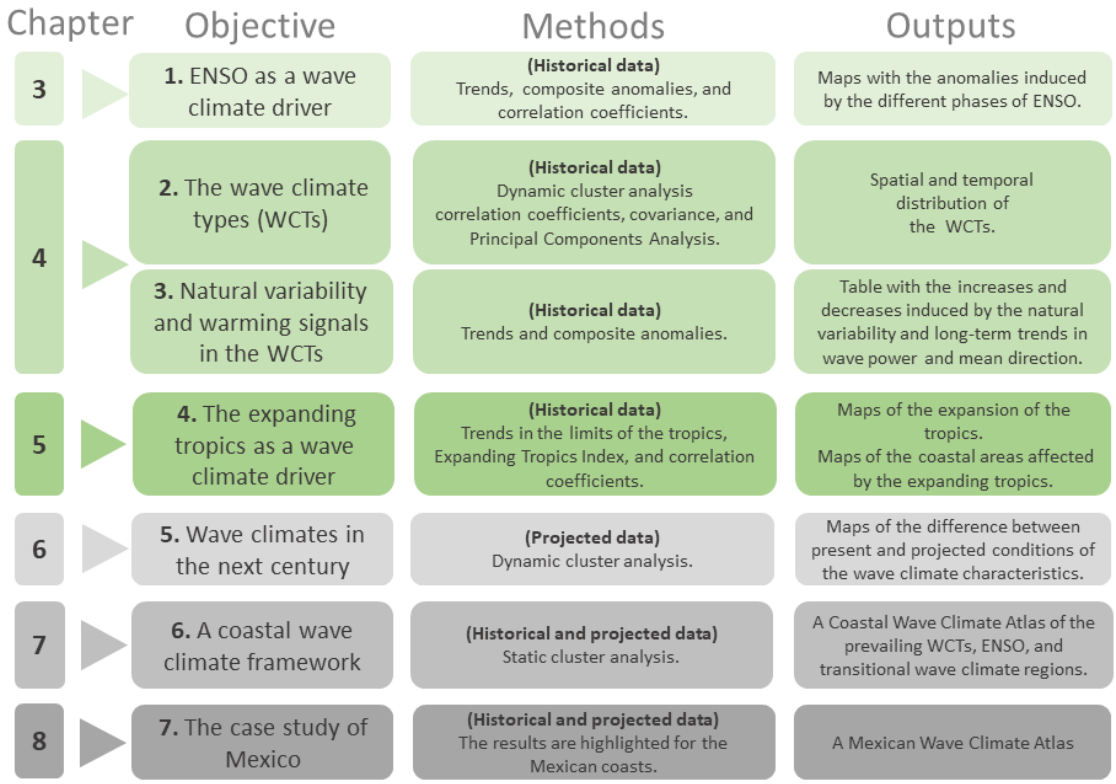


Figure 2. 1 The methodological framework and organization of this thesis.

## 2.1 Data

In this thesis, only the monthly average wave power and mean direction of deep-water wave climate is examined; local effects and extreme events are not. This thesis uses wave and wind parameters from ERA5 (Hersbach et al., 2020), the latest wave reanalysis dataset from the ECMWF (European Centre for Medium-Range Weather Forecasts).The ocean wave and wind parameters of the ERA5 (Hersbach et al., 2020) dataset for 1979 to 2018 (0.5 x 0.5° and 0.25 x 0.25° respectively), with an hourly resolution, were used. The wave model was forced by HRES-WAM (Guenther et al., 1992) using wave spectra with 24 directions and 30 frequencies. The work examined the wave power and the mean wave direction as the characteristic parameters of wave climate. The wave power for irregular waves was computed under the following assumptions, the total wave energy of a wave spectrum is $E_{tot} = \rho g \int_0^\infty S(f)df = \rho g m_0 \rightarrow E = \frac{1}{16}\rho g H_{m0}^2$. Where $m_0 = \left(\frac{H_{m0}}{4}\right)^2 = \frac{{H_{m0}}^2}{16}$. The total wave power is the result of adding the wave power of the individual waves that make up the total wave spectrum (Neill & Hashemi, 2018).

$$\Delta P = \rho g C_g(\sigma)\Delta S(\sigma) = \rho g C_g S(\sigma)\Delta(\sigma) = \rho g \frac{\sigma}{k}\left[\frac{1}{2}\left(1+\frac{2kh}{senh\ 2kh}\right)\right]S(\sigma)\Delta(\sigma)$$

(2. 1)

Consequently, the total power is

$$P = \rho g \int_0^\infty C_g(\sigma)S(\sigma)d\sigma = \rho g \int_0^\infty \frac{\sigma}{k}\left[\frac{1}{2}\left(1+\frac{2kh}{senh\ 2kh}\right)\right]S(\sigma)d\sigma$$

(2. 2)

In the case of deep waters the dispersion equation is simplified because $\tanh(kd) \approx 1 \rightarrow \sigma = \sqrt{gk} \rightarrow C_g = \frac{d\sigma}{dk} = \frac{g}{2}\frac{1}{\sqrt{gk}} = \frac{g}{2\sigma} = \frac{gT}{4\pi}$. Then, the wave power can be expressed as

$$P = \rho g \int_0^\infty C_g(\sigma)S(\sigma)d\sigma = \rho g \int_0^\infty \frac{g}{2\sigma}S(\sigma)d\sigma = \frac{\rho g^2}{2}\int_0^\infty \sigma^{-1}S(\sigma)d\sigma = \frac{\rho g^2}{2}m_{-1}$$

(2. 3)

Using the approximation of deep waters, the group velocity is $C_g = \frac{gT_E}{4\pi}$. And finally, the wave power for irregular waves is

$$P = EC_g = \frac{\rho g^2}{4\pi}H_{mo}^2 T_E = \frac{\rho g^2}{32\pi}\left(\frac{H_{m0}}{\sqrt{2}}\right)^2 T_E = \frac{\rho g^2}{64\pi}{H_{m0}}^2 T_E$$

(2. 4)

Where $\rho$ is the water density; $g$ is the acceleration of gravity; $T_e$ (s) is the wave energy period; and $H_s$ (m) is the significant wave height of combined wind sea and swell. The wave energy period ($T_e, s$) was obtained using the approximation $T_e = \alpha T_{01}$; where the parameter $\alpha = 1.08$ was used (Webb & Fox-Kemper, 2011).

## 2.2 Methods to address Objective 1 (Chapter 3)

This chapter addresses the quantification of the impacts of ENSO in the wave climate characteristics.

### 2.2.1 Validation of ERA 5

First, ERA 5 was validated with observations of altimetry data and buoys. Four estimators were used, the bias (equation (2. 5)), the Root Mean Square Error (RMSE, equation (2. 6)), the Pearson correlation coefficient (equation (2. 7)) and R-squared (equation (2. 8)). The buoys 46072 (2002-2018), 51000 (2009-2018), 46047 (1991-2018), 41040 (2005-2017), from NDBC meteorological/ocean program of the National Oceanographic and Atmosphere Administration of USA, were selected to cover different points in the Atlantic and Pacific.

The time series of the buoys have some gaps in time and do not cover the entire area of this work. The altimetry Globwave dataset, which integrates different satellite altimeter missions (GEOSAT, ERS-1/2, TOPEX/Poseidon, GFO, Envisat, Jason-1/2, and CryoSAT), (Gavrikov *et al.*, 2016), was used to cover all the basins from 1985 onwards. The parameter compared was the significant wave height ($H_s$). To evaluate the buoys, the 4 estimators were used.

$$Bias(\hat{\theta}) = E_{x|\theta}(\hat{\theta}) - \theta = \frac{\sum_{i=1}^{n}(\hat{\theta} - \theta)}{n}$$

(2. 5)

$$RMSE[\hat{\theta}] = \sqrt{E_{x|\theta}\left((\hat{\theta} - \theta)^2\right)} = \sqrt{\frac{\sum_{i=1}^{n}(\hat{\theta} - \theta)^2}{n}}$$

(2. 6)

$$R(\hat{\theta}, \theta) = \frac{1}{n-1}\sum_{i=1}^{N}\overline{\left(\frac{\hat{\theta}_i - \overline{x_{\hat{\theta}}}}{s_{\hat{\theta}}}\right)}\left(\frac{\theta_i - \overline{x_{\theta}}}{s_{\theta}}\right)$$

(2. 7)

$$R^2 = 1 - \frac{SS_{res}}{SS_{tot}} = 1 - \frac{\sum_i(\hat{\theta}_i - \theta_i)^2}{\sum_i\left(\hat{\theta}_i - \bar{\hat{\theta}}\right)^2}$$

(2. 8)

Where $\hat{\theta}$ is the estimator (buoys and altimetry datasets), and ERA5 is the estimated value $\theta$.

To validate the ERA 5 data with GlobWave, the time period of 1992-2013 was used. The grid of both datasets did not match, so the values of ERA5 were interpolated with the grid of GlobWave. In this case, only the bias was computed.

The seasonal variability was examined with the average of the variables using the seasons: December, January, and February (DJF), March, April, and May (MAM); June, July, and August (JJA); and September, October, and November (SON). The inter-annual validation of ERA 5 was computed with GlobWave, the correlation coefficients R were calculated between ENSO climate indices (ONI, MEI, SOI, Nino3.4, defined in detail in section 2.2.3) and the significant wave height ($H_s$), as explained in section 2.2.2. The Bias of R between both datasets was used for inter-annual validation.

### 2.2.2 ENSO as a wave climate driver

ENSO climate indices can be classified into: those that use sea level pressure (e.g., Southern Oscillation Index, SOI, Equatorial Southern Oscillation, and ESO), the sea surface temperature indices (e.g., Niño1, Niño 1.2, Niño 3, Niño 4 and Niño 3.4), those that consider OLR (Outgoing Longwave Radiation), and finally, those that use wind or other parameters, combining more than one variable.

Previous studies focusing on ocean waves have used the SOI (Reguero *et al.,* 2015), Niño3 (Reguero *et al.,*2019), Niño 3.4., (Shimura *et al.,* 2013a; Stopa and Cheung, 2014), and MEI (Barnard *et al.,* 2015, 2017). However, these authors did not explain why one or another climate index was used in their work. In Chapter 3, four climate indices of the National Oceanographic and Atmospheric Administration (NOAA) Earth System Research Laboratory were used. Each climate index was analysed for its statistical significance against wave power and direction, in order to identify which was most appropriate for the description of the global wave climate response to ENSO.

1. The SOI (Southern Oscillation Index) is calculated using the monthly mean SLP (Sea Level Pressure) difference between Tahiti and Darwin. During the phase of El Niño (La Niña), negative (positive) values of SOI, negative (positive) anomalies are found in Tahiti, while positive (negative) anomalies are found in Darwin.
2. The Niño3.4 is the SST (Sea Surface Temperature) anomalies of the region (5°N-5°S, 170°W-120°W) in the tropical Pacific. This index has previously been found to be the most representative for these SST regions (Trenberth and Hoar, 1997).
3. The ONI (Oceanic Niño Index), is a 3-month moving average of the SST anomalies in the Niño3.4 region. Values greater than 0.5 are El Niño phenomena, less than -0.5 are La Niña and values between -0.5 and 0.5 correspond to neutral phases.
4. The MEI.v2 (Multivariate ENSO Index Version 2) is a bi-monthly index of the Empirical Orthogonal Function (EOF), considering five variables (SLP, SST, OLR, zonal and meridional components of the surface wind), over the tropical Pacific (30°S-30°N and 100°E-70°W).

The composite anomalies for ENSO phases (El Niño and La Niña) were computed to depict the general behaviour of the atmosphere and wave climate. Anomalies of individual extreme ENSO events were analysed to detect dissimilarities that may exist between individual events. For this, the monthly anomalies ($A_{i,j} = x_{i,j} - \mu_j$; $j = 1,2,\dots,12$) of SLP, $P_w$, and $Dir_m$ were calculated as the value ($x_{i,j}$) of the year *i* and month *j* analysed, minus the average of the corresponding month $\mu_j$ for all the years.

The general effects of ENSO on mean wave direction and wave power were calculated using the correlation coefficient between the residual time series of $P_w$ and $Dir_m$ and the MEI climate indices. The time series were considered as an Additive Model and the seasonal component was calculated by applying a moving average for the 12 months. The correlation coefficients were calculated using the Pearson approach (Kendall, 1948), with a level of confidence of 95%. When the probability was less than 5% ($p<0.05$) the correlation coefficient was considered as statistically significant. Cross correlation was computed within a 12 month lag window to find the moment when the maximum value of R was obtained. The results of all the months are presented as absolute values.

## 2.3 Methods to address Objective 2 (Chapter 4)

Chapter 4 describes the classification of the wave climate into types, and compares the long-term impacts induced by climate patterns, and trends associated with ocean warming.

### 2.3.1 Classification of wave climate into types

The planetary wind systems were classified using a dynamic clustering technique, followed by a regionalization criterion. The wave climates were obtained using dynamic clustering, and the Wave Climate Types (WCTs, from here) were obtained by identifying isolated WCTs and relating them with their basin-scale wind origin, Figure 2. 2.

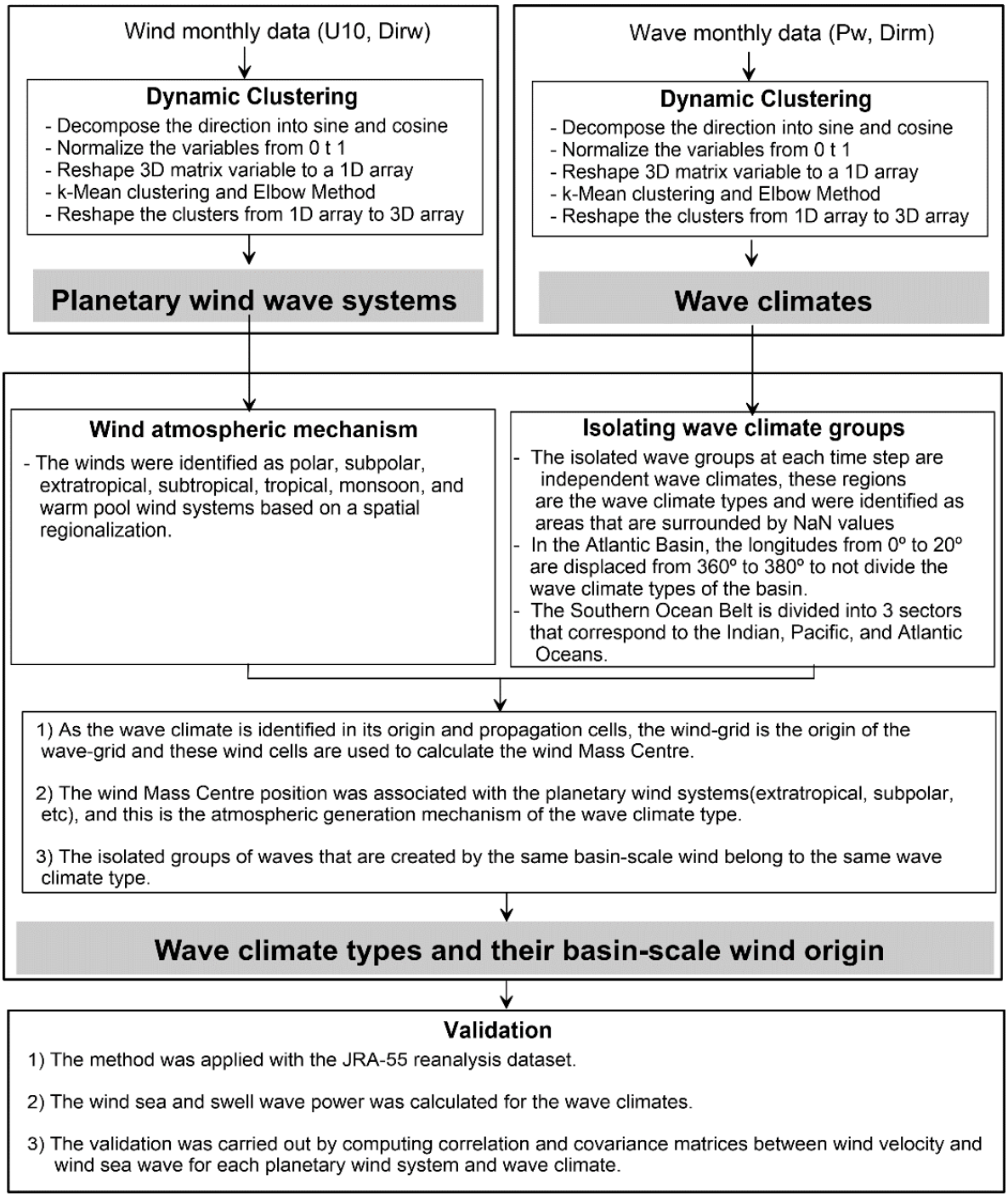


Figure 2. 2 A general perspective of the methods used to identify the wave climate types.

#### 2.3.1.1 Dynamic Clustering: planetary wind systems and wave climates

First, we examined the planetary wind systems using the monthly-averaged near surface wind velocity ($U_{10,}$ m/s) and wind direction ($Dir_{w,}$ °). This provided a set of spatial-temporal indices to identify the atmospheric circulation and its variability. Next, the wave climates associated with the

planetary wind systems were calculated using the same 'dynamic clustering' algorithm, but this time the input variables were the monthly-averaged wave direction ($Dir_m$, °) and wave power ($P_w$, kW/m).

The dynamic clustering technique used, involved *k-means* (MacQueen, 1967), which identified data patterns from the data characteristics, defined as variables. *k-means* is a non-supervised classification method that minimizes the sum of the Euclidian distances between each data variable and the centroids of each cluster, equation 2.9. The centroid of the cluster is defined as the average of all the variables that belong to this cluster (Berkhin, 2006).

$$\min_{s} E(\mu_k) = \min_{s} \sum_{k=1}^{n} \sum_{x_i} \left|\left|x_i - \mu_k\right|\right|^2$$

(2. 9)

Where $x_i$ is a variable, $\mu_k$ is the centroid, *k is* the cluster number and *n* is the total number of clusters. The method consists of the following steps, i) random centroids and the variables are assigned to the nearest cluster centroid. ii) Then, the process is repeated with the new centroids that are the average of the dataset belonging to each cluster. iii) This step is replicated until the centroids do not change. iv) The next step is to select the number of partitions, n. For this, the Elbow Method (Ketchen & Shook, 1996) was applied, using 2 to 10 clusters to compute the sum of the squared of error (SSE) of the distances of each object in the clusters from its centroid. The number of clusters (x axis) versus the SSE of the distance are represented and the optimal number of clusters is the number in which there is an abrupt change.

The data patterns depend on the input variables and their configuration. In wave and wind climate analysis, a time-step of each parameter is usually an input variable of *k-means*, and the result is a spatial distribution (called here 'static clustering', see Figure 2. 3 a). In contrast, the approach we applied is novel, in that we used a dynamic clustering technique that consists of all the time-steps and space-grid values of a parameter as a unique variable. That means we reshaped the 3D matrix of a parameter (longitude, latitude, time) to a 1D array. See the configuration in equation (2. 10) for the wind (input $U_{10}$, cos ($Dir_w$), sin ($Dir_w$)) and the ocean-wave variables (input $P_w$, cos ($Dir_m$), sin ($Dir_m$)), where $id_k$ is the cluster assigned. The direction is a circular variable that was decomposed into sine and cosine components. All the variables were normalized from 0 to 1, so that they all had the same weight when computing the distances. Once we obtained the cluster indexes, we reshaped them from 1D to 3D and then the classification was assigned in space and time.

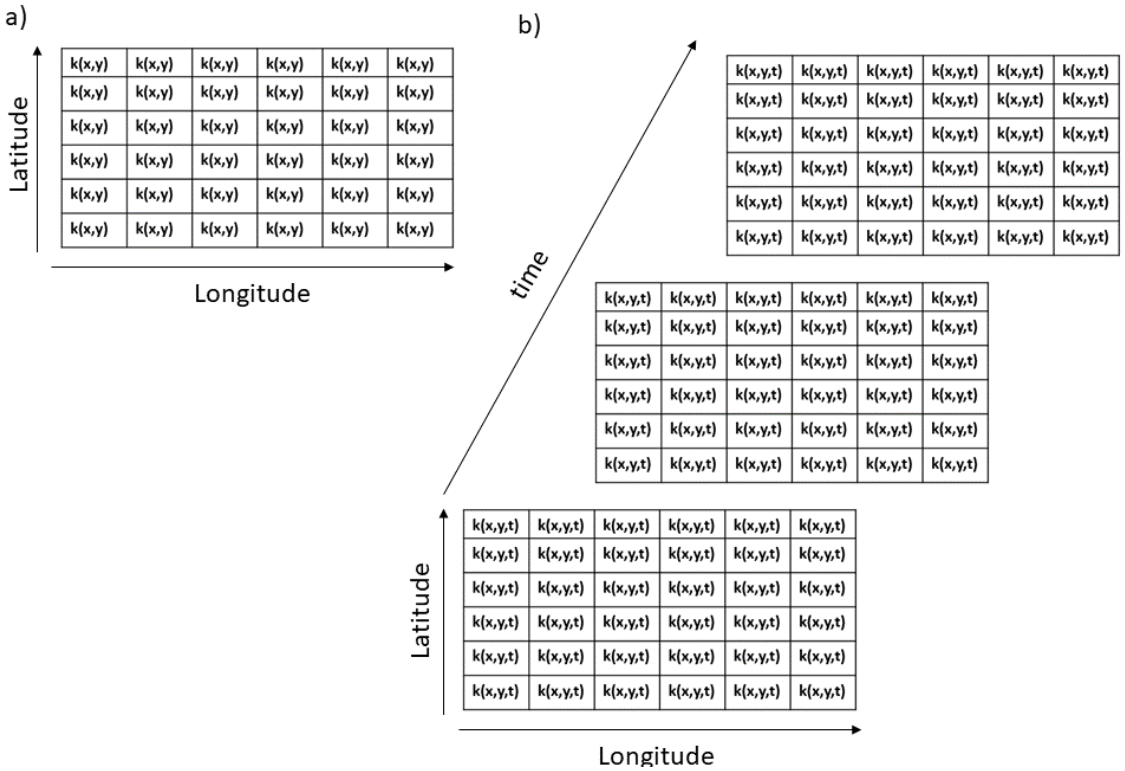


Figure 2. 3 Conceptual difference between a) static clustering, where the resulting classification k is assigned to (x and y) and b) dynamic clustering, where the classification is obtained in 3 dimensions (x, y and t).

$$\begin{pmatrix} U_{10n_{1,1,1}} & cos(Dir_{1,1,1})_n & sin(Dir_{1,1,1})_n \\ U_{10n_{2,1,1}} & cos(Dir_{2,1,1})_n & sin(Dir_{2,1,1})_n \\ \vdots & \vdots & \vdots \\ U_{10n_{i,1,1}} & cos(Dir_{i,1,1})_n & sin(Dir_{i,1,1})_n \\ \vdots & \vdots & \vdots \\ U_{10n_{1,j,1}} & cos(Dir_{1,j,1})_n & sin(Dir_{1,j,1})_n \\ \vdots & \vdots & \vdots \\ U_{10n_{i,j,1}} & cos(Dir_{i,j,1})_n & sin(Dir_{i,j,1})_n \\ \vdots & \vdots & \vdots \\ U_{10n_{1,1,t}} & cos(Dir_{1,1,t})_n & sin(Dir_{1,1,t})_n \\ U_{10n_{2,1,t}} & cos(Dir_{2,1,t})_n & sin(Dir_{2,1,t})_n \\ \vdots & \vdots & \vdots \\ U_{10n_{i,1,t}} & cos(Dir_{i,1,t})_n & sin(Dir_{i,1,t})_n \\ \vdots & \vdots & \vdots \\ U_{10n_{1,j,t}} & cos(Dir_{1,j,t})_n & sin(Dir_{1,j,t})_n \\ U_{10n_{2,j,t}} & cos(Dir_{2,j,t})_n & sin(Dir_{2,j,t})_n \\ \vdots & \vdots & \vdots \\ U_{10n_{i,j,t}} & cos(Dir_{i,j,t})_n & sin(Dir_{i,j,t})_n \end{pmatrix} \rightarrow \begin{pmatrix} id_{k_{1,1,1}} \\ id_{k_{2,1,1}} \\ \vdots \\ id_{k_{i,1,1}} \\ \vdots \\ id_{k_{1,j,1}} \\ \vdots \\ id_{k_{i,j,1}} \\ \vdots \\ id_{k_{1,1,t}} \\ id_{k_{2,1,t}} \\ \vdots \\ id_{k_{i,1,t}} \\ \vdots \\ id_{k_{1,j,t}} \\ id_{k_{2,j,t}} \\ \vdots \\ id_{k_{i,j,t}} \end{pmatrix}; \begin{pmatrix} P_{wn_{1,1,1}} & cos(Dir_{1,1,1})_n & sin(Dir_{1,1,1})_n \\ P_{wn_{2,1,1}} & cos(Dir_{2,1,1})_n & sin(Dir_{2,1,1})_n \\ \vdots & \vdots & \vdots \\ P_{wn_{i,1,1}} & cos(Dir_{i,1,1})_n & sin(Dir_{i,1,1})_n \\ \vdots & \vdots & \vdots \\ P_{wn_{1,j,1}} & cos(Dir_{1,j,1})_n & sin(Dir_{1,j,1})_n \\ \vdots & \vdots & \vdots \\ P_{wn_{i,j,1}} & cos(Dir_{i,j,1})_n & sin(Dir_{i,j,1})_n \\ \vdots & \vdots & \vdots \\ P_{wn_{1,1,t}} & cos(Dir_{1,1,t})_n & sin(Dir_{1,1,t})_n \\ P_{wn_{2,1,t}} & cos(Dir_{2,1,t})_n & sin(Dir_{2,1,t})_n \\ \vdots & \vdots & \vdots \\ P_{wn_{i,1,t}} & cos(Dir_{i,1,t})_n & sin(Dir_{i,1,t})_n \\ \vdots & \vdots & \vdots \\ P_{wn_{1,j,t}} & cos(Dir_{1,j,t})_n & sin(Dir_{1,j,t})_n \\ P_{wn_{2,j,t}} & cos(Dir_{2,j,t})_n & sin(Dir_{2,j,t})_n \\ \vdots & \vdots & \vdots \\ P_{wn_{i,j,t}} & cos(Dir_{i,j,t})_n & sin(Dir_{i,j,t})_n \end{pmatrix} \rightarrow \begin{pmatrix} id_{k_{1,1,1}} \\ id_{k_{2,1,1}} \\ \vdots \\ id_{k_{i,1,1}} \\ \vdots \\ id_{k_{1,j,1}} \\ \vdots \\ id_{k_{i,j,1}} \\ \vdots \\ id_{k_{1,1,t}} \\ id_{k_{2,1,t}} \\ \vdots \\ id_{k_{i,1,t}} \\ \vdots \\ id_{k_{1,j,t}} \\ id_{k_{2,j,t}} \\ \vdots \\ id_{k_{i,j,t}} \end{pmatrix}$$

(2. 10)

Our "dynamic clustering" has several advantages over "static clustering", or other statistical methods used to detect variability patterns in that:

1. **The wind and wave climates are defined by multivariate criteria** (wave climate: $P_w$, $Dir_m$; planetary wind system: $U_{10}$, $Dir_w$). Otherwise, using a variability analysis, such as Principal Component Analysis, we would analyse variability patterns and not a wave climate/wind systems.

2. **Wave climate tracking.** Our approach identifies the similarities that exist between neighbouring data (spatially and temporally). From this, the track of wave generation and subsequent propagation is obtained. As the classification identifies the wave origin, the wave climates are derived from their wind drivers, and classified through this approach. This procedure does not need tuning parameters, unlike other works that examine wave parametric relationships with neighbouring points. (e.g., Delpey et al., 2010; Hanson & Phillips, 2001; Jiang, 2019; or the method implemented in WAVEWATCH III).

3. **The method identifies wave patterns that are similar and separates geographical areas that are driven by different wind systems.** In general, to identify teleconnection patterns, Empirical Orthogonal Functions are applied that detect distant variability patterns. Instead of identifying variability patterns, using dynamic clustering, we were looking for similar spatial patterns of the wind and wave climate in time. In this way, the results are not biased by the time step analysed, and the classification is applied to the complete time series of the variables. From this, the variability patterns of the spatial-temporal classification can be examined.

As the input dataset plays an important role in the classification, the method was applied to two different wave reanalysis datasets, ERA5 and JRA-55, to evaluate its robustness. The approach was applied to both datasets for the same period, 1979-2017.

#### 2.3.1.2 Wave climate types and their basin-scale wind origins

Through dynamic clustering the geographical location of wave climate genesis and subsequent propagation is identified, meaning that the regional wind drivers can be detected and can be tracked through time and space. Other, more traditional, means of analysis could also infer the wind/wave relationship, by using, for example, a Singular Value Decomposition (SVD) analysis of the covariance matrix between two variables. However, in doing so the definition of the wave climates would be reduced to one variable, instead of two. Secondly, the covariance between a pair wind and wave parameters (e.g. $P_w$-$U_{10}$) would identify areas with the same, or different, spatial-temporal response for both parameters. However, forced by distant winds, ocean waves can propagate over large distances. So, a SVD analysis of the covariance matrix only allows the wind sea and wind with high covariance (extratropical regions, polar, and monsoon) to be identified, and regions dominated by swell would not be distinguished (the subtropics and tropics).

In the dynamic clustering classification of the wind, the global atmospheric circulation cells were well defined by latitude. The geographic limits (Figure 2.4) were applied to define the planetary wind system (Polar, Subpolar, Extratropical, Subtropical, Trade, Monsoon and Warm Pool winds).

The wind regionalization was as follows:

Southerly wind

- Subpolar Southern Hemisphere (<40ºS),
- Subtropical Southern Hemisphere (40ºS to 10ºN),
- Subtropical Northern Hemisphere (10ºN to 35ºN),
- Subpolar Northern Hemisphere (>35ºN),

Westerly wind

- Extratropical Southern Hemisphere (<15ºS),

- Tropical (15ºS to 10ºN),
- Extratropical Northern Hemisphere (>10ºN),
- Monsoon (30ºE to 160ºW; 0º to 30ºN),
- Warm Pool (30ºE to 120ºW; 25ºS to 0º),

Easterly wind

- Polar Southern Hemisphere (<40ºS),
- Tropical Southern Hemisphere (40ºS to 35ºN),
- Polar Northern Hemisphere (>35ºN)

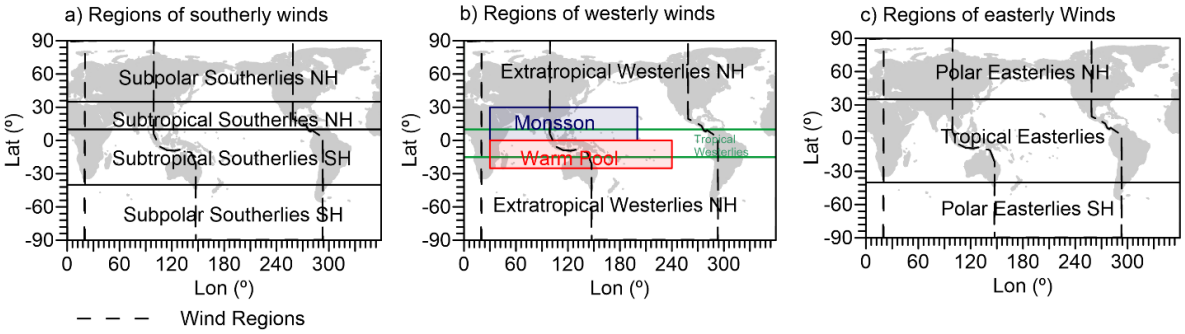


Figure 2. 4 Regional classification of the planetary wind systems.

Figure 2.5 shows how the major wave climates can be further decomposed by isolating regions by groups of cells that we refer to as WCTs. The WCTs are identified by groups of cells that are surrounded by NaN values. In particular, the extratropical westerly wave climate in the Southern Ocean only has one isolated region. However, for practical analysis, this belt was divided into three areas; the South Indian (20ºE; 147ºE), South Pacific (147 ºE; 67ºW), and South Atlantic (67ºW; 20 ºE) Oceans.

The WCTs are independent wave climates that are generated by basin-scale wind systems and propagate outwards from the generation zone. So, if the spatial area and directional range of a WCT is shared by a wind system, the WCT will be generated by the paired wind system. If the WCT has no obvious wind system pairing, the origin of the WCT is considered as swell with an undefined wind system origin.

The location of the mass centre of the wind system was calculated (Equations in 2.11), using only the cells that coincided with the WCT, see Figure 2.5b.

$$MC_{Lat} = \frac{1}{U_{10T}} \sum_{i=1}^{n} U_{10i} Lat_i \; ; \; MC_{Lon} = \frac{1}{U_{10T}} \sum_{i=1}^{n} U_{10i} Lon_i$$

(2. 11)

Where $U_{10T}$ is the total surface wind velocity, and *Lon* and *Lat* are the corresponding positions for each $U_{10}$. The resulting mass centre of the wind, ($MC_{Lat}$ and $MC_{Lon}$) was linked to the wind regions (Figure 2.5 c), with this being the atmospheric origin of the WCTs. To validate this step, the wind sea-wave power of the wave climates was calculated and the correlation and covariance matrices between $U_{10,}$ and wind sea-wave power was obtained.

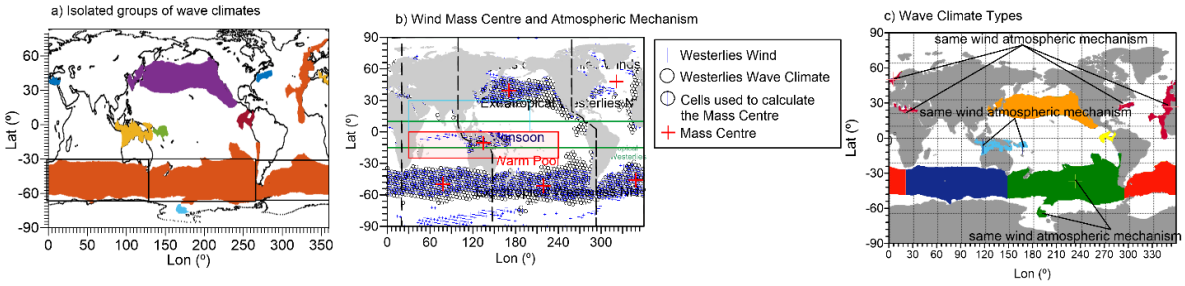


Figure 2. 5 Example of the process used to identify westerly wave climate types in January, 1979; a) identification of the isolated groups of wave climates; b) mass centre of the wind with the wind-grid that coincides with the wave-grid; c) the isolated wave climate groups that are generated by the same basin-scale wind are considered to belong the same wave climate type.

In the months: Feb-1983, Feb-1986, Jan-1992, Feb-1998, and Nov-2016, the westerly wave climate extended its cover of the Pacific Ocean. In these months, the identification of WCTs was made using the wind regionalization method, instead of isolating regions.

To validate that the wave climates are driven by planetary wind systems, the wind sea wave power and wind velocity pertaining to each WCT were correlated. The covariance was also computed, using standardized values. In addition, the SLP average yearly, DJF seasonal average, and JJA seasonal average, as well as the three main components of SLP that result from applying Empirical Orthogonal Functions (EOFs) after de-trending SLP monthly data were computed. The EOFs, also called Principal Components Analysis (PAC), consists of finding the eigenvectors, which contribute to the maximum variance of the data (mean square value) and are used to depict spatial-time temporal variability patterns. The PAC method uses the Singular Decomposition Values (SDV) approach that rotates the axes of the coordinate system of the original variables to new orthogonal axes, so that these axes coincide with the direction of the maximum variance of the data. SDV solves the classic Eigen function, where A is the data matrix, $\lambda$ are the eigenvalues, x is the eigenvector, and I the identity matrix.

$$A \cdot x = \lambda \cdot x; [A - \lambda I] \cdot x = 0$$

(2. 12)

The first eigenvector preserves most of the variance of the data, the second eigenvector maintains the largest remaining variance, and so on. If we have correlated quantitative variables, that means the data contains redundant information. The method reduces the variable to transformed variables (principal components) that explain a large part of most of the variability in the data.

## 2.4 Methods to address Objective 3 (Chapter 4)

### 2.4.1 Wave climate type parameters: an analysis in time

The main disadvantage of the "dynamic clustering" method is that the total time-series of 408 measurements (34 years (1985-2018) x 12 months) was subdivided into several time-series, one for each WCT. This generates a non-homogenous space-time data matrix, and makes any post-analysis of the wave climate types difficult. We tried to avoid the heterogeneity by using the WCTs as categorical variables, but that did not work for all the space cells, as some WCTs are identified very few times. To solve this, we created spatially-averaged characteristics of the WCT that extend the

length of the time series, although the spatial information was filtered. The time series of the total area, the spatially-averaged wave direction, and the mean wave power (2.13) of the WCTs were obtained.

$$Dir_m(t) = \frac{1}{N_t}\sum_{i=1}^{n} Dir_{mi,t}\ ;\ Pw_m(t) = \frac{1}{N_t}\sum_{i=1}^{n} Pw_{mi,t}\ ;\ A_T(t) = \sum_{i=1}^{n} A_{i,t}$$

(2. 13)

Where $Dir_{mi,t}, Pw_{mi,t}, A_{i,t}$ are the mean direction, wave power, and the area of each cell at a time step $t$. $N_t$ are the number of cells of each WCT at time step *t*.

#### 2.4.1.1 Natural variability

The time series of the spatial average of $P_w$ and $Dir_m$ were de-trended and then the monthly anomalies ($A_{i,j} = x_{i,j} - \mu_j;\ j = 1,2,\dots,12$) were computed as the value ($x_{i,j}$) of the year *i* and month *j*, minus the average of the corresponding month $\mu_j$ for all the years.

Subsequently, the composite anomalies were calculated for periods of ENSO, ENSO-PDO coupling, and ENSO-SAM coupling over the satellite era (1985-2018) (Ribal & Young, 2019), and only those that were statistically significant were considered. ENSO phases were identified using the ONI (Oceanic Niño Index), and PDO phases with the PDO index of NOAA. The SAM phases were calculated using the monthly AAO index, (where positive SAM >$\mu+\sigma$; and negative SAM <$\mu-\sigma$), following the indications of (Godoi & Torres Júnior, 2020; Marshall et al., 2018). The statistical significance of the composite anomalies was calculated using a two-tailed Student's t test with the null hypothesis of no difference in means ($\mu_1 = \mu_2$) and the alternative hypothesis of $\mu_1 \neq \mu_2$ at the 95% confidence level, where the population is the whole time series and the sample is the time series of the composited period. The degree of freedom was the number of samples, minus one.

#### 2.4.1.2 Long-term trends and global warming

The long-term trends of the spatially-averaged $P_{wm}$ and $Dir_m$ of the WCTs were calculated using the Least Squares approach, for the same period as the natural variability (1985 to 2018).The Mann-Kendall (Hirsch et al., 1982) approach was used, at the 95% level of confidence, to calculate the significance of the trends.

In order to address the underlying mechanisms responsible for these trends, we also calculated trends for the spatially averaged velocity of near surface wind ($U_{10}$) systems and the SST for the same areas occupied by each WCT over the same period. The same spatial distribution of SST as that of the WCTs was created by interpolating the SST grid. A spatial average of the SST grid was computed, giving a time series of SSTs for the cells occupied by each WCT. We assume that any long-term trends in wave power and direction of the WCTs that is concurrent with trends in SSTs or surface winds in the same climate region, have a causal relationship.

#### 2.4.1.3 Ocean wave teleconnections

The total area, $A_T$, and spatial-averages of $Dir_m$, and $P_{wm}$ of each WCT were correlated with those of every other WCT to quantify their interconnection, using the Pearson correlation coefficient (Kendall, 1948) with a level of confidence of 95%. In equation 2.14, $\bar{x}$ and $s_x$ are the mean and standard deviations of the variable of one WCT *X*, and $\bar{y}$ and $s_y$ of the same variable of another WCT *Y*:

$$R(X,\mathrm{Y}) = \frac{1}{N-1}\sum_{i=1}^{N}\overline{\left(\frac{X_i - \bar{\mathrm{x}}}{s_X}\right)\left(\frac{Y_i - \bar{\mathrm{y}}}{s_Y}\right)}$$

(2. 14)

## 2.5 Methods to address Objective 5 (Chapter 6)

In this chapter, the tropics on the Earth's surface are identified to analyse the impacts of their expansion on the near surface winds and waves. Some authors have defined the limits of the tropics as the latitude where the sign of the direction of the surface zonal wind changes. We use a similar criterion, but, instead of zonal wind, take the wind classification presented in Objective 2 (Chapter 4). Thus, the tropical limits were identified as the highest latitudes of the trade wind systems. The annual and seasonal linear trends of the tropical limits were calculated for each longitudinal cell. Only those that were statistically significant at 95 % confidence level by the Mandal Kendall approach were considered.

Then, five Expanding Tropics indices (ETIs) were calculated to analyse the potential impacts of the phenomenon in the wave parameters. The ETIs were computed as follows: the spatially averaged latitude anomalies of the tropical limits in regions N1 (180ºE; 110ºW) N2 (50ºW; 20ºW), S1 (60 ºE; 90 ºE), S2 (170 ºE; 135ºW), and S3 (100ºW; 80ºW) were obtained. These regions were selected because they have a high correlation with the WCTs characteristics and show expansion, seasonally, and yearly, as will be explained in detail in Chapter 5.

$$\mathrm{LATA}_{ij} = LAT_{ij} - \overline{LAT_{ij}}$$

(2. 15)

Next, a 3-month moving average was applied.

$$eti_i = \frac{1}{3}\sum_{n=i-1}^{n=i+1}\mathrm{LATA}_n$$

(2. 16)

Then, the index was computed by standardizing the results assuming a t-Student distribution. NaN values were not considered in the processes.

$$ETI = \frac{eti - \overline{eti}}{S}$$

(2. 17)

The correlation coefficients, using the Pearson correlation approach, were computed between these ETIs and the wave power and mean wave direction.

## 2.6 Methods to address Objective 5 (Chapter 6)

The wave climates were examined for the next century, using the scenarios of RCP 2.6 and 8.5. The RCP 2.6 maintains the current levels of $CO_2$, up to ~1°C, while the second scenario is the most conservative, ~ 4.3°C by 2100. The wave climate projection (Shimura & Mori, 2020), forced by atmospheric conditions (wind and ice cover), from the Japanese Meteorological Research Institute-Atmospheric General Circulation Model (MRI-AGCM) was used. The wave climate was modelled with the spectral wave model WaveWatch III version 5 (Tolman et al., 2014) with a 0.5º spatial and

hourly temporal resolution. The time range is 25 years, from 1979 to 2003, for the historical conditions, and from 2075 to 2099 for the RCP2.6 and RCP8.5 scenarios.

The same method of dynamic clustering, explained in Objective 2, was applied for present conditions (1979-2003). For the two scenarios of climate change, RCP2.6 and RCP8.5, the method was the same, but the centroids to cluster the data were predetermined, as those obtained for the present conditions, see Figure 2. 6. Then, the results of the projections were grouped according to the present conditions; resulting in the same clusters. Thus, the results are not different climates, but are their projected characteristics.

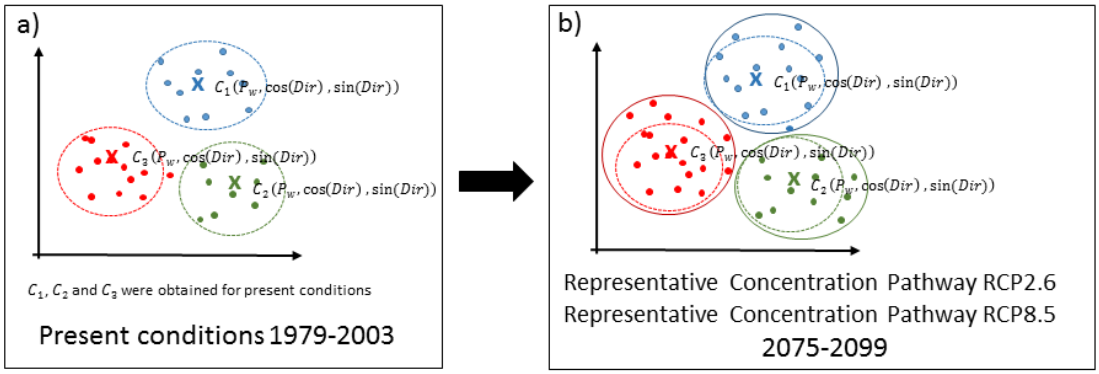


Figure 2. 6 Conceptual explanation of the method applied for a) present conditions, and b) projected scenarios using the centroids calculated in (a).

## 2.7 Methods to address Objective 6 (Chapter 7)

The chapter aims to identify the wave climate patterns, a driver of coastal hazards, around the world. The three atlases of coastal wave climate was produced by applying the "statistic clustering" *k-means* technique. The results show coastal regions with similar wave climate patterns. For each atlas the input matrix was different, defined below.

For ENSO atlas the matrix consists of normalized Pearson correlation coefficients between MEI climate index and wave power ($R_{lag0}$ (MEI- $P_W$)), and mean wave direction ($R_{lag0}$ (MEI-$Dir_m$)) for each spatial cell of all coasts worldwide.

$$\begin{pmatrix} R_{Pw_{\mathrm{n1}}} & R_{Dirm_{\mathrm{n1}}} \\ R_{Pw_{\mathrm{n2}}} & R_{Dirm_{\mathrm{n2}}} \\ \vdots & \vdots \\ R_{Pw_{\mathrm{ni}}} & R_{Dirm_{\mathrm{ni}}} \end{pmatrix} \rightarrow \begin{pmatrix} id_1 \\ id_2 \\ \vdots \\ id_i \end{pmatrix}$$

(2. 18)

For the prevailing wave climates atlas, the input matrix was formulated as the annual, DJF, JJA, SON and MAM seasonal average of wave frequency, wave power, and mean wave direction of each WCT. See the configuration in equation (2. 19).

$$\begin{pmatrix} PC_{n_{1,k,0}} & PC_{n_{1,k,1}} & \dots & PC_{n_{1,k,4}} & P_{wn_{1,k,0}} & P_{wn_{1,k,1}} & \dots & P_{wn_{1,k,4}} & Dir_{mn_{1,k,0}} & Dir_{mn_{1,k,1}} & \dots & Dir_{mn_{1,k,4}} \\ PC_{n_{2,k,0}} & PC_{n_{2,k,1}} & \dots & PC_{n_{2,k,4}} & P_{wn_{2,k,0}} & P_{wn_{2,k,1}} & \dots & P_{wn_{2,k,4}} & Dir_{mn_{2,k,0}} & Dir_{mn_{2,k,1}} & \dots & Dir_{mn_{2,k,4}} \\ \vdots & \vdots & \ddots & \vdots & \vdots & \vdots & \ddots & \vdots & \vdots & \vdots & \ddots & \vdots \\ PC_{n_{i,k,0}} & PC_{n_{i,k,1}} & \dots & PC_{n_{i,k,4}} & P_{wn_{i,k,0}} & P_{wn_{i,k,1}} & \dots & P_{wn_{i,k,4}} & Dir_{mn_{i,k,0}} & Dir_{mn_{i,k,1}} & \dots & Dir_{mn_{i,k,4}} \end{pmatrix} \rightarrow \begin{pmatrix} id_1 \\ id_2 \\ \vdots \\ id_i \end{pmatrix}$$

(2. 19)

Where sub-index *n* are the standardized variables, *i* corresponds to the cell number, the sub-index *k* is the WCT (1=subtropical, 2=subpolar; 3=Extratropical, 4= warm pool; 5=Monsoon, 6=Tropical and 7 =Polar), and *j* indicates the season (0=year, 1=DJF, 2=MAM, 3=JJA, 4= SON). $id$ is the cluster to which each cell belongs.

## 2.8 Methods to address Objective 7 (Chapter 8)

In Chapter 8, the results obtained in the previous objectives are highlighted for the coast of Mexico. A resulting wave climate atlas is then presented, which includes sea state analysis, seasonal variability, long-term variability, the wave climate types, and the wave climate projections. The results offer a robust basis to analyse coastal hazards and from this, coastal risk and climate change adaptation.

### References

Barnard, P. L., Short, A. D., Harley, M. D., Splinter, K. D., Vitousek, S., Turner, I. L., et al. (2015). Coastal vulnerability across the Pacific dominated by El Niño/Southern Oscillation. *Nature Geoscience*, *8*, 801. Retrieved from https://doi.org/10.1038/ngeo2539

Barnard, P. L., Hoover, D., Hubbard, D. M., Snyder, A., Ludka, B. C., Allan, J., et al. (2017). Extreme oceanographic forcing and coastal response due to the 2015–2016 El Niño. *Nature Communications*, *8*, 14365. Retrieved from https://doi.org/10.1038/ncomms14365

Berkhin, P. (2006). A Survey of Clustering Data Mining Techniques BT - Grouping Multidimensional Data: Recent Advances in Clustering. In J. Kogan, C. Nicholas, & M. Teboulle (Eds.) (pp. 25–71). Berlin, Heidelberg: Springer Berlin Heidelberg. https://doi.org/10.1007/3-540-28349-8_2

Delpey, M. T., Ardhuin, F., Collard, F., & Chapron, B. (2010). Space - time structure of long ocean swell fields, *115*(May), 1–13. https://doi.org/10.1029/2009JC005885

Gavrikov, A. V, Krinitsky, M. A., & Grigorieva, V. G. (2016). Modification of Globwave satellite altimetry database for sea wave field diagnostics. *Oceanology*, *56*(2), 301–306. https://doi.org/10.1134/S0001437016020065

Guenther, H., Hasselmann, S., & Janssen, P. A. E. M. (1992). *The WAM model cycle 4*. Germany. Retrieved from http://inis.iaea.org/search/search.aspx?orig_q=RN:26000788

Hanson, J. L., & Phillips, O. M. (2001). Automated Analysis of Ocean Surface Directional Wave Spectra. *Journal of Atmospheric and Oceanic Technology*, *18*, 277–294.

Hersbach, H., Bell, B., Berrisford, P., Hirahara, S., Horányi, A., Muñoz-Sabater, J., et al. (2020). The ERA5 global reanalysis. *Quarterly Journal of the Royal Meteorological Society*, *146*(730), 1999–2049. https://doi.org/https://doi.org/10.1002/qj.3803

Hirsch, R. M., Slack, J. R., & Smith, R. A. (1982). Techniques of trend analysis for monthly water quality data. *Water Resources Research*, *18*(1), 107–121. https://doi.org/10.1029/WR018i001p00107

Jiang, H. (2019). Spatially Tracking Wave Events in Partitioned Numerical Wave Model Outputs. *Journal of Atmospheric and Oceanic Technology*, *36*(10), 1933–1944. https://doi.org/10.1175/JTECH-D-18-0228.1

Kaufman, L., & Rousseeuw, P. J. (1990). Finding Groups in Data: An Introduction to Cluster Analysis. John Wiley.

Kendall, M. G. (1948). *Rank correlation methods. Rank correlation methods.* Oxford, England: Griffin.

KETCHEN, D. J., & SHOOK, C. L. (1996). THE APPLICATION OF CLUSTER ANALYSIS IN STRATEGIC MANAGEMENT RESEARCH: AN ANALYSIS AND CRITIQUE. *Strategic Management Journal*, *17*(6), 441–458. https://doi.org/https://doi.org/10.1002/(SICI)1097-0266(199606)17:6<441::AID-SMJ819>3.0.CO;2-G

MacQueen, J. (1967). Some methods for classification and analysis of multivariate observations. In *Proceedings of the Fifth Berkeley Symposium on Mathematical Statistics and Probability, Volume 1: Statistics* (pp. 281–297). Berkeley, Calif.: University of California Press. Retrieved from https://projecteuclid.org/euclid.bsmsp/1200512992

Neill, S. P., & Hashemi, M. R. (2018). Chapter 5 - Wave Energy. In S. P. Neill & M. R. B. T.-F. of O. R. E. Hashemi (Eds.), *E-Business Solutions* (pp. 107–140). Academic Press. https://doi.org/https://doi.org/10.1016/B978-0-12-810448-4.00005-7

Reguero, B G, Losada, I. J., & Méndez, F. J. (2015). A global wave power resource and its seasonal, interannual and long-term variability. *Applied Energy*, *148*, 366–380. https://doi.org/https://doi.org/10.1016/j.apenergy.2015.03.114

Reguero, Borja G., Losada, I. J., & Méndez, F. J. (2019). A recent increase in global wave power as a consequence of oceanic warming. *Nature Communications*, *10*(1), 1–14. https://doi.org/10.1038/s41467-018-08066-0

Ribal, A., & Young, I. R. (2019). 33 years of globally calibrated wave height and wind speed data based on altimeter observations. *Scientific Data*, *6*(1), 77. https://doi.org/10.1038/s41597-019-0083-9

Saha, S., Moorthi, S., Pan, H.-L., Wu, X., Wang, J., Nadiga, S., et al. (2010). NCEP Climate Forecast System Reanalysis (CFSR) Selected Hourly Time-Series Products, January 1979 to December 2010. Boulder, CO: Research Data Archive at the National Center for Atmospheric Research, Computational and Information Systems Laboratory. https://doi.org/10.5065/D6513W89

Saha, S., Moorthi, S., Wu, X., Wang, J., Nadiga, S., Tripp, P., et al. (2011). NCEP Climate Forecast System Version 2 (CFSv2) 6-hourly Products. Boulder, CO: Research Data Archive at the National Center for Atmospheric Research, Computational and Information Systems Laboratory. https://doi.org/10.5065/D61C1TXF

Shimura, T., & Mori, N. (2019). High-resolution wave climate hindcast around Japan and its spectral representation. *Coastal Engineering*, *151*, 1–9. https://doi.org/https://doi.org/10.1016/j.coastaleng.2019.04.013

Shimura, T., & Mori, N. (2020). FUTURE CHANGES IN SPECTRAL WAVE CLIMATE AROUND JAPAN UNDER GLOBAL WARMING. *Coastal Engineering Proceedings*, (36v SE-Waves). https://doi.org/10.9753/icce.v36v.waves.10

Shimura, T., Mori, N., & Mase, H. (2013). Ocean waves and teleconnection patterns in the northern hemisphere. *Journal of Climate*, *26*(21), 8654–8670. https://doi.org/10.1175/JCLI-D-12-00397.1

Stopa, J. E., & Cheung, K. F. (2014). Periodicity and patterns of ocean wind and wave climate. *Journal of Geophysical Research: Oceans*, *119*(8), 5563–5584. https://doi.org/10.1002/2013JC009729

Trenberth, K. E., & Hoar, T. J. (1997). El Niño and climate change. *Geophysical Research Letters*, *24*(23), 3057–3060. https://doi.org/10.1029/97GL03092

Webb, A., & Fox-Kemper, B. (2011). Wave spectral moments and Stokes drift estimation. *Ocean Modelling*, *40*(3), 273–288. https://doi.org/https://doi.org/10.1016/j.ocemod.2011.08.007

# CHAPTER 3

## El Niño-Southern Oscillation, a Wave Climate Driver

This chapter analysed the impacts of ENSO on wave power and mean wave direction. The supporting information is given in APPENDIX A1.

This chapter is based on

Odériz, I., Silva, R., Mortlock, T.R., & Mori, N. (2020). ENSO Impacts on global wave climate and Potential coastal hazards. *Journal of Geophysical Research: Oceans*, 125, e2020JC016464. https://doi.org/10.1029/2020JC016464

## 3.1 Introduction

At a global scale, many studies have been carried out to identify the wave parameters response to ENSO (Semedo *et al.,* 2010; Stopa and Cheung, 2014; Reguero *et al.,* 2015, 2019; Mori *et al.,* 2018). Although these contributions have reinforced the knowledge, more data is needed on ENSO coastal morphological hazards, particularly for data-poor locations. In particular, the mean wave directional response to ENSO, (Barnard *et al.,* 2015; Morim *et al.,* 2019; Ranasinghe, 2016; Toimil *et al.,* 2020), still remains undocumented on a global scale. Therefore, this chapter aims to quantify ENSO effects on global wave direction and wave power. In this section interannual variability of the wave climate characteristics induced by ENSO is analysed. The potential differences that may exist between individual events are also highlighted.

## 3.2 Validation of ERA5 seasonal to interannual variability

Prior to address this analysis, we validate the interannual variability performance of ERA5 in wave heights against global altimetry measurements (GlobWave). In general, significant wave heights from ERA5 are negatively biased for seasonal variability when compared to the altimetry dataset Globwave (see Appendix A1). Occasionally, ERA 5 is positive biased on the western coasts of the Atlantic and Pacific basins, these areas generally affected by larger swells originated in the Southern Ocean. The Asian Monsoon region also presented a positive bias. In regard to interannual variability, ERA5 showed a good performance compared to altimetry data (see the R-maps in Appendix A1 and the R-bias in Figure 3. 1). Results show low values of bias (±0.2).

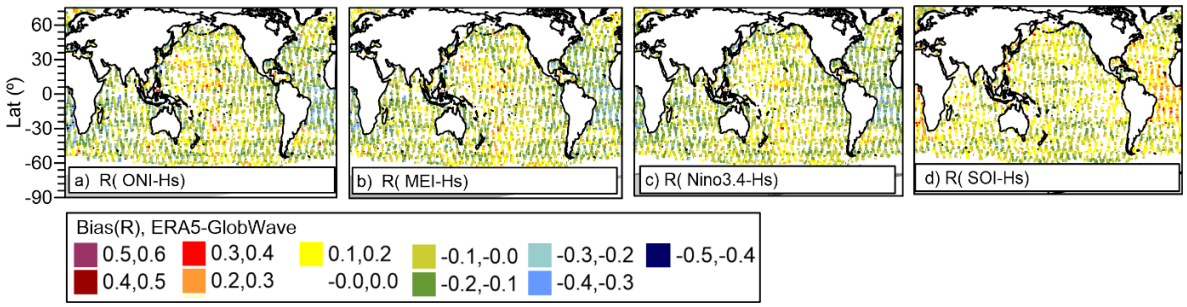


Figure 3. 1. Bias of correlation coefficients (calculated sequentially between ENSO climate indices and ERA-5 derived $H_s$, and same again for GlobWave $H_s$) from 1992 to 2013. a) ONI, b) MEI, c) Nino 34, and d) SOI.

## 3.3 ENSO as a wave climate driver

### 3.1.1 ENSO climate indices

There is no specific climate index that is best to analyse ENSO impacts. It depends on the region and the variable studied. In this section, we analyse which ENSO index is best for an analysis of global wave power and direction. For this, the statistical significance of correlation coefficients (Figure 3. 2) between $P_w$ and $Dir_m$ and each climate index, were calculated for all the ocean basins. The climate index with the most statistically significant points will be that covers the ENSO phenomenon spatially best over the global scale.

Each climate index is computed with different oceanographic and atmospheric parameters of different regions. The SOI uses the SLP for part of the southern hemisphere show the poorest result globally. Meanwhile, the ONI, MEI, and Niño 3.4, which are calculated with parameters of the tropical Pacific shows better results. Although, the ONI and Niño 3.4 use the same SST database, the

first is computed using a 3 moving average approach of the anomalies of SST, and the second uses the monthly average. The differences between both indexes for the *Pw* and $Dir_m$ might be associated with the delay in ENSO impact in the *Pw* (>1 month to see ENSO impacts in the *Pw*), while the $Dir_m$ response to ENSO is immediate. For instance, the climate index Niño 3.4 is highly correlated with the wave direction, Figure 3. 2h). However, correlation between wave power and Niño 3.4 is the second-worst performer of all indices. Instead, ONI or MEI perform better in wave power, Figure 3. 2 e, g). This suggests that the wave power response to ENSO may be lagged in accordance with monthly-average used by the MEI and ONI.

The spatial response to ENSO is different for the two variables wave power and mean wave direction. $P_w$ responds more to ENSO than $Dir_m$ globally. The Indian Ocean, in particular, is more affected by ENSO in the mean wave direction. While the Pacific is the ocean basin with the largest area of wave power response to ENSO, followed by the Indian Ocean, and then the Atlantic. In the Southern Ocean, the wave power is significantly correlated across the whole belt, but not wave direction. The common regions of statistical significance of R for all the ENSO climate indices are where the individual ENSO events impact similarly always (Figure 3. 2). Nevertheless, those regions where the statistical significance is not consistent for all the climate indices shows regions where the individual ENSO events impact differently from time to time. The difference in magnitude (see Appendix A1) shows that MEI reaches higher values globally distributed. However, Niño 3.4 shows higher values of R in the Monsoon area, while the wave power has the higher correlation values in the Southern Hemisphere, and SOI index were the highest in the East Indian Ocean.

Globally, no large differences in magnitude nor in spatial patterns were found between the climate indices. The climate index selected for this work was the MEI, because from a global perspective this index gives the best results for $P_w$, and the second best for $Dir_m$.

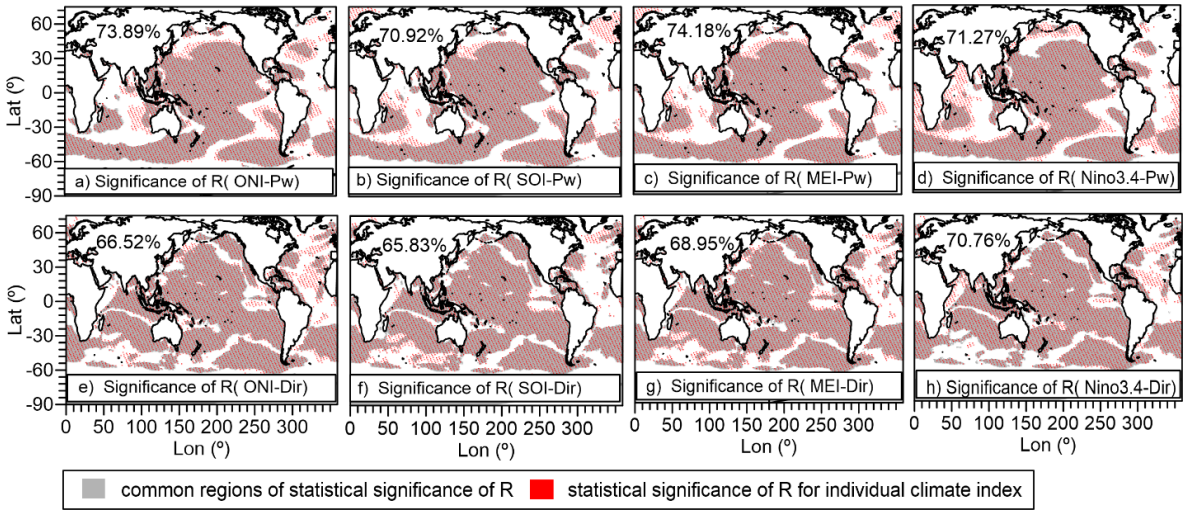


Figure 3. 2**.** Statistical significance of ENSO Climate Indices for wave power and mean wave direction. The top and bottom panels are $P_w$ and $D_{irm}$, respectively. The first column shows the SOI, the second the ONI, the third the Nino3.4, and the fourth the MEI. The red dots mark significant correlation points and the values are the percentage of statistically significant spatial cells worldwide.

### 3.1.2 Composite anomalies for ENSO phases

In this section we investigate the composite anomalies (1979-2018) of atmospheric and ocean configurations in ENSO phases (neutral, La Niña, and El Niño phase). In Chapter 2, section

2.2.2 the methods is described in detail. Figure 3. 3 describes the anomalies in SLP, $P_w$, and $Dir_m$ for El Niño and La Niña. In Appendix A1, anomalies are depicted for three extreme ENSO events: El Niño 1997-1998, La Niña 2010-2011 and El Niño 2015-2016.

The ENSO forms in the tropical Pacific. During El Niño events, the tropical Pacific shows positive anomalies in SLP in the west and negative anomalies in the east Pacific. El Niño weakens the trade winds, or even shifts their direction (Reiter, 1978), in contrast to the strengthening of wave power in this area (see Figure 3. 3, b). In the North Pacific, the winds shift clockwise, forced by positive anomalies of SLP over the northern subtropical Pacific (Wallace & Gutzler, 1981; H. Wang et al., 2012). Furthermore, El Niño events produce a deeper Aleutian Low (Figure 3. 3a) and extratropical wind and waves strengthen and shift anticlockwise in the Northwest Pacific coast (Figure 3. 3c). However, during the 2015-2016 event, wave fields rotated towards the south, caused by different SLP patterns during this event (Appendix A1). In the South Pacific, two blocking high pressure systems become quasi-stationary in this area (Fogt & Bromwich, 2006) that leads to a reduction and a rotation of the wave field northward around the Magellan Straits. In the rest of the Southern Ocean, the wave power increases during El Niño.

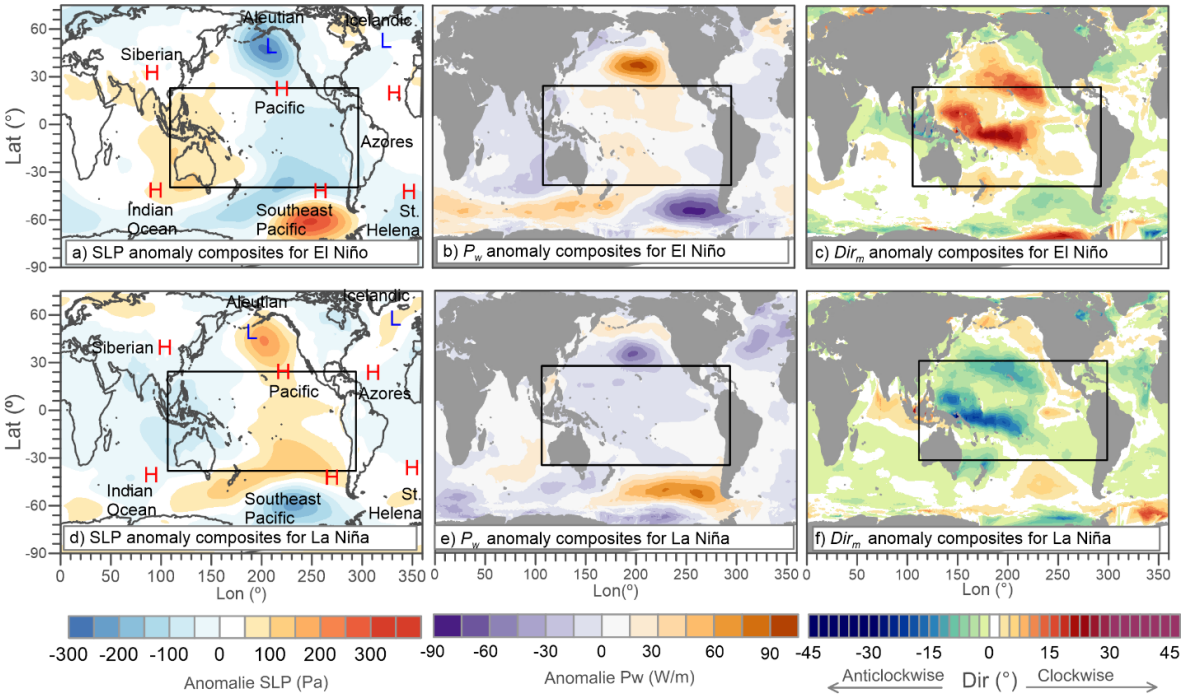


Figure 3. 3. SLP (a, d), $P_w$ (b, e) and $Dir_m$ (c, f) composite anomalies for warm and cold phases of ENSO. Top panels (a, b, c), correspond to El Niño and bottom panels to La Niña. H and L in the SLP panels indicate high and low pressure systems.

Wave response were found different between 2015-2016 and 1997-1998 El Niño events (Barnard et al., 2017). During the 2015-2016 event, an increase in wave power was experienced in the North Pacific, while the South Pacific showed larger positive anomalies in wave power during the 1997-1998 event. In the Indian Ocean, during El Niño, the strong positive anomalies that occur over the Philippine Sea (East Pacific) weaken the wave power. In the North Atlantic, the Icelandic Low intensifies (Moron & Gouirand, 2003), which increases wave power and rotates the wave field clockwise. In general, La Niña events tend to be weaker than El Niño and are more similar between

each other (Timmermann *et al.,* 2018). During La Niña, the SLP anomalies patterns are inverted with respect to EL Niño events (Wang et al., 2000) (Figure 3. 3d), and the wave power increases in the East Indian Ocean, the Northwest Pacific, the Northwest Atlantic, and part of the Southern Ocean, and decrease in the rest of the oceans. It was found that wave fields turn clockwise in the Northeast Indian Ocean during this cold phases.

### 3.1.3 ENSO as a driver of wave climate: general patterns

In an effort to generalise wave patterns response, the Correlation coefficients between the MEI and the residuals time series of $P_w$ and $Dir_m$ were calculated (Figure 3. 4). See section 2.2.2 in Chapter 2 for more detailed description of the methods. During warm phases of ENSO, wave power in the Southern Ocean intensified and the waves were more northerly, with the exception of the Southeast Pacific, due to the blocking pressure in this area, as mentioned earlier. The Hadley Cell contracted and strengthened and westerlies intensified and shifted poleward in both hemispheres (Lu *et al.,* 2008; Reichler, 2009). However, the wave power increased in the central Pacific ($R$~0.4). Thus suggests that this increment was due to the swell radiated from the extratropical belts to the tropical regions. During El Niño, it is known that the monsoon winds are weaken (Wang *et al.,* 2000; Zhang *et al.,* 2016), and here we detected that the wave energy reduced.

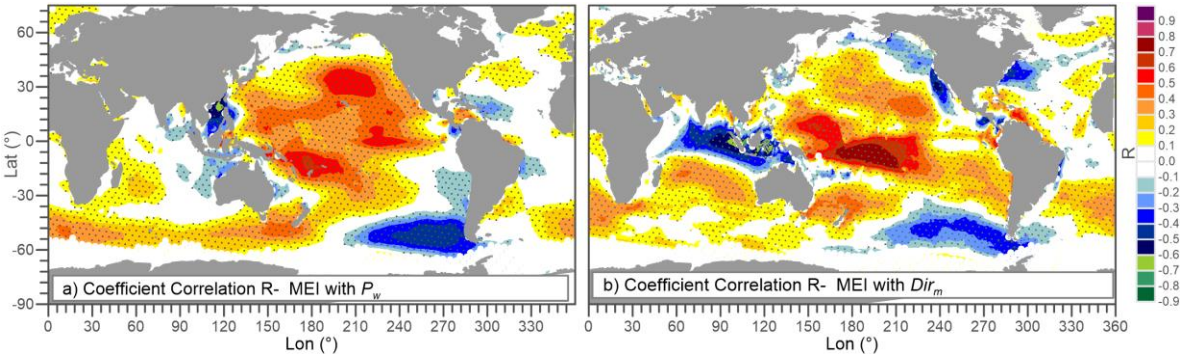


Figure 3. 4. Correlation coefficients of MEI and; a) wave power; b) mean wave direction. The black dots mark significant correlation points at a significance level of 95%.

Overall, in ENSO events the mean wave direction followed a well-defined spatial pattern. It was positively correlated in the north and in the subtropics of the Indian Ocean, ($R$~ 0.3), southern subtropics of all the basins, and tropics of the Pacific ($R$ from 0.3 to 0.7) and the Atlantic ($R$~ 0.2). At the same time, in the tropical Indian Ocean, tropical Pacific, and North Atlantic, $R$ acquired negative values in the North Pacific (central and east), ($R$~ -0.3), and northern extratropics of the Atlantic ($R$~ -0.25). The extratropics and subtropics were positively correlated ($R$~0.15) in the Atlantic. This was a response to the poleward movement of the subtropical jets during El Niño (Reichler, 2009). Stronger correlations were seen in the Caribbean Sea ($R$~0.4).

The effects of ENSO varied temporally, as it was shown in the lagged cross-correlation analysis. For wave power, in the Pacific basin and the Southern Ocean region of Australia, the effects were almost immediate (highest $R$ values within 0 to 3 months). In contrast, in the Atlantic, the wave power response was lagged by up to 12 months. The mean wave direction responded earlier than wave power. In Appendix A1 the maximum values of R within a given 12 month period are shown. In general, the extratropics of all ocean basins were the most influenced by the ENSO signal in wave power, while the direction response was most significant in the Northern Hadley Cell and Subtropical Ridge regions of the North Pacific.

## 3.4 Conclusions

From the findings, general patterns of ENSO can be seen that force a latitudinal response in wave climate forced by anomalies identified in the atmospheric circulation. However, not all ENSO events produced the same anomalies in SLP, or in $P_w$ and $Dir_m$, and the coastal hazards can be expected to vary on an event-by-event, depending on the ENSO characteristics, such as was the case for the 1997-1998 and 2015-2016 El Niño events. The results explained global patterns of interannual variability of wave direction and wave power driven by ENSO, as one of the primary climate-related driver of coastal vulnerability (Barnard *et al.,* 2015; Morim *et al.,* 2019). In the analysis of global direction and wave power, all ENSO climate index performance similarly. In this study, the MEI was selected as the most appropriate climate index to analyse wave direction (the second best) and wave power (the best) at the global scale.

The results showed a general global ENSO wave climate pattern. In particular, during El Niño, wave power increased in the extratropics of both hemispheres for the three ocean basins, in response to the strength of the extratropical winds (Timmermann *et al.,* 2018). In the tropics, the intensification of wave power was caused by the swell propagated from the extratropics. This is consistent with the strengthening of the subtropical jets in both hemispheres during El Niño (Lu *et al.,* 2008; Reichler, 2009). The Indian Monsoon and the Warm Pool showed a decrease in wave power during ENSO warm phases. The direction showed a latitudinal variation; in the southern subtropics this turned clockwise, while in the extratropics, particularly in the northern hemisphere, coming southerly direction. Caused by the Aleutian Low strengthened and displaced northeast, producing more southerly winds at the land-sea boundary of North America. This is in line with the observations found by Lu *et al.,*(2008) and Reichler (2009), that the subtropical jets move poleward during El Niño events. The most immediate impacts of ENSO were found in the Pacific Ocean, followed by the Indian Ocean, while the effected delay 7-12 months to impact Atlantic Ocean. These findings are in agreement with the results of other authors (Reguero *et al.,* 2019; Semedo *et al.,* 2010; Shimura *et al.,* 2013; Stopa and Cheung, 2014) and are consistent with the theoretical mechanism of ENSO.

While there are general patterns of wave direction and wave power produced during ENSO events, the anomalies also highlighted dissimilarities in these parameters in different events, such as was the case for the 1997-1998 and 2015-2016 El Niño events, as noted by (Barnard *et al.,* 2017). These anomalies are relevant for individual events that can impact long-shore and cross-shore sediment transport. The estimation of particular ENSO characteristics impacts on wave climate needs more investigation, such as intensity, temporal evolution, or asymmetry. For example, the asymmetry of ENSO is related to the intensification of extratropical winds during El Niño events (Timmermann *et al.,* 2018). A more accurate prediction of the wave climate impacts under different ENSO characteristics may lead to a reduction in the uncertainties of ENSO-driven coastal hazards.

## References

Barnard, P. L., Short, A. D., Harley, M. D., Splinter, K. D., Vitousek, S., Turner, I. L., et al. (2015a). Coastal vulnerability across the Pacific dominated by El Niño/Southern Oscillation. *Nature Geoscience*, *8*, 801. Retrieved from https://doi.org/10.1038/ngeo2539

Barnard, P. L., Short, A. D., Harley, M. D., Splinter, K. D., Vitousek, S., Turner, I. L., et al. (2015b). Coastal vulnerability across the Pacific dominated by El Niño/Southern Oscillation. *Nature Geoscience*, *8*(10), 801–807. https://doi.org/10.1038/ngeo2539

Barnard, P. L., Hoover, D., Hubbard, D. M., Snyder, A., Ludka, B. C., Allan, J., et al. (2017). Extreme oceanographic forcing and coastal response due to the 2015–2016 El Niño. *Nature Communications*, *8*,

14365. Retrieved from https://doi.org/10.1038/ncomms14365

Fogt, R. L., & Bromwich, D. H. (2006). Decadal Variability of the ENSO Teleconnection to the High-Latitude South Pacific Governed by Coupling with the Southern Annular Mode. *Journal of Climate*, *19*(6), 979–997. https://doi.org/10.1175/JCLI3671.1

Lu, J., Chen, G., & Frierson, D. M. W. (2008). Response of the Zonal Mean Atmospheric Circulation to El Niño versus Global Warming. *Journal of Climate*, *21*(22), 5835–5851. https://doi.org/10.1175/2008JCLI2200.1

Mori, N., Kishimoto, R., & Shimura, T. (2018). WAVE CLIMATE VARIABILITY AND RELATED CLIMATE INDICES. *Coastal Engineering Proceedings*, *1*(36), 75. https://doi.org/10.9753/icce.v36.risk.75

Morim, J., Hemer, M., Wang, X. L., Cartwright, N., Trenham, C., Semedo, A., et al. (2019). Robustness and uncertainties in global multivariate wind-wave climate projections. *Nature Climate Change*, *9*(9), 711–718. https://doi.org/10.1038/s41558-019-0542-5

Moron, V., & Gouirand, I. (2003). Seasonal modulation of the El Niño–southern oscillation relationship with sea level pressure anomalies over the North Atlantic in October–March 1873–1996. *International Journal of Climatology*, *23*(2), 143–155. https://doi.org/10.1002/joc.868

Ranasinghe, R. (2016). Assessing climate change impacts on open sandy coasts: A review. *Earth-Science Reviews*, *160*, 320–332. https://doi.org/https://doi.org/10.1016/j.earscirev.2016.07.011

Reguero, B G, Losada, I. J., & Méndez, F. J. (2015). A global wave power resource and its seasonal, interannual and long-term variability. *Applied Energy*, *148*, 366–380. https://doi.org/https://doi.org/10.1016/j.apenergy.2015.03.114

Reguero, Borja G., Losada, I. J., & Méndez, F. J. (2019). A recent increase in global wave power as a consequence of oceanic warming. *Nature Communications*, *10*(1), 1–14. https://doi.org/10.1038/s41467-018-08066-0

Reichler, T. (2009). Chapter 7 - Changes in the Atmospheric Circulation as Indicator of Climate Change. In T. M. B. T.-C. C. Letcher (Ed.) (pp. 145–164). Amsterdam: Elsevier. https://doi.org/https://doi.org/10.1016/B978-0-444-53301-2.00007-5

Reiter, E. R. (1978). The Interannual Variability of the Ocean-Atmosphere System. *Journal of the Atmospheric Sciences*, *35*(3), 349–370. https://doi.org/10.1175/1520-0469(1978)035<0349:TIVOTO>2.0.CO;2

Semedo, A., Sušelj, K., Rutgersson, A., & Sterl, A. (2011). A Global View on the Wind Sea and Swell Climate and Variability from ERA-40. *Journal of Climate*, *24*(5), 1461–1479. https://doi.org/10.1175/2010JCLI3718.1

Shimura, T., Mori, N., & Mase, H. (2013). Ocean waves and teleconnection patterns in the northern hemisphere. *Journal of Climate*, *26*(21), 8654–8670. https://doi.org/10.1175/JCLI-D-12-00397.1

Stopa, J. E., & Cheung, K. F. (2014). Periodicity and patterns of ocean wind and wave climate. *Journal of Geophysical Research: Oceans*, *119*(8), 5563–5584. https://doi.org/10.1002/2013JC009729

Timmermann, A., An, S.-I., Kug, J.-S., Jin, F.-F., Cai, W., Capotondi, A., et al. (2018). El Niño–Southern Oscillation complexity. *Nature*, *559*(7715), 535–545. https://doi.org/10.1038/s41586-018-0252-6

Toimil, A., Camus, P., Losada, I. J., Le Cozannet, G., Nicholls, R. J., Idier, D., & Maspataud, A. (2020). Climate change-driven coastal erosion modelling in temperate sandy beaches: Methods and uncertainty treatment. *Earth-Science Reviews*, *202*, 103110. https://doi.org/https://doi.org/10.1016/j.earscirev.2020.103110

Wallace, J. M., & Gutzler, D. S. (1981). Teleconnections in the Geopotential Height Field during the Northern Hemisphere Winter. *Monthly Weather Review*, *109*(4), 784–812. https://doi.org/10.1175/1520-0493(1981)109<0784:TITGHF>2.0.CO;2

Wang, B., Wu, R., & Fu, X. (2000). Pacific–East Asian Teleconnection: How Does ENSO Affect East Asian Climate? *Journal of Climate*, *13*(9), 1517–1536. https://doi.org/10.1175/1520-

0442(2000)013<1517:PEATHD>2.0.CO;2

Wang, H., Kumar, A., Wang, W., & Xue, Y. (2012). Influence of ENSO on Pacific Decadal Variability: An Analysis Based on the NCEP Climate Forecast System. *Journal of Climate*, *25*(18), 6136–6151. https://doi.org/10.1175/JCLI-D-11-00573.1

Zhang, W., Jin, F.-F., Stuecker, M. F., Wittenberg, A. T., Timmermann, A., Ren, H.-L., et al. (2016). Unraveling El Niño's impact on the East Asian Monsoon and Yangtze River summer flooding. Geophysical Resear*ch Letters*, *43*(21), 11,311-375,382. https://doi.org/10.1002/2016GL071190

# CHAPTER 4

## Global Wave Climate Framework

This chapter analyzed the global wave climate types and studied signals of natural variability and global warming. The supporting information is given in APPENDIX A2.
This chapter is based on

Odériz, I., Silva, R., Mortlock, T. R., Mori, N., Shimura, T., Webb, A., Padilla-Hernández R., and Villers S. (2021). Natural Variability and Warming Signals in Global Ocean Wave Climates. *Geophysical Research Letters*, 48, e2021GL093622. https://doi.org/10.1029/2021GL093622

## 4.1 Introduction

In this chapter we classify the global wave climate into types that are intrinsically linked to the atmospheric circulation responsible for their genesis. Then, we evaluate the impact of each source, natural variability and global warming, on historical data. Moreover, we depict ocean-wave teleconnection patterns that connect the coasts with similar wave climate variability across the word. Then, the major wave climates are defined as regions with similar prevailing wave conditions, in homology to the major climate regions (e.g., tropical, temperate, polar, tundra).

For a better understanding of the methods it is recommended to read Chapter 2 of this document (section 2.3). To sum up, the planetary wind systems and wave climates classification are based on a dynamic clustering technique. The major wave climates are decomposed by isolating regions of groups of cells that we refer to as Wave Climate Types (WCTs). Once the WCTs were obtained in time and space, the time series of the total area covered $A_{T,t}$, and the spatially-averaged $Dir_{m,t}, Pw_{m,t}$, were calculated. With this parameter the net long-term trends and variation of each WCT over the last three decades (1985-2018) was examined. The natural variability of these parameters were analysed by computing the composite monthly anomalies of the periods of ENSO, ENSO-PDO, and ENSO-SAM coupling. The long-term trend was computed with least squares regression approach, and the teleconnection patterns with correlation coefficient between the parameter of WCTs.

## 4.2 Ocean wave climate types driven by atmospheric circulation

The results of the dynamic clustering show three major wave climates (Figure 4.4) and the planetary wind systems(Figure 4.3) (westerlies, southerlies, and easterlies). The westerly wave climate is defined as a high-energy system with wave directions from 209° to 352°. The southerly wave climate is defined as a moderate-energy system, which travels in a northward direction (between 135° and 216°). The easterly wave climate is defined as a low-energy system with directions between 6° and 138°. The direction follows the metereological convection. The westerly wave climates encompass the extratropical, monsoon, and warm pool WCTs. The Southerly wave climates include the subtropical and subpolar WCTs. While the easterly wave climates include the tropical and polar WCTs. The dynamic clustering of wave climate was validated with JRA-55 dataset. The centroids for both reanalysis datasets are similar (see Figure 4.1 and Table 4.2). Differences were found in wave power as JRA-55 (ERA5) has a positive (negative) bias in the significant wave height, compared with the altimetry data of GlobWave (see Appendix A1 ).

Table 4.1. Centroids of wind and ocean wave climates identified by dynamic clustering.

| | ERA 5- winds | | | ERA 5- ocean waves | | |
|---|---|---|---|---|---|---|
| Centroids of | $U_{10}$ (m/s) | cos(Dir$_{wnd}$) | sin(Dir$_{wnd}$) | P$_w$ (kW/m) | cos($Dir_m$) | sin($Dir_m$) |
| Southerlies | 5.32 | 0.94 | -0.06 | 26.63 | -0.93 | 0.03 |
| Westerlies | 7.57 | 0.49 | 0.79 | 59.30 | -0.28 | -0.89 |
| Easterlies | 6.20 | 0.25 | -0.87 | 17.502 | -0.09 | 0.88 |

Table 4.2. Centroids for each variable ($P_w$, sin ($Dir_m$), cos ($Dir_m$)), wave power, and mean direction for the westerly, easterly and southerly climate type for JRA-55 (1979-2017) and ERA5 (1979-2017).

| Centroid of | ERA 5 | | | JRA-55 | | |
|---|---|---|---|---|---|---|
| | $P_w$ (W/m) | cos($Dir_m$) | sin($Dir_m$) | $P_w$ (W/m) | cos($Dir_m$) | sin($Dir_m$) |
| Westerlies | 142.41 | -0.28 | -0.89 | 199.82 | -0.24 | -0.90 |
| Southerlies | 62.95 | -0.93 | 0.03 | 76.01 | -0.93 | -0.04 |
| Easterlies | 37.95 | -0.1 | 0.88 | 43.17 | -0.12 | 0.87 |

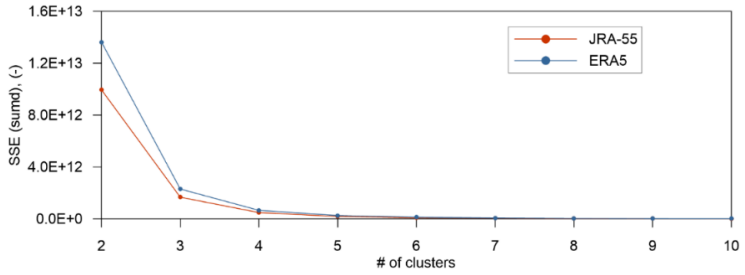


Figure 4.1.Elbow method applied for both reanalyses dataset, JRA-55 and ERA 5.

The response of WCT is forced by the atmospheric circulation, induced by the variation of the semi-permanent High and Low-pressure systems. These SLP belts are the ascent and descent branches of the atmospheric cell circulation (Polar, Ferrer, and Hadley). Figure 4.2 depicts the SLP average yearly, DJF, and JJA seasonally average, as well as the three main principal components of SLP that result from applying Empirical Orthogonal Functions after de-trending SLP monthly data. The SLP variation, shown in Figure 4.2, creates the well-known planetary wind systems variability. For example, the two modes (DJF and JJA) of the Icelandic Low and Aleutian Low induce higher or lower pressure gradients that impact the westerly and polar winds (Pickart *et al*., 2009; Dodet, Bertin and Taborda, 2010). In the DJF, these Low-pressure centres produce higher pressure gradients and stronger extratropical winds (Pickart *et al.*, 2009; Dodet, Bertin and Taborda, 2010). On the other hand, during JJA, the Icelandic and Pacific High anticyclones dominate the northern basins; leading to stronger subtropical and weaker extratropical winds and waves climate types. However, in the Southern Hemisphere, the high and low-pressure belt is fairly constant and there are westerly winds all year round. On the other hand, the Monsson winds are created when the Intertropical Convergence Zone (ITCZ) moves further north over the Asian continent (SANIL KUMAR *et al.*, 2012) (Figure 4.2c and f). Then, the variability of the polar and extratropical WCTs of the North Pacific and North Atlantic response to the strength and position of the Aleutian Low and the Icelandic Low. While variations in the tropical WCTs are induced by the trade winds. On the other hand, the subtropical WCTs are controlled by the position and strength of the subtropical ridges, whereas the subpolar WCTs are linked to the subpolar ridges.

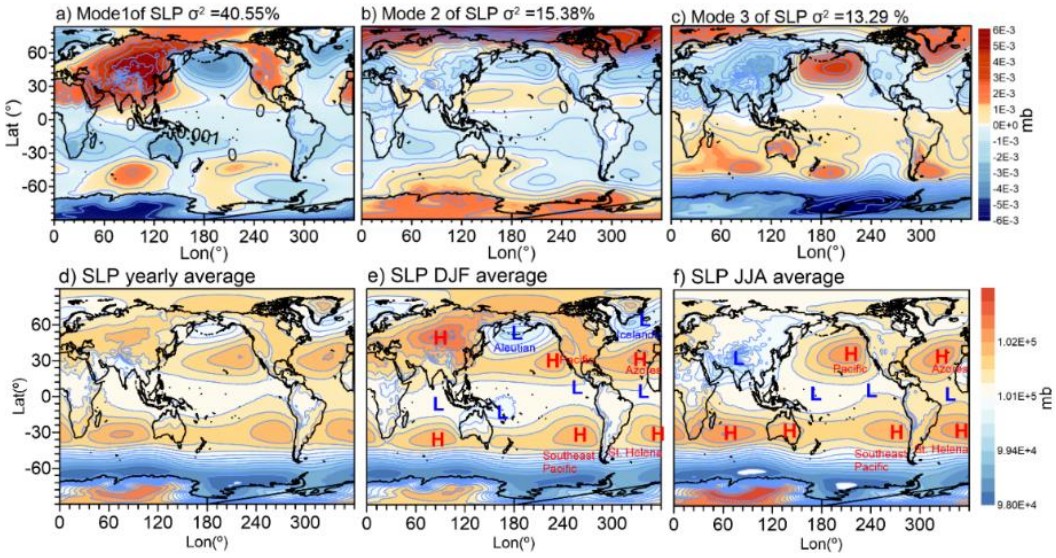


Figure 4.2. (a, b, c) Principal components of SLP, b) yearly, e) DJF, f) JJA seasonal average.

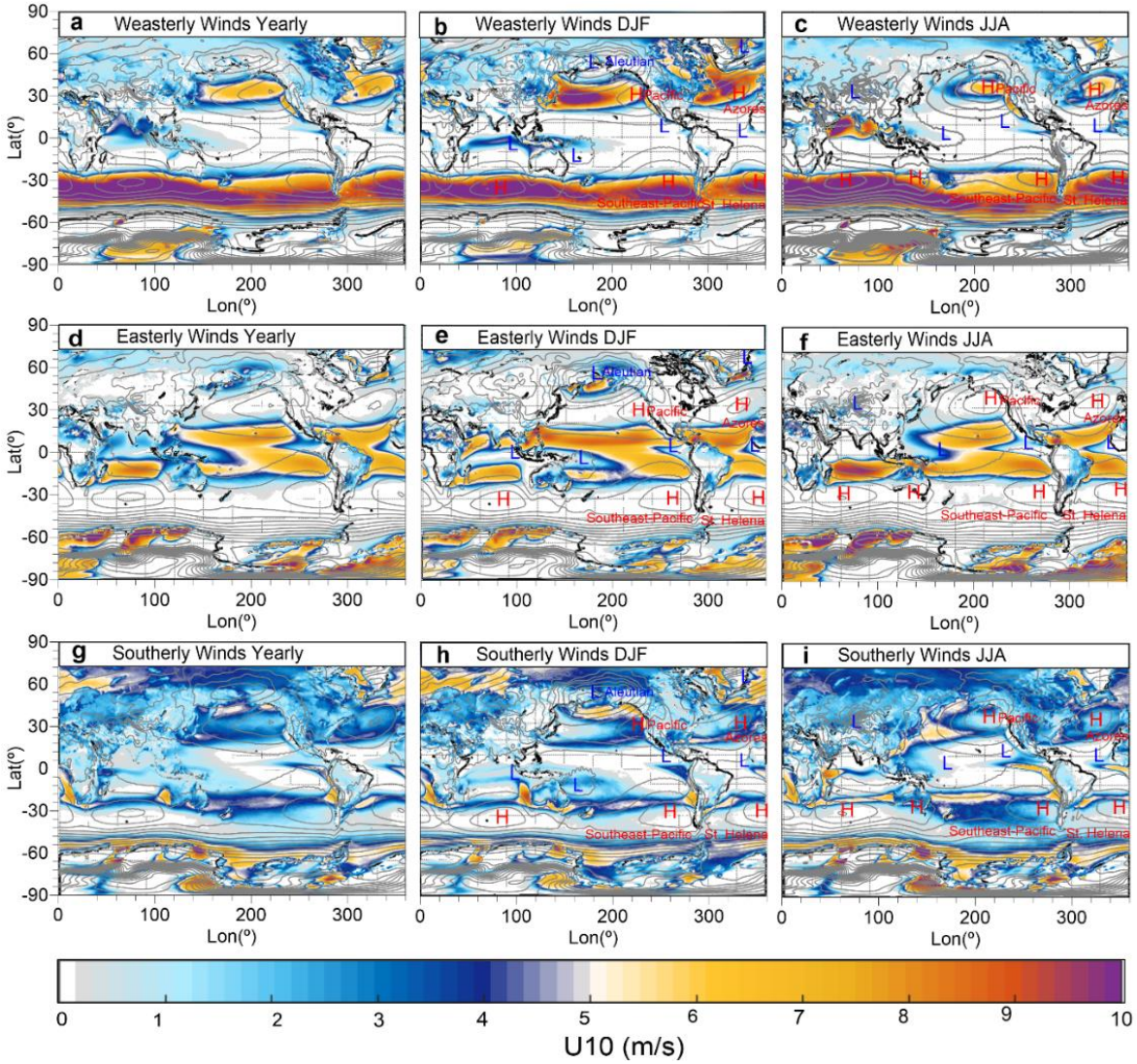


Figure 4.3.Planetary near surface wind systems $U_{10}$ (m/s) classified by dynamic clustering. Yearly averaged (a, d, g), DJF (b, e, h), and JJA, (c, f, i) of the westerly, (a b c), easterly (d, e, f), southerly (g, h, i) winds. Grey contour lines indicate the average SLP. H and L indicate the high and low-pressure centres of SLP.

As it was expected and in accordance with (Echevarria, Hemer and Holbrook, 2019), the wave power has a pan-hemispheric response. In the boreal winter (DJF), the wave climates of the Northern Hemisphere intensify. While in the boreal summer (JJA), the wave climates of the Southern Hemisphere do. In the Southern Hemisphere, in JJA, the gradient of the circumpolar high-low pressure belts strengthens and the subtropical WCTs intensify, affecting the South-eastern coasts of the ocean basins. The polar WCT (all) shift southward (northward) in DJF (JJA). In the Northern Hemisphere, in DJF, the polar winds and waves intensify and extend, influenced by the Aleutian, excepting for the North Atlantic that expands in MAM and JJA.

In JJA, in the Pacific and Atlantic, the tropical WCTs shift northward, as the high-pressure belt is interrupted by the appearance of low-pressure systems in the Asian and American continents and create a shift in the trade winds northward. Both Hadley cells are well defined in the Atlantic and the Pacific all year round. Meanwhile, in the Indian Ocean the Northern Hadley Cell is seasonally intermittent. In the DJF, between both Hadley Cells, the Warm Pool winds and waves are generated.

Nevertheless, the Trade winds are induced by the Southern Hadley cell in the JJA and the Intertropical Convergence Zone (ITCZ) moves further north in the Indian Ocean (SANIL KUMAR *et al.*, 2012) creating the monsoon winds and WCT. The monsoon WCT shifts clockwise in DJF and MAM, induced by the positions of the ITCZ, which shows a seasonal displacement toward the warmer hemisphere (Broccoli, Dahl and Stouffer, 2006).

All the wave climates are swell-dominated, in agreement with (Semedo *et al.*, 2011; Li, 2016). In particular, this is more notorious for the easterly and southerly wave climates (see Appendix A2). To validate the paired wave climates and basin-scale wind systems, the wind sea wave power and wind velocity of the corresponding systems were correlated. The results show high correlation, R>0.7 for all the systems and very high for the easterlies and westerlies R=0.9. Also the covariance was calculated using standardized values. The results show high covariabitliy, see Figure 4.5. Furthermore, the seasonal variation of win-sea wave power is plotted for each wave climate, see Figure 4.5. This figure shows the areas of generation of the wave climates forced by the planetary systems. These WCTs, their variation, and the wave generation region, are in agreement with, and reinforce the findings of previous studies (Echevarria et al., 2020; Hemer et al., 2013; Reguero et al., 2019; Shimura et al., 2013; Stopa & Cheung, 2014).

| Wave Climates | Wave Climates Types (WCTs) | Ocean Basin |
|---|---|---|
| Easterly | Polar<br>Tropical | North Atlantic, North Pacific Oceans<br>Atlantic, Pacific, Indian Oceans |
| Southerly | Subtropical<br>Subpolar | South Pacific, North Pacific, North Atlantic, South Atlantic,Indian Oceans<br>North Atlantic, North Pacific Oceans |
| Westerly | Extratropical<br>Monsoon<br>Warm Pool | South Pacific, North Pacific, North Atlantic, South Atlantic, and Indian Oceans<br>Indian Ocean<br>Indian and Pacific Oceans |

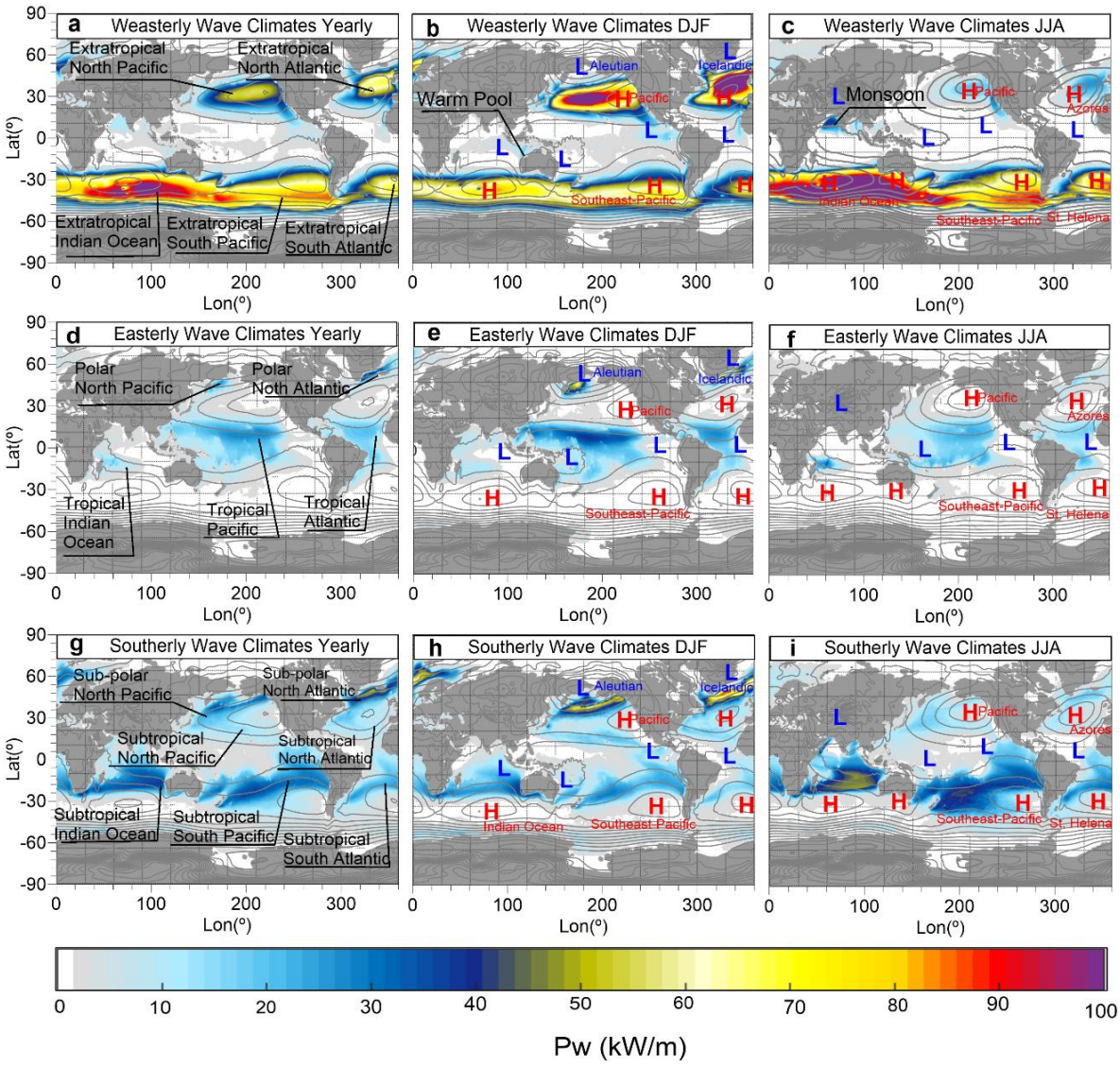


Figure 4.4. Wave climates classified by dynamic clustering. $P_w$ (kW/m) yearly averaged (a, d, g), DJF (b, e, h), and JJA (c, f, i) of the westerly, (a b c), easterly (d, e, f), southerly (g, h, i) wave climates.

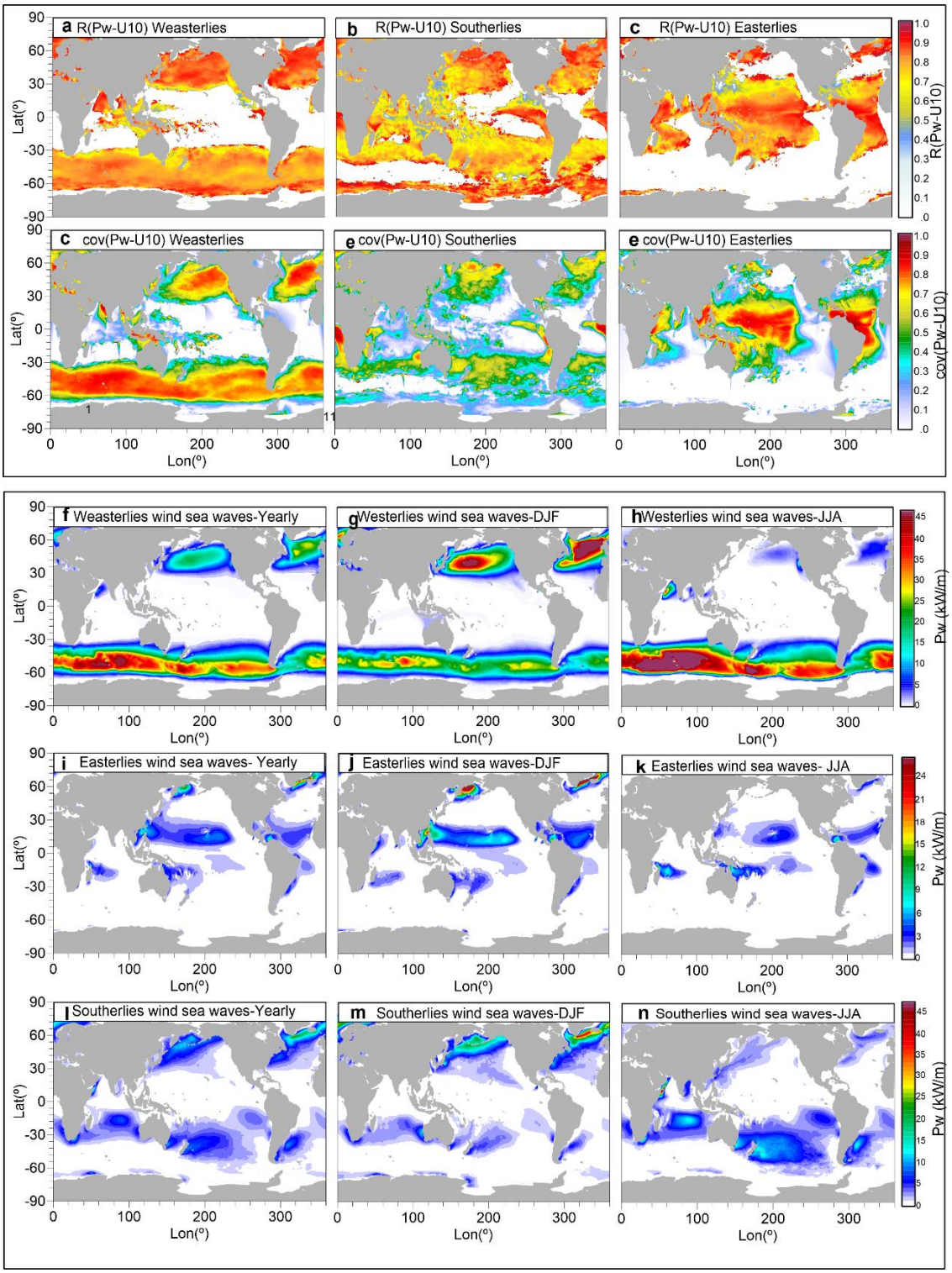


Figure 4.5. Correlation coefficient between wind sea wave power and wind velocity for (a) westerly wave climate and wind systems. b) For southerly wave climate and wind systems. c) For easterly wave climate and wind systems. Only those statistically significant are shown. Covariance between wind sea wave power and wind velocity for (d) westerly wave climate and wind systems. e) For southerly wave climate and wind systems. f) For easterly wave climate and wind systems. Wind-sea wave power for each wave climate: westerlies (a, b, c), easterlies (d, e, f), and southerlies (g, h, i) for the yearly (a, d, g), DJF, (b, e, h) and JJA (c, f, i) periods.

## 4.3 Tropical and extratropical natural variability

In this section, we examine the WCTs' response to ENSO, and ENSO when co-occurred with SAM and PDO climate patterns. For each WCT, the composite monthly anomalies of the spatially-averaged wave power are shown in Table 4.3 and for mean wave direction in Table 4.4.

Overall, the wave power of the zonal WCTs (westerlies and easterlies) are most affected by tropical-extratropical climate variability (ENSO, PDO and SAM). El Niño produces a strengthened Aleutian Low (Li et al., 2015), as consequence El Niño reinforces the extratropical WCT in the North Pacific (~ 3 kW/m). The ENSO and PDO positive phases, when occur simultaneously, create a much-deepened Aleutian Low (Bonsal, Shabbar and Higuchi, 2001) and the wave power intensifies even more (~ 4 kW/m). These results are in line with previous studies that focused on the impact of the PDO (Bromirski et al., 2013; Odériz et al., 2020) and ENSO ( Izaguirre et al., 2011; Shimura et al., 2013; Stopa & Cheung, 2014; Yang & Oh, 2020) on wave parameters separately.

Positive SAM phase intensifies the westerly wind due to an increment of the SLP gradient between the high and low pressure belts (Wang & Cai, 2013) and intensifies the swells generated in the Southern Ocean (Godoi and Júnior, 2020). Consequently, positive SAM also intensifies the ENSO wave power signal in the extratropical WCTs of the Southern Hemisphere in the Indian Ocean and the South Pacific (by ~3 to ~6 kW/m, respectively). However, La Niña increases the wave power of the monsoon WCT (~ 0.6 kW/m), due to the increase of the SLP gradient between the Indian Ocean and East Pacific (Wang et al., 2000; Wang & He, 2012; Zhang et al., 1996). The PDO reinforces this pattern (Wang et al., 2008), and when La Niña and a negative PDO co-occurred, the monsoon WCT strengths (~ 0.7 kW/m). Positive SAM also produces this effect when co-occurred with La Niña on wave power for this WCT (~ 2 kW/m). The extratropical WCT in the South Pacific intensifies the most in wave power when the ENSO and positive SAM are coupled (~ ±9 kW/m). Previously, in the extratropical belt of the Southern Ocean, highly natural variation of waves and winds has been identified (Clem et al., 2020; Hemer et al., 2010; Wang & Cai, 2013).

Table 4.3. Mean wave power composite anomalies induced by tropical and extratropical variability, and trends of mean wave power, wind-sea wave power, near surface wind velocity, and SST. Only the anomalies and trends that are significant at 95% confident levels are shown. Colours in red and blue represent intensification and reduction in the last 34 yrs. Colours green-yellow shows the level of SST warming.

| Wave Climate | Wave Climate Type | Basin | Natural variability: Tropical and extratropical Composite anomalies $P_{wm}$(kW/m) | | | | | | | | | | Trends Increment in 34 yr. | | | Global Warming Increment in 34 yr. |
|---|---|---|---|---|---|---|---|---|---|---|---|---|---|---|---|---|
| | | | ENSO + | ENSO - | ENSO + PDO + | ENSO + PDO - | ENSO + SAM + | ENSO + SAM - | ENSO - PDO + | ENSO - PDO - | ENSO - SAM + | ENSO - SAM - | $P_{wm}$ (kW/m) | $P_{wm-ws}$ Wind sea (kW/m) | $U_{10}$ (m/s) | SST (Cº) |
| Southerly | Subtropical | Indian Ocean | - | 0.74 | - | -1.1 | - | - | - | 1.04 | 2.11 | - | 3.95 | 0.36 | 0.18 | 0.63 |
| Southerly | Subtropical | South Pacific | - | - | - | - | 2.45 | - | - | - | - | -2.11 | - | - | - | - |
| Southerly | Subtropical | North Pacific | - | - | - | - | - | - | - | - | - | 9.98 | - | - | - | - |
| Southerly | Subpolar | North Pacific | - | - | - | - | - | - | - | - | - | - | - | - | - | - |
| Southerly | Subtropical | South Atlantic | - | - | - | - | - | - | - | - | - | - | 2.76 | 0.47 | 0.25 | - |
| Southerly | Subtropical | North Atlantic | - | - | - | - | - | - | - | - | - | -8.92 | - | - | - | - |
| Southerly | Subpolar | North Atlantic | - | - | - | - | - | - | - | - | - | -7.52 | - | -2.68 | - | - |
| Westerly | Extratropical | Indian Ocean | - | - | 2.15 | - | 6.8 | - | - | - | 5.53 | - | 9.03 | - | 0.17 | 0.33 |
| Westerly | Warm Pool | Indian Ocean | - | - | - | -1.4 | - | - | - | - | 2.33 | - | 1.59 | - | - | 0.68 |
| Westerly | Monsoon | Indian Ocean/Pacific | - | 0.71 | - | - | -1.06 | - | - | 0.8 | 2.9 | - | - | - | - | 0.84 |
| Westerly | Extratropical | South Pacific | -1.58 | 2.88 | - | -3.37 | 5.49 | -9.32 | - | 4.5 | 9.67 | -7.77 | 6.52 | - | - | - |
| Westerly | Extratropical | North Pacific | 2.58 | - | 3.4 | - | 4.48 | 3.89 | - | - | - | - | - | - | - | - |
| Westerly | Extratropical | South Atlantic | - | - | 1.54 | - | 4.17 | - | -2.8 | - | - | - | 5.9 | 1.76 | 0.29 | - |
| Westerly | Extratropical | North Atlantic | - | - | - | - | - | - | - | - | - | - | - | - | - | - |
| Easterly | Tropical | Indian Ocean | -1.14 | - | -1.75 | - | - | - | - | - | 2.37 | - | - | - | - | 0.63 |
| Easterly | Tropical | Pacific | 0.79 | - | 0.78 | - | 2.06 | - | -1.24 | - | - | - | 2.52 | 0.36 | 0.23 | 0.55 |
| Easterly | Polar | North Pacific | - | - | - | - | - | - | - | - | - | - | - | - | - | - |
| Easterly | Tropical | Atlantic | - | - | - | - | - | - | - | - | - | - | 1.83 | 0.4 | 0.15 | 0.61 |
| Easterly | Polar | North Atlantic | - | -3.48 | - | - | - | - | -7.67 | - | - | -6.23 | - | - | - | - |

Table 4.4. Mean wave direction composite anomalies induced by tropical and extratropical variability, and trends of mean wave direction and SST. Only the anomalies and trends that are significant at 95% confident levels are shown. Colours in red and blue represent clockwise and anticlockwise rotations in the last 34 years. Colours green-yellow shows the level of SST warming.

| Wave Climate | Wave Climate Type | Basin | Natural variability: Tropical and extratropical Composite anomalies of $Dir_m$ (º) | | | | | | | | | | Trend Increment in 34 yr. | Global Warming Increment in 34 yr. |
|---|---|---|---|---|---|---|---|---|---|---|---|---|---|---|
| | | | ENSO + | ENSO - | ENSO+ PDO + | ENSO+ PDO - | ENSO+ SAM + | ENSO+ SAM - | ENSO - PDO + | ENSO - PDO - | ENSO - SAM + | ENSO - SAM - | $Dir_m$ (º) | SST (Cº) |
| Southerlies | Subtropical | Indian Ocean | - | - | - | - | - | 1.53 | - | - | -1.2 | 1.68 | - | 0.63 |
| Southerlies | Subtropical | South Pacific | - | - | - | - | - | - | - | - | - | - | - | - |
| Southerlies | Subtropical | North Pacific | - | - | - | - | -6.1 | - | - | - | - | - | - | - |
| Southerlies | Subpolar | North Pacific | - | 2.23 | - | - | - | - | - | 3.54 | 4.14 | - | - | - |
| Southerlies | Subtropical | South Atlantic | - | - | - | - | - | - | - | -0.8 | -1.1 | - | -1.36 | - |
| Southerlies | Subtropical | North Atlantic | - | - | - | - | - | 4.98 | - | - | - | - | - | - |
| Southerlies | Subpolar | North Atlantic | - | - | - | - | - | - | - | - | - | - | - | - |
| Westerly | Extratropical | Indian Ocean | - | - | - | - | 2.98 | -2.3 | - | - | 2.03 | -3 | - | 0.33 |
| Westerly | Warm Pool | Indian Ocean | - | - | - | - | - | - | - | - | - | - | - | 0.68 |
| Westerly | Monsoon | Indian Ocean/Pacific | - | - | - | - | - | - | - | - | - | - | - | 0.84 |
| Westerly | Extratropical | South Pacific | - | - | - | - | 2.93 | -5.7 | - | - | 3.3 | -3.4 | - | - |
| Westerly | Extratropical | North Pacific | 1.25 | - | 1.71 | - | - | - | - | - | - | - | - | - |
| Westerly | Extratropical | South Atlantic | - | - | - | - | - | -2.3 | - | - | 3.22 | - | - | - |
| Westerly | Extratropical | North Atlantic | - | - | - | - | - | - | - | - | - | - | - | - |
| Easterly | Tropical | Indian Ocean | -1 | - | -1.7 | - | - | -2.6 | 1.85 | - | - | - | - | 0.63 |
| Easterly | Tropical | Pacific | 1.24 | -1.3 | 1.29 | - | 2.57 | - | - | -1.3 | -2.7 | - | - | 0.55 |
| Easterly | Polar | North Pacific | - | - | - | - | - | - | - | - | - | - | - | - |
| Easterly | Tropical | Atlantic | - | - | - | - | - | - | -1.8 | - | - | - | - | 0.61 |
| Easterly | Polar | North Atlantic | - | - | - | - | - | - | 4.37 | - | - | - | -2.85 | - |

## 4.4 Historical variability and ocean warming

This section shows the long-term trend of the spatially-averaged wave direction ($Dir_m$), wave power (both the mean wave power of the combined swell and wind seas, $P_{wm}$, and wind seas, $P_{wm\text{-}ws}$), in addition to the total area ($A_T$) for each WCT calculated for the same period as natural variability analysis (1985-2018); see Figure 4.6, Table 4.3, Table 4.4. Only those trends that are significant to the 95 % confidence level are discussed here.

Over the past 34 years, in the Southern Hemisphere there has been an increase in wave power (~ 3 to 9 kW/m) in both the extratropical and subtropical WCTs, supporting the signs of an intensification in the Southern Hemisphere wave climate suggested by other authors (Liu et al., 2016; Ribal & Young, 2019; Young et al., 2011). In the Indian and South Atlantic Oceans the wave power, wind seas (+0.4 kW/m) and winds (+0.1 to 0.3 m/s) trend to increase. In addition, the region of the Indian Ocean occupied by the subtropical WCT has experienced SST warming of ~ 0.6 ºC.

Likewise, in the Pacific and Atlantic Oceans, both wind speeds (~0.2 m/s) and wave power (for the total swell and wind sea combined, ~2 kW/m, and wind sea, ~0.4 kW/m) of the tropical WCTs have increased, as previously detected by (England et al., 2014; Young & Ribal, 2019). The tropical regions of all the oceans have experienced warming of approximately 0.6 ºC. Similarly, the warm pool WCT shows an upward trend in wave power (~ 1.6 kW/m) and SSTs (~ 0.7 ºC). The monsoon WCT increases in wave power, but the trend is non-significant. However, this trend is in agreement with previous findings (Anoop *et al.*, 2015), and this region has the highest rate of SST warming (~ 0.8 ºC). Against, the wave power has decreased in the North Atlantic (Morim et al., 2019; Reguero et al., 2019), which we can now show it is associated with the reduction in wave power of the subpolar WCT. Although no links with SST warming and wind in this area were found. The results indicate that the area covered by this WCT has reduced in the last decades.

Statistically significant trends in wave direction were only found for subtropical of the South Atlantic and polar of the North Atlantic WCTs. Although, these changes appear to not be related to SST warming, suggesting an alternative climate driver for these shifts in wave direction. However, a general pattern has been identified, the high-latitude WCTs (polar and extratropical) shifting poleward and the subtropical WCTs shifting toward the tropics. In the Southern Hemisphere, this pattern is forced by a decrease in pressure across the high-latitudes (Clem *et al*., 2020).

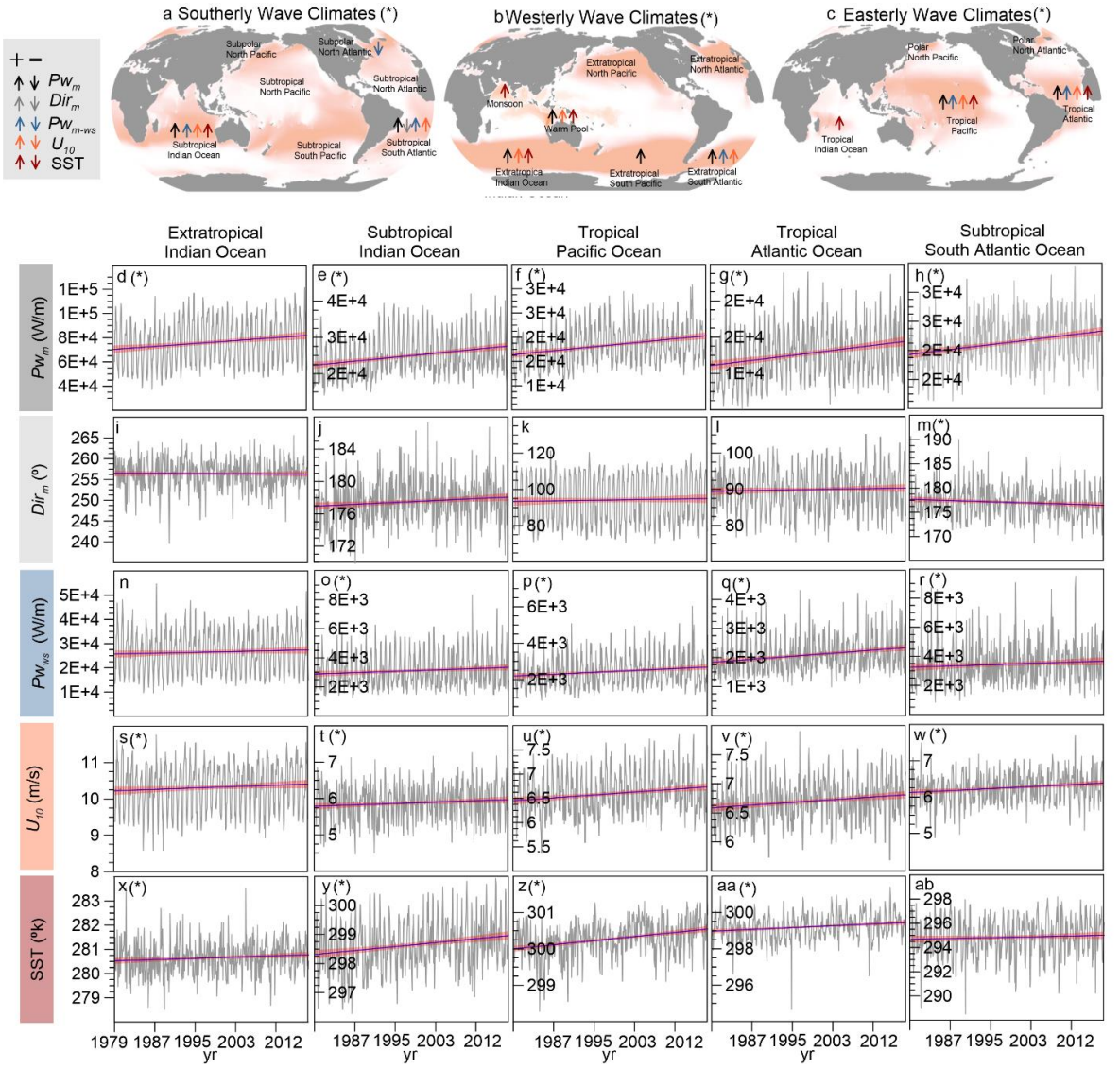


Figure 4.6. Trends of wave power ($P_{wm}$), mean wave direction ($Dir_m$), wave power for wind seas ($P_{wm\text{-}ws}$), near surface wind velocity $U_{10}$, and *SST* for a) westerly, b) easterly, and c) southerly WCTs. Time series and trends of, (d-h) $P_{wm}$, (i-m) $Dir_m$, (n-r) $P_{wm\text{-}ws}$, (s-w) $U_{10}$, (x-ab) *SST*, for (d, i, n, s, x) extratropical Indian Ocean, (e, j, o, t, y) subtropical Indian Ocean, (g, k, p, u, z) tropical Pacific Ocean, (g, l, q, v, aa) tropical Atlantic Ocean, and (h, m, r, w, ab) subtropical South Atlantic Ocean. (*)Trends in these panels are significant to the 95% confidence level.

## 4.5 Ocean-wave teleconnection patterns: a basis for global adaptation schemes

Ocean-wave teleconnection patterns are defined as remote wave climates which their variability is related. Results indicate that there are inter-basin, tropical-extratropical-subtropical, and inter-hemispheric connections between WCTs, forced by their origins in the atmospheric circulation. To analyse the interconnections between WCTs, the Pearson correlation coefficient (R) was calculated for spatially-averaged wave power ($P_{wm}$), direction ($Dir_m$), and total area ($A_T$) for each WCT.

The WCTs in wave power show a pan-hemispheric interconnection that is governed by seasonal variability, as shown in Figure 4.7, in line with other authors (Echevarria, Hemer and Holbrook, 2019;

Jiang, 2020). In the Southern Hemisphere, the extratropical and subtropical WCTs exhibit the same response to atmospheric forcing, as both WCTs have in common the atmospheric mechanism of the subtropical high pressure belt. In the Atlantic and Pacific basins, the tropical WCTs intensify simultaneously with the extratropical and subtropical WCTs of the Northern Hemisphere (see Figure 3. 3. and Figure 4.4). This same behaviour shows that these WCTs are all forced by the intensity and position of the Northern Hemisphere subtropical high-pressure belt.

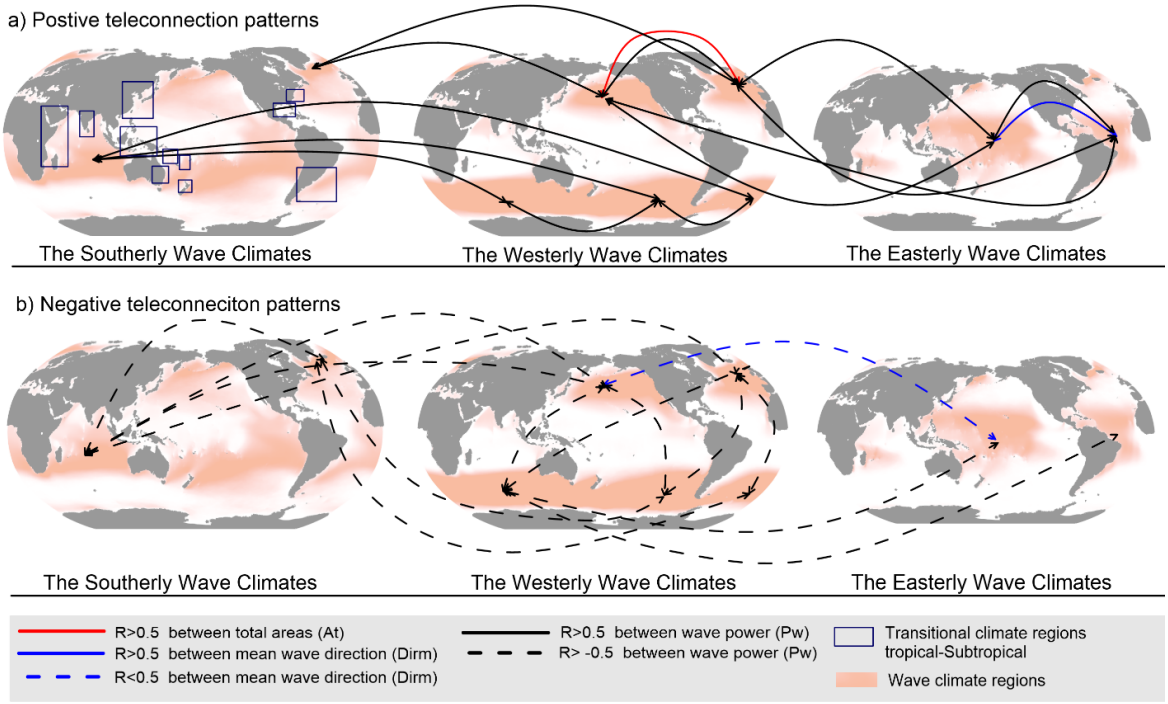


Figure 4.7. Correlations coefficient R, significant at 95% confidence level, for mean wave power, mean wave direction and total area between the WCTs. a) Positive correlations shows increase/increase or decrease/decrease, and b) negative shows increase/decrease between the variables analysed.

For wave direction, in the Pacific and Indian Ocean, the subtropical WCT rotates in the opposite direction to the extratropical WCTs. All extratropical WCTs rotate in the same direction. The exception was found in those of the North Atlantic basin, which is dominated by the position and intensity of the Icelandic Low. The tropical WCTs in the Atlantic and Pacific, forced by the trade winds, rotates in response to the Hadley cells displacement to the warmer hemisphere.

In general, we identify coasts where extratropical WCTs prevail, such as those of Chile, the Mexican Pacific, Northwest Europe, Southern Africa and South Australia, and those where tropical WCTs prevail, including those bounding the Caribbean Sea, Indonesia, Madagascar or East of Australia. Both of these regions have the same wave conditions throughout the year (Fairl*ey et al.*, 2020). Other regions are dominated by both tropical and subtropical WCTs (e.g., the coasts of Japan and Argentina, Eastern New Zealand, and Eastern USA).

## 4.6 Conclusions

The global ocean wave climate is classified into the extratropical, monsoon, warm pool, subtropical, subpolar, polar, and tropical WCTs. In general, results suggest that in the long-term, the wave direction around the world is driven by natural variability. There is a net increase in global

wave power of the WCTs in the Southern Hemisphere. The global warming signal lies outside the upper bounds of natural variability in wave power for warm pool, the subtropical and the extratropical WCTs of the Indian Ocean, and the tropical WCTs of the Atlantic and Pacific basins. In the North Atlantic, a strong downward trend in wave power associated with the subpolar WCT was found, but exceeded by natural variability when both the negative ENSO and SAM phases occur. For the subtropical of the South Pacific, the monsoon, the extratropical of North Pacific, the tropical of Indian Ocean and the Polar WCTs, the long-term trends over the past decades remain inside the bounds of natural variability.

WCTs with large natural variability may mask a global warming signal that is emerging. Special attention should be paid to the Pacific sector of the Southern Ocean that has a strong natural fluctuations (Hemer, Church and Hunter, 2010; Clem *et al*>, 2020). Although we could not identify the driver, a strong long-term trend was detected in the extratropical WCT of the South Pacific (~6 kW/m) but was masked by natural variability when positive phases of ENSO and SAM occurred (up to 10kW/m). The WCTs exhibit strong inter-basin, inter-hemisphere, and tropical-subtropical-extratropical-subpolar teleconnections in different regions of the world.

**References**

Alves, J.-H. G. M. (2006) 'Numerical modeling of ocean swell contributions to the global wind-wave climate', *Ocean Modelling*, 11(1), pp. 98–122. doi: https://doi.org/10.1016/j.ocemod.2004.11.007.

Anoop, T. R. *et al.* (2015) 'Surface Wave Climatology and Its Variability in the North Indian Ocean Based on ERA-Interim Reanalysis*', *Journal of Atmospheric and Oceanic Technology*, 32(7), pp. 1372–1385. doi: 10.1175/JTECH-D-14-00212.1.

Bonsal, B. R., Shabbar, A. and Higuchi, K. (2001) 'Impacts of low frequency variability modes on Canadian winter temperature', *International Journal of Climatology*. John Wiley & Sons, Ltd, 21(1), pp. 95–108. doi: 10.1002/joc.590.

Broccoli, A. J., Dahl, K. A. and Stouffer, R. J. (2006) 'Response of the ITCZ to Northern Hemisphere cooling', *Geophysical Research Letters*, 33(1), pp. 1–4. doi: 10.1029/2005GL024546.

Bromirski, P. D. *et al.* (2013) 'Wave power variability and trends across the North Pacific', *Journal of Geophysical Research: Oceans*, 118(12), pp. 6329–6348. doi: 10.1002/2013JC009189.

Clem, K. R. *et al.* (2020) 'Record warming at the South Pole during the past three decades', *Nature Climate Change*, 10(8), pp. 762–770. doi: 10.1038/s41558-020-0815-z.

Dodet, G., Bertin, X. and Taborda, R. (2010) 'Wave climate variability in the North-East Atlantic Ocean over the last six decades', *Ocean Modelling*. Elsevier Ltd, 31(3–4), pp. 120–131. doi: 10.1016/j.ocemod.2009.10.010.

Echevarria, E. R. *et al.* (2020) 'Influence of the Pacific-South American Modes on the Global Spectral Wind-Wave Climate', *Journal of Geophysical Research: Oceans*. John Wiley & Sons, Ltd, 125(8), p. e2020JC016354. doi: 10.1029/2020JC016354.

Echevarria, E. R., Hemer, M. A. and Holbrook, N. J. (2019) 'Seasonal Variability of the Global Spectral Wind Wave Climate', *Journal of Geophysical Research: Oceans*. John Wiley & Sons, Ltd, 124(4), pp. 2924–2939. doi: 10.1029/2018JC014620.

England, M. H. *et al.* (2014) 'Recent intensification of wind-driven circulation in the Pacific and the ongoing warming hiatus', *Nature Climate Change*, 4(3), pp. 222–227. doi: 10.1038/nclimate2106.

Fairley, I. *et al.* (2020) 'A classification system for global wave energy resources based on multivariate clustering', *Applied Energy*, 262, p. 114515. doi: https://doi.org/10.1016/j.apenergy.2020.114515.

Godoi, V. A. and Júnior, A. R. (2020) 'A global analysis of austral summer ocean wave variability during SAM–

ENSO phase combinations', *Climate Dynamics*, 54(9), pp. 3991–4004. doi: 10.1007/s00382-020-05217-2.

Hemer, M. A., Church, J. A. and Hunter, J. R. (2010) 'Variability and trends in the directional wave climate of the Southern Hemisphere', *International Journal of Climatology*. John Wiley & Sons, Ltd, 30(4), pp. 475–491. doi: 10.1002/joc.1900.

Hemer, M. A., Katzfey, J. and Trenham, C. E. (2013) 'Global dynamical projections of surface ocean wave climate for a future high greenhouse gas emission scenario', *Ocean Modelling*, 70, pp. 221–245. doi: https://doi.org/10.1016/j.ocemod.2012.09.008.

I. R. Young, S. Zieger, A. V. B. (2011) 'Global Trends in Wind Speed and Wave Height', *Science*, 332(April), pp. 451–456.

Izaguirre, C. *et al.* (2011) 'Global extreme wave height variability based on satellite data', *Geophysical Research Letters*, 38(10), pp. 1–6. doi: 10.1029/2011GL047302.

Jiang, H. (2020) 'Wave Climate Patterns from Spatial Tracking of Global Long-Term Ocean Wave Spectra', *Journal of Climate*, 33(8), pp. 3381–3393. doi: 10.1175/JCLI-D-19-0729.1.

Li, F., Wang, H. and Gao, Y. (2015) 'Modulation of Aleutian Low and Antarctic Oscillation co-variability by ENSO', *Climate Dynamics*, 44(5), pp. 1245–1256. doi: 10.1007/s00382-014-2134-4.

Li, X.-M. (2016) 'A new insight from space into swell propagation and crossing in the global oceans', *Geophysical Research Letters*. John Wiley & Sons, Ltd, 43(10), pp. 5202–5209. doi: https://doi.org/10.1002/2016GL068702.

Liu, Q. *et al.* (2016) 'Wind and Wave Climate in the Arctic Ocean as Observed by Altimeters', *Journal of Climate*. American Meteorological Society, 29(22), pp. 7957–7975. doi: 10.1175/JCLI-D-16-0219.1.

Morim, J. *et al.* (2019) 'Robustness and uncertainties in global multivariate wind-wave climate projections', *Nature Climate Change*, 9(9), pp. 711–718. doi: 10.1038/s41558-019-0542-5.

Odériz, I. *et al.* (2020) 'Climate drivers of directional wave power on the Mexican coast', *Ocean Dynamics*, 70(9), pp. 1253–1265. doi: 10.1007/s10236-020-01387-z.

Pickart, R. S. *et al.* (2009) 'Seasonal Evolution of Aleutian Low Pressure Systems: Implications for the North Pacific Subpolar Circulation', *Journal of Physical Oceanography*. American Meteorological Society, 39(6), pp. 1317–1339. doi: 10.1175/2008JPO3891.1.

Reguero, B. G., Losada, I. J. and Méndez, F. J. (2019) 'A recent increase in global wave power as a consequence of oceanic warming', *Nature Communications*. Springer US, 10(1), pp. 1–14. doi: 10.1038/s41467-018-08066-0.

Ribal, A. and Young, I. R. (2019) '33 years of globally calibrated wave height and wind speed data based on altimeter observations', *Scientific Data*, 6(1), p. 77. doi: 10.1038/s41597-019-0083-9.

SANIL KUMAR, V. *et al.* (2012) 'Variations in nearshore waves along Karnataka, west coast of India', *Journal of Earth System Science*, 121(2), pp. 393–403. doi: 10.1007/s12040-012-0160-3.

Semedo, A. *et al.* (2011) 'A Global View on the Wind Sea and Swell Climate and Variability from ERA-40', *Journal of Climate*. American Meteorological Society, 24(5), pp. 1461–1479. doi: 10.1175/2010JCLI3718.1.

Shimura, T., Mori, N. and Mase, H. (2013) 'Ocean waves and teleconnection patterns in the northern hemisphere', *Journal of Climate*, 26(21), pp. 8654–8670. doi: 10.1175/JCLI-D-12-00397.1.

Stopa, J. E. and Cheung, K. F. (2014) 'Periodicity and patterns of ocean wind and wave climate', *Journal of Geophysical Research: Oceans*. John Wiley & Sons, Ltd, 119(8), pp. 5563–5584. doi: 10.1002/2013JC009729.

Wang, B., Wu, R. and Fu, X. (2000) 'Pacific–East Asian Teleconnection: How Does ENSO Affect East Asian Climate?', *Journal of Climate*. American Meteorological Society, 13(9), pp. 1517–1536. doi:

10.1175/1520-0442(2000)013<1517:PEATHD>2.0.CO;2.

Wang, G. and Cai, W. (2013) 'Climate-change impact on the 20th-century relationship between the Southern Annular Mode and global mean temperature', *Scientific Reports*, 3(1), p. 2039. doi: 10.1038/srep02039.

Wang, H. and He, S. (2012) 'Weakening relationship between East Asian winter monsoon and ENSO after mid-1970s', *Chinese Science Bulletin*, 57(27), pp. 3535–3540. doi: 10.1007/s11434-012-5285-x.

Wang, L., Chen, W. and Huang, R. (2008) 'Interdecadal modulation of PDO on the impact of ENSO on the east Asian winter monsoon', *Geophysical Research Letters*. John Wiley & Sons, Ltd, 35(20). doi: 10.1029/2008GL035287.

Yang, S. and Oh, J.-H. (2020) 'Effects of modes of climate variability on wave power during boreal summer in the western North Pacific', *Scientific Reports*, 10(1), p. 5187. doi: 10.1038/s41598-020-62138-0.

Young, I. R. and Ribal, A. (2019) 'Multiplatform evaluation of global trends in wind speed and wave height', *Science*, 364(6440), pp. 548 LP – 552. doi: 10.1126/science.aav9527.

Young, I. R., Zieger, S. and Babanin, A. V (2011) 'Global Trends in Wind Speed and Wave Height', *Science*, 332(6028), pp. 451 LP – 455. doi: 10.1126/science.1197219.

Zhang, R., Sumi, A. and Kimoto, M. (1996) 'Impact of El Niño on the East Asian Monsoon', *Journal of the Meteorological Society of Japan. Ser. II*, 74(1), pp. 49–62. doi: 10.2151/jmsj1965.74.1_49.

# CHAPTER 5

## The Expanding Tropics, a Wave Climate Driver

This chapter explores the widening of the tropical regions in the last four decades and their impacts on wave climate.

## 5.1 Introduction

The expanding tropics is one of the main consequences of climate change in the atmospheric circulation (Reichler, 2009). The widening and strengthening of the Hadley cells have implications for the surrounding climatic zones in the context of a changing climate (Reichler, 2009; Seidel et al., 2008). Many regions across the world (i.e. Australia, the Mediterranean region, North America, and South America) have reported more frequent droughts related to changes in climate regions (tropical to subtropical). Concerning the climate patterns, such as ENSO that operates over the Hadley cells and Walker cell, generate significant fluctuations in wave climate. All of these factors point to the expanding tropics being a potential wave climate driver. This chapter presents the tropical limits and their trends over the last 40 years. The regions of tropical limits that most affect the WCTs were identified and used to calculate five Expanding Tropics Indices. After, these new climate indices were correlated with the anomalies of mean wave direction and wave power on the coasts. The impacts on wave climate were evaluated across the global coastlines, and its comparison with ENSO was discussed. The results show that the expanding tropics modulate the long-term wave climate.

## 5.2 The tropical limits

One of the challenges to identify the expansion of the tropics is the definition itself. This topic has been approached by atmospheric science, in this area of knowledge the limits of the tropics are the Hadley cells. Also, in oceanography, mainly in Australia, it has been reached using the subtropical high-pressure ridge as its indicator (Mortlock et al., 2020; Timbal & Drosdowsky, 2013; Wandres et al., 2016). This is motivated by the fact that subtropical High-Pressure systems drives the Southeast Australian climate, although the subtropical High-Pressure ridge itself is not the definition of the tropical limits, rather a consequence of it. As such, this indicator does not differentiate between tropical and subtropical regions. Lucas et al. (2014) review the expanding tropics issue and summarize four approaches to identify their limits: tropopause methods, satellite methods, Jetstream function, and stream function. All of these methods analyse the Hadley cells in upper levels of the atmosphere.

Nonetheless, we aim to explore the expansion over the near-surface winds and waves. After all, our goal is to evaluate the impacts on the ocean waves and the consequences on the coast. Thereby, we define the tropics on the Earth's surface as the upper (Northern Hemisphere) and lower (Southern Hemisphere) latitude that delimited the trade winds. For this, the wind classification presented in Chapter 4 is used. Figure 5. 1 shows the process carried out to identify the tropical limits at each time step. The area where the trade winds is shown in grey, in red the northern tropical limit, and in blue the southern tropical limit. To avoid data noise the isolated regions composed by less than 40 cells were not included in this analysis. The time series of latitudinal position was obtained at every longitudinal 0.5 degrees.

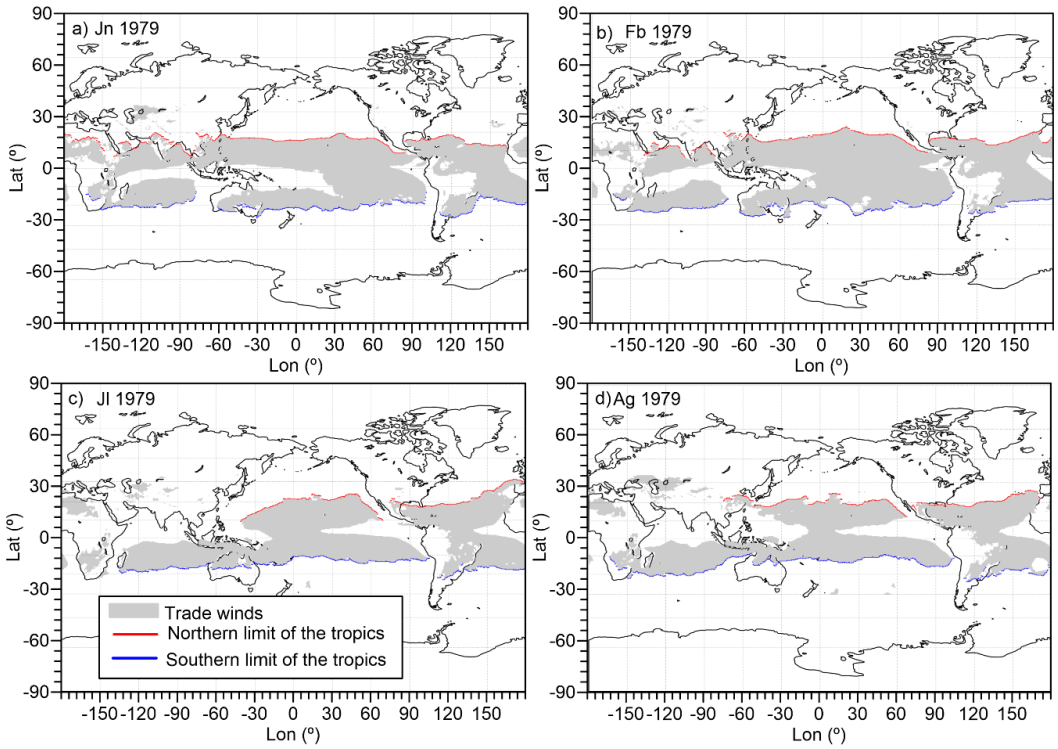


Figure 5. 1. Examples of the tropical limits based on near surface wind classification. For a) January 1979, b) July 1979, c) February 1979, and d) August 1979.

The average and deviation standard were calculated yearly and seasonally (DJF, MAM, JJA, and SON). The results are shown in Figure 5. 2 and Figure 5. 3, and are in line with general understanding of tropical behaviour. For instance, the tropical zone is displaced to the warmer hemisphere, in JJA northward and in DJF southward, in agreement with Broccoli et al (2008). Moreover, in JJA, in the Indian Ocean, the ITCZ localizes over the Asian Continent. This phenomenon leads to the Monsoon winds. In DJF and MAM, a larger variation is found in the Southern Hemisphere, and drastic changes of tropical limits are found in the land-sea boundaries. This is particularly representative in the East Pacific Basin.

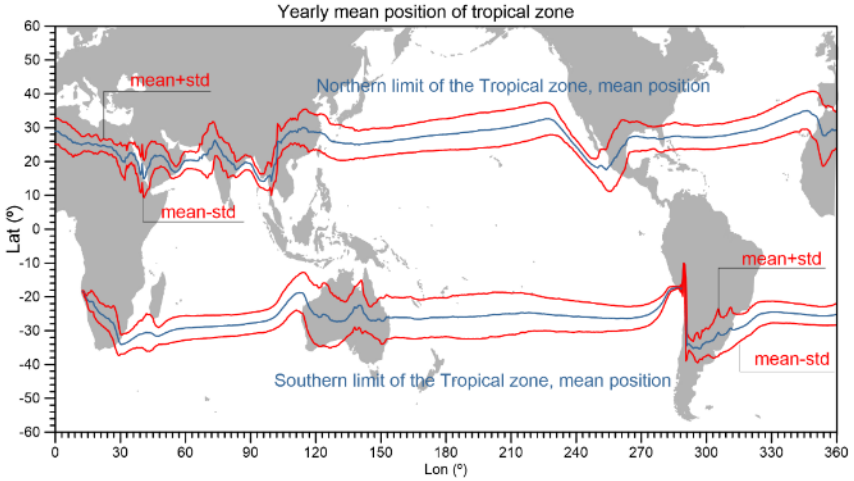


Figure 5. 2. Mean and standard deviation of the tropical limits, yearly.

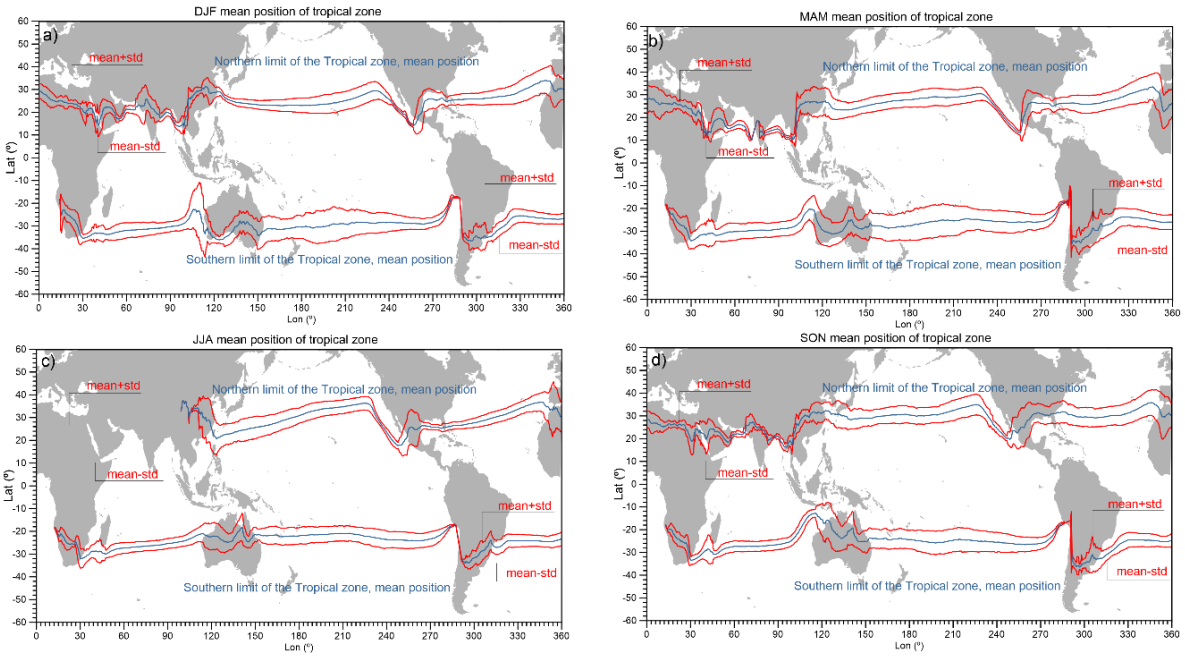


Figure 5. 3. Mean and standard deviation of the tropical limits in a) DJF, b) MAM c) JJA, d) SON.

## 5.3 The expanding tropics

The linear trends, yearly and seasonally, of tropical limits were calculated for each longitudinal cell. Only those that were statistically significant at 95 % confidence level by the Mandal Kendall approach were considered. In general, our results show a similar pattern of expansion reported in previous studies that utilized another reanalysis NCEP, ERA 40, CFSR, or MERRA (Davis & Rosenlof, n.d.; Yongyun Hu et al., 2011), see table 5.1. All these works identified an expansion of the tropical belt in both hemispheres since 1979 (Lucas et al, 2014).

Table 5. 1. Tropical widening in degrees latitude per decade from different studies and approaches (Reichler, 2009).

| | Indicator | Data | Widening º |
|---|---|---|---|
| (ROSENLOF, 2002) | Tropical upwelling(60 hPa) | Analyses | 3.0 |
| (T. Reichler, I. Held,2005) | Tropopause height | Radiosonde | 0.4 |
| | Tropopause height | Reanalyses | 0.7 |
| (Fu et al., 2006) | Tropospheric temperatures | MSU | 0.7 |
| (Hudson et al., 2006) | total ozone | TOMS | 1.0 (NH only) |
| (Seidel & Randel, 2007) | Tropopause height | Radiosonde, Reanalyses | 1.8-3.1 |
| (Y Hu & Fu, 2007) | Outgoing longwave radiation | Various satellite sensors | 1.5 |
| | Mean meridional circulation | Reanalyses | 1.0 |
| (Archer & Caldeira, 2008) | Jet stream separation | Reanalyses | 0.3 |
| (Seidel et al., 2008) | Jet stream separation | Reanalyses | 1.0 |

The results show that seasonality is larger than the year-on-year trend, and the expansion is longitudinally irregular. In JJA, the warmer season in the northern hemisphere, the tropics over the North Atlantic and the North Pacific contracted (by an average of -0.5° and -0.9°, respectively). For this hemisphere, the expansion is produced for colder seasons. In MAM, the expansion in the Indian

Ocean was up to +1.2°, in SON and DJF, in the Pacific Ocean was up to +0.8°, and in the Atlantic in DJF was up to +0.9°. In contrast, the expansion in the Southern Hemisphere is permanent all year round. Except for the Indian Ocean, where a contraction was found in JJA (+0.14°). Although the higher rates of expansion were found in the warmer and temperate seasons of this hemisphere, in the Pacific Ocean during DJF and MAM, and in the Atlantic during SON. In DJF, the expansion was notable for both hemispheres. In the Southern Hemisphere, the expansion has been associated with stratospheric ozone depletion (Min & Son, 2013). The higher contraction was found in MAM and JJA on the northcentral Pacific and northeast Atlantic basin (1.5-2.5°), and the higher expansion (3-6°) was produced in Africa (South and North, +6°), Australia (up to 4°), and the Arabian Peninsula (up to 5°) in MAM.

Table 5. 2. Tropical widening in degrees in the last 40 years by region.

| Degrees of expansion (red, positive sign) and contraction (blue, negative sign) in 40 years between 1979-2018 Northern region | | | | | | Degrees of expansion(red, negative sign) and contraction(blue, positive sign) in 40 years between 1979-2018 Southern region | | | | | |
|---|---|---|---|---|---|---|---|---|---|---|---|
| Region | Annual | DJF | MAM | JJA | SON | Region | Annual | DJF | MAM | JJA | SON |
| Indian Ocean (NH) | 0.49 | 0.37 | 1.23 | NaN | -0.63 | Indian Ocean (SH) | -0.41 | -0.58 | -0.13 | 0.14 | -0.30 |
| Pacific Ocean (NH) | 0.15 | 0.74 | -0.51 | -0.91 | 0.76 | Pacific Ocean (SH) | -0.52 | -0.81 | -1.00 | -0.66 | 0.01 |
| Atlantic Ocean (NH) | 0.33 | 0.87 | 0.12 | -0.47 | 0.37 | Atlantic Ocean (SH) | -0.42 | -0.17 | -0.49 | -0.14 | -1.06 |

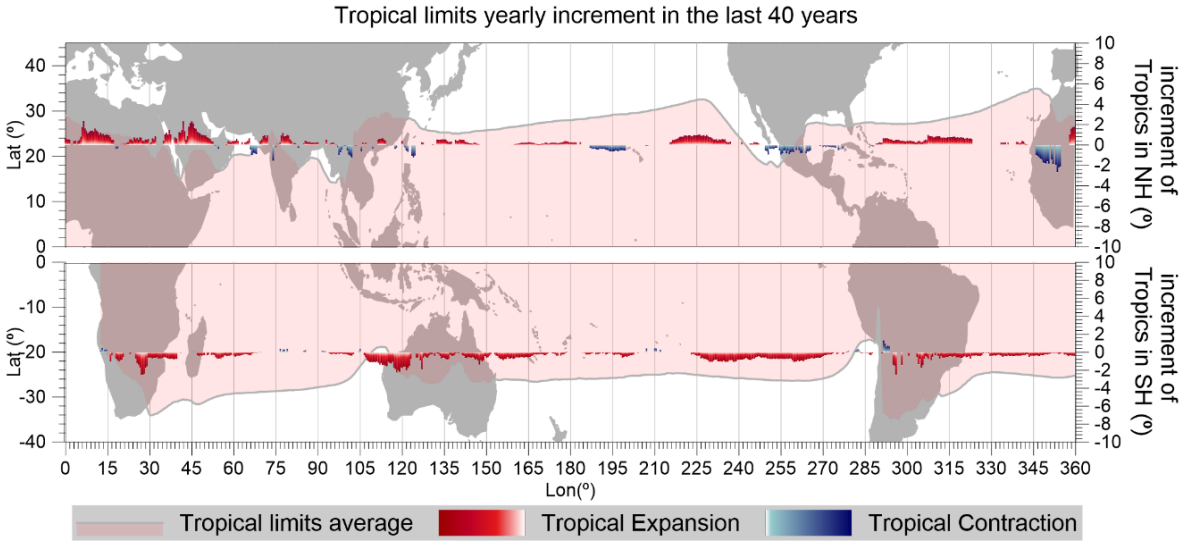


Figure 5. 4. Expansion and contraction of the tropical limits in the las 40 years, yearly.

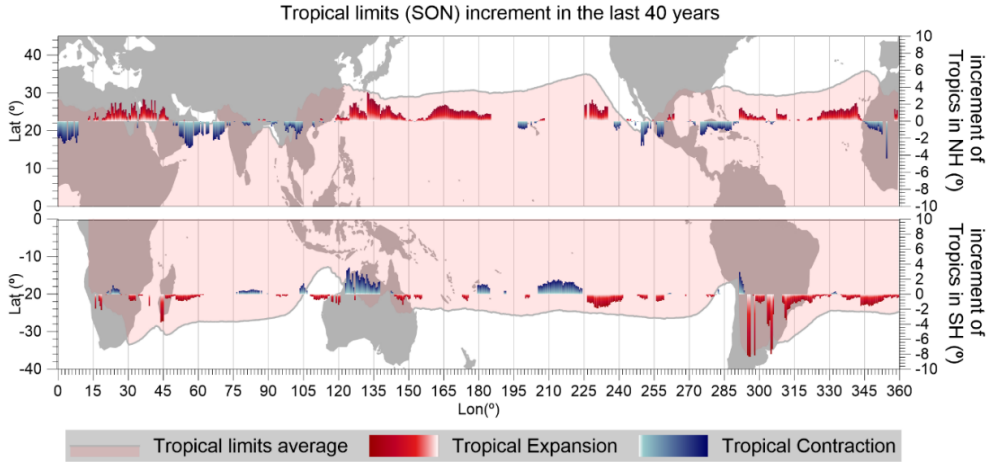


Figure 5. 5. Expansion and contraction of the tropical limits in the las 40 years, SON.

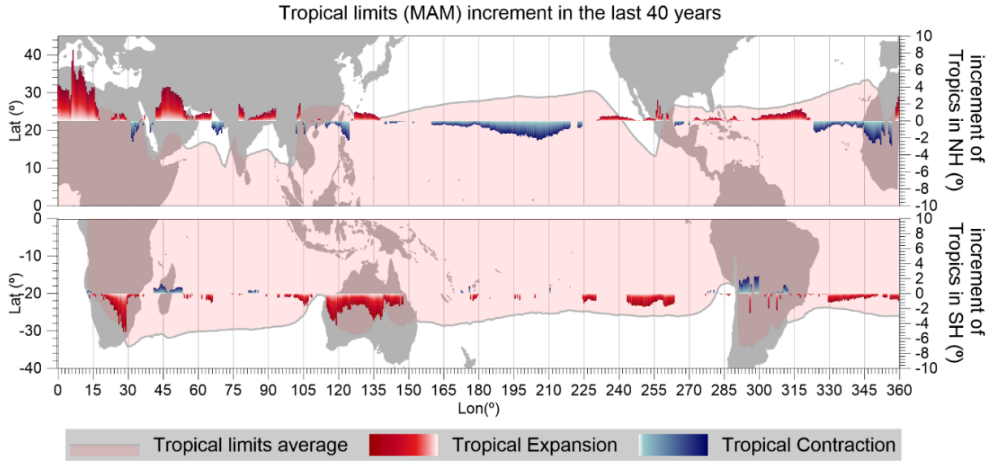


Figure 5. 6. Expansion and contraction of the tropical limits in the las 40 years, MAM.

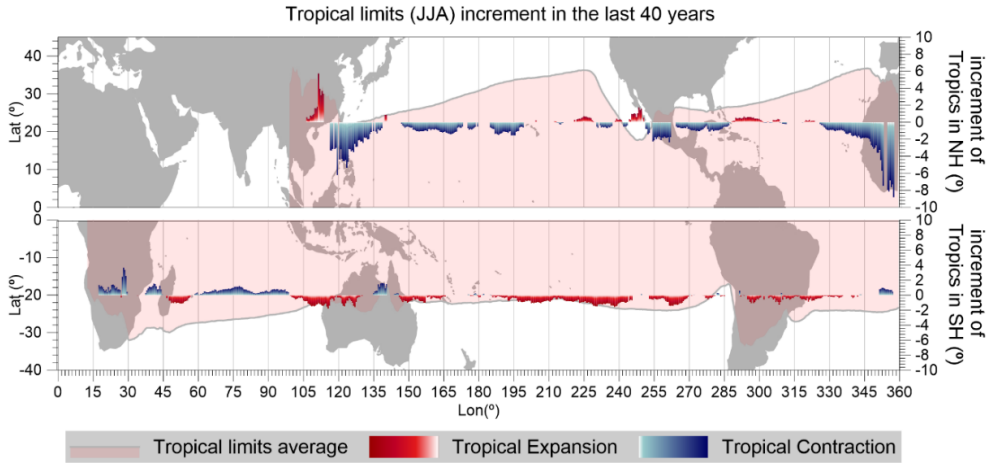


Figure 5. 7. Expansion and contraction of the tropical limits in the las 40 years, JJA.

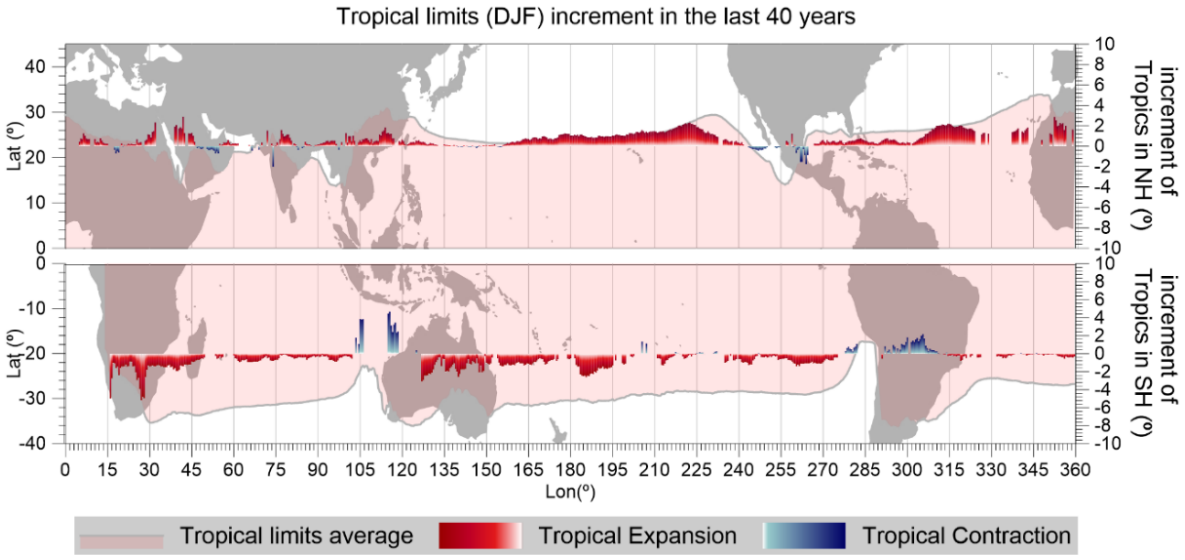


Figure 5. 8. Expansion and contraction of the tropical limits in the las 40 years, DJF.

## 5.4 Expanding tropics impacts on the wave climate types

We examined the relationship that exists between the tropics and WCT variability in order to investigate the regions of the tropics that most affected on wave climate characteristics. The correlation coefficient (R) between the tropical limits and the spatially-averaged wave power and mean wave direction of each WCT (those shown in Chapter 4) was calculated using the Pearson approach. Only those values statistically significant were used. Figure 5. 9 depicts the parts of the tropics that affect each WCT. The northern tropical limits are positive in latitude, while the southern tropical limits are negative. In consequence, the correlation coefficient signs behave opposite. When R in the Northern Hemisphere is positive, there is an increase in wave power and a clockwise rotation, and vice-versa when R is negative. However, in the tropical limits of the Southern Hemisphere, a positive correlation means a decrease in wave power and anticlockwise rotation when the tropical limits are displaced southward.

In chapter 4, we demonstrated that the planetary wind and pressure systems drive the wave climate variability. The High and Low-pressure belts of descending and ascending branches of the Hadley cells are the atmospheric mechanisms of the almost WCTs. The gradient in pressure between the subtropical ridge and the ITZC belt creates the trade winds and, consequentially, the tropical wave climates. The monsoon and warm pool dependent on the ITZC position, while the extratropical winds and wave climates are forced by the gradient of the high-pressure ridge between the Hadley cell and the low pressure of the polar systems. In addition, the subtropical wave climate is governing by the subtropical ridges. Thereby, the position and width of the Hadley cells will impact all of the aforementioned mechanisms with consequences in the wave characteristics. We explain those impacts below.

In general, all the extratropical and tropical WCTs, and the subtropical of the Indian Ocean present extreme sensitivity to the displacement of the tropics. In the Northern Hemisphere, the westerlies WCTs decrease in wave power and turn anticlockwise when the tropics displace northward and opposite when displacing southward. The reason is that the Hadley cells displace to the warmer hemisphere (Broccoli et al., 2006). In the boreal summer, they displace northward and that creates a weak and poleward extratropical wave climate. In contrast, in the Southern Hemisphere, the bearing is contrary. The tropical wave climates respond to the displacement of

Hadley cells equal to the extratropical WCTs. However, in the Atlantic, the tropical WCT intensifies when the northern tropic displaces northward.

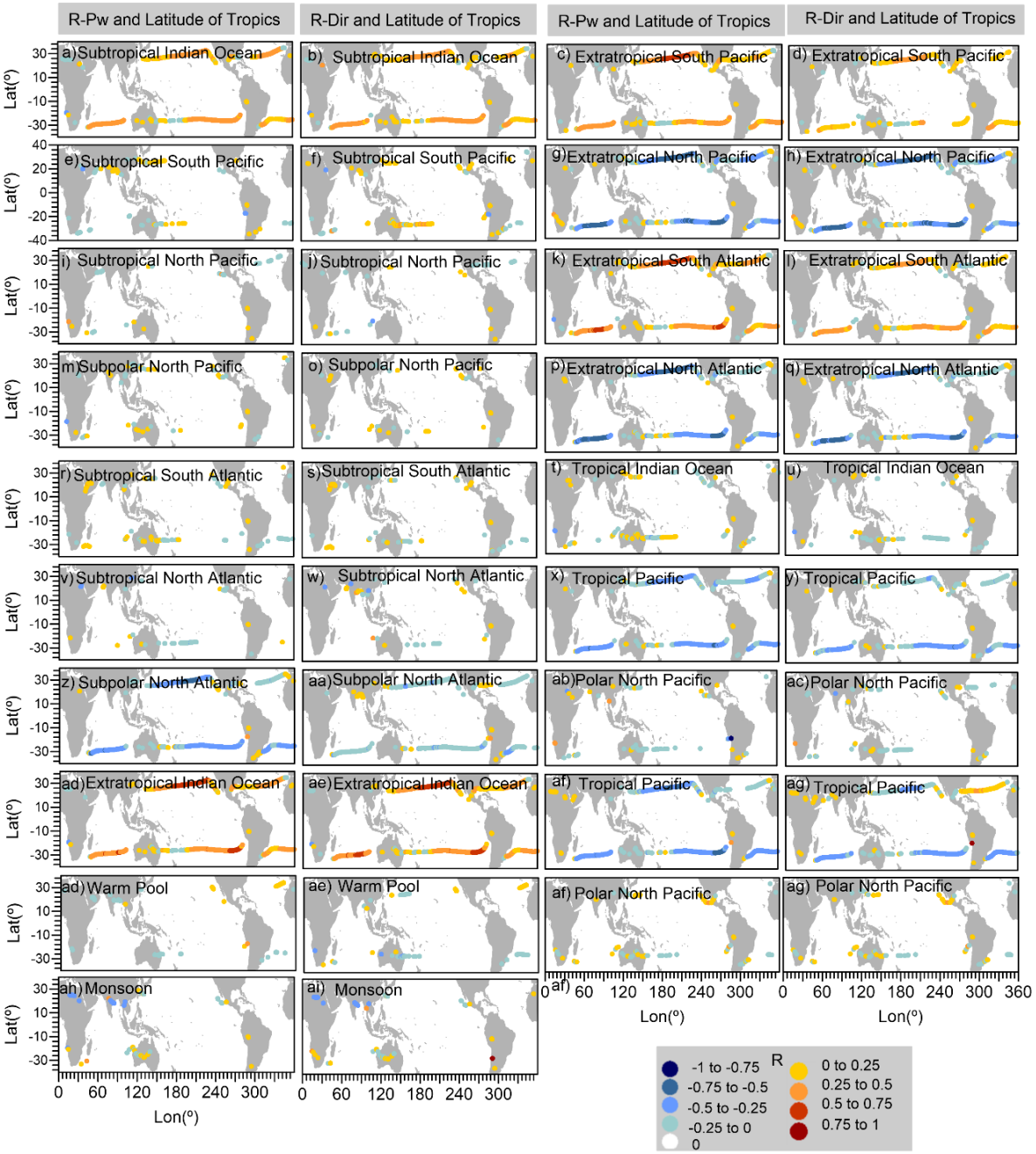


Figure 5. 9. Correlation coefficients between the latitude of tropical limits and wave power and mean wave direction of the wave climates types.

This analysis demonstrates that wave climates are more sensitive to displacements of particular regions. These regions showed high correlation coefficients and are depicted in Figure 5. 9 (deep red and blue), and were used to calculate the Expanding Tropics Indices. These areas are in the southern tropical limit: Central Indian Ocean, the Central and East Pacific. In the northern tropical limit: the Central Atlantic and Central-east Pacific.

## 5.5 Expanding tropics indices

Five Expanding Tropics indices (ETIs) were proposed to analyse the potential impacts of the phenomenon in the wave parameters. To see how the ETIs are calculated see section 2.5 in Chapter 2. One ETI was proposed for each regions N1 (180ºE; 110ºW) N2 (50ºW; 20ºW), S1 (60 ºE; 90 ºE), S2 (170 ºE; 135ºW), and S3 (100ºW; 80ºW). These regions were selected because they have a higher correlation with the WCTs and show expansion, seasonally and yearly. The ETIs have an upward trend in the northern regions and downward trend in the Southern regions, which means expanding, see Figure 5.10.

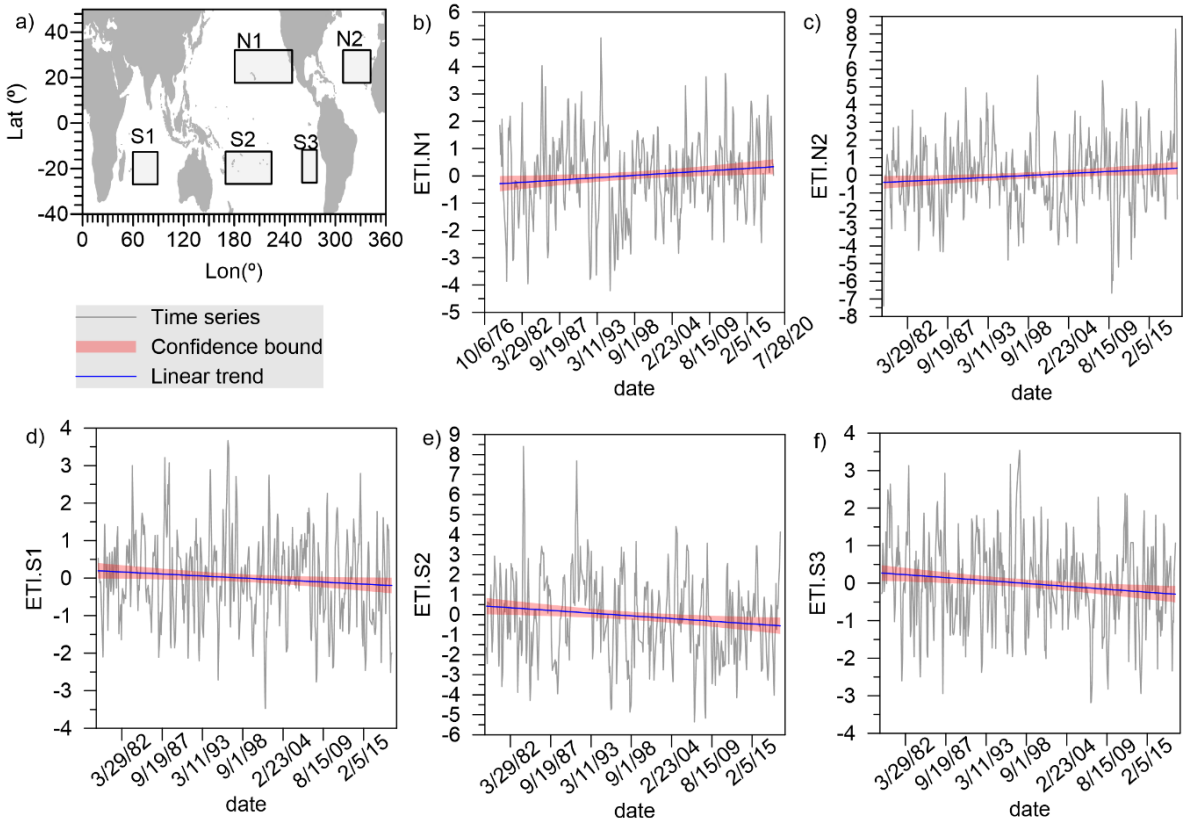


Figure 5. 10. a) Regions used for each ETI, and time series and trends of b) ETI.N1, c) ETI.N2, d) ETI.S1, e) ETI.S2, f) ETI.S2, and g) ETI.S3.

## 5.6 Expanding tropics impact the global coasts

This section shows the correlation between ETI indices and the monthly anomalies of wave power and mean wave direction on the coasts. The whole time series of the wave characteristics were used, instead of wave climate classification. The correlation with each ETI expresses how the tropical expansion at each region drives the wave climate.

When region N1 (North Pacific) expands, the wave power decreases in the eastern Pacific, and increases in the western tropical Northeast Atlantic and Pacific. The response in wave climate to N2 expansion (North Atlantic) is the same as N1, except for an intensification in the western Indian Ocean. The tropical expansion in the southern Pacific (S1) induced an increase in wave power in the East Pacific and a decrease in Eastern Atlantic. The widening of the tropical limits in the South Atlantic drives an increment in the wave power on the eastern of the Atlantic and Pacific Basins.

Although, a decrease in wave power was found in the Southern Caribbean Sea, Northeast Atlantic and West Pacific. The expansion of the tropics in the southeast Pacific intensifies the wave climate in the east Pacific and Indian Ocean, and reduces in the western tropical Pacific.

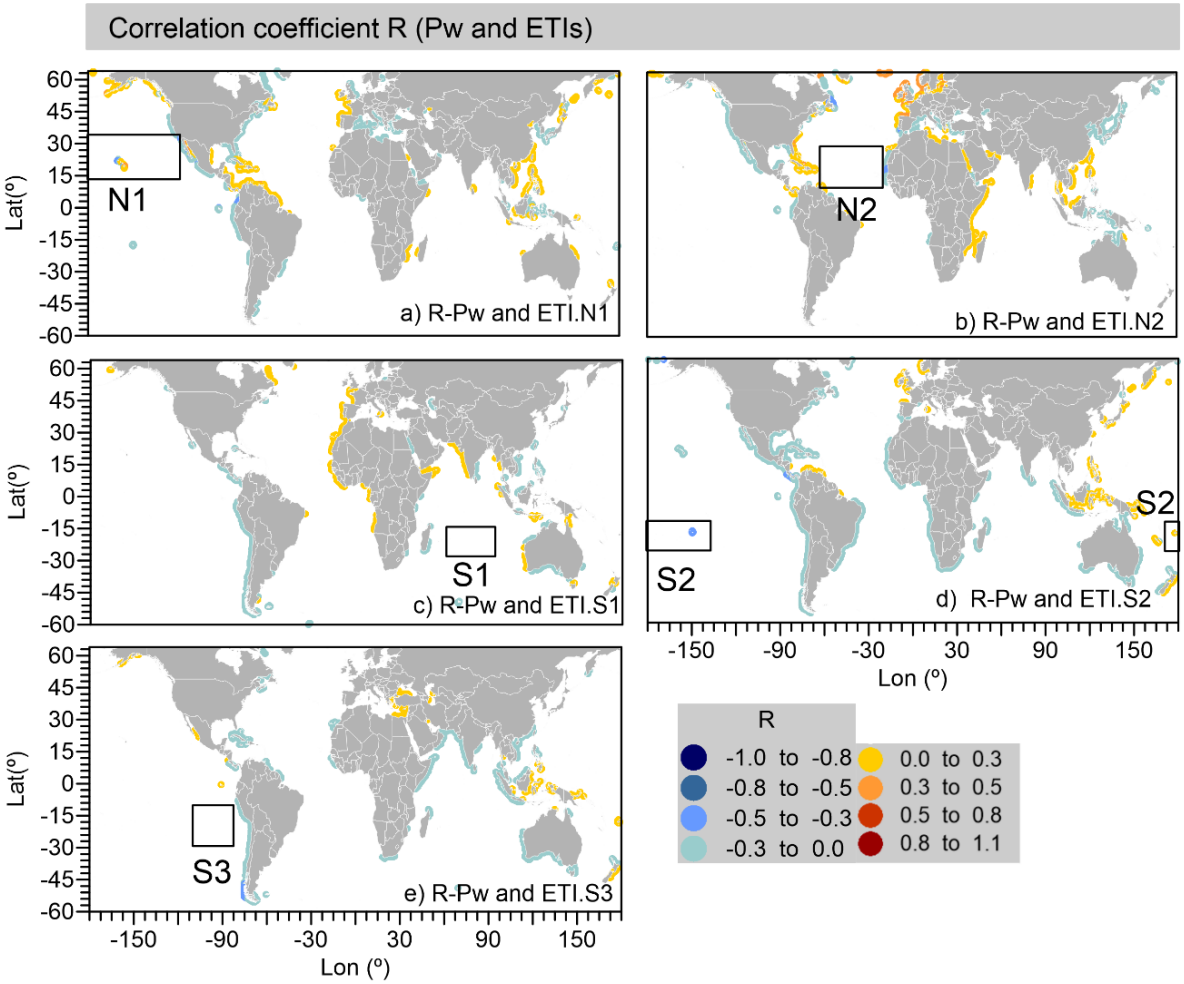


Figure 5. 11. Correlation coefficient between ETIs and the anomalies of wave power.

The wave direction shows a higher sensitivity to expanding tropics than wave power. The relative positions of Low and High-Pressure belts impact the wave direction, while their intensification impact the wave power. In this regard, it seems logical to have higher correlation coefficients with the direction than with the wave power. Furthermore, uncertainties exist about how the expansion /contraction of the tropics is related to the strength of the Hadley cells. Despite, it is known that ENSO (El Niño/La Niña) reinforces/reduces the Hadley cells when narrowing/widening. In this sense, we found opposite wave direction behavior to El Niño- pattern, especially in the Pacific basin. The expansion of the Southern regions porduced a general anticlockwise rotation for the southern basins. This aligns with the projections of the poleward expansion of the extratropical circulation.

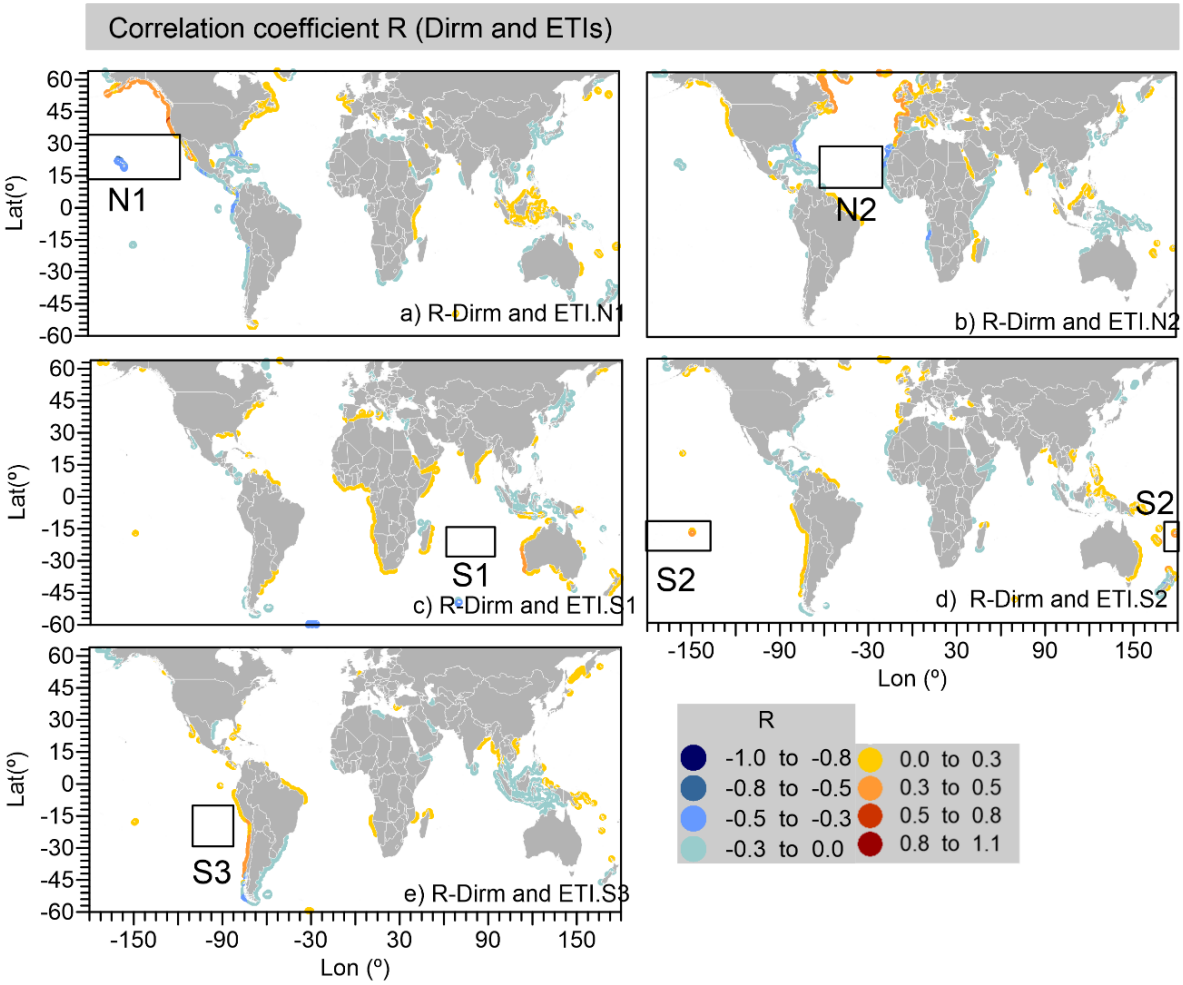


Figure 5. 12. Correlation coefficient between ETIs and the anomalies of mean wave direction.

## 5.7 Conclusions

One of the great challenges in present day climate science is to differ the inherent fluctuation forced by natural variability from those forced by climate change. This chapter analyses the expanding tropics and Chapter 3 the ENSO as wave climate drivers. The first is a consequence of the climate change and the second is a natural climate pattern. Both, expanding tropics and ENSO, have the capacity to impact the atmospheric circulation and affect the Hadley cells dynamics. As a consequence, both impact wave climate and must be considered for sustainable coastal management. While the expanding tropics appear to have an El Niño-like temperature distribution in the Pacific, the meridional response does not conform to this (Lu *et al.,* 2008). In the warm phases of ENSO, the Hadley Cells contract and intensify, the extratropical winds shift equatorward, the subtropical highs move towards the equator, which is the opposite to what happens with expanding tropics. However, both of them weaken the Walker Circulation (Lu et al., 2009; Lucas et al., 2014; Reichler, 2009).

The results show a tropical expansion in both Hemispheres (up to 3º). In MAM, some contractions were found in the boundaries sea-land of the Northern Hemisphere. Furthermore, a better understanding of the expanding tropics impacts on the ocean surface was developed. This could be relevant in the physics and validation of GCMs that perform the expansion but

underestimate its magnitude (Lucas et al., 2014).The regions of expansion that more impact wave climate are identified as N1 (Northeast Pacific), N2 (North Pacific), S1 (South Pacific), S2 (South Indian Ocean), and S3 (Southeast Pacific). For each region, five climate indices were proposed as indicators of the phenomenon, called ETIs (Expanding Tropics Indices). The width of tropics variation around the Earth is heterogeneous, as are its effects on wave climates. In Chapter 4, we have shown the wave climates types are driven by different planetary wind systems that are forced by a gradient of the permanent High Low-pressure belt. The Hadley cell limits (tropical limits) were demonstrated to be one of their generation mechanism. Thus, the expansion affects mainly the extratropical and tropical WCTs, and exceptionally the subtropical WCT in the Indian Ocean.

The wave direction was more sensitive to tropical expansion than wave power. As a result, in the North Pacific, the response of wave direction is opposite to ENSO warm phase. Then, the consequence of expanding tropics when coupled with ENSO will be different around the world, and they can either amplify or dampen impacts at the coasts. Concluding that the expanding tropics is happening and is a driver of wave climate, principally of wave direction, and should be integrated in coastal risk assessment.

**References**

Alves, J.-H. G. M. (2006). Numerical modeling of ocean swell contributions to the global wind-wave climate. *Ocean Modelling*, *11*(1), 98–122. https://doi.org/https://doi.org/10.1016/j.ocemod.2004.11.007

Archer, C. L., & Caldeira, K. (2008). Historical trends in the jet streams. *Geophysical Research Letters*, *35*(8). https://doi.org/https://doi.org/10.1029/2008GL033614

Babanin, A. V, Rogers, W. E., de Camargo, R., Doble, M., Durrant, T., Filchuk, K., et al. (2019). Waves and Swells in High Wind and Extreme Fetches, Measurements in the Southern Ocean. *Frontiers in Marine Science*, *6*, 361. https://doi.org/10.3389/fmars.2019.00361

Broccoli, A. J., Dahl, K. A., & Stouffer, R. J. (2006). Response of the ITCZ to Northern Hemisphere cooling. *Geophysical Research Letters*, *33*(1), 1–4. https://doi.org/10.1029/2005GL024546

Davis, S. M., & Rosenlof, K. H. (n.d.). A Multidiagnostic Intercomparison of Tropical-Width Time Series Using Reanalyses and Satellite Observations. *Journal of Climate*, *25*(4), 1061–1078. https://doi.org/10.1175/JCLI-D-11-00127.1

Fu, Q., Johanson, C. M., Wallace, J. M., & Reichler, T. (2006). Enhanced Mid-Latitude Tropospheric Warming in Satellite Measurements. *Science*, *312*(5777), 1179 LP – 1179. https://doi.org/10.1126/science.1125566

Hu, Y, & Fu, Q. (2007). Observed poleward expansion of the Hadley circulation since 1979. *Atmospheric Chemistry and Physics*, *7*(19), 5229–5236. https://doi.org/10.5194/acp-7-5229-2007

Hu, Yongyun, Zhou, C., & Liu, J. (2011). Observational evidence for poleward expansion of the Hadley circulation. *Advances in Atmospheric Sciences*, *28*(1), 33–44. https://doi.org/10.1007/s00376-010-0032-1

Hudson, R. D., Andrade, M. F., Follette, M. B., & Frolov, A. D. (2006). The total ozone field separated into meteorological regimes – Part II: Northern Hemisphere mid-latitude total ozone trends. *Atmospheric Chemistry and Physics*, *6*(12), 5183–5191. https://doi.org/10.5194/acp-6-5183-2006

Lu, J., Chen, G., & Frierson, D. M. W. (2008). Response of the Zonal Mean Atmospheric Circulation to El Niño versus Global Warming. *Journal of Climate*, *21*(22), 5835–5851. https://doi.org/10.1175/2008JCLI2200.1

Lu, J., Deser, C., & Reichler, T. (2009). Cause of the widening of the tropical belt since 1958. *Geophysical Research Letters*, *36*(3). https://doi.org/10.1029/2008GL036076

Lucas, C., Timbal, B., & Nguyen, H. (2014). The expanding tropics: A critical assessment of the observational

and modeling studies. *Wiley Interdisciplinary Reviews: Climate Change*, *5*(1), 89–112. https://doi.org/10.1002/wcc.251

Min, S.-K., & Son, S.-W. (2013). Multimodel attribution of the Southern Hemisphere Hadley cell widening: Major role of ozone depletion. *Journal of Geophysical Research: Atmospheres*, *118*(7), 3007–3015. https://doi.org/https://doi.org/10.1002/jgrd.50232

Mortlock, T. R., Baillie, Z., Goodwin, I. D., & Browning, S. (2020). Influence of the subtropical ridge on directional wave power in the southeast Indian Ocean. *International Journal of Climatology*, *n/a*(n/a). https://doi.org/10.1002/joc.6522

Reichler, T. (2009). Chapter 7 - Changes in the Atmospheric Circulation as Indicator of Climate Change. In T. M. B. T.-C. C. Letcher (Ed.) (pp. 145–164). Amsterdam: Elsevier. https://doi.org/https://doi.org/10.1016/B978-0-444-53301-2.00007-5

ROSENLOF, K. H. (2002). Transport Changes Inferred from HALOE Water and Methane Measurements. *Journal of the Meteorological Society of Japan. Ser. II*, *80*(4B), 831–848. https://doi.org/10.2151/jmsj.80.831

Seidel, D. J., & Randel, W. J. (2007). Recent widening of the tropical belt: Evidence from tropopause observations. *Journal of Geophysical Research: Atmospheres*, *112*(D20). https://doi.org/https://doi.org/10.1029/2007JD008861

Seidel, D. J., Fu, Q., Randel, W. J., & Reichler, T. J. (2008). Widening of the tropical belt in a changing climate. *Nature Geoscience*, *1*(1), 21–24. https://doi.org/10.1038/ngeo.2007.38

Timbal, B., & Drosdowsky, W. (2013). The relationship between the decline of Southeastern Australian rainfall and the strengthening of the subtropical ridge. *International Journal of Climatology*, *33*(4), 1021–1034. https://doi.org/https://doi.org/10.1002/joc.3492

Wandres, M., Pattiaratchi, C., Wijeratne, E. M. S., & Hetzel, Y. (2016). The Influence of the Subtropical High-Pressure Ridge on the Western Australian Wave Climate. *Journal of Coastal Research*, *75*(sp1), 567–571. https://doi.org/10.2112/SI75-114.1

# CHAPTER 6

# Wave Climate in the Next Century

This work in this chapter was made possible through the 2019 DPRI Collaborative Research (2019L-03) at the Disaster Prevention Research Institute of Kyoto University, under the supervision of Prof. Mori and in collaboration with Dr. Shimura and Dr. Webb. The chapter explores wave climate changes in the next century, for the RCP 2.6 and 8.5. The supporting information is given in APPENDIX A3.

The chapter is based on

Odériz I. Mori N. Shimura, Web A. Silva R., Mortlock R.M. Changes in Prevailing Wave Climates on the Global Continental and Polar Coasts under Warmer Scenarios (In preparation)

## 6.1 Introduction

This chapter seeks to identify and quantify wave climate changes driven by the atmospheric circulation using the scenarios of RCP 2.6 and 8.5. The wave climates, postulated in Chapter 4, were identified for climate change scenarios. Then, we examined the seasonal differences in wave climates of present conditions and climate change scenarios, studying wave power, direction, and area covered. We related these to shifts in the atmospheric circulation.

The results for the RCP 2.6 are shown in APPENDIX A3. A more detailed description of the method is found in Chapter 2 (section 2.6).

## 6.2 Net projected changes in wave climate

Before addressing changes induced by climate change in the wave climates, (previously defined in Chapter 4), we analysed the projected net global wave climate variation for the next century. The dataset is part of the ensemble used in Morim et al. (2019). In consequence, the results of this section are in agreement with their findings. However, we also examined wave power to understand the implications on energy harvesting and variations in wave energy distribution across the oceans. Figure 6.1 and Figure 6.2 show the differences between present conditions and the RCP 8.5 scenario, for yearly and seasonally averages, respectively.

The wave power of the Southern Ocean and Southeast Pacific is projected to increase in JJA (+ 5 to +30 kW/m). Whilst in DJF, the wave power will increase in the entire basin (+0.5 to +5 kW/m). In the South Atlantic, wave power will increase in JJA (+2 to +10 kW/m) and SON (+0.5 to +2 kW/m). Whereas in the Indian Ocean, the wave climate only intensifies in JJA (up to +1 kW/W). In DJF, there will be a significant decrease in wave power in the Northwest Pacific (up to-20 kW/m), the North Atlantic (up to -25 kW/m), and the Indian Ocean (up to – 4 kW/m).

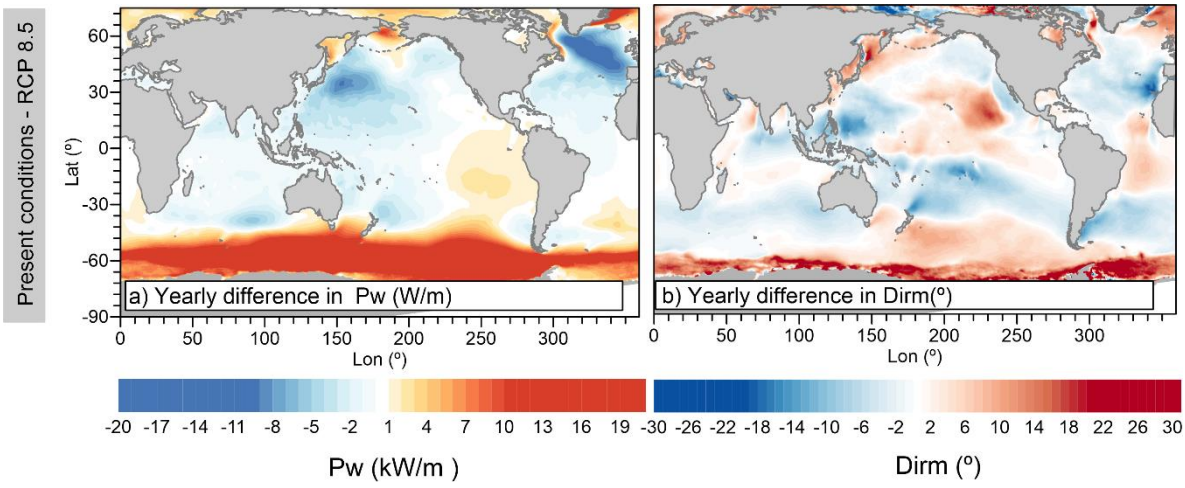


Figure 6.1 Differences between RCP 8.5 conditions (2075-2099) and present conditions (1979-2003) in a) wave power and b) mean wave direction.

Throughout a year, in the Northern Hemisphere, including the Indian Ocean, the mean wave direction will have an El Niño-like pattern. Meanwhile, in the Southern Hemisphere, it will have a La Niña-like pattern. In the Indian Ocean, the wave mean direction will shift anticlockwise in JJA (up to -15º). In contrast, in DJF and SON, on the western coast of the Indian Ocean and in the subtropical belt, the wave mean direction will shift clockwise (up to +11°). In DJF, in the extratropical latitudes

of the North Pacific the wave mean direction will shift clockwise (up to +30°), and in the rest of the Pacific region it will shift anticlockwise (up to -30°). For the other seasons (SON, MAM, and JJA), the wave mean direction in the Northcentral and tropical Pacific will shift clockwise (up to +25°), and in the Northeast Pacific anticlockwise (up to -30°), following an El Niño-like pattern. All year round, the wave mean direction in the Pacific part of the Southern Ocean will shift clockwise (up to +15°) and anticlockwise in the Atlantic and Indian Ocean parts. In general, the subtropical belt of the Southern Hemisphere will shift anticlockwise (up to -15°). All year round, the mean wave direction in the Atlantic Ocean will shift clockwise (up to +20°), with the exception of the tropical and mid-latitudes of the North Atlantic, where it will shift anticlockwise (up to -25°). In MAM, in the Atlantic, the mean wave direction will shift anticlockwise (up to +15°) and in the North Atlantic, clockwise (up to +8°).

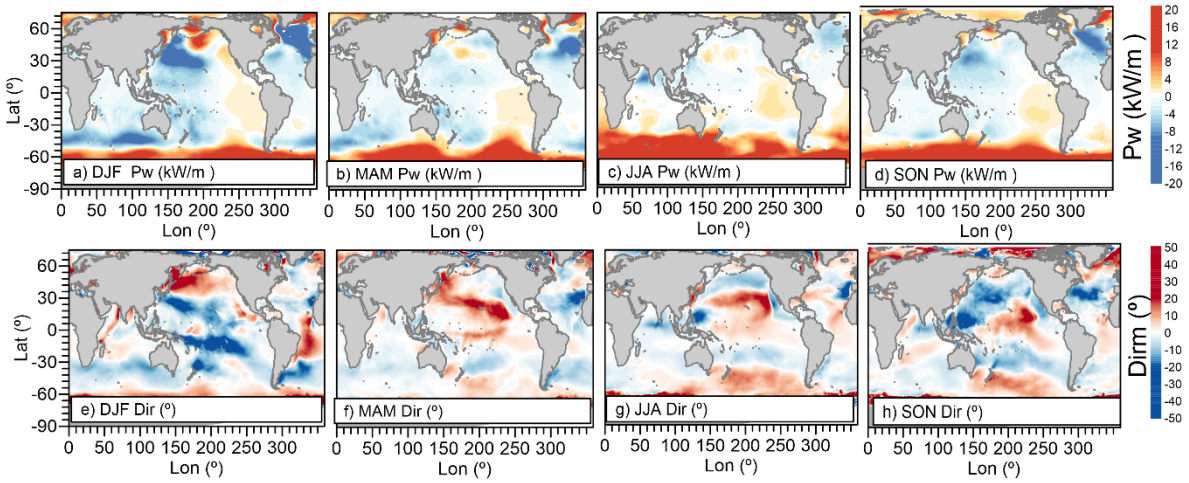


Figure 6.2 Differences between RCP 8.5 (2075-2099) and present conditions (1979-2003) in (a, b, c, d) wave power and (e, f, g, h) mean wave direction in, (a, e) DJF, (b, f) MAM, (c, g) JJA, and (d, h) SON.

## 6.3 Projected changes in wave climates induced by atmospheric circulation

The dynamic *k-mean* clustering technique was applied to present day conditions using the computed method of Chapter 4. The centroids obtained for the dataset of present conditions (1979-2003) were similar to those obtained from the reanalysis datasets ERA5 (1979-2018 and 1979-2017) and JRA-55 (1979-2017), obtaining the same wave climates(see Chapter 4). The classification was repeated for the RCP 2.6 and 8.5 scenarios, using the previously obtained centroids from present day conditions, rather than generating new ones. The same wave climates were identified for the next century (Figure 6.3) by the classification for the two RCP scenarios. Shifts in wave climates are the consequence of changes in atmospheric circulation, as the wave climates are implicitly linked to their origin in the planetary wind systems.

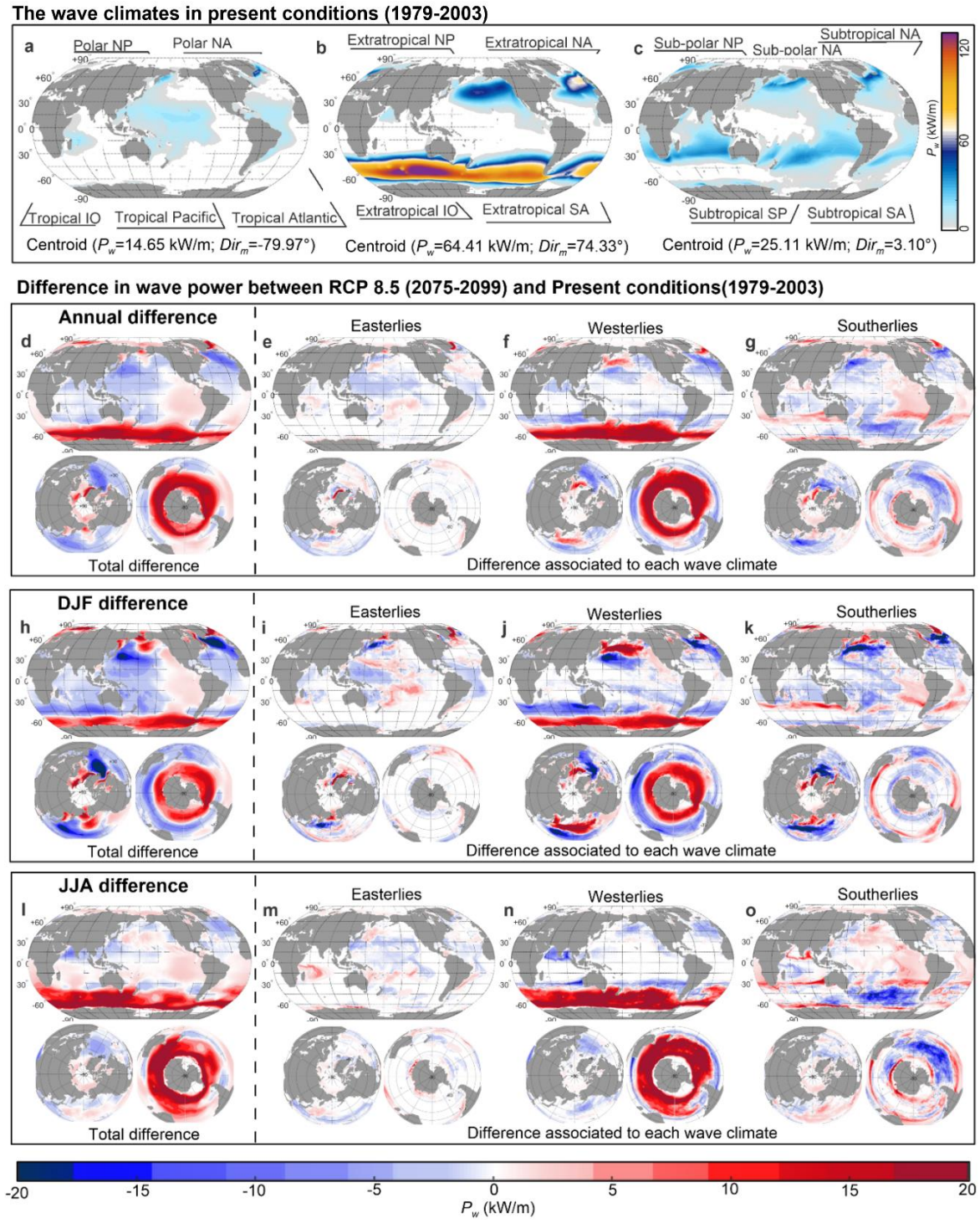


Figure 6.3 Annual average of wave power for 1979-2003, of the (a) easterly, (b) westerly, and (c) southerly wave climates. (d, h, l) Differences in net wave power between RCP 8.5 and present conditions. Difference in wave power associated with the easterly, (e, i, m) westerly (f j, n), and southerly (g, k, o) wave climates, (d-g) annual, (h-k) DJF, and (l-o) JJA.

### 6.3.1 Changes in wave power

Figure 6.3 compares changes in wave power for the climates in the projected RCP 8.5 scenario with those of present conditions. In the North Atlantic, the wave power in the polar climate will increase to +20 kW/m. This coincides with the intensification in the projected polar atmospheric circulation, caused by lower pressure than there is at present over the poles (Screen et al., 2018) and an increasing positive phase of the annular modes (Arctic Oscillation for the Northern Hemisphere). The coasts of Greenland and Northeast Russia will be affected by these changes (up to +20 and +10 kW/m, respectively). The intensification is greater in DJF, MAM, and SON. In addition, the wave power of the subpolar wave climates of the North Pacific and North Atlantic will increase in DJF and MAM (up to +10 and +20 kW/m) caused by the stronger northern polar circulation. The escalation in wave power has repercussions in the Atlantic and Pacific (Figure 6.3).

The polar atmospheric circulation is key in the global wind systems (Screen et al., 2018) and changes in it modify the surface westerly winds. Under negative pressure and an increasing positive phase of the Arctic and Southern Antarctic Oscillations, more intense, poleward extratropical winds will be produced (Miller et al., 2006; Nazarenko et al., 2015). This phenomena will intensify the extratropical wave climate in the high-latitudes of the Northeast Atlantic, Northeast Pacific (+10-25 kw/m), and in the Southern Ocean (+20 kW/m). On the other hand, the extratropical wave climate will weaken in the mid-latitudes of the aforementioned regions. In the Southern Ocean, the highest wave intensification will be in JJA, due to the more positive trend projected for the SAM in this season, and its impacts on the extratropical winds (Lim et al., 2016).

Overall, the tropical wave climate is projected to decrease as a response to greenhouse gas emissions, causing a weakening in the east-west tropical circulation (Held & Soden, n.d.; Lu et al., 2009). Some exceptions can be found in the boundaries of the South Atlantic and South Pacific wave climates that are projected to have a small gain in wave power. This gain could be caused by an increase in frequency of this wave climate in DJF. This is probably related to the expansion of the tropics (Lucas et al., 2014), which is more apparent during DJF in the Southern Hemisphere. In the south of the Indian Ocean, an increase is produced in JJA and MAM (up to +10 kW/m). A similar case is seen in the southern Caribbean Sea, where in the same seasons there is an increase in wave power (see Appendix A4). This occurs because the Caribbean Sea is getting warmer than the Atlantic Ocean, creating a strong pressure gradient (Nazarenko et al., 2015), which increases wind velocity (Costoya et al., 2019) and wave power over the region.

A decrease of -20 kW/m wave power for the monsoon wave climate is expected, coinciding with the weakened monsoon winds. This is forced by the ITCZ displacement toward the warmer Northern Hemisphere (Seth et al., 2019), see Figure 6.3.

Figure 6.3 (k, d, o, h) shows that the subtropical wave climate of the North Pacific is projected to weaken, up to -10 kW/m, forced by a debilitated Northeast Pacific subtropical high pressure centre. In contrast, this wave climate in the southeast Pacific will strengthen, up to +15 kW/m, all year round, but more energetic in JJA and SON, caused by the intensification of the South Pacific subtropical high (He et al., 2017).

In the Indian and South Atlantic Oceans, the subtropical wave climate will lessen in line with the weakening high-pressure belts in these regions (Cherchi et al., 2018), see Figure 6.3. However, an exception exists in the belt that limits the extratropical and subtropical wave climates. In these regions the wave power is projected to strengthen. This may be related to the poleward displacement of the extratropical winds (He & Zhou, n.d.; Shaw & Voigt, 2015). In these latitudes the southerlies wave climate will be more prevalent.

Overall, the increase in total wave power will be concentrated in the high-latitudes, more so in the Southern Hemisphere (extratropical and subtropical wave climates) than in the Northern Hemisphere (polar and subpolar wave climates). In the Southern Hemisphere, all the wave climates will show an increase in wave power. While in the Northern Hemisphere, the tropical, the extratropical in mid-latitudes, and subtropical wave climates will have less energy, on average.

### 6.3.2 Changes in wave direction

The projected changes in mean wave direction are calculated only for those areas where the frequency of each wave climate is over 60%. Unlike the wave power, the mean wave direction cannot be divided by the complete temporal range, it is divided by the number of months in which the wave climate occurs. Otherwise, the physical magnitude of the direction loses its meaning. Therefore, in the areas where the wave climate frequency is low, the difference in mean wave direction is not representative for the mid and long-term.

For the most part, the results show an anticlockwise rotation in high-latitudes and clockwise for the rest of the oceans, in line with (Morim et al., 2019), except for the high-latitudes of the Southern Ocean and the North Pacific. In the Atlantic, anticlockwise shifts in mean wave direction of the tropical wave climate are limited to the northern region, and are induced by the shift to the northwest of the High-Pressure system (Choi et al., 2016; Shaw & Voigt, 2015). In the South Atlantic, the wave climate shifts clockwise (~ +15°), forced by a displacement southward of the High Pressure of this region (He et al., 2017), and linked with the expanding tropics (Lucas et al., 2014).

In the Pacific Ocean, the tropical wave climate shifts anticlockwise (~-20°) in DJF, and clockwise in MAM and JJA (~ +15°). In the North Pacific, in DJF, the extratropical and subpolar wave climate will shift clockwise, forced by the displacement southeast of the Aleutian Low (Choi et al., 2016). In DJF, the increasing positive phase of the Southern Antarctic Oscillation will produce a poleward shift in the extratropical winds (Miller et al., 2006; Nazarenko et al., 2015), and therefore in these wave climates (~ +20°). Between the latitudes 45°S and 30°S, the subtropical wave climate will shift anticlockwise, associated with the displacement southward of the South Pacific, Indian Ocean, and South Atlantic High Pressure centres (He et al., 2017).

### 6.3.3 Changes in the area covered by each wave climate

The area of the easterly wave climates will expand globally by 2.5%, and even more in the Pacific (up to 3.7 %), Figure 6.5. The opposite occurs to the westerlies, which have a reduction in area globally (-1%), but most in the Indian Ocean (-5%) and in the Pacific, -3.5%.

There is, however, an exception in the Southern Ocean, where the area covered by the easterlies falls almost -12% and increases +22% for the westerlies. This is related to the reduction of the Marginal Ice Zone (MIZ) and the poleward displacement of the extratropical atmospheric circulation (Chen et al., 2008). In SON, the area of all the wave climates expands in this region. The southerlies expand globally, with the greatest expansion being in the Indian Ocean (+4.5 %), while there is a reduction of -8.4% in the Southern Ocean.

In the Indian Ocean, in DJF, the area of the southerlies will increase (+8 %), while that of the easterlies will decrease (-2 %). The westerly wave climate will also decrease in area (-7 %). In this region, the area of the easterly wave climate will increase in JJA by +5 %.

In the Pacific Ocean, the area covered by the easterlies will increase most in SON (+8.4 %) and DJF (+5.8 %), while the westerlies will decrease, and the southerlies will increase in area all year round, except in SON.

In the Atlantic Ocean, the area of the easterlies will expand in all seasons, except in JJA, on the contrary, the area of the westerlies will generally decrease, and will expand up to + 3% in JJA. Meanwhile, the area of the southerlies will expand during DJF and MAM (up to +6%).

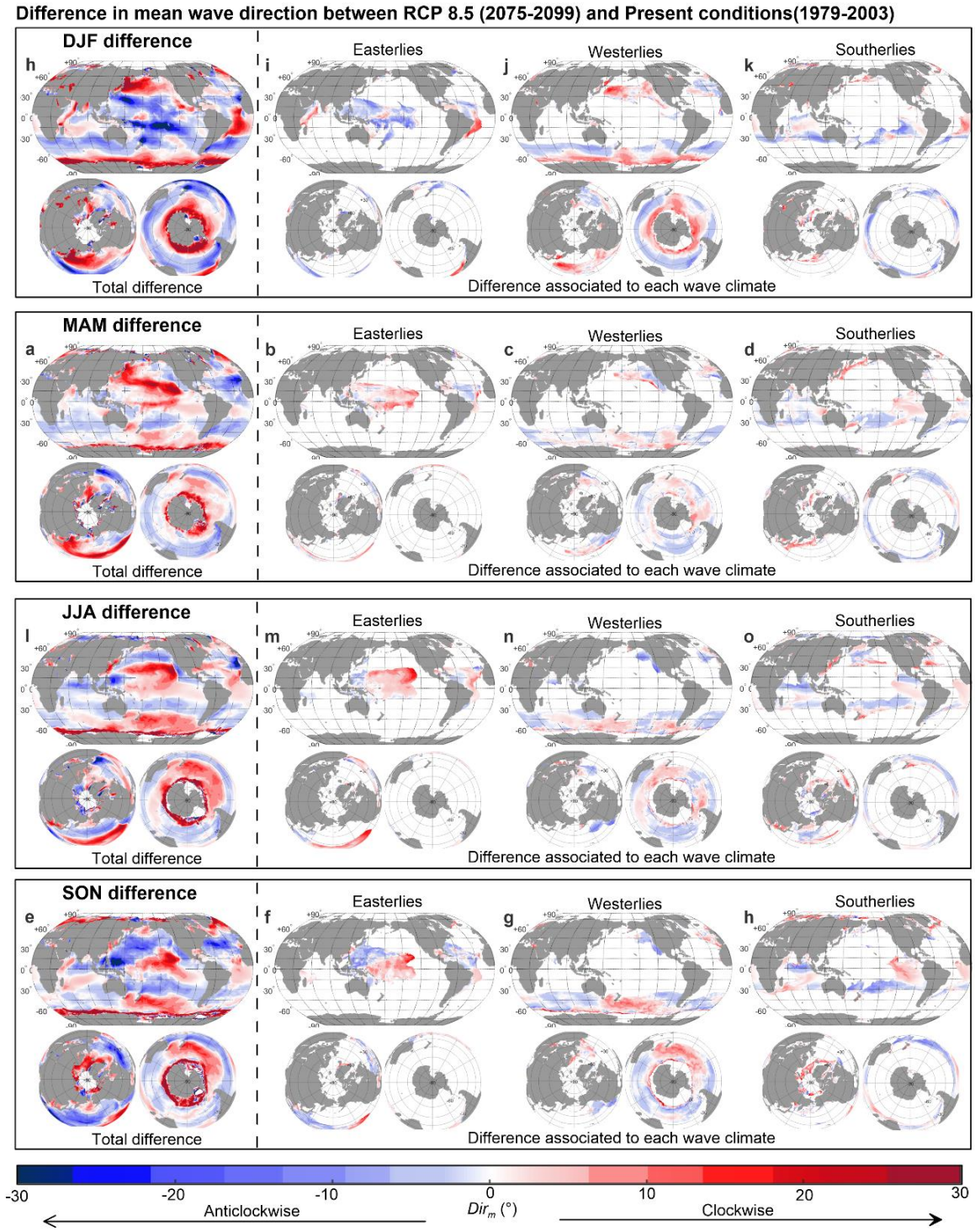


Figure 6.4 Differences between RCP 8.5 and present conditions in mean wave direction, (a, d, g and j) for the easterlies, (b, e, h, k) for the westerlies, and (c, f, I, l) for the southerlies, (a, b, c) in DJF, (d, e, f) in MAM, (g, h, i) JJA, and (j, k, l) in SON.

a

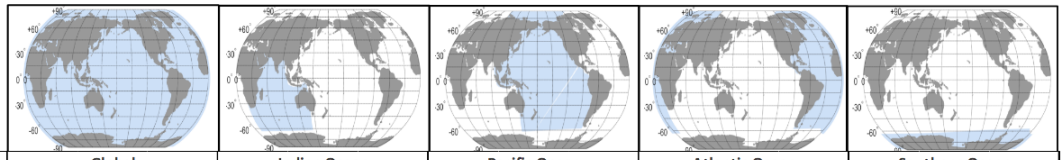

| Season | Wave climate | Global | | | Indian Ocean | | | Pacific Ocean | | | Atlantic Ocean | | | Southern Ocean | | |
|---|---|---|---|---|---|---|---|---|---|---|---|---|---|---|---|---|
| | | Present Conditions | RCP 2.6 | RCP 8.5 | Present Conditions | RCP 2.6 | RCP 8.5 | Present Conditions | RCP 2.6 | RCP 8.5 | Present Conditions | RCP 2.6 | RCP 8.5 | Present Conditions | RCP 2.6 | RCP 8.5 |
| | | Extension (%) | Relative (%) increase/ decrease | Relative(%) increase/ decrease | Extension (%) | Relative (%) increase/ decrease | Relative(%) increase/ decrease | Extension (%) | Relative (%) increase/ decrease | Relative(%) increase/ decrease | Extension (%) | Relative (%) increase/ decrease | Relative(%) increase/ decrease | Extension (%) | Relative (%) increase/ decrease | Relative(%) increase/ decrease |
| Year | Easterlies | 18.38 | 0.45 | 2.51 | 8.29 | 1.72 | 0.01 | 27.28 | -0.09 | 3.64 | 17.15 | 0.61 | 1.60 | 3.56 | 14.16 | -12.39 |
| | Westerlies | 23.34 | 0.75 | -1.41 | 29.93 | -1.05 | -4.85 | 23.20 | 1.78 | -3.53 | 19.07 | -0.21 | -2.11 | 29.72 | 4.23 | 22.23 |
| | Southerlies | 27.12 | 1.03 | 2.32 | 31.69 | 0.56 | 4.51 | 30.67 | 0.27 | 1.66 | 23.42 | 1.99 | 2.72 | 11.48 | 9.77 | -8.38 |
| DJF | Easterlies | 18.12 | 2.62 | 3.20 | 12.80 | -1.66 | -1.71 | 24.64 | 6.07 | 5.80 | 16.37 | -2.00 | 1.91 | 5.76 | -2.08 | -23.72 |
| | Westerlies | 27.46 | 0.19 | -2.06 | 27.88 | -1.08 | -7.76 | 30.66 | -0.52 | -3.20 | 22.07 | 1.42 | -2.69 | 38.40 | 3.51 | 18.34 |
| | Southerlies | 23.79 | -0.36 | 3.34 | 29.24 | 1.75 | 7.91 | 25.37 | -3.91 | 1.90 | 20.50 | 4.04 | 5.64 | 15.52 | -2.57 | -25.43 |
| MAM | Easterlies | 17.72 | -0.24 | 0.94 | 6.04 | 4.91 | 0.16 | 27.77 | -1.73 | -0.21 | 15.78 | 1.88 | 4.46 | 3.87 | 2.74 | -12.06 |
| | Westerlies | 22.68 | 1.81 | -2.15 | 27.02 | -0.45 | -5.47 | 22.04 | 3.51 | -1.79 | 18.75 | 0.88 | -5.10 | 37.80 | 2.52 | 11.22 |
| | Southerlies | 28.70 | 0.20 | 3.74 | 36.85 | -0.48 | 3.99 | 30.89 | -0.01 | 3.34 | 24.23 | 0.85 | 5.05 | 14.39 | 4.17 | -3.14 |
| JJA | Easterlies | 18.54 | 0.61 | -0.11 | 5.49 | 12.32 | 5.05 | 28.80 | -2.42 | 0.72 | 17.72 | 3.45 | -2.77 | 2.53 | 49.21 | -5.63 |
| | Westerlies | 20.83 | -0.11 | 0.96 | 34.59 | -2.45 | -2.55 | 17.20 | 2.88 | -1.80 | 17.77 | -1.83 | -0.94 | 20.38 | 3.33 | 42.34 |
| | Southerlies | 29.12 | 1.90 | 1.98 | 29.84 | 0.59 | 1.83 | 35.63 | 2.14 | 1.85 | 25.01 | 0.05 | 2.94 | 9.05 | 35.16 | -3.05 |
| SON | Easterlies | 19.14 | -1.12 | 5.90 | 8.82 | -2.17 | -1.21 | 27.92 | -1.48 | 8.41 | 18.73 | -0.86 | 3.15 | 2.09 | 37.56 | 0.51 |
| | Westerlies | 22.40 | 1.17 | -2.06 | 30.23 | 0.05 | -4.23 | 22.90 | 2.35 | -6.94 | 17.69 | -1.76 | 0.71 | 22.30 | 9.19 | 28.69 |
| | Southerlies | 26.86 | 2.21 | 0.31 | 30.84 | 0.65 | 4.47 | 30.80 | 1.83 | -0.42 | 23.93 | 3.40 | -2.33 | 6.95 | 15.84 | 5.75 |

Figure 6.5 Differences in the area covered by the wave climates between the two RCP scenarios and present conditions, by basin.

## 6.4 The transitional wave climate regions

We assume that severe impacts in sediment transport and energy flux that alter the coastal environment will be induced not only by changes in storminess but also by the spatial changes affecting the prevailing wave climates, meaning that they will impact areas where, until now, they did not. We call these areas the “transitional wave climate regions”. These will undergo substantial modifications in their prevailing climate characteristics (e.g. tropical-subtropical, subtropical–extratropical, extratropical–polar) and are seen as critical areas in the face of climate change (Duarte et al., 2020). The “coastal transitional wave climate regions” have not been yet investigated in wave climate research. In this work we identify them and explore changes in the critical areas, continental coasts, the effects on sea ice, and on permafrost coastlines, according to the Special Report on the Ocean and Cryosphere (H.-O. Pörtner et al., 2019).

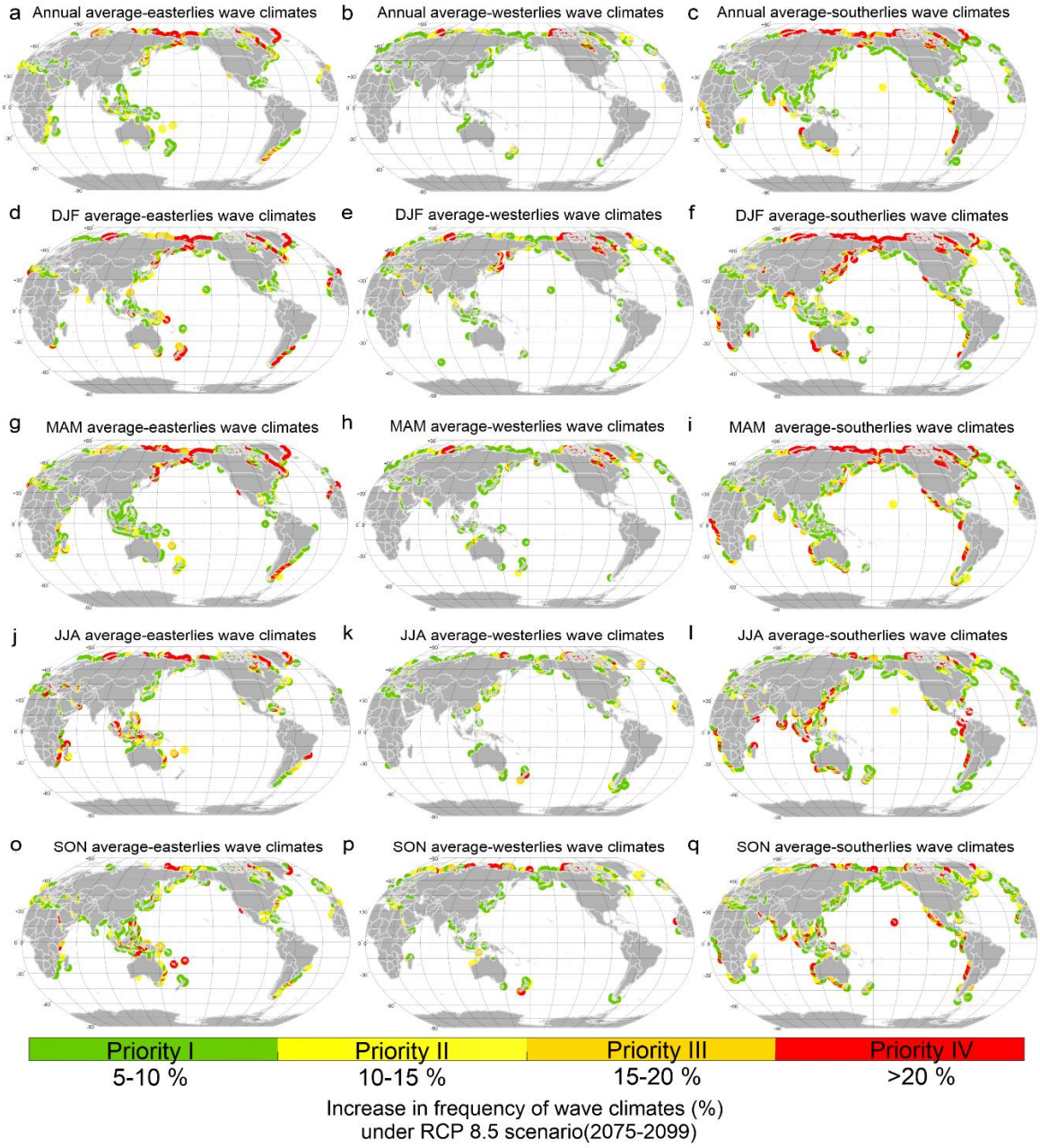


Figure 6.6 The transitional wave climate regions in RCP 8.5 scenarios in the continental coasts of (a, d, g, j, o) easterlies, (b, e, h, k, p) westerlies, and (c, f, i, l, q) southerlies. For (a-c) annual, (d-f) DJF, (g-i) MAM, (j-l) JJA, and (o-q) SON.

As mentioned earlier, the wave climates described in this chapter are classified by direction and wave power. In that sense, an increase in their frequency will affect near-shore wave conditions. Hence, we classified the coasts using a priority scale, based on the increase in frequency of the wave climates (I: 5-10 %, II: 10-15 %; III: 15-20 %; and IV: >20 %), see Figure 6.6, 6.7, and 6.8.

Overall, in the East Pacific (e.g. Chile, Mexico, Colombia, Peru, Ecuador), the Southeast Atlantic (i.e. Cameroon, Nigeria, Gabon, Republic of Congo, Angola), and south and east of Australia the southerlies wave climate will prevail more, being more frequent in MAM and JJA. In the Northwest

Atlantic and in the Southwest of all the ocean basins, this wave climate will decrease in frequency and the easterlies wave climate will be more prevalent. The extratropical wave climate will decrease in the mid-high latitudes, and will increase in frequency in the North Polar Region and New Zealand, due to the displacement poleward of the extratropical winds (Miller et al., 2006; Nazarenko et al., 2015). In some regions, the seasonal variability will increase the bimodality of the wave climates. For instance, in Hawaii, the southerly wave climate will become more prevalent all year-round, but the easterly wave climate will increase in frequency in DJF. The southerly wave climate will increase up to +2 kW/m in the North Indian Ocean, and up to +8 kW/m in Chile, Peru, Namibia, and South Africa. In general, in MAM, JJA and SON, the extratropical wave climate will decrease in frequency in all the ocean basins, with the exception of the higher latitudes of Chile, Australia, New Zealand, and in the Northern Hemisphere all year round. The wave power of the easterly wave climate will increase up to +2 kW/m on the east coast of the U.S.A, the southeast of Africa (Kenya, Tanzania, Mozambique, and Madagascar), the southeast Pacific, and the northeast of the Atlantic and Pacific basins.

In a changing planet, due to the melting ice, the areas affected by sea ice will be potential new marine regions, and will play an essential role in wave-ice interaction. This interaction will increase the fetch of the waves, if the broken ice melts, or will decrease the wave development if the ice freezes again (Liu et al., 2016; Rogers et al., 2018; Thomson & Rogers, 2014). On the other hand, the waves in polar regions may act as an ecological driver, transport new species, pollution, alter the carbon cycle, accelerate ice retreat and expose the coast to erosion (Fraser et al., 2018; Lantuit et al., 2012). In the case of the RCP 8.5 scenario, the retreat of sea ice is critical, (see Appendix A4). The results we show for the polar regions must be interpreted cautiously, because current wave models do not address the waves-ice interaction.

In the Arctic circle, a sea-level rise of 0.2 m is predicted; higher than the average for the rest of the world (Pörtner et al., 2019). Furthermore, an average coastal erosion of 0.5 m/year has already been reported in these areas (Lantuit et al., 2012). Our work also shows that the Arctic shoreline will be more exposed to the subpolar and polar wave climates. Parts of Canada and Russia will be more exposed to westerlies in SON. The subpolar wave climate will be prevalent in SON and DJF, while the polar wave climate will affect Greenland and Alaska. The Siberian coast, where the highest rate of erosion for permafrost coastlines (above 3 m/year) has been detected (Lantuit et al., 2012), will be the most impacted by changes of the three climates; in DJF and MAM by the subpolar and polar WCTs, in SON by the subpolar and extratropical WCTs, and in JJA by the polar WCT.

In Antarctica, the part corresponding to the Indian Ocean (0°-180°E) will be most affected by the extratropical WCT in DJF, the polar WCT in JJA, and subpolar WCT in JJA and SON. The Weddell Sea will be protected from the westerlies by the Antarctica peninsula, but will be affected by the easterlies and southerlies. The Ross Sea will be affected by southerlies all year round, with the exception of DJF, when more easterlies and westerlies waves reach its coasts.

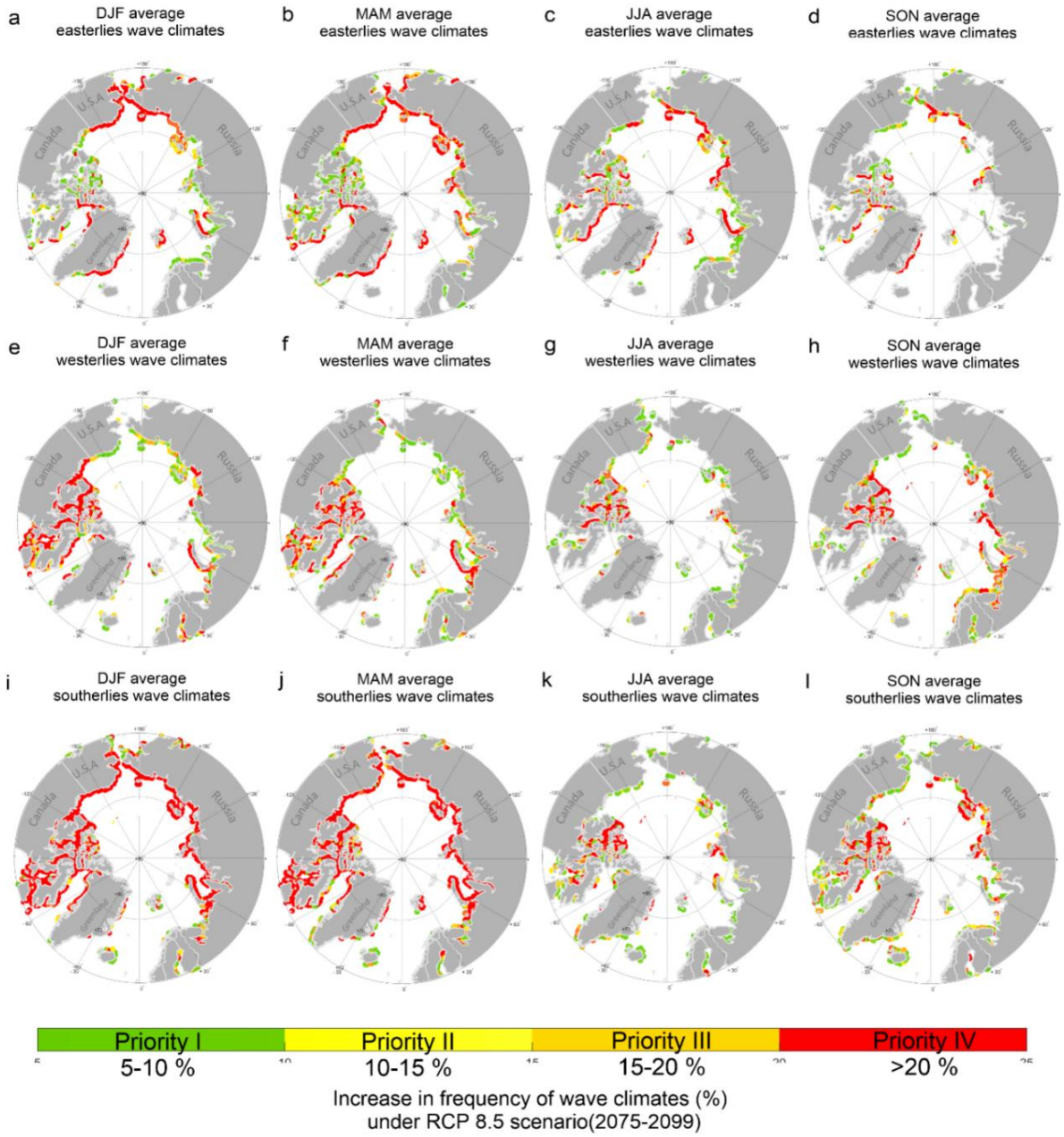


Figure 6.7 The transitional wave climate regions in RCP 8.5 scenarios in the Arctic coasts of (a, -d) easterlies, (e-f) westerlies, and (i-l) southerlies. For (a, e, i) DJF, (b, f, h) MAM, (c, g, k) JJA, (d, h, l) SON.

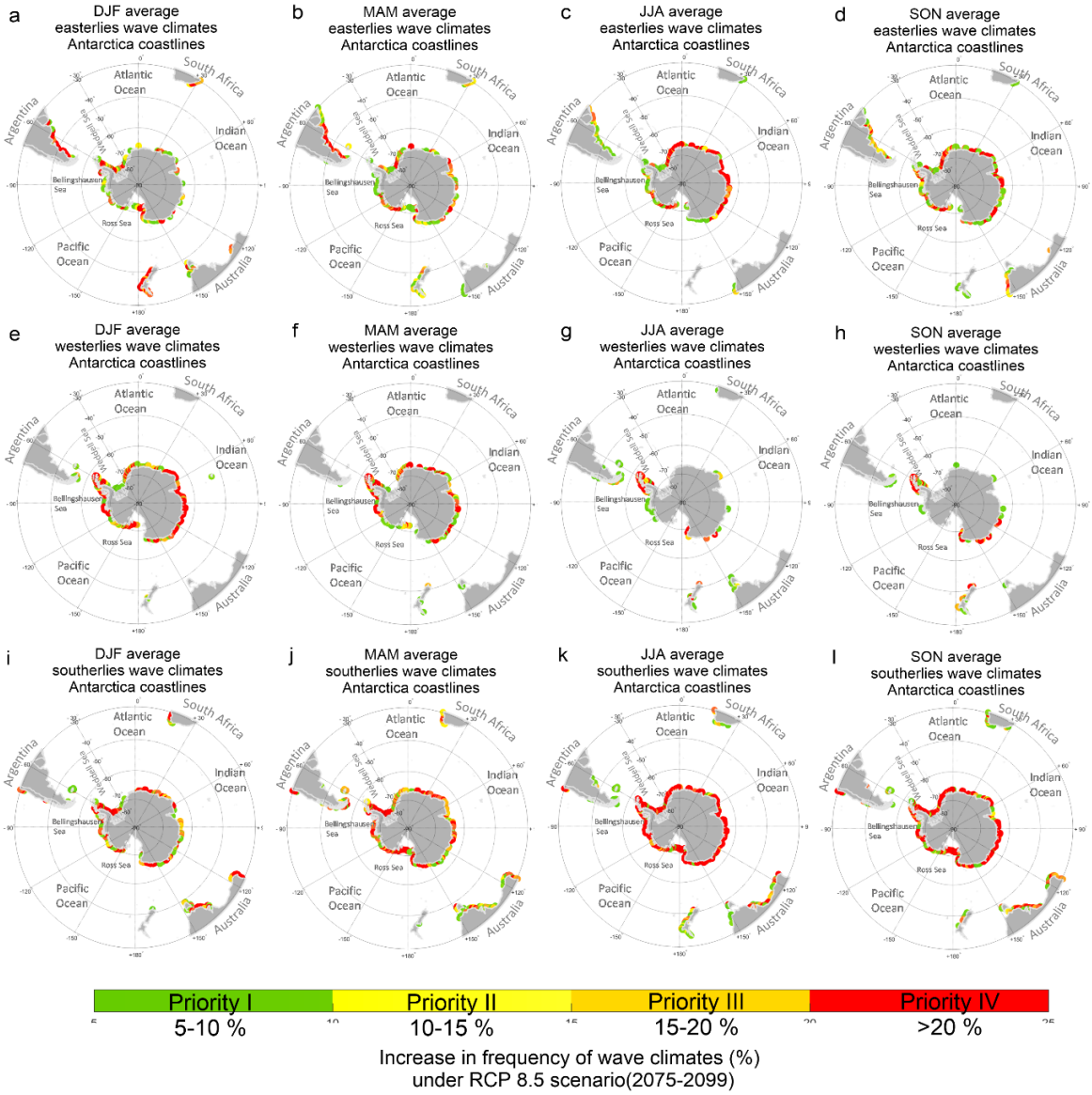


Figure 6.8 The transitional wave climate regions in RCP 8.5 scenarios in the Antarctic coasts of (a, -d) easterlies, (e-f) westerlies, and (i-l) southerlies. For (a, e, i) DJF, (b, f, h) MAM, (c, g, k) JJA, (d, h, l) SON.

## 6.5 Conclusions

In this chapter we identified the major westerly, southerly, and easterly wave climates driven by the wind planetary systems in the next century for the scenarios of RCP 2.6 and 8.5. Changes induced in them by atmospheric circulation were also described. This analysis provides a comprehensive spatial-temporal variation of projected changes under warmer scenarios.

The increase in wave power will be most noticeable in the Polar Regions and in the Southern Hemisphere. The extratropical wave climate will increase in wave power in the high-latitudes and decrease in mid-latitudes, due to the intensification and poleward displacement of the extratropical atmospheric circulation. In the Northern Hemisphere, the polar atmospheric circulation, with systems of lower pressure, will intensify the wave power of the subpolar and polar wave climates. The monsoon wave climate is projected to weaken. In general, the tropical wave climate will reduce

by 20% for the far future; but in the northern and southern limits, over the Atlantic and Pacific basins, it will increase due to the expanding tropics. Over the Caribbean Sea, this wave climate will also increase, caused by an intensification of the regional wind systems.

Particular attention is paid to the continental, sea ice and permafrost coastlines, because of the importance they have for industries and for ecosystems. As is the case in other fields of research (Duarte et al., 2020), we point out that the transitional regions are those where the impacts of climate change will be most exacerbated. The transitional regions will be affected by more frequent wave climates. Therefore, the transitional wave climate regions have been identified and given a priority classification, based on the increase in frequency of the new prevailing wave climates. Overall, in the eastern basins, the coasts will be affected more by southerly wave climates, and in the western basins, by the easterlies. New Zealand, Chile, and South Africa will be affected by an increase in the extratropical wave climate that is intensifying and being displaced poleward.

The analysis of the polar regions shows which parts will be affected by the major wave climates. As wave-ice interaction is not considered by wave models, this analysis can be seen as a preliminar approach to define adaptation and conservancy strategies in the polar regions. Futher work on this will be decisive in developing more accurate wave climate projections (Babanin et al., 2019), especially in these regions.

Our results show that the Polar circulation plays a fundamental role in changes in extratropical circulation, and also in the waves generated in high and mid-latitudes that propagate towards the tropics. The Arctic amplification (warming of the North Pole) is occurring more rapidly than the Antarctic (warming of the South Pole), but the latter will have important implications for the wave climates of the Southern Hemisphere and for the eastern coasts of the basins. This pan-hemispheric asymmetry in the atmospheric system could be critical for the adaptation timeline of countries facing climate change. This is especially true for coasts that face wave climate bimodality, originating in both hemispheres, as in the East Pacific.

To summarize, this study (i) improves the understanding of cause-effect of the atmospheric system–ocean waves; (ii) identifies transitional wave climate regions in climate change scenarios; and (iii) offers a more precise classification of regional wave climate that will assist in developing roadmaps for coastal risk adaptation. This work is believed to be the first wave climate projection that focuses on coastlines at the circumpolar scale.

**References**

Babanin, A. V, Rogers, W. E., de Camargo, R., Doble, M., Durrant, T., Filchuk, K., et al. (2019). Waves and Swells in High Wind and Extreme Fetches, Measurements in the Southern Ocean. *Frontiers in Marine Science*, *6*, 361. https://doi.org/10.3389/fmars.2019.00361

Chen, G., Lu, J., & Frierson, D. M. W. (2008). Phase Speed Spectra and the Latitude of Surface Westerlies: Interannual Variability and Global Warming Trend. *Journal of Climate*, *21*(22), 5942–5959. https://doi.org/10.1175/2008JCLI2306.1

Cherchi, A., Ambrizzi, T., Behera, S., Freitas, A. C. V., Morioka, Y., & Zhou, T. (2018). The Response of Subtropical Highs to Climate Change. *Current Climate Change Reports*, *4*(4), 371–382. https://doi.org/10.1007/s40641-018-0114-1

Choi, J., Lu, J., Son, S.-W., Frierson, D. M. W., & Yoon, J.-H. (2016). Uncertainty in future projections of the North Pacific subtropical high and its implication for California winter precipitation change. *Journal of Geophysical Research: Atmospheres*, *121*(2), 795–806. https://doi.org/https://doi.org/10.1002/2015JD023858

Costoya, X., deCastro, M., Santos, F., Sousa, M. C., & Gómez-Gesteira, M. (2019). Projections of wind energy resources in the Caribbean for the 21st century. *Energy*, *178*, 356–367. https://doi.org/https://doi.org/10.1016/j.energy.2019.04.121

Duarte, C. M., Agusti, S., Barbier, E., Britten, G. L., Castilla, J. C., Gattuso, J.-P., et al. (2020). Rebuilding marine life. *Nature*, *580*(7801), 39–51. https://doi.org/10.1038/s41586-020-2146-7

Fraser, C. I., Morrison, A. K., Hogg, A. M., Macaya, E. C., van Sebille, E., Ryan, P. G., et al. (2018). Antarctica's ecological isolation will be broken by storm-driven dispersal and warming. *Nature Climate Change*, *8*(8), 704–708. https://doi.org/10.1038/s41558-018-0209-7

H.-O. Pörtner, D.C. Roberts, V. Masson-Delmotte, P. Zhai, M. Tignor, E. Poloczanska, K. Mintenbeck, A. Alegría, M. Nicolai, A. Okem, J. Petzold, B. Rama, N. M. W. (eds. . (2019). *IPCC, 2019: IPCC Special Report on the Ocean and Cryosphere in a Changing Climate*.

He, C., & Zhou, T. (n.d.). Responses of the Western North Pacific Subtropical High to Global Warming under RCP4.5 and RCP8.5 Scenarios Projected by 33 CMIP5 Models: The Dominance of Tropical Indian Ocean–Tropical Western Pacific SST Gradient. *Journal of Climate*, *28*(1), 365–380. https://doi.org/10.1175/JCLI-D-13-00494.1

He, C., Wu, B., Zou, L., & Zhou, T. (2017). Responses of the Summertime Subtropical Anticyclones to Global Warming. *Journal of Climate*, *30*(16), 6465–6479. https://doi.org/10.1175/JCLI-D-16-0529.1

Held, I. M., & Soden, B. J. (n.d.). Robust Responses of the Hydrological Cycle to Global Warming. *Journal of Climate*, *19*(21), 5686–5699. https://doi.org/10.1175/JCLI3990.1

Lantuit, H., Overduin, P. P., Couture, N., Wetterich, S., Aré, F., Atkinson, D., et al. (2012). The Arctic Coastal Dynamics Database: A New Classification Scheme and Statistics on Arctic Permafrost Coastlines. *Estuaries and Coasts*, *35*(2), 383–400. https://doi.org/10.1007/s12237-010-9362-6

Lim, E.-P., Hendon, H. H., Arblaster, J. M., Delage, F., Nguyen, H., Min, S.-K., & Wheeler, M. C. (2016). The impact of the Southern Annular Mode on future changes in Southern Hemisphere rainfall. *Geophysical Research Letters*, *43*(13), 7160–7167. https://doi.org/https://doi.org/10.1002/2016GL069453

Liu, Q., Babanin, A. V, Zieger, S., Young, I. R., & Guan, C. (2016). Wind and Wave Climate in the Arctic Ocean as Observed by Altimeters. *Journal of Climate*, *29*(22), 7957–7975. https://doi.org/10.1175/JCLI-D-16-0219.1

Lu, J., Deser, C., & Reichler, T. (2009). Cause of the widening of the tropical belt since 1958. *Geophysical Research Letters*, *36*(3). https://doi.org/10.1029/2008GL036076

Lucas, C., Timbal, B., & Nguyen, H. (2014). The expanding tropics: A critical assessment of the observational and modeling studies. *Wiley Interdisciplinary Reviews: Climate Change*, *5*(1), 89–112. https://doi.org/10.1002/wcc.251

Miller, R. L., Schmidt, G. A., & Shindell, D. T. (2006). Forced annular variations in the 20th century Intergovernmental Panel on Climate Change Fourth Assessment Report models. *Journal of Geophysical Research: Atmospheres*, *111*(D18). https://doi.org/10.1029/2005JD006323

Morim, J., Hemer, M., Wang, X. L., Cartwright, N., Trenham, C., Semedo, A., et al. (2019). Robustness and uncertainties in global multivariate wind-wave climate projections. *Nature Climate Change*, *9*(9), 711–718. https://doi.org/10.1038/s41558-019-0542-5

Nazarenko, L., Schmidt, G. A., Miller, R. L., Tausnev, N., Kelley, M., Ruedy, R., et al. (2015). Future climate change under RCP emission scenarios with GISS ModelE2. *Journal of Advances in Modeling Earth Systems*, *7*(1), 244–267. https://doi.org/10.1002/2014MS000403

Pörtner, H.-O., D.C. Roberts, V. Masson-Delmotte, P. Zhai, M. Tignor, E. Poloczanska, K. Mintenbeck, A. A., & M. Nicolai, A. Okem, J. Petzold, B. Rama, N. M. W. (eds. . (2019). *IPCC Special Report on the Ocean and Cryosphere in a Changing Climate*.

Rogers, W. E., Posey, P. G., Li, L., & Allard, R. (2018). Forecasting and Hindcasting Waves In and Near the Marginal Ice Zone: Wave Modeling and the ONR Sea State Field Experiment.

Screen, J. A., Bracegirdle, T. J., & Simmonds, I. (2018). Polar Climate Change as Manifest in Atmospheric Circulation. *Current Climate Change Reports*, *4*(4), 383–395. https://doi.org/10.1007/s40641-018-0111-4

Seth, A., Giannini, A., Rojas, M., Rauscher, S. A., Bordoni, S., Singh, D., & Camargo, S. J. (2019). Monsoon Responses to Climate Changes—Connecting Past, Present and Future. *Current Climate Change Reports*, *5*(2), 63–79. https://doi.org/10.1007/s40641-019-00125-y

Shaw, T. A., & Voigt, A. (2015). Tug of war on summertime circulation between radiative forcing and sea surface warming. *Nature Geoscience*, *8*(7), 560–566. https://doi.org/10.1038/ngeo2449

Thomson, J., & Rogers, W. E. (2014). Swell and sea in the emerging Arctic Ocean. *Geophysical Research Letters*, *41*(9), 3136–3140. https://doi.org/https://doi.org/10.1002/2014GL059983

# CHAPTER 7

## Coastal Wave Climate Frameworks for the Near and Far Future

This chapter is structured as a diagnostic handbook for coastal adaptation based on long-term and projected changes in wave climate. It summarizes and translates the results of Chapters 3, 4, 6 into useful information to reduce barriers in understanding coastal hazards for climate change adaptation projects.

The chapter is based on

Odériz, I., Silva, R., Mortlock, T.R., & Mori, N. (2020). ENSO Impacts on global wave climate and Potential coastal hazards. *Journal of Geophysical Research: Oceans*, 125, e2020JC016464. https://doi.org/10.1029/2020JC016464

## 7.1 Introduction

Adaptation to climate change in coastal areas is a complex process that involves a series of steps (understanding, planning, and management) and depends on various factors in the context of the governance, social and biophysical environments (Eisenack et al., 2014; Moser & Ekstrom, 2010). There are two frameworks, "top-down" and "down-top" (Klein et al 2014), for implementing adaptation strategies. The first approach identifies climate scenarios and prioritizes the climate-related drivers of coastal hazards, whereas the second starts by identifying local vulnerability and the adaptive capability of the local social and biophysical environment, giving more importance to areas with higher social vulnerability. Neither is better than the other, in fact, both are recommended to address adaptation strategies efficiently. One of the most difficult challenges in implementing an adaptive framework is the climatic time-scale constraints to which they are subjected (Eisenack et al., 2014; Moser & Ekstrom, 2010).

Therefore, in order to plan a temporary hierarchy of actions for coastal adaptation, the temporal and spatial scales of the long-term variability and projected changes of wave climate should be outlined. In the previous chapters these long-term fluctuations have been analysed, induced by both natural variability and climate change (historical data and projections), establishing a global understanding of the wave climate. Accordingly, this chapter proposes a "top-down" framework and the compilation of three atlases, based on time scale. Each atlas was produced with a coastal classification using the static *k-means* clustering, explained in Chapter 2.

This chapter is based on the framework proposed by (Moser & Ekstrom, 2010). For reference, a summary of this framework is presented in the following section. To delve into this complex field it is recommended to read for a general perspective AR-5 (Chapters 14, 15, and 16), and specific examples of the normative approach the Spanish case (Losada et al., 2019), or the New Zealand case (Lawrence et al., 2018).

## 7.2 The coastal adaptation framework

We have selected the Moser & Ekstrom (2010) framework for improving adaptation assessment schemes of because it is proactive. This framework is also compatible with other impact-based approaches, such as the seven steps approach of the IPCC (Carter et al., 1994; Parry and Carter, 1998; Noble et al. 2014):

(1) define the problem (including the study area and the sectors to be examined),
(2) select the method of problem assessment,
(3) test the methods/ perform sensitivity analysis,
(4) select and apply climate change scenarios,
(5) assess biophysical and socio-economic impacts,
(6) assess autonomous adjustments,
(7) evaluate adaptation strategies.

The Moser & Ekstrom (2010) framework is based on three main stages: understanding, planning, and managing, as shown in Figure 7.1. Each stage has sub-elements on which the structural elements work. The structural elements are the actors (local institutions, local governments, non-government organizations, and civil society organizations), the systems of interest (natural and human coastal systems), the governance context, and the social and biophysical environment. Each sub-element may have insurmountable limits and barriers that must be worked around to avoid, deflect, delay, reduce or overcome them.

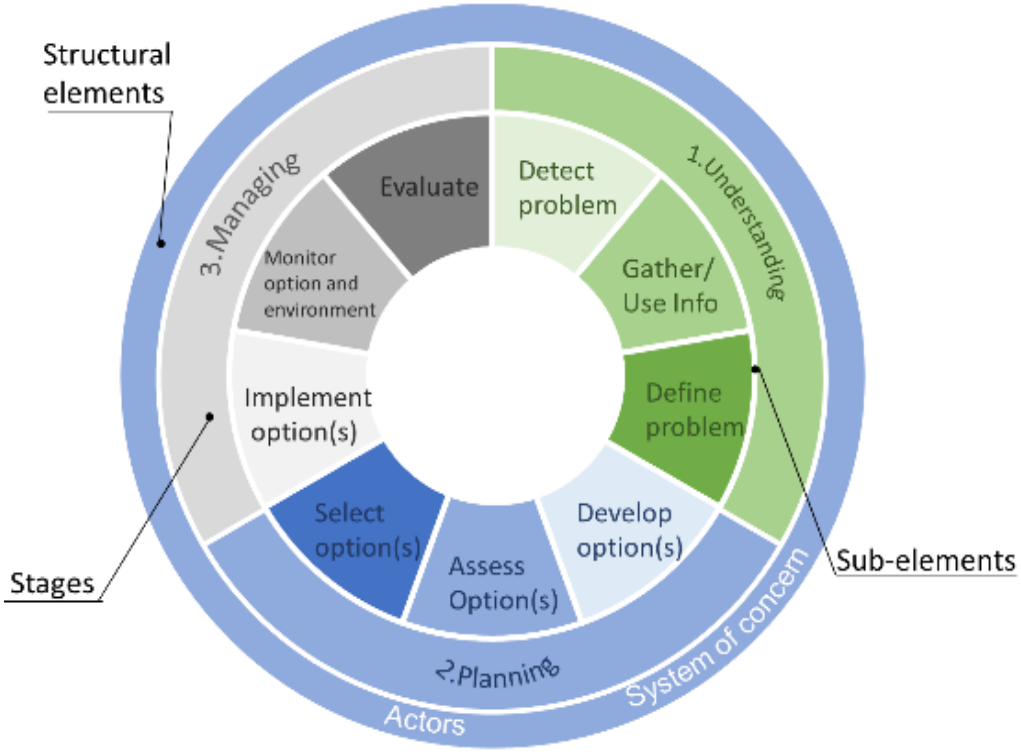


Figure 7. 1 The Moser & Ekstrom (2010) framework for reducing and overcoming barriers to adaptation to climate change, adapted from (Moser & Ekstrom, 2010).

This chapter works on the structural element "Understanding" of the wave climate. The atlases can be used as temporal and geographical frameworks that identify those coasts affected by wave climates with signals of natural variability, global warming, and climate change. To overcome the barrier in understanding wave climate, we propose a coastal regionalization, based on wave impacts in the near and far future:

1. The global coastal atlas for the near future (1979-2018).

1.1. This atlas analyses the impact of ENSO. The coasts were classified according to the wave climate response to ENSO; those coasts where ENSO should already be integrated in coastal projects are highlighted.

1.2. This atlas includes the coasts where the wave climate types prevail. In this classification the coasts where the warming sign has already emerged and where coastal adaptation is relevant are identified.

2. The global coastal atlas for the far future (2075-2099). This atlas identifies the transitional wave climate regions for the RCP 8.5 scenario, where the prevailing wave climates will change in frequency.

The atlases can serve as a basis for coastal managing adaptation actions and identify the coasts where wave climate types prevail, where global warming has already emerged, where it is important to account for natural variability, and which are transitional wave climate regions under the RCP 8.5 scenario. Tables 7.1, 7.2, and 7.3 can be used to determine how the atlas helps to reduce the barriers to understanding. This information is practical for coastal managers to better prioritize and develop adaptation strategies at national levels. However, it is beyond the scope of this chapter to establish a normative framework of good practices for the entire process of adaptation to climate change.

Table 7. 1 How the atlases overcome the barriers for the sub-element "Detect the problem" of the framework Moser & Ekstrom (2010).

| Sub-element: Detect problem | |
|---|---|
| **Barriers** | **Use of atlases** |
| Existence of a signal | Natural variability and climate change |
| Detection (and perception) of a signal | Identification of both signals (natural variability and climate change) in the wave climate of the global coasts |
| Threshold of concern (initial framing as problem) | Identification of which signals have a strong impact on the wave climate |
| Threshold of response need and feasibility (Initial framing of response) | Regions where climate change should be considered, regions where the climate variability should be considered, regions where both should be considered. Or regions where more data, monitoring, and research are needed. |

Table 7. 2 How the atlases overcome the barriers for the sub-element "Gather/Use info" of the framework Moser & Ekstrom (2010).

| Sub-element: Gather/Use info | |
|---|---|
| **Barriers** | **Use of atlases** |
| Interest and focus (and consensus, if needed) | Establish a consensus and a common interest for all the actors on long-term variability of wave climate. |
| Availability | Present a global scheme for all the coasts of the world, especially useful for areas with poor data. |

Table 7. 3 How the atlases overcome the barriers for the sub-element "(Re) Define problem" of the framework Moser & Ekstrom (2010).

| Sub-element: (Re)Define problem | |
|---|---|
| **Barriers** | **Use of atlases** |
| Threshold of concern (reframing of the problem) | A starting point to establish a normative framework by nations. |
| Threshold of response need | Characterize the prevailed wave climates. |
| | Regions where climate change has already emerged |
| | Regions where the natural variability has a high rate of perturbation in the wave climate |
| | The impact of the combination of both climate change and natural variability. |
| | Identification of the transitional wave climate regions as the most critical in adaptation to climate change. |
| Level of agreement or consensus | Establish a wave climate basis and knowledge, common to all the actors |

## 7.3 The global coastal atlas for the present

To classify the global coasts according to wave climate variation in ENSO events, the *R-lag 0* results of *MEI-$P_w$* and *MEI-$Dir_m$* (see Chapter 3) were obtained for global coastlines. The optimal number of clusters was found to be 5. The results plotted in Figure 7.2 show the level of coastal response to ENSO events, and each type is briefly described as follows:

**Coasts of Low response to ENSO events**: These coasts respond to El Niño and La Niña but within a range of ±0.2 for *R ($P_w$* and *$Dir_m$)*.

**Coasts of High Niña 1 ENSO response**: These areas exhibit a reduction (increase) in wave power and a clockwise (anticlockwise) rotation of the wave field during El Niño (La Niña). The coastal response is 0 to 0.6 for *R-$Dir_m$* and -0.6 to 0 for *R-$P_w$*. In all cases one or both of the *R-$Dir_m$* and *R-$P_w$* values are > 0.2.

**Coasts of High Niña 2 ENSO response**: In these areas wave power reduces (increases) but turns anticlockwise (clockwise) during El Niño (La Niña) events. Both *$Dir_m$* and *$P_w$* are negative, and at least one is < -0.2, with a correlation *R* ranging from -0.6 to 0.

**Coasts of High Niño 1 ENSO response**: wave power increases (reduces) and turns anticlockwise (clockwise) during El Niño (La Niña) events. For *$P_w$* 0 to 0.5 and for *$Dir_m$*. -0.5 to 0, with one of the variables always exceeding ±0.2 of *R*.

**Coasts of High Niño 2 ENSO response**: In these areas the wave power increases (reduces) and turns clockwise (anticlockwise) during El Niño (La Niña) events. In this classification both *$P_w$* and *$Dir_m$* are positively correlated and the highest of *R* values are found.

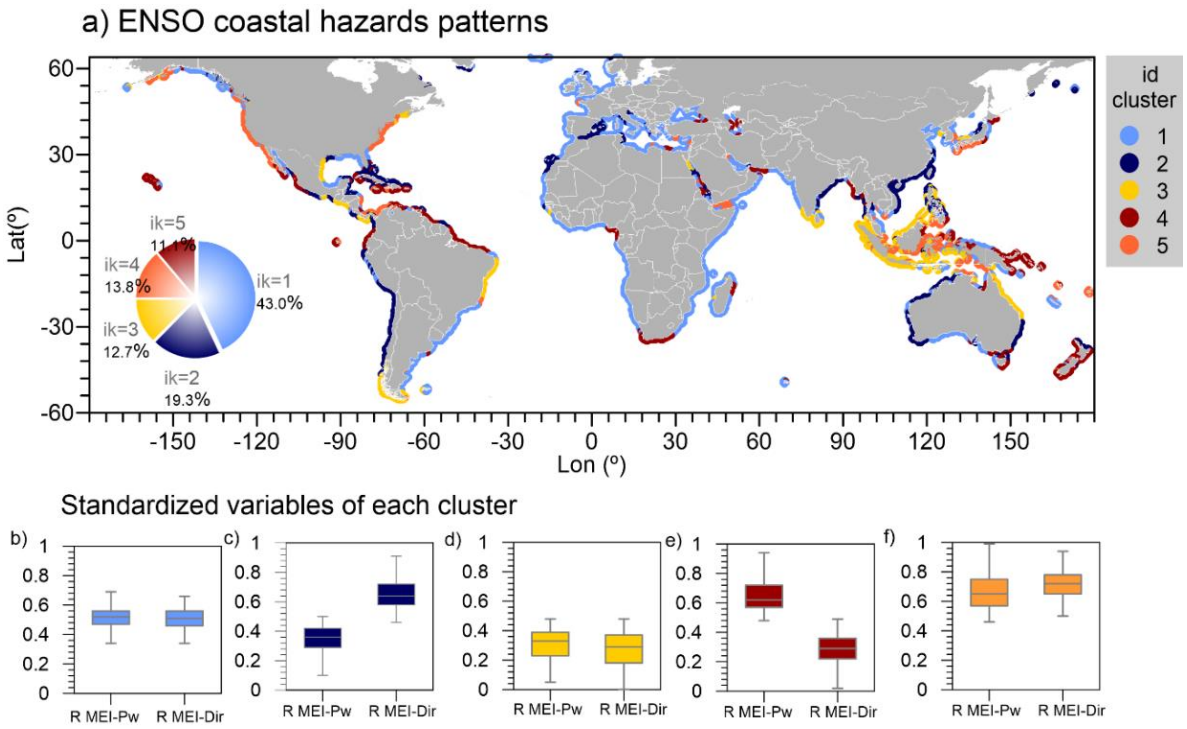


Figure 7. 2 Coastal wave climate atlas for the near future. Coastal classification based on the mean wave direction and power response to ENSO.

## 7.4 The global coastal atlas for the near future

This classification uses the annual and seasonal variability of the WCTs to identify the coastal regions where they prevail. The signals of global warming and natural variability were identified in the global wave climate types, and therefore on the coasts affected by them. The global shorelines were classified into 8 types, depicted in Figure 7.3, and their characteristics are described below. The response of WCTs to global warming is shown in Table 7.4, and to natural variability in Table 7.5.

**Coast type id=1** are coasts dominated by tropical WCT in all seasons. These coasts are the eastern tropical regions of the Atlantic and Pacific, and parts of the Indian Ocean. In the Atlantic and Pacific Oceans, evidence of global warming has already been reported, though not in the Indian Ocean. The natural variability, modulated by ENSO+SAM+PDO, plays an important role in the Pacific and Indian Ocean.

**Coast type id=2** are coasts dominated by monsoon WCT, but the subtropical WCT is more prevalent in DJF. On these coasts, the natural variability of ENSO, PDO, and SAM has to be taken into account. However, the global warming sign has not yet been detected.

**Coast type id=3** are those coasts where polar, extratropical, and subtropical WCTs prevail. In DJF, the extratropical WCT increases in frequency. Subpolar and subtropical increase in JJA. Where the effects of global warming have not yet emerged, but ENSO and SAM have an impact on the wave climate and should be included in wave climate analysis.

**Coast type id=4** are coasts mainly governed by subtropical and secondary tropical WCTs. In the Indian Ocean, these coasts have already been affected by ocean warming. In the Pacific and North Atlantic, they have a strong natural variability forced by ENSO+SAM, and in the Indian Ocean, this is driven by ENSO+SAM+PDO.

**Coast type id=5** are coasts governed by the extratropical WCT all year round. Only in the Indian Ocean, the global warming signal has already been detected. However, the South Pacific and South Atlantic parts of the Southern Ocean will potentially be affected by climate change. In the Pacific, Indian, and South Atlantic Oceans, ENSO, PDO and SAM influence this wave climate and should be considered in coastal projects.

**Coast type id=6** are coasts governed by subtropical and tropical WCTs in JJA, and warm pool WCT in DFJ. Global warming and natural variability induced by ENSO+PDO+SAM affect the coastal wave climate of these regions.

**Coast type id=7,** these coasts are not well classified by this methodology.

**Coast type id=8,** these are coasts where the tropical WCT prevails all year round, followed by the subtropical WCT. In the Indian, tropical Pacific and tropical Atlantic Oceans, the global warming signal has already emerged. The natural variability on these coasts should be considered only in the Indian Ocean.

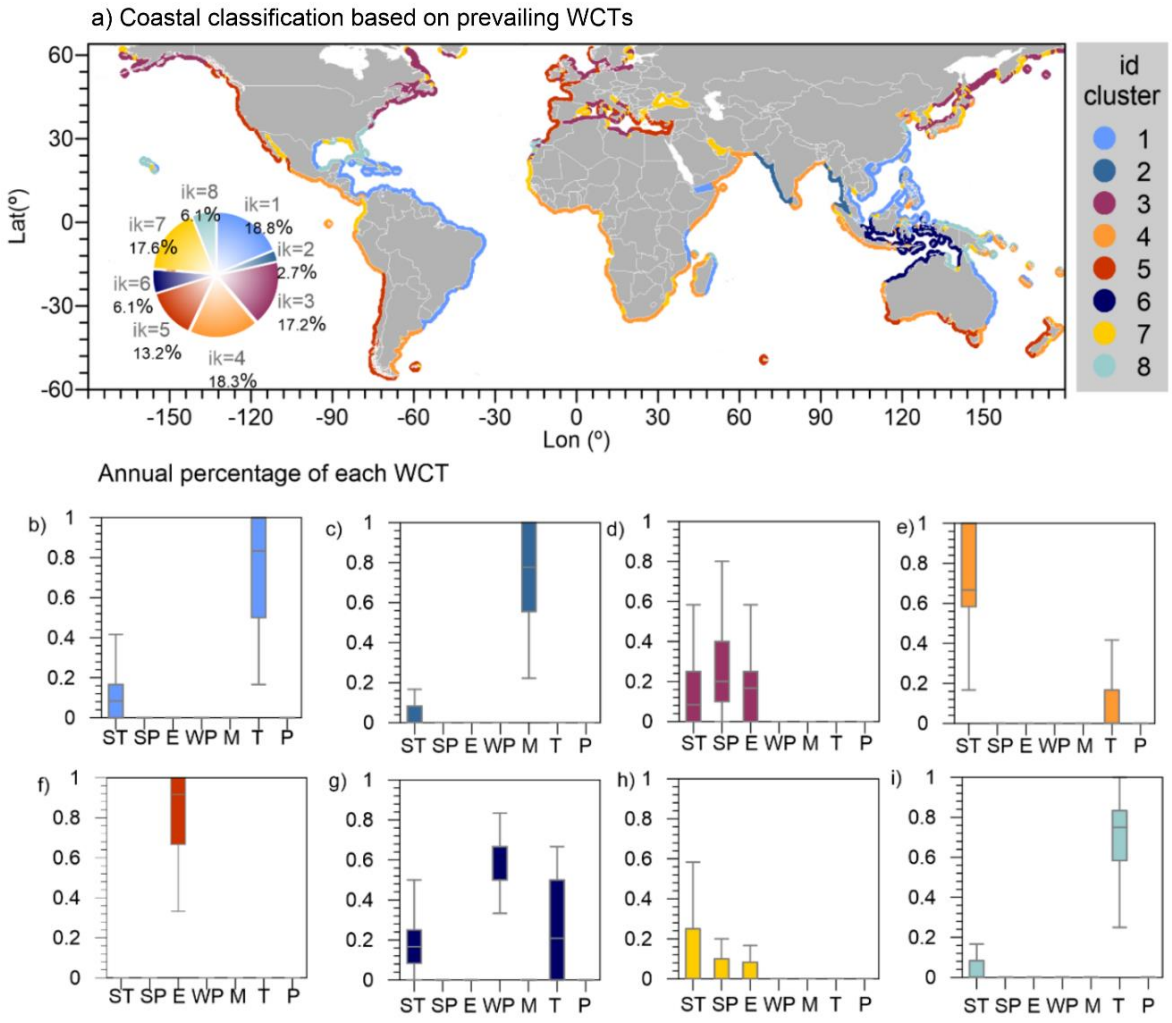


Figure 7. 3 Coastal wave climate atlas for the near future. Coastal classification based on the prevailing WCTs.

Table 7. 4 Characteristics of the coastal classification, global warming evidence.

| idx | **Prevailing WCT** | | | **Global warming evidence** | | | | | | |
|---|---|---|---|---|---|---|---|---|---|---|
| | all year around | DJF | JJA | Indian Ocean | South Pacific | Tropical Pacific | North Pacific | South Atlantic | Tropical Atlantic | North Atlantic |
| 1 | tropical | tropical | tropical | no | - | yes | - | - | yes | - |
| 2 | monsoon | subtropical | monsoon | no | - | - | - | - | - | - |
| 3 | subpolar+ extratropical+ subtropical | subpolar | subpolar | no+yes+yes | - | - | no+no+no | | | no+no+no |
| 4 | subtropical | subtropical | subtropical | yes | no | | no | no | - | no |
| 5 | extratropical | extratropical | extratropical | yes | no | - | no | no | - | no |
| 6 | tropical+ warm pool + subtropical | warm pool | subtropical + tropical | no+ yes+ yes | - | yes+ yes +no | - | - | - | - |
| 7 | not classified | | | | | | | | | |
| 8 | tropical + subtropical | tropical | subtropical | no+yes | - | yes+no | - | - | yes+no | - |

Table 7. 5 Characteristics of the coastal classification, natural variability.

| idx | **Prevailing WCT** | | | **Strong natural variability forced by** | | | | | | |
|---|---|---|---|---|---|---|---|---|---|---|
| | all year around | DJF | JJA | Indian Ocean | South Pacific | Tropical Pacific | North Pacific | South Atlantic | Tropical Atlantic | North Atlantic |
| 1 | tropical | tropical | tropical | ENSO+PDO+SAM | - | ENSO+PDO+SAM | - | - | - | - |
| 2 | monsoon | subtropical | monsoon | ENSO+PDO+SAM | - | - | - | - | - | - |
| 3 | subpolar+ extratropical+ subtropical | subpolar | subpolar | - | - | - | - | - | - | - ENSO+SAM ENSO+SAM |
| 4 | subtropical | subtropical | subtropical | ENSO+PDO+SAM | ENSO+SAM | - | ENSO+SAM | - | - | ENSO+SAM |
| 5 | extratropical | extratropical | extratropical | ENSO+PDO+SAM | ENSO+PDO+SAM | - | ENSO+PDO+SAM | ENSO+PDO+SAM | - | - |
| 6 | tropical+ warm pool + subtropical | warm pool | subtropical and tropical | ENSO+PDO+SAM ENSO+PDO+SAM ENSO+PDO+SAM | - | - | - | - | - | - |
| 7 | not classified | | | | | | | | | |
| 8 | tropical and subtropical | tropical | subtropical | ENSO+PDO+SAM | - | - | - | - | - | - |

## 7.5 The global coastal atlas for the far future

In Chapter 6, we have explained that changes in sediment transport and wave energy flux on coastal environments will be induced by changes in the frequency of the prevailing wave climate types. The wave climates are classified by direction and wave power, and an increase in their frequency will affect coastal wave hydrodynamic. We have called these zones the "transitional wave climate regions"; we identified those changes in the critical areas, continental coasts, the effects on sea ice, and permafrost coastlines. We classified these coasts using a priority scale based on the increase in the frequency of the wave climates. The atlases for the continental coasts are shown in Figure 6.6, for Arctic coasts in Figure 6.7, and Antarctic coast in Figure 6.8. The changes on those coasts are described in detail in section 6.4 of Chapter 6.

**Coasts of Priority I** (increase in frequency of wave climates, 5-10 %)

**Coasts of Priority II** (increase in frequency of wave climates, 10-15 %)

**Coasts of Priority III** (increase in frequency of wave climates, 15-20 %)

**Coasts of Priority IV** (increase in frequency of wave climates, >20 %)

## 7.6 Conclusions

The work of this chapter defines the prevailing wave climate of the coastal regions, where natural variability should be considered, where global warming has already emerged, as well as the transitional wave climate regions for the RCP 8.5 scenario.

Overall, for the Indian Ocean, eastern Pacific and southeast Atlantic coasts, coastal projects should include analysis of the potential effect of the SAM, PDO, and ENSO. The Pacific, northwest Atlantic and the eastern Indian Ocean are the regions with highest response to ENSO, while the African and European coasts have lower responses. In the Indian Ocean, global warming is already emerged on all the coasts, with the exception of eastern Madagascar, the eastern Arabian Sea, eastern Bay of Bengal and Tanzania. In the Pacific Ocean, the northern and eastern coasts of Australia, Indonesia, the South China Sea and the Philippine Sea are experiencing the impact of global warming on wave climate. In the Atlantic, the coasts where global warming has already emerged are: the southern and eastern Gulf of Mexico, and the USA states of Florida and Georgia, and from Central America to South America, excluding Argentina.

In the far future, we pay special attention to continental coasts, those affected by sea ice and permafrost because of their value for industries and ecosystems. In agreement with other authors who highlighted that transitional regions will be those where the impacts of climate change will be more severe, we have considered that in addition to storms, in those areas affected by different prevailing wave climates the effects of climate change will be more drastic. We have therefore identified transitional wave climate regions and classified the coasts with a priority scale based on the increased frequency of new prevailing wave climates. In general, coasts will be affected more by southerlies wave climates in the eastern basins and by the easterlies in the western basins. New Zealand, Chile, and South Africa will be affected by an increase in extratropical wave climate that undergoes poleward displacement and intensification.

A diagnosis of coastal wave climate can produce an anticipatory, rather than reactive, response to natural variability and climate change, and the prioritisation of the regions where adaptation strategies are most needed. This is most beneficial in areas where there are limited observations or insufficient information.

The atlases produced for each wave climate region can be used to:

i. provide guidance on wave climate impact responses; by identifying regions where further adaptation strategies, monitoring, research and technical analysis are needed
ii. calibrate efforts and channel the financial instruments of governments
iii. engage industries (tourism, wave energy, port operability, fishing, etc.), communities, organizations, and governments; and build the capacity of these actors
iv. promote the exchange and dissemination of information
v. build international partnerships between countries with the same wave climate characteristics.

**References**

Eisenack, K., Moser, S. C., Hoffmann, E., Klein, R. J. T., Oberlack, C., Pechan, A., et al. (2014). Explaining and overcoming barriers to climate change adaptation. *Nature Climate Change*, *4*(10), 867–872. https://doi.org/10.1038/nclimate2350

Klein, R.J.T., G.F. Midgley, B.L. Preston, M. Alam, F.G.H. Berkhout, K. Dow, and M.R. Shaw, 2014: Adaptation opportunities, constraints, and limits. In: Climate Change 2014: Impacts, Adaptation, and Vulnerability. Part A: Global and Sectoral Aspects. Contribution of Working Group II to the Fifth Assessment Report of the Intergovernmental Panel on Climate Change [Field, C.B., V.R. Barros, D.J. Dokken, K.J. Mach, M.D. Mastrandrea, T.E. Bilir, M. Chatterjee, K.L. Ebi, Y.O. Estrada, R.C. Genova, B. Girma, E.S. Kissel, A.N. Levy, S. MacCracken, P.R. Mastrandrea, and L.L.White (eds.)]. Cambridge University Press, Cambridge, United Kingdom and New York, NY, USA, pp. 899-943.

Lawrence, J., Bell, R., Blackett, P., Stephens, S., & Allan, S. (2018). National guidance for adapting to coastal hazards and sea-level rise: Anticipating change, when and how to change pathway. *Environmental Science & Policy*, *82*, 100–107. https://doi.org/https://doi.org/10.1016/j.envsci.2018.01.012

Losada, I. J., Toimil, A., Muñoz, A., Garcia-Fletcher, A. P., & Diaz-Simal, P. (2019). A planning strategy for the adaptation of coastal areas to climate change: The Spanish case. *Ocean & Coastal Management*, *182*, 104983. https://doi.org/https://doi.org/10.1016/j.ocecoaman.2019.104983

MacQueen, J. (1967). Some methods for classification and analysis of multivariate observations. In *Proceedings of the Fifth Berkeley Symposium on Mathematical Statistics and Probability, Volume 1: Statistics* (pp. 281–297). Berkeley, Calif.: University of California Press. Retrieved from https://projecteuclid.org/euclid.bsmsp/1200512992

Moser, S. C., & Ekstrom, J. A. (2010). A framework to diagnose barriers to climate change adaptation. *Proceedings of the National Academy of Sciences*, *107*(51), 22026 LP – 22031. https://doi.org/10.1073/pnas.1007887107

Noble, I.R., S. Huq, Y.A. Anokhin, J. Carmin, D. Goudou, F.P. Lansigan, B. Osman-Elasha, and A. Villamizar, 2014: Adaptation needs and options. In: Climate Change 2014: Impacts, Adaptation, and Vulnerability. Part A: Global and Sectoral Aspects. Contribution of Working Group II to the Fifth Assessment Report of the Intergovernmental Panel on Climate Change [Field, C.B., V.R. Barros, D.J. Dokken, K.J. Mach, M.D. Mastrandrea, T.E. Bilir, M. Chatterjee, K.L. Ebi, Y.O. Estrada, R.C. Genova, B. Girma, E.S. Kissel, A.N. Levy, S. MacCracken, P.R. Mastrandrea, and L.L.White (eds.)]. Cambridge University Press, Cambridge, United Kingdom and New York, NY, USA, pp. 833-868.

United Nations Department of Economic and Social Affairs. (2020). Recovering better: economic and social challenges and opportunities A compilation of the High-level Advisory Board on Economic and Social Affairs. New York, New York 10017, United States of America.

# CHAPTER 8

# Case Study, Mexico

This chapter focuses on wave climate on the Mexican coasts and the implications for climate change mitigation and adaptation. The supporting information is given in APPENDIX A4.

This chapter is based on

Odériz, I., Silva, R., Mortlock T.R., Mendoza E. (2020) Climate drivers of directional wave power on the Mexican coast. Ocean Dynamics, 70 (9), 1253-1265. https://doi.org/10.1007/s10236-020-01387-z

## 8.1 Introduction

Mexico is surrounded by 11,122 km of coast along the Atlantic and Pacific basins. In addition, its oil, fishing, sports, and tourism industries are linked to the wave climate. By 2015, 15.8 % of the total population lived in coastal municipalities. Thence, a deep understanding of the wave climate is essential to carry out efficient adaptation and mitigation projects. This chapter shows the sea states analysis, long-term fluctuations based on historical data, and wave climate changes under future scenarios along the Mexican coast.

In this chapter, we use boreal seasons nomenclature (winter: DJF; spring: MAM; summer: JJA; autumn: SON).

## 8.2 Long-term analysis (sea states)

This section describes the wave climate using a long-term statistical analysis of the sea states. For this, we considered, instead of monthly data, hourly data from 1979-2018 with the ERA 5 dataset. We calculated the mean, the percentile 90 %, 95%, and 99% of the $H_s$, $T_m$, $T_P$, and $P_w$. The annual average is shown in Figure 8.1, and the seasonal average in APPENDIX A4. The higher mean $H_s$ was found in the North Pacific, while the waves that exceed 99 percent were presented on the coast of Veracruz. On the other hand, low frequencies were found on the Pacific basin that are coasts affected by distant swells, as has been explained in Chapter 4. The wave power is a function of the squared significant wave height and energy period ($H^2T$), thereby high values in the mean and percentile 90$^{th}$ of wave power were shown in the Pacific coast, particularly in the Central South Pacific coasts. While high energy conditions (percentiles 95$^{th}$ and 99$^{th}$ of wave power) were found in the Gulf of Mexico and Baja California State.

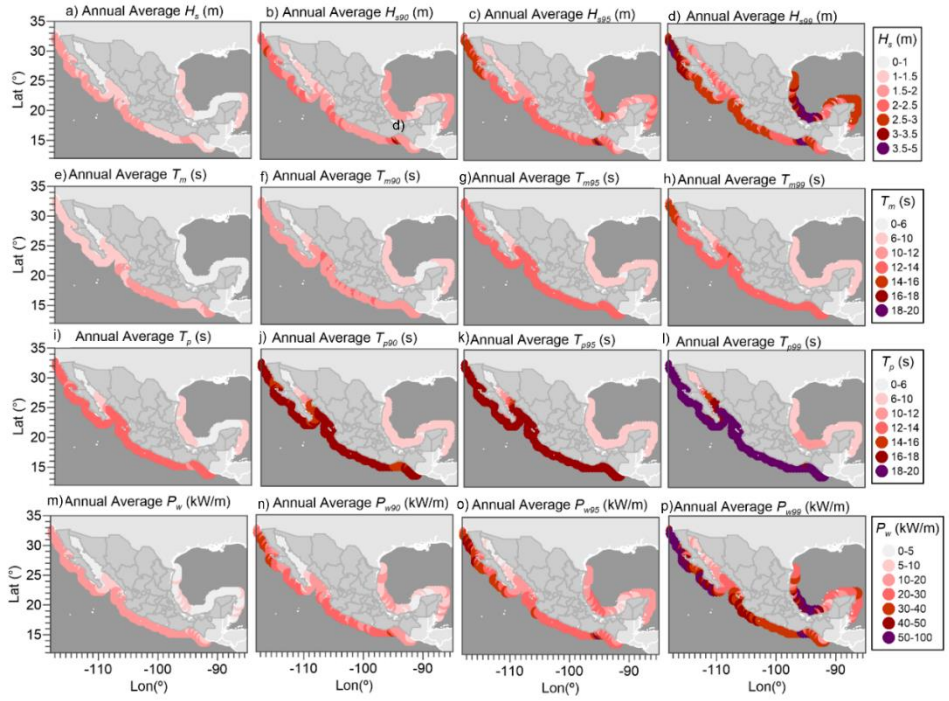


Figure 8.1. Annual values of a) mean of $H_s$, b) percentile 90 % of $H_s$, c) percentile 95% of $H_s$, and d) percentile 99% of $H_s$, e) mean of $T_m$, f) percentile 90 % of $T_m$, g) percentile 95% of $T_m$, and h) percentile 99% of $T_m$, i) mean

of $T_P$, j) percentile 90 % of $T_P$, k) percentile 95% of $T_P$, and l) percentile 99% of $T_P$, m) mean of $P_w$, n) percentile 90 % of $P_w$, o) percentile 95% of $P_w$, and p) percentile 99% of $P_w$.

Following the indications of (Fairley et al. (2020) and Silva et al. (2013), the joint probability of $H_s$ and $T_e$ (Equation 13) was calculated. The $pdf(H_s, T_e) = P(H_s) \cdot P(T_e)$ was computed for a total of 195 sea states ($H_s$: 0.5 to 12.5 m; and $T_e$: 4.5 to 18.5 s) by intervals of 1.0 m and 1.0 s, respectively. For each sea state, the wave power generated in a year was calculated by multiplying the wave power, by the joint probability $pdf(H_s, T_m)$, and by the hours in a non-leap year (8760). The results shown in Figure 8.1 identify each local sea state with more accumulated wave power in a year, in which the design WEC devices should focus on optimizing their efficiency.

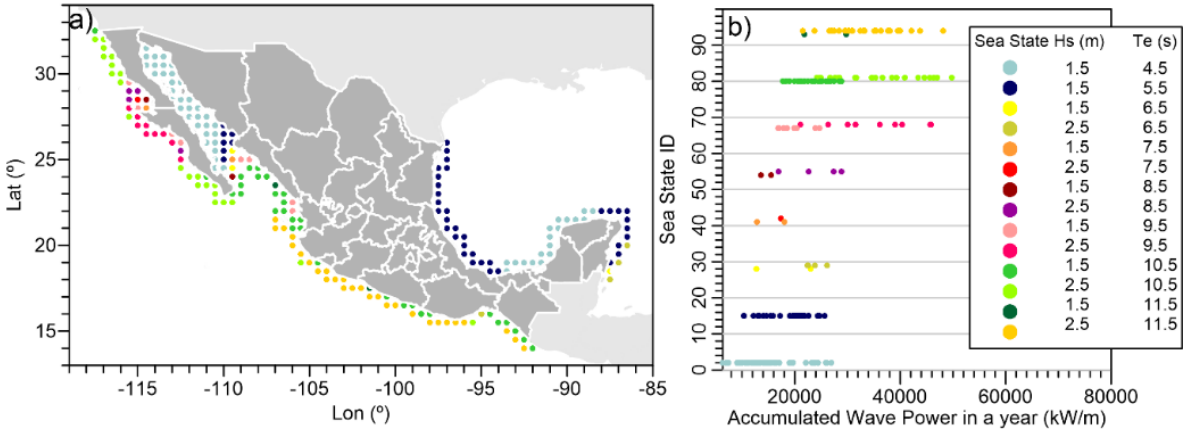


Figure 8.2.Local sea states that generate the more accumulated wave power in a year.

In coastal engineering, extreme events are applied to select the design sea state. The storm waves are selected with a time-dependent Peak Over Threshold (POT) approach to the significant wave height. It is common to address the Annual Maximum methods, such as distribution Poisson or Weibull. These models consist of applying cumulative distribution function to the annual maximums. Then, the significant wave height for a return period is selected. However, this approach uses only a storm event per year. Méndez et al. (2006) solve this problem by selecting the event for one year return period. An alternative way is to use the significant wave height that exceeds the percentile 90$^{th}$ ($Hs_{90}$) or the percentile 99$^{th}$ ($H_{s99}$) (Bromirski et al., 2013).

In this chapter, the extremes events were those sea states that exceed $H_{S99}$, and those obtained by using $H_{S90}$ are shown in APPENDIX A4. The minimal time interval between two events was 12 hours. The parameters of storm analysed in this chapter were: duration, time intervals of storm cluster (IN), mean significant wave height ($H_s$), maximum significant wave height ($H_{smax}$), peak period ($T_p$), mean wave direction ($Dir_m$), mean wave power ($P_{wE}$), and wave directional spectral width ($S_w$). Time interval of storm cluster(IN, days) is the time elapsed between storms (Dissanayake et al., 2015). Long storm duration occurred on the Pacific coasts, in contrast to more clustering storms in the Gulf of Mexico. High significant heights impacted the North Pacific and Veracruz State. While the North Pacific showed long periods. The coasts of the central Pacific show wide spectral width $S_w$, as these coasts are affected by distant swells generated in both hemispheres.

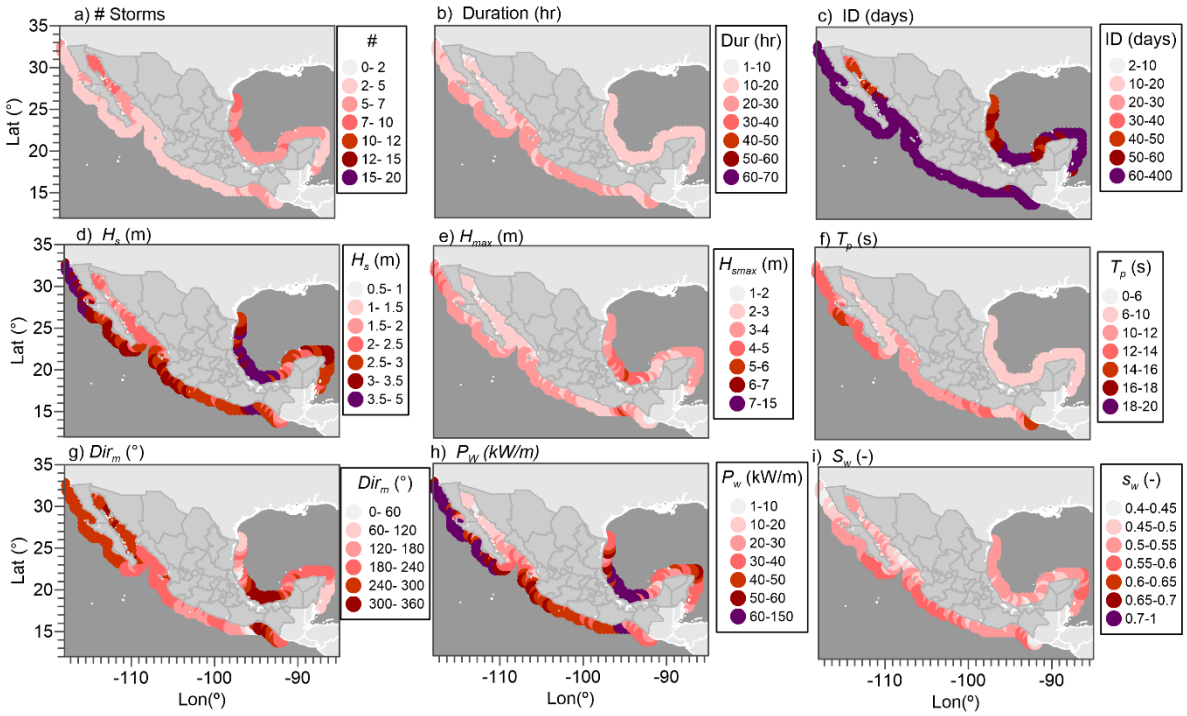


Figure 8.3. Annual average of a) number, b) duration, c) time intervals of the storm cluster (*IN*), d) significant height ($H_s$), e) maximum significant wave height ($H_{smax}$), f) peak period ($T_p$), g) mean wave direction($Dir_m$), h) wave power ($P_{wE}$), and I) the wave directional spectral width ($S_w$) of storm events obtained with percentile 99%.

## 8.3 The wave climate types

The three wave climates identified in Chapter 4, westerlies, southerlies, and, easterlies were evaluated for the Mexican coasts. The results showed that these three wave climates directly influence the coast of Mexico. Figure 8.4 shows the mean winter (a-c) and summer (d-f) $P_w$ for each wave climates. Figure 8.5 shows the contribution of each wave climate to the total wave power along the coast, and Figure 8.6 the mean direction of each wave climate, respectively. Overall, the results show that both extratropical and subtropical WCTs impact the Mexican Pacific coast, with considerable seasonal variation. While the Atlantic coast is influenced by the tropical WCT, year-round.

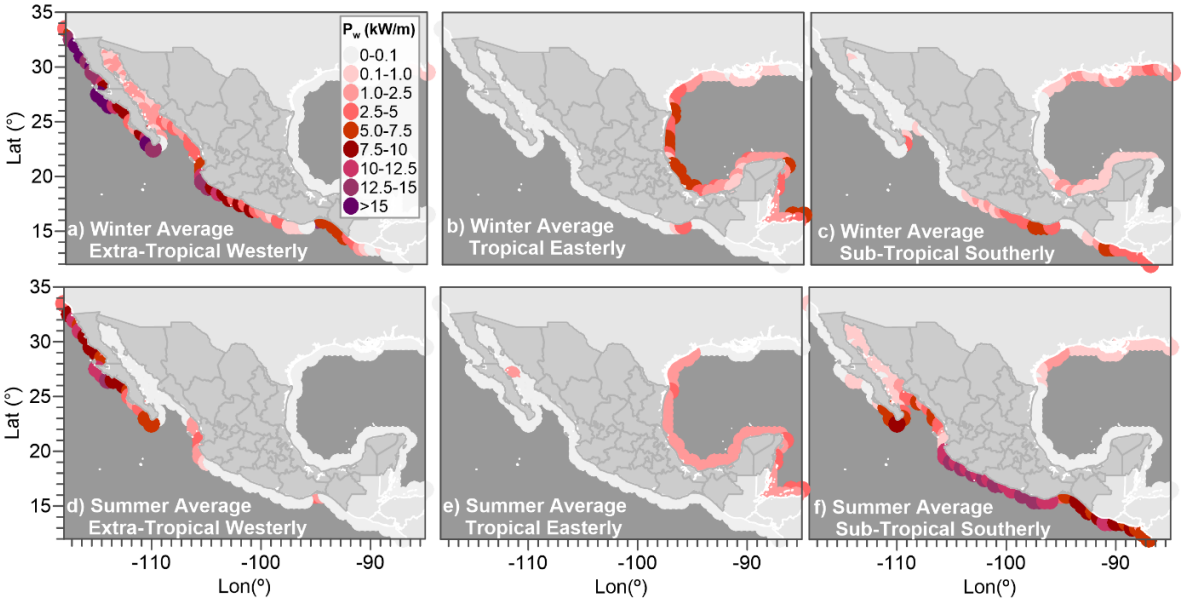


Figure 8.4. Wave power averages by season for each wave climate type. a) Extratropical $P_w$ average for winter; b) tropical $P_w$ average for winter; c) subtropical $P_w$ average for winter; d) extratropical $P_w$ average for summer; e) tropical $P_w$ average for summer; f) subtropical $P_w$ average of wave climates for summer.

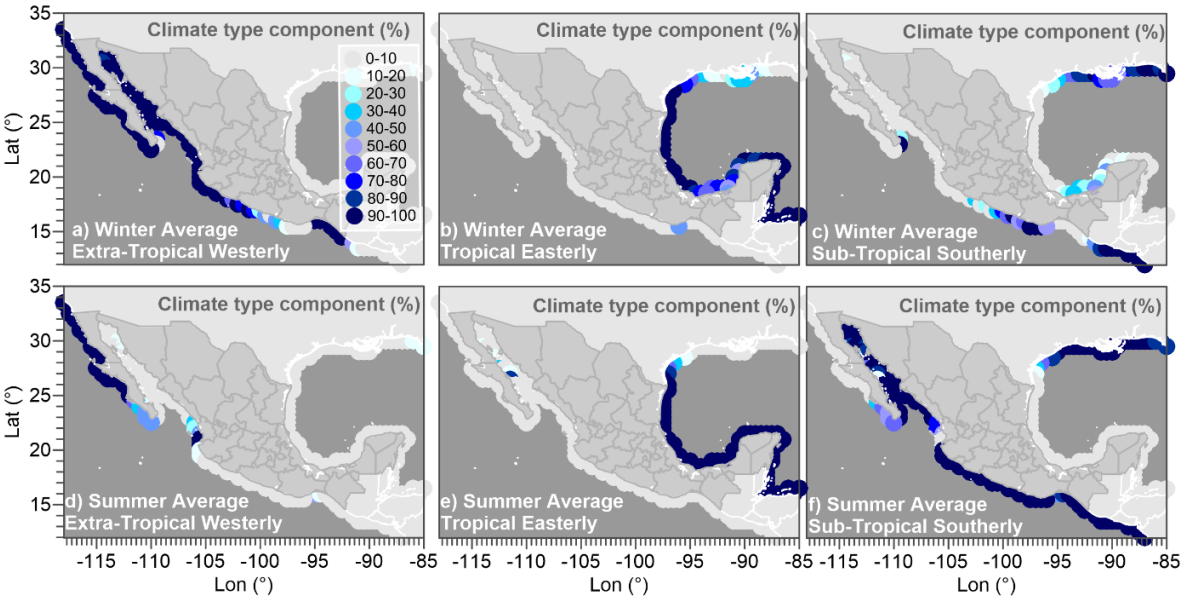


Figure 8.5. Wave climate type percentage contribution by season average. a) Extratropical percentage contribution for winter average; b) tropical percentage contribution for winter average; c) subtropical percentage contribution for winter average; d) extratropical percentage contribution for summer average; e) tropical percentage contribution for summer average; f) subtropical percentage contribution of wave climates for summer.

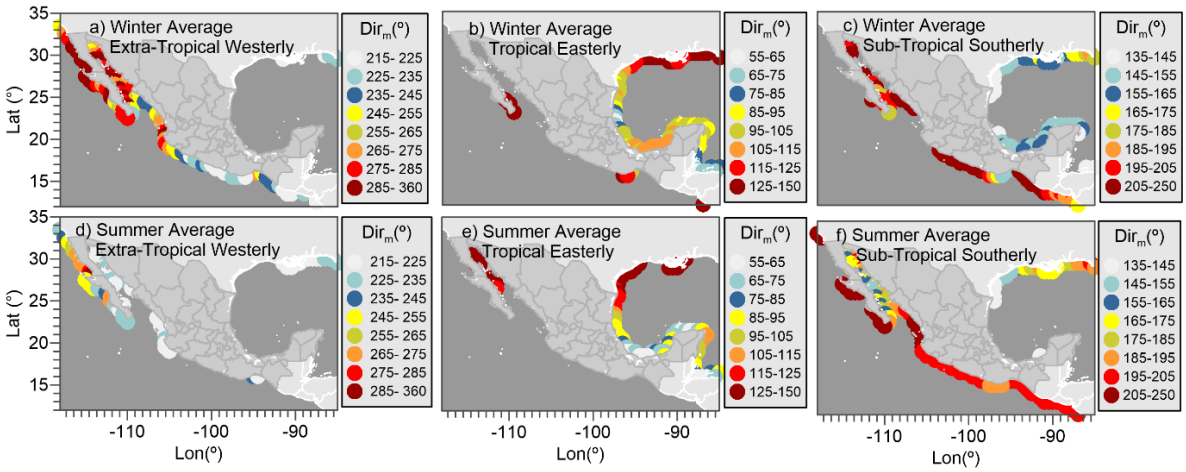


Figure 8.6. Wave climate type mean wave direction by season. a) Extratropical mean direction for winter; b) tropical mean direction for winter; c) subtropical mean direction for winter; d) extratropical mean direction for summer; e) tropical mean direction for summer; f) subtropical mean direction for summer. Direction follows meteorological convection.

During winter, the extratropical WCT impacts the entire Mexican Pacific coast, with a wave power average of approximately 15 kW/m in the north and 7.5 kW/m in the south. At this time of the year, in the south, only the coasts of Guerrero and Oaxaca are influenced by the Southerlies WCTs. In summer, the extratropical WCT is confined to the Baja California peninsula, Nayarit, and Jalisco (Pw ~10 kW/m), while the subtropical wave climate becomes more prevalent, affecting almost all of the Pacific coast (~15 kW/m). Both, the subtropical and extratropical WCTs, exhibit a clockwise rotation of around 10 and 25 degrees in winter, respectively. In the Gulf of Mexico and the Mexican Caribbean, the tropical WCT is the prevailing system all year round. An anticlockwise rotation in this WCT of approximately 20 degrees is evident during the summer.

## 8.4 Long-term variability

Interannual variability in the wave climate was analysed for ENSO events. The correlations were computed between ONI and monthly wave direction ($Dir_m$) and wave power ($P_w$). Previously, the trend and seasonal components of the time series were removed. Figure 8.7 shows the correlation between $P_w$ and Firm with the ONI. A positive (negative) correlation for $P_w$ indicates an increase (decrease) in wave power. A positive (negative) correlation for $Dir_m$ indicates a clockwise (anticlockwise) rotation in wave direction.

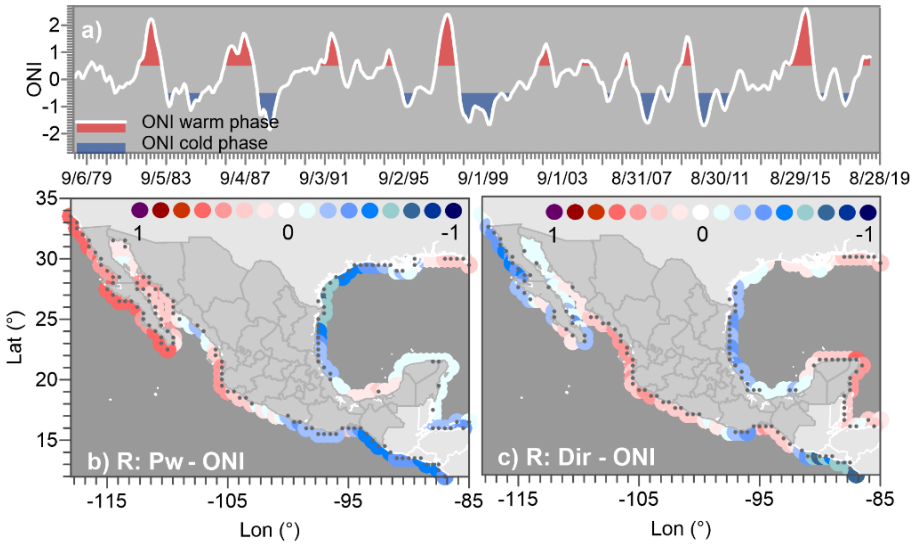


Figure 8.7. a) Time series of ONI, in blue are the cold phases (La Niña) and in red the warm phases (El Niño); b) correlation coefficient (R) with ONI and wave power, and; c) Correlation coefficient with ONI and mean wave direction. Points indicate correlation coefficient at 95 % confidence level.

Figure 8.7 shows a moderate-strong positive correlation between wave power and the ONI along the north and central Mexican Pacific coast, with the highest values seen on the coast of Baja California. This falls to a moderate-strong negative correlation along the south Pacific Mexican coast. This suggests that wave power increases (decreases) during El Niño (La Niña) on the north and central Pacific coast, but this relationship is inverse along the south Mexican and Central American Pacific coast. The wave power response to ENSO on the Caribbean coast is weaker.

Wave direction is negatively moderate-strong correlated with the ONI on the coasts of northern Baja California, Central America, and the Gulf of Mexico, suggesting that an anti-clockwise (clockwise) rotation of the wave field occurs in these areas during El Niño (La Niña). Conversely, wave direction is moderately positively correlated with the ONI on the Yucatan Peninsula, centre and south Pacific coast, except for Oaxaca, indicating a significant clockwise (anti-clockwise) rotation of the wave field during the El Niño (La Niña).

Multi-decadal variability in the wave climate was analysed using the PDO and AMO. Figure 8.8 shows the correlation between monthly $P_w$ and $Dir_m$ and the PDO, while Figure 8.9 shows the same for the AMO.

On the Pacific coast, the multi-decadal wave climate responses to PDO (Figure 8.8 b) is similar to the response to ENSO (Figure 8.7 b); an increase (decrease) in wave power occurs along the north and central Mexican Pacific during PDO positive (La Niña-like, negative) periods, while the opposite relationship occurs on the south Mexican and Central American Pacific coast. This suggests that the PDO may amplify the wave power response to individual ENSO events along the Pacific coast. Similarly, the response of wave direction to the PDO (Figure 8.8 c) is similar to that of ENSO (Figure 8.7 c). There is a moderate negative correlation on the Pacific coasts of Baja California and Central America and in the Gulf of Mexico, with a positive response along the central Pacific Mexican coast and on the Yucatan Peninsula.

The AMO shows a moderate positive correlation on the entire Pacific coast and Yucatan Peninsula for wave power and direction, and weaker negative correlation in the Gulf of Mexico. This indicates that AMO positive (negative) drives an increase (decrease) in wave power with the opposite occurring on the Gulf coast. Figure 8.8 and Figure 8.9 indicate a coupling of wave climate response to the PDO and AMO on the north and central Pacific coast of Mexico and the Yucatan Peninsula.

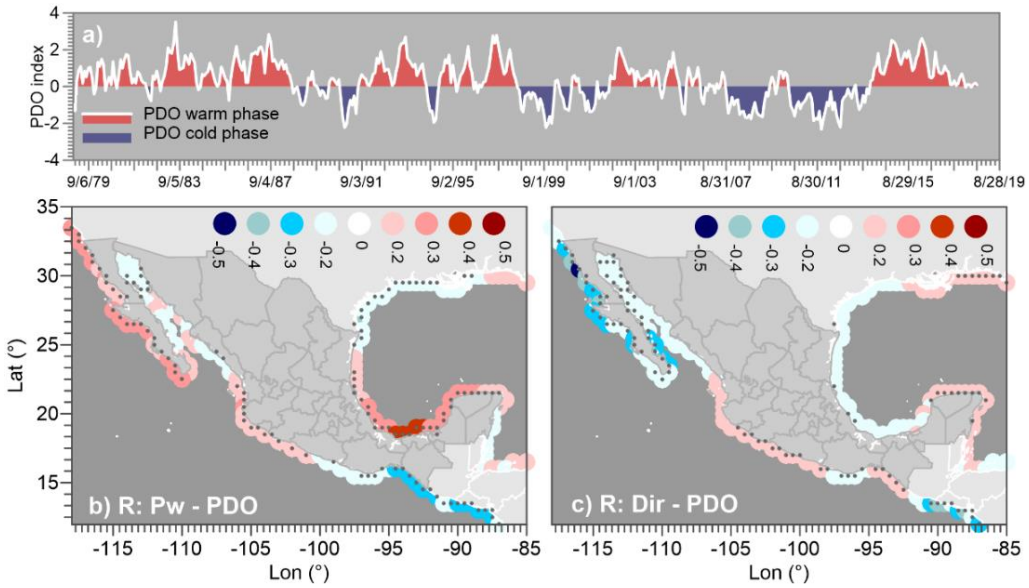


Figure 8.8. a) Time series of PDO climate index, in blue are the cold phases and in red the warm phases; b) and c) correlation coefficient of the PDO phases with wave power (b) and wave direction (c). Points indicate correlation coefficient at 95% confidence level.

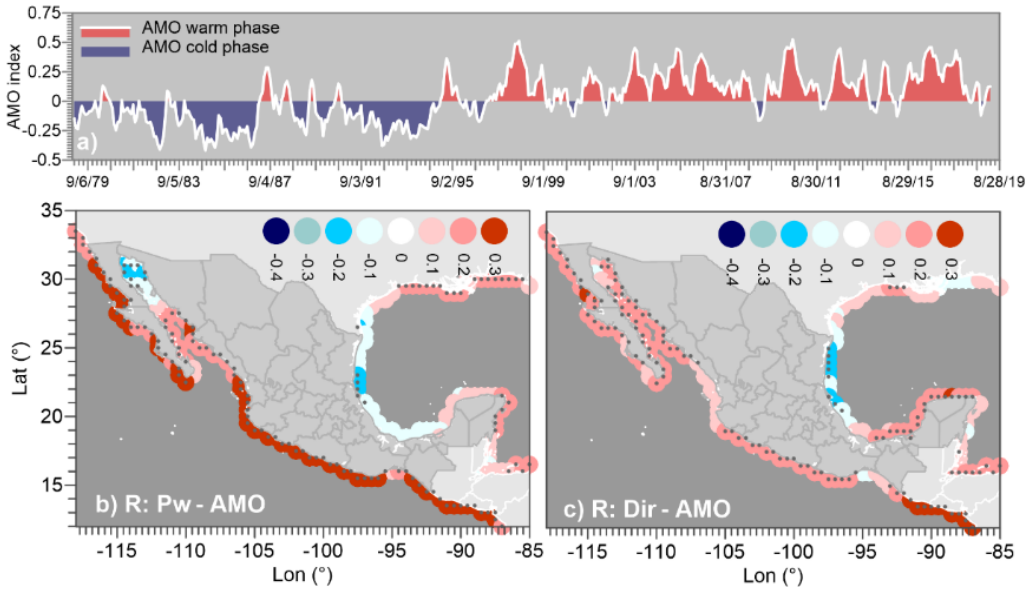


Figure 8.9. a) Time series of AMO climate index, in blue are the cold phases and in red the warm phases, b) and c) correlation coefficient (*R*) with the AMO and wave power, c) correlation coefficient with the AMO and mean wave direction. Points indicate correlation coefficient at 95% confidence level.

## 8.5 Climate change projections

Moderate (RCP 2.6) and severe (RCP 8.5) scenarios of climate change were analysed for wave power and mean wave direction. In the RCP 2.6 scenario, the wave power is projected to increase in Baja California all year round, and only from June to November in the South Pacific. In contrast to the RCP 8.5 scenario that is projected to increase in the Pacific Basin all year round. On the other hand, in the Atlantic basin, the wave power is projected to reduce. The seasonal analysis is shown in Appendix A$. Overall, under the RCP 8.5 scenario, the wave direction is projected to shift anticlockwise in the Pacific and clockwise in the Gulf of Mexico and the Caribbean Sea. While in the RCP 2.6 scenario wave climate shift similar in the Gulf of Mexico, but in the Pacific, the wave fields will shift clockwise in winter and spring seasons.

Regarding the WCTs, in the next century, for the most severe scenario, RCP 8.5, the southerly wave climate becomes more prevailing all year round. Although, it will be more notorious during the autumn season. These results are shown in APPENDIX A4.

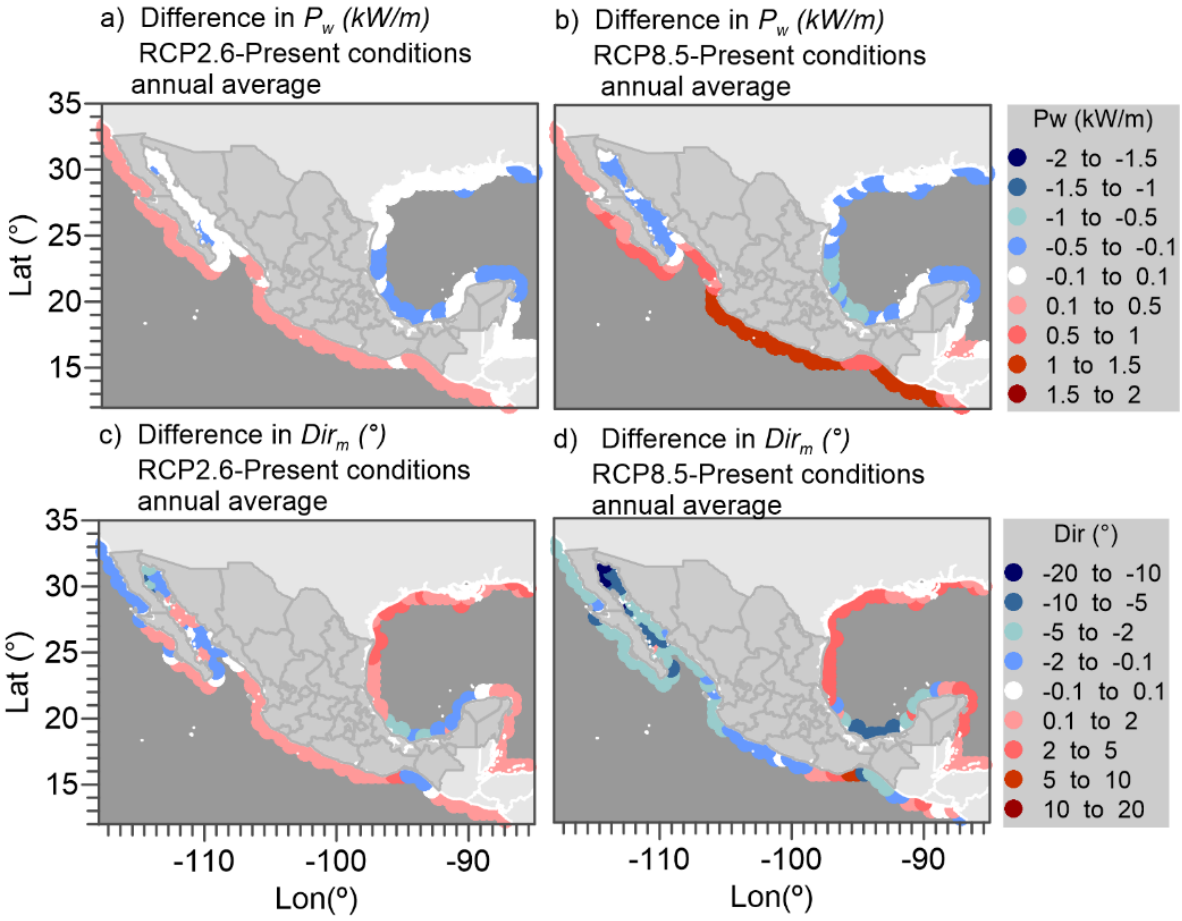


Figure 8.10. Annual differences in wave power between present conditions and a) RCP2.6 scenario, b) RCP 8.5. Annual differences in mean wave direction between present conditions and c) RCP2.6 scenario, d) RCP 8.5.

## 8.6 Potential partners

This work established that the coasts are interconnected around the world affected by the same wave climates. This coastal connectivity can be a window of opportunities to reinforce economic, governmental, and research alliances looking for solutions to face similar problems. In a similar mean, as the research institutions of the Arctic and Antarctic collaborate. For example, they can develop joint research, educative and training programs, consortium of companies, and a governmental alliance between the states in order to address climate adaptation strategies, ecosystems conservancy, rebuilding coastal environments, or WEC design to optimize their efficiency under similar climates.

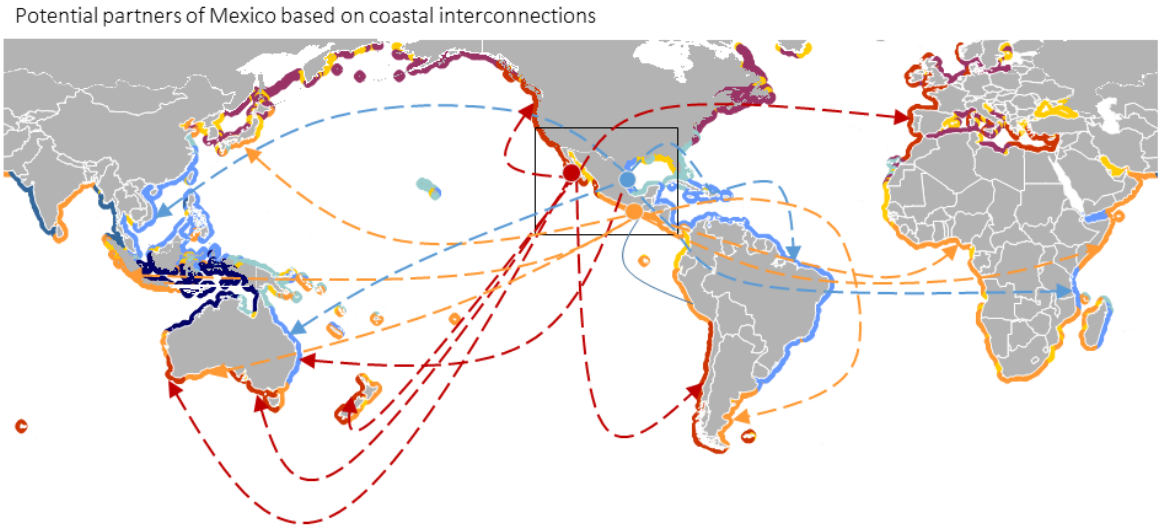


Figure 8.11. Potential partners of Mexico based on common prevailing wave climates. Colours identify coasts affected by the same wave climates types.

## 8.7 Conclusions

The results show two distinct wave climate regimes; a bimodal wave climate (extratropical and subtropical WCTs) on the Mexican Pacific coast and a modal wave climate (tropical WCT) on the Mexican Caribbean coast. The bimodality of the Mexican Pacific is altered by long-term variability and climate change along the Mexican Pacific coast. In contrast, the variability of the tropical wave climate in the Gulf of Mexico and Yucatan Peninsula is lower comparing this found on the Pacific coast.

Results show that wave climate increases (decreases) and rotates anti-clockwise (clockwise) during El Niño (La Niña) on the north and central Pacific coast. That behaviour changes southward of the Pacific coasts, on the Central Pacific coast, the wave power decreases (increases), and wave direction rotates clockwise (anti-clockwise) during El Niño (La Niña). On multi-decadal climate patterns, the response of wave climate to PDO exhibits a similar bearing to ENSO on the Pacific coast, suggesting that changes during individual ENSO events are amplified or dampened when ENSO coupled with PDO. The influence of both climate patterns is weaker on the Caribbean coast. In contrast, AMO shows a significant response on both coasts.

Under climate change scenarios, ocean wave rotations are expected at both side's coasts, and the wave power is projected to increase in the Pacific side, while it will reduce in the Atlantic.

This chapter generates a comprehensive long-term analysis of the wave climate on the Mexican coasts. This wave climate framework establishes a baseline for climate change adaptation and mitigation planning for the near and far future.

## References

Bromirski, P. D., Cayan, D. R., Helly, J., & Wittmann, P. (2013). Wave power variability and trends across the North Pacific. Journal of Geophysical Research: Oceans, 118(12), 6329–6348. https://doi.org/10.1002/2013JC009189

Dissanayake, P., Brown, J., Wisse, P., & Karunarathna, H. (2015). Effects of storm clustering on beach/dune evolution. Marine Geology, 370, 63–75. https://doi.org/https://doi.org/10.1016/j.margeo.2015.10.010

Fairley, I., Lewis, M., Robertson, B., Hemer, M., Masters, I., Horrillo-Caraballo, J., et al. (2020). A classification system for global wave energy resources based on multivariate clustering. Applied Energy, 262, 114515. https://doi.org/https://doi.org/10.1016/j.apenergy.2020.114515

Méndez, F. J., Menéndez, M., Luceño, A., & Losada, I. J. (2006). Estimation of the long-term variability of extreme significant wave height using a time-dependent Peak Over Threshold (POT) model. Journal of Geophysical Research: Oceans, 111(C7). https://doi.org/https://doi.org/10.1029/2005JC003344

Silva, D., Rusu, E., & Soares, C. G. (2013). Evaluation of Various Technologies for Wave Energy Conversion in the Portuguese Nearshore. Energies . https://doi.org/10.3390/en6031344

# CONCLUSIONS

## Conclusions

Wave climate is the principal driver of coastal processes, and as such, many economic activities depend on ocean wave conditions: sun-sand tourism, leisure, renewable energy, fishing, commerce, etc. In the long-term both, natural variability (forced by climate patterns) and climate change (caused by greenhouse gas emissions) shift the atmosphere and ocean systems and affect the global, regional, and local climate. This doctoral research sought to evaluate the long-term impacts of natural variability and climate change on global average wave climate, focusing on wave power and mean wave direction.

Natural variability was studied; we analysed ENSO in detail, which is the principal driver of global wave climate variability at the interannual time scale. Its effects on wave climate, when coupled with the multidecadal climate patterns Pacific Decadal Oscillation (PDO) and Southern Annular Mode (SAM), were also evaluated. The expansion of the tropics is a principal effect of climate change on atmospheric circulation and has already been detected by other authors. However, no previous studies exist that examine its effects on global wave climate. This thesis delves into this phenomenon, and we demonstrated that is a wave climate driver that should be included in coastal risk assessment. Subsequently, the wave climate projections were examined for the climate change scenarios of RCP 2.6 (low emissions) and RCP 8.5 (high emissions). The results of the world's coasts were highlighted intending to make up a comprehensive long-term wave climate framework for coastal applications. Finally, the case study of Mexico was analysed in depth. The main conclusions are described below, in the order of the objectives established in this thesis.

The analysis of ENSO shows that El Niño events (warm phase of ENSO) impact the waves generated in the extratropical latitudes. El Niño intensifies the Hadley cells, increasing the pressure in the subtropical belts and the gradient between mid-high latitudes that leads to the intensification of extratropical winds, and therefore of wave power. These areas are where the major swells of the world are generated and reach many eastern coasts of the ocean basins, including the coast of the Mexican Pacific. On the other hand, the highest impacts on the wave direction were found in the subtropical and tropical regions of the basins. It was also identified that the characteristics of ENSO (asymmetry, amplitude, and intensity) modify the wave climate. More understanding is needed in this regard to enhance coastal risk prediction under ENSO phases.

Despite the remarkable efforts carried out to decipher inherent fluctuations of natural and global warming signals on wave climate, nowadays is still a challenge for science. To deeper analyse both phenomena, the wave climate was classified into types in homology to the major climate regions (polar, temperate, tropical, etc.). These wave climate types (southerlies: subpolar and subtropical; easterlies: tropical and polar; and westerlies: warm pool, monsoon, and extratropical) are driven by planetary wind systems (extratropical, tropical, polar, subpolar, subtropical, warm pool, and monsoon) and therefore their variations are related to the semi-permanent High and Low-pressure centres. This wave climate framework was proposed with a novel *k-means* technique called dynamic clustering. The results explain and reinforce previous knowledge of global wave climate, such as variability patterns and wave generation. Furthermore, they agree with recent works that address the issue of wave climate and planetary wind systems.

For each wave climate type, the long-term trends of the wave characteristics associated with the warming of the oceans were evaluated, using the sea surface temperature as an indicator. They were compared with the anomalies induced by ENSO phases and when ENSO co-occurs with PDO and SAM. The results show that in the last three decades, natural variability was the main signal in the subtropical climate of the South Pacific Ocean, the monsoon, the extratropical of the Pacific, the

tropical of the Indian Ocean, and the polar wave climate types. The climates in which global warming was detected and exceeded the thresholds of natural variability, were the warm pool, the extratropical and subtropical of the Indian Ocean, and the tropical of the Atlantic and Pacific. Wave climates with great natural variability can mask a sign of emerging global warming. This could be happening in the Pacific sector of the Southern Ocean, which has large natural fluctuations forced by SAM and ENSO.

Expansion of the tropics was detected in several oceanic regions and showed some heterogeneity across the ocean basins. Specifically, five areas were identified where the tropical widening impacts most on the wave climate. For each region, we proposed five indices called Expanding Tropics Indices (ETIs). We demonstrated that the poleward displacement of the tropical limits significantly influences global wave conditions, with the most impact seen on wave direction rather than wave power. In consequence, the expanding tropics is a wave climate driver that coastal risk assessments should include.

For the far future, the wave climate was examined under different climate change scenarios of RCP 2.6 (low emissions) and RCP 8.5 (high emissions). Changes in wave climates (southerlies, easterlies, and westerlies) were quantified in frequency, direction, wave power, and area. Those changes were induced by projected shifts in tropical, extratropical, and polar circulation. For instance, the extratropical wave climates will increase their power at high-latitudes, but they will decrease at mid-latitudes caused by a poleward displacement of the extratropical circulation. We identified the transitional wave climate regions that should be priority areas for coastal adaptation to climate change. We concluded that the easterly and southerly wave climates will become more prevalent under global warming with implications for coastal environments. Furthermore, for the first time, our analysis depicts wave climate projections at the circumpolar scale, where new marine regions may emerge, due to melting ice.

From these results, we propose three coastal wave climate atlases that classify the coasts according to the wave response to natural variability, global warming signal, and those regions that will suffer changes in the frequency of the prevailing wave climates under the RCP 8.5 scenario. The classification identifies and connects coasts throughout oceans; from this, some bases can establish to plan coastal adaptation at national and transnational scales.

Finally, all of the datasets and analyses developed in this thesis were applied to the case of Mexico to carry out a detailed assessment of long-term changes in wave climate. The Pacific coasts present a bimodal climate between the extratropical and subtropical wave climates types that highly respond to climate patterns. In the Gulf of Mexico and the Caribbean Sea, the tropical wave climate type prevails all year round and fewer fluctuations were detected. An increase in wave power is projected for the Pacific coast, caused partly by an increase in the frequency of the subtropical wave climate type.

**Future lines of investigation**

Although this work focuses on average wave climate at the global scale, coastal adaptation cannot be limited to this climate-related driver alone. Similarly, coastal processes at the local scale also involve complex interactions with other factors, such as relative sea level, extreme events, sediment budget, land use, and the conservancy state of ecosystems. Furthermore, the long-term wave climate changes must be evaluated at the local scale. Thereby, it is necessary to carry out downscaling methods (numerical modelling or statistical approaches) to quantify the interactions of wave climate with these local factors and its consequences on erosion, flooding, ecosystem

connectivity, and coastal squeeze, among others. In addition, storm waves deserve special attention, since extreme events can produce episodic erosion and flooding that affect the resilience of coastal systems. Therefore, a comprehensive assessment, including climate, biophysical, socioeconomic, and governmental perspectives, must be implemented if we are to develop optimal adaptation projects.

**Contribution of this thesis**

Research on which this thesis is based.

Peer reviewed

1. **Odériz I.**, Rodolfo S., Mortlock T.R., Mori N., Shimura T., Webb A., Padilla-Hernandez R., Villers S. (2021) "Natural Variability and warming signal in global ocean wave climates". Geophysical Research Letters, 48, e2021GL093622.

2. **Odériz I.**, Rodolfo S., Mortlock T.R., and Mori N. (2020) "El Niño-Southern Oscillation impacts on Global Wave Climate and potential Coastal Hazards". Journal of Geophysical Research Oceans. e2020JC016464.

3. **Odériz I.,** Silva R., Mortlock T.R., and Mendoza E. (2020). "Climate Drivers of Directional Wave Power on the Mexican Coast". Ocean Dynamics 70(9), 1253–65.

4. **Odériz I.**, Mori N., Shimura, Web A., Silva R., and Mortlock T.R. "Changes in Prevailing Wave Climates on the Global Continental and Polar Coasts under Warmer Scenarios". (In preparation)

5. **Odériz I.**, Silva R., Mori N., and Mortlock T.R. "The Expanding Tropics, a wave climate driver with implications in coastal environments". (In preparation)

International conferences

1. **Odériz I**., Mori N., Mortlock T. R., Mendoza E.G., and Silva R. (2020). "Transitional Impacts of ENSO on wave climate in coastal regions". Coastal Engineering Proceedings, 36v, 22-22.

2. Silva R., **Odériz I**., Mortlock T.R., and Mariño-Tapia I. (2020). "Climate Variability induced shifts of the wave climate in Mexico". In virtual International Conference on Coastal Engineering 2020. Coastal Engineering Proceedings, 36v, 21-21.

3. **Odériz I.,** Mortlock T.R., Silva R., and Sentic S. (2019). "Directional Wave Changes Induced by the Expanding Tropics". Poster in 2nd International Workshop on Waves Storm Surges and Coastal Hazards at Melbourne, Australia 2019.

4. **Odériz I.,** Silva R., Mortlock T.R., and Mendoza E (2018). "Climate Drivers of Directional Wave Power on the Mexican Coast". LatWaves, Medellin, Colombia.

Research related to this thesis

Peer reviewed

1. Guimarais, M.; Zúñiga-Ríos, A.; Cruz-Ramírez, C.J.; Chávez, V.; **Odériz, I.;** van Tussenbroek, B.I.; Silva, R. (2021) "The Conservational State of Coastal Ecosystems on the Mexican Caribbean Coast: Environmental Guidelines for Their Management". Sustainability, *13*, 2738.

2. Martell R., Mendoza E., Mariño-Tapia I., **Odériz I**., and Silva R. (2020). "How Effective Were the Beach Nourishments at Cancun?". *J. Mar. Sci. Eng.* 8(*6),* 388.

3. **Odériz I.,** Gómez I., Ventura Y., Díaz V., Escalante A., Gómez D.T, Bouma T.J., and Silva R. (2020). "Understanding Drivers of Connectivity and Resilience Under Tropical Cyclones in Coastal Ecosystems at Puerto Morelos, Mexico". Journal of Coastal Research 95(sp1), 128–32.

4. **Odériz I.,** Knöchelmann N., Silva R., Feagin R. A., Martínez M.L., and Mendoza E. (2020). "Reinforcement of Vegetated and Unvegetated Dunes by a Rocky Core: A Viable Alternative for Dissipating Waves and Providing Protection?". Coastal Engineering, 158, 103675.

# CONCLUSIONES (español)

**Conclusiones**

El oleaje es el principal impulsor de los procesos costeros y, como tal, muchas actividades económicas dependen de éste, como son el turismo de playa, ocio, energías renovables, pesca, comercio, etc. A largo plazo, tanto la variabilidad natural (inducida por patrones climáticos) como el cambio climático (causado por las emisiones de gases de efecto invernadero) cambian el sistema atmósfera-océano, afectando así el clima en la escala global, regional y local. Esta tesis evaluó los impactos a largo plazo de la variabilidad natural y el cambio climático en el oleaje. El estudio analizó la potencia y dirección media del oleaje en el ámbito global.

En la variabilidad natural se estudió *El Niño-Southern Oscillation* (ENSO) en detalle, ya que es el principal impulsor de la variabilidad interanual del oleaje a escala global. También se evaluaron sus efectos sobre el oleaje, cuando se combinan con los patrones climáticos multidecadales *Pacific Decadal Oscillation* (PDO) y *Southern Annular Mode* (SAM). La expansión de los trópicos ha sido identificada como uno de los principales efectos del cambio climático en la circulación atmosférica. Sin embargo, no existen estudios previos que examinen sus impactos sobre el oleaje. Esta tesis profundiza en este fenómeno y demuestra que es un impulsor de cambio que debe incluirse en la evaluación de riesgos costeros. Posteriormente, se examinaron las proyecciones de oleaje para dos escenarios de cambio climático RCP 2.6 (bajas emisiones) y RCP 8.5 (altas emisiones). Se destacaron los resultados de las costas del mundo para desarrollar un marco de trabajo integral sobre el clima de oleaje a largo plazo. Finalmente, se estudió en profundidad el caso de México. Las principales conclusiones se describen a continuación en el orden de los objetivos establecidos en esta tesis.

El análisis de ENSO muestra que los eventos de El Niño (fase positiva de ENSO) impactan principalmente en los oleajes de las regiones extratropicales. Estas regiones son esenciales en la generación del oleaje y sus impactos; en ellas se generan los oleajes (*swells*) más energéticos del mundo e impactan en la mayoría de las costas este de las cuencas oceánicas, incluida la costa del Pacífico mexicano. El Niño intensifica las celdas de Hadley aumentando la presión en los cinturones de altas presiones subtropicales y el gradiente entre latitudes medias-altas, que produce la intensificación de los vientos extratropicales, y por tanto de la potencia de las olas. Por otro lado, los mayores impactos en la dirección del oleaje se encontraron en las regiones tropicales y subtropicales de las cuencas oceánicas. También se detectó que las características del ENSO (asimetría, amplitud e intensidad) modifican el clima de oleaje y se necesita un mayor entendimiento en este sentido para mejorar la predicción del riesgo costero en las fases del ENSO.

A pesar de los notables esfuerzos realizados para identificar las fluctuaciones inherentes asociadas a las señales de variabilidad natural y cambio climático en el oleaje, a día de hoy sigue siendo un desafío para la ciencia. Para analizar en profundidad ambos fenómenos, se clasificó el clima de oleaje en tipos, en homología con las principales regiones climáticas (polar, templada, tropical, etc.). Estos tipos de clima de oleaje (provenientes del sur: subpolar y subtropical, provenientes del este: tropical y polar, y provenientes del oeste: *warm pool*, monzón y extratropical) son impulsados por los sistemas de vientos planetarios (extratropical, tropical, polar, subpolar, subtropical, *warm pool* y monzón) y en consecuencia sus variaciones están relacionadas con los centros semipermanentes de altas y bajas presiones. Este marco climático de oleaje se desarrolló con una nueva técnica de *k-medias* llamada agrupación dinámica. Los resultados explican y refuerzan el conocimiento previo del clima global de oleaje, sus patrones de variabilidad y la generación de olas. Además, los resultados coinciden con trabajos recientes que abordan el oleaje y su relación con los sistemas de vientos planetarios.

Para cada tipo de clima de oleaje, se evaluaron las tendencias a largo plazo de sus características asociadas con el calentamiento de los océanos, utilizando la temperatura superficial del mar como indicador. Las anomalías inducidas por las fases del ENSO y ENSO cuando ocurre al mismo tiempo que PDO y SAM fueron comparadas con las tendencias asociadas al calentamiento. Los resultados mostraron que, en las últimas tres décadas, la variabilidad natural fue la principal señal en el clima subtropical del Pacífico Sur, en el monzón y en el extratropical del Pacífico, en el clima tropical del Océano Índico y en todos los climas polares de oleaje. Los climas de oleaje que se vieron afectados por el calentamiento global, y que excedieron los umbrales de la variabilidad natural, fueron el *warm pool*, el extratropical y subtropical del Océano Índico y el tropical del Atlántico y Pacífico. Se debe poner especial atención en el sector correspondiente al Pacífico Sur del Océano Austral, donde se detectó una fuerte tendencia, pero fue menor a las fluctuaciones naturales forzadas cuando SAM y ENSO ocurren al mismo tiempo. Es de suma importancia analizar en detalle las regiones climáticas con gran variabilidad natural, ya que pueden enmascarar señales de calentamiento que están emergiendo o emergerán en un futuro.

La expansión de los trópicos es heterogénea a lo largo de las cuencas oceánicas. En particular, se detectaron cinco áreas donde el ensanchamiento tropical afecta más a las características del oleaje. Para cada una de estas regiones, se propusieron cinco índices denominados Índices de la Expansión de los Trópicos (ETIs, por sus siglas en inglés). De la correlación de estos índices con las características del oleaje, se demostró que el desplazamiento hacia los polos de los trópicos influye significativamente al oleaje, con mayor impacto en la dirección que en la potencia. En consecuencia, la expansión de los trópicos es un impulsor de cambio del oleaje que se debe incluir en las evaluaciones de riesgo costero.

El clima de oleaje se examinó bajo los escenarios de cambio climático, RCP 2.6 (bajas emisiones) y RCP 8.5 (altas emisiones). Los cambios inducidos por el cambio climático en los climas de oleaje (provenientes del sur, este y oeste) se cuantificaron en frecuencia, dirección, potencia y área. Estos cambios fueron inducidos por cambios proyectados en la circulación tropical, extratropical y polar. Por ejemplo, los climas de oleaje extratropicales aumentarán su potencia en latitudes más altas, pero disminuirán en las latitudes medias debido al desplazamiento hacia los polos de la circulación extratropical. También se identificaron las regiones climáticas de transición del oleaje que deben ser áreas prioritarias para la adaptación al cambio climático. Se observó que los climas de oleaje provenientes del este y del sur serán más frecuentes en un clima cambiante con implicaciones en los ambientes costeros. Además, por primera vez, las proyecciones de clima de oleaje se presentaron en la escala circumpolar, que debido al deshilo, las regiones polares pueden ser nuevas regiones marinas.

Con estos resultados, se propusieron tres atlas de clima de oleaje para las costas del mundo que se basan en la respuesta del oleaje a la variabilidad natural, al calentamiento global y a cambios en la frecuencia de los climas de oleajes bajo el escenario RCP 8.5. Estos atlas pueden servir para establecer la planificación en la adaptación costera a escalas nacionales y transnacionales. Además, esta clasificación identifica las zonas costeras que están interconectadas por tener las mismas características de oleaje.

Finalmente, se realizó una evaluación detallada de los cambios a largo plazo en el clima de oleaje a escala nacional. Para ello, los datos y análisis desarrollados en esta tesis se aplicaron al caso de México. Las costas del Pacífico presentaron un clima bimodal, con oleajes provenientes de ambos hemisferios (subtropical y extratropical) que respondieron en gran medida a los patrones climáticos. En el Golfo de México y el Mar Caribe, el clima de oleaje tropical se presenta durante todo el año y

en él se detectaron menos fluctuaciones inducidas por variabilidad natural. Para los futuros escenarios de cambio climático, se proyectó un aumento en la potencia del oleaje en las costas del Pacífico, causado en parte por un aumento en la frecuencia del clima subtropical proveniente del Hemisferio Sur.

**Futuras líneas de investigación**

Este trabajo sólo se centra en el oleaje en condiciones medias a escala global. Sin embargo, los procesos costeros a escala local también involucran interacciones complejas con otros factores, como el nivel relativo del mar, los eventos extremos, el balance de sedimentos, el uso de suelo o el estado de conservación de los ecosistemas. Además, es necesario evaluar los impactos que las fluctuaciones a largo plazo del oleaje tienen en la escala local, para lo que se deberán aplicar metodologías de reducción de escala, mediante modelación numérica o estadística, que permitan cuantificar las consecuencias de los cambios en el oleaje en la erosión, inundación, conectividad de ecosistemas y *coastal squeeze*, entre otros. Por otro lado, el oleaje generado por tormentas merece especial atención en futuros estudios, ya que los eventos extremos pueden producir episodios drásticos de erosión e inundación con importantes consecuencias en la resiliencia de los sistemas costeros. Por lo tanto, se debe implementar una evaluación integral, que incluya perspectivas climáticas, biofísicas, socioeconómicas y gubernamentales, si queremos desarrollar proyectos eficientes de adaptación al cambio climático.

# APPENDIX A1

This appendix is the supporting information for Chapter 3

List of figures

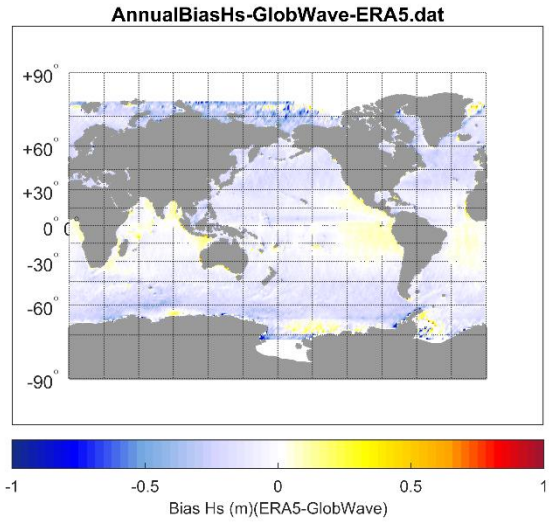


Figure A 1.1.Bias of annual significant height $H_s$, Era5 vs GlobWave from 1992 to 2013.

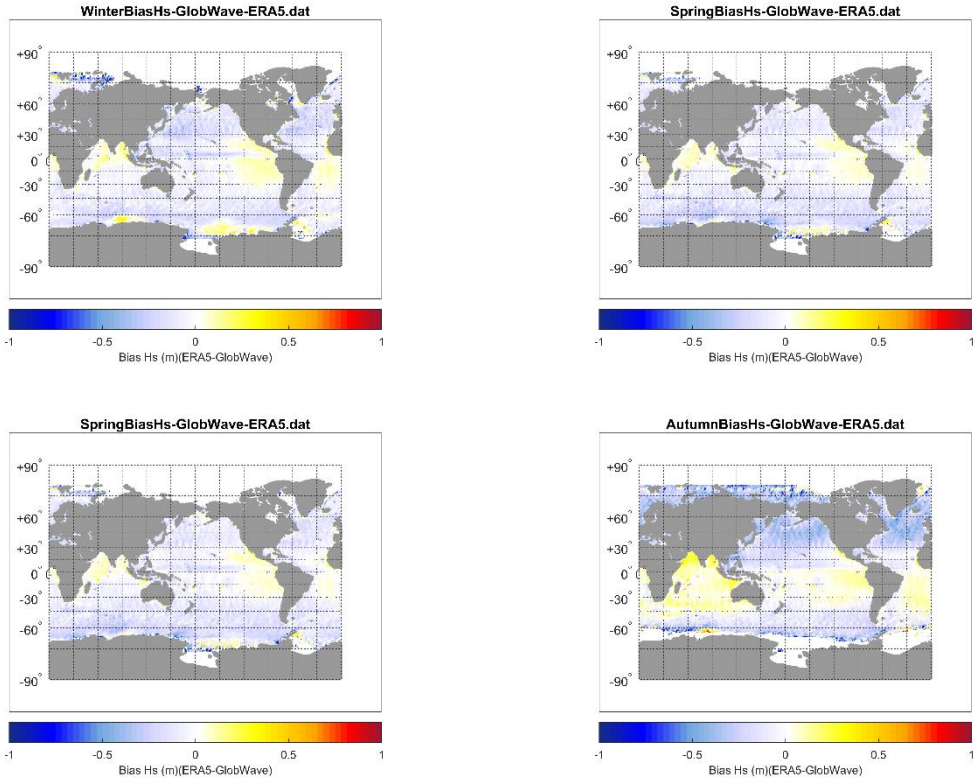


Figure A 1.2. Bias of seasonal significant height $H_s$, Era5 vs GlobWave from 1992 to 2013.

Buoy 51000

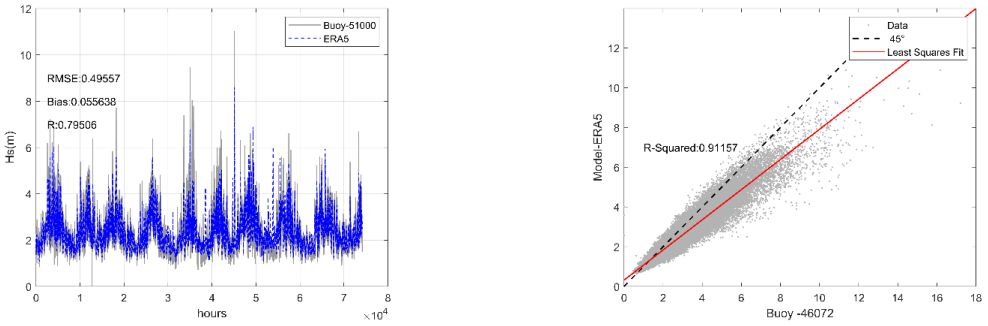


Buoy 46072

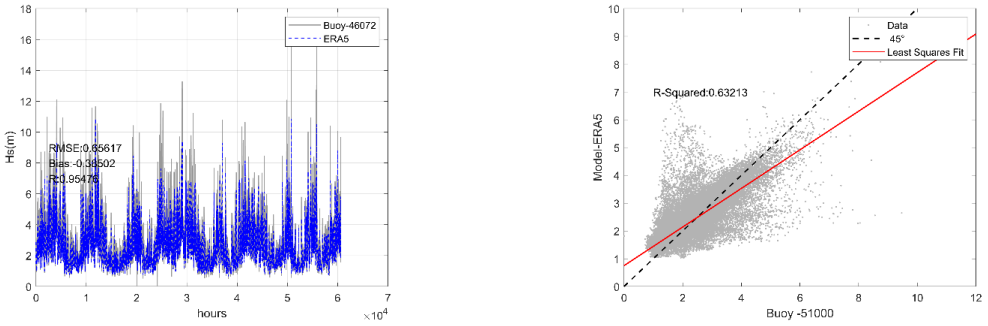


Buoy 46047

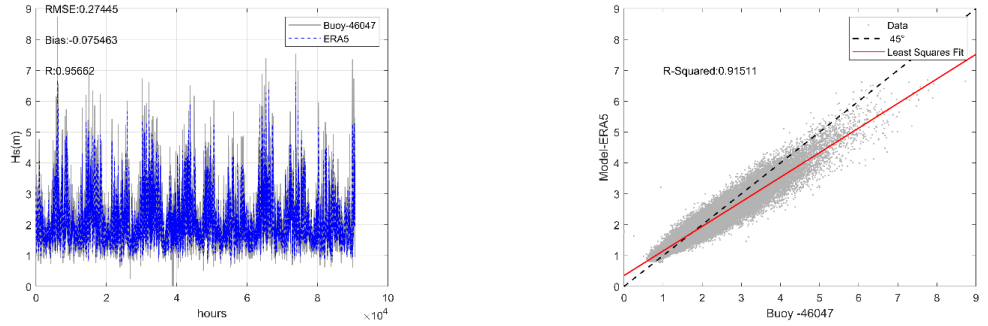


Buoy 41040

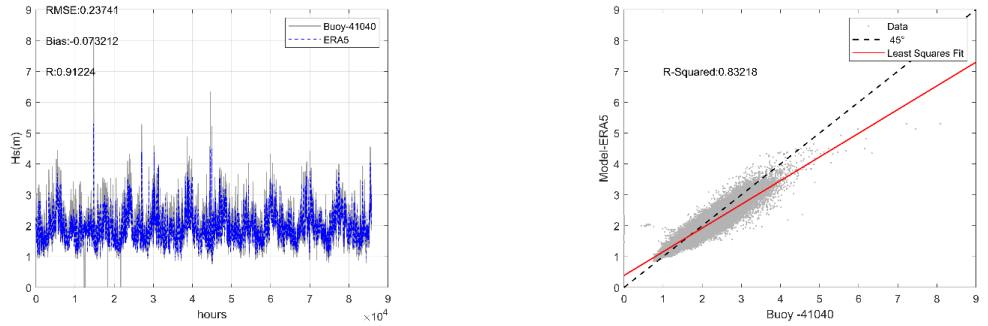


Figure A 1.3. Time series of $H_s$, ERA 5 vs buoy; and Scatter plot, buoy vs ERA 5.

The $H_s$ of the reanalysis was compared with Globwave dataset as a relative error. The results for ERA-5 are shown in Figure A 1.4 for ERA5 and in Figure A 1.5 for JRA-55.ERA 5 sub-estimated the significant waves with the exception of the North Indian basin and southeast Pacific and Atlantic basins. Meanwhile, JRA-55 is positive biased in the whole basins with the exception of tropical region in the east Pacific.

$$Hs_{\mathrm{RE}-GW} = 100 \cdot {}^{(Hs_{RE} - Hs_{GW})}/_{Hs_{GW}} \quad (1)$$

Where:

$Hs_{\mathrm{RE}-GW}$ = Relative error [%]
$Hs_{RE}$ = Significant Height of reanalysis dataset[m]
$Hs_{GW}$ = Significant Height of altimeter data Globwave [m]

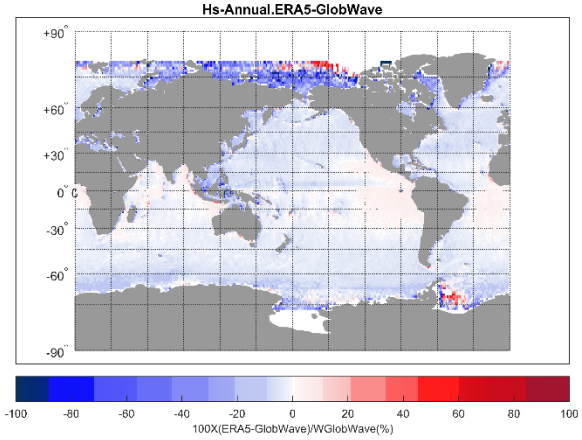


Figure A 1.4 Percentage of difference in Significant Height $H_s$, between ERA5 and Globwave (1992-2013),

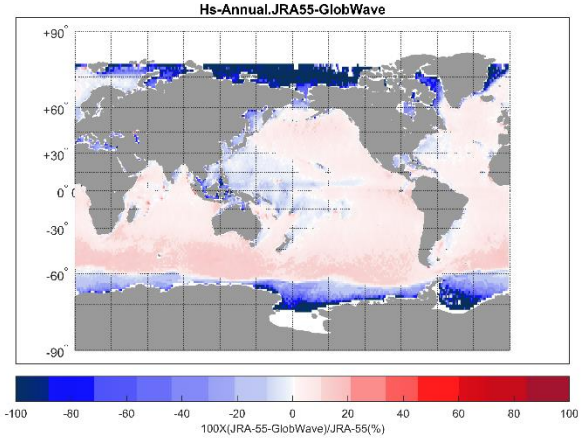


Figure A 1.5 Percentage of difference in Significant Height Hs, between JRA-55 and Globwave (1992-2013).

Then the comparison between both reanalysis is in accordance with the previous results in the significant height. However, the difference between the mean wave periods $T_{01}$ is the opposite, the ERA5 has larger periods for all the basins. The direction parameter fluctuates more spatially, the eastern of the Pacific and Atlantic basins, and the Indian Ocean is further clockwise in the JRA-55 and further anti-clockwise in the northwest and in the Southern Ocean for JRA-55.

$$Hs_{\mathrm{JRA55-ERA5}} = 100 \cdot {\left(Hs_{\mathrm{JRA55}} - Hs_{\mathrm{ERA5}}\right)}/{Hs_{\mathrm{JRA55}}} \quad (2)$$

Where:

$Hs_{\mathrm{JRA55-ERA5}}$ = Relative error [%]
$Hs_{\mathrm{JRA55}}$ = Significant Height of JRA55 reanalysis dataset [m]
$Hs_{\mathrm{ERA5}}$ = Significant Height of ERA5 reanalysis dataset [m]

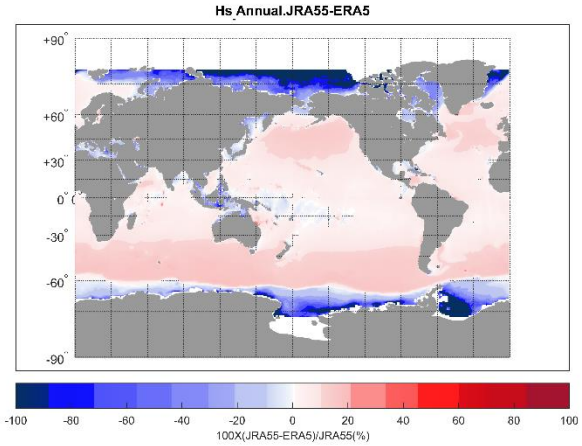


Figure A 1.6 Percentage of difference between JRA-55 and ERA5, $H_s$ (1979-2017).

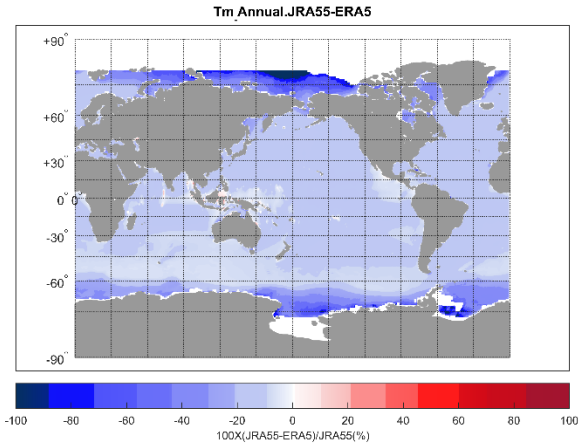


Figure A 1.7 Percentage of difference between JRA-55 and ERA5, T01 (1979-2017).

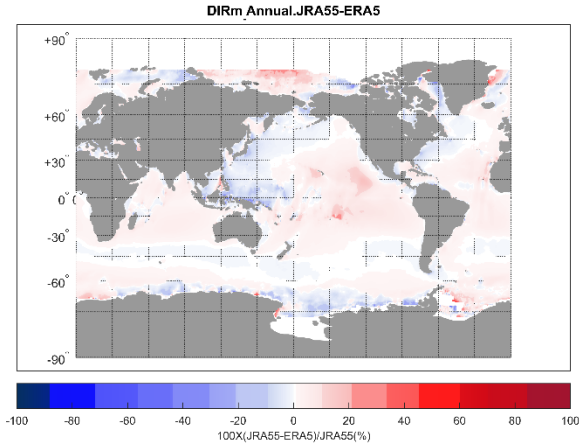


Figure A 1.8 Percentage of difference between JRA-55 and ERA5, $Dir_m$ (1979-2017).

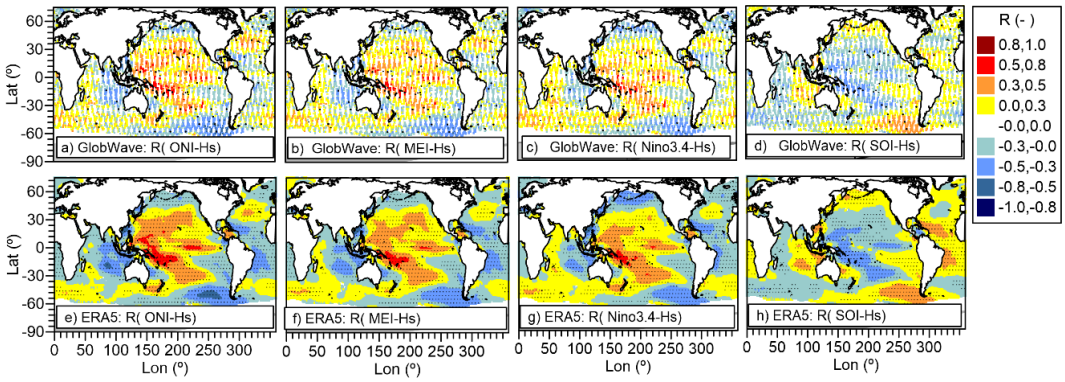


Figure A 1.9**.** Worldwide correlation coefficients of the ENSO climate Indexes and significant Height $H_s$, ERA5 (e, f, g, h) and GlobWave (e, f, g, h) from 1992 to 2013.

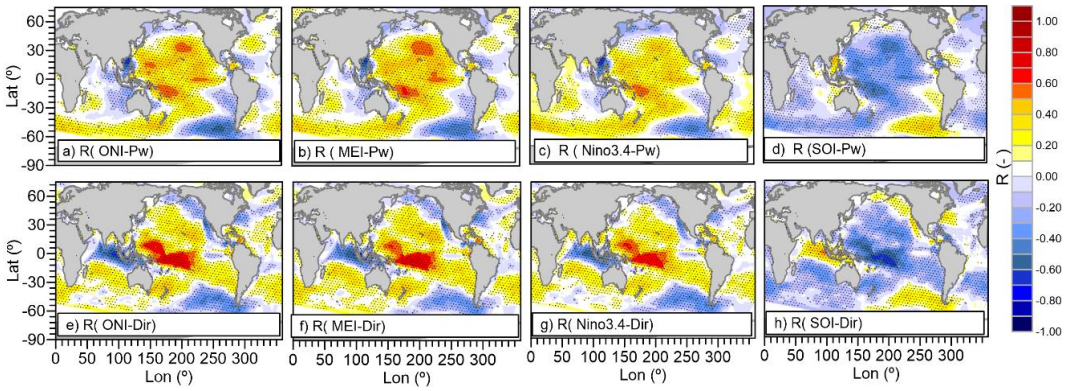


Figure A 1.10. Worldwide correlation coefficients of the ENSO climate indexes and wave power (a, b, c, d) mean wave direction (e, f, g, h).

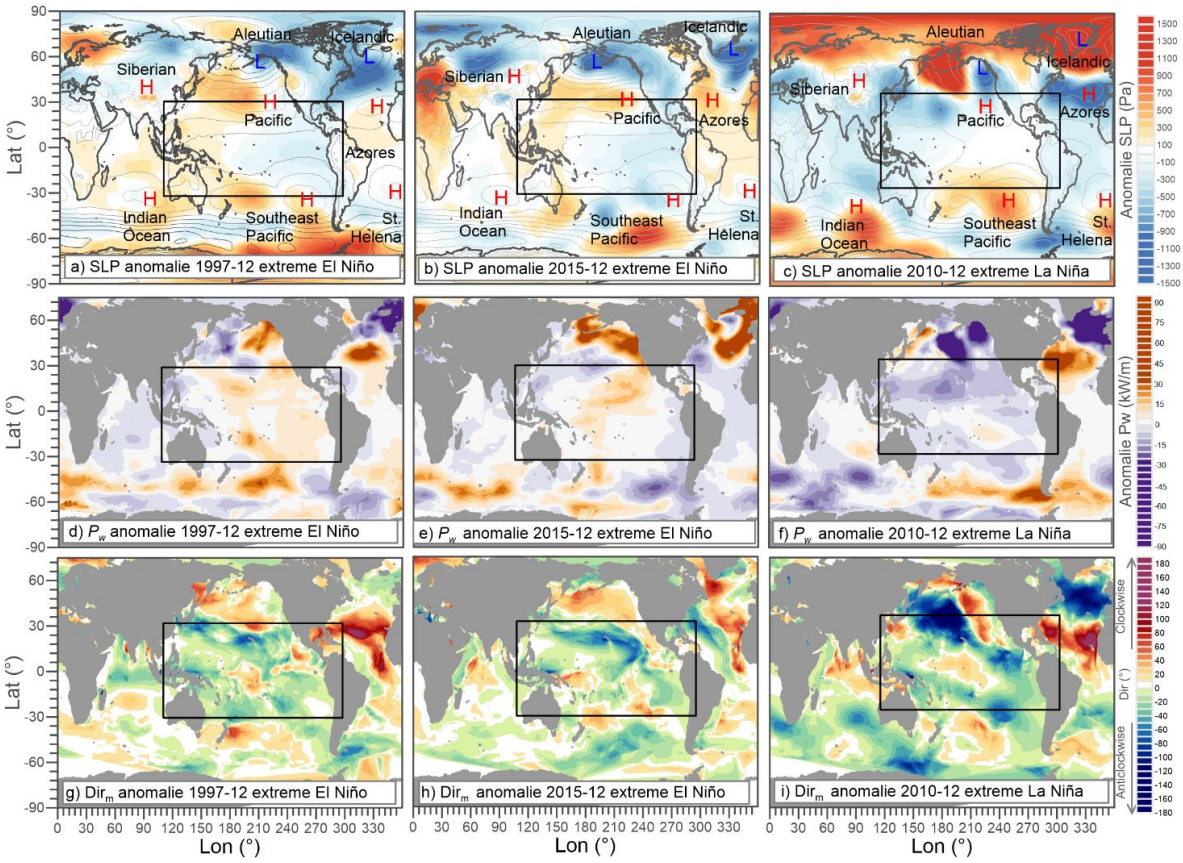


Figure A 1.11. SLP anomalies during extreme warm and cold phases of ENSO. Top, middle and bottom panels are SLP, $P_w$ and $Dir_m$, respectively. Left, middle and right panels are anomalies in December, 1997 (El Niño), 2015 (El Niño) and 2010 (La Niña), respectively. H and L in the top panels indicate high and low pressure systems.

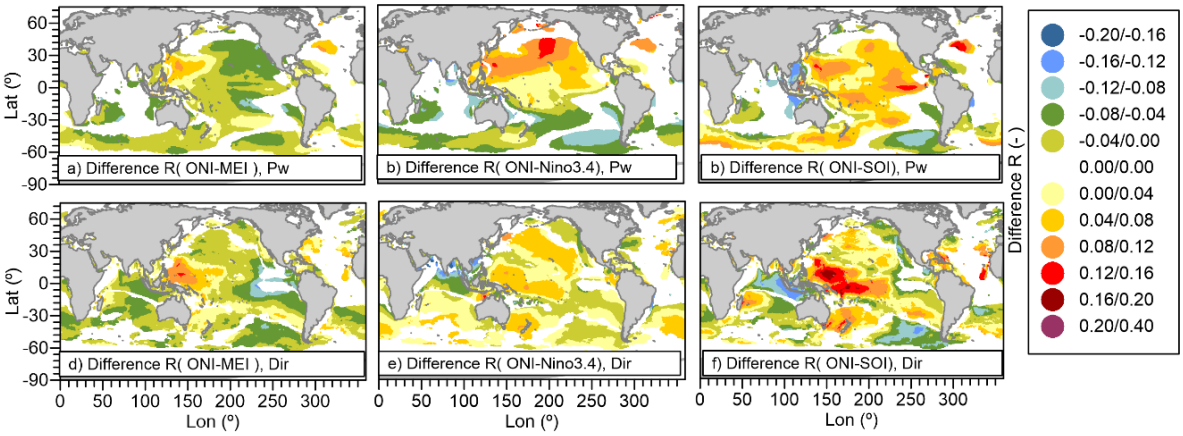


Figure A 1.12. Difference between ONI and other ENSO coefficients and wave power (a, b, c) and mean wave direction (d, e, f). Differences in the correlation coefficient are only represented in those common locations with significant correlation with both ENSO indices

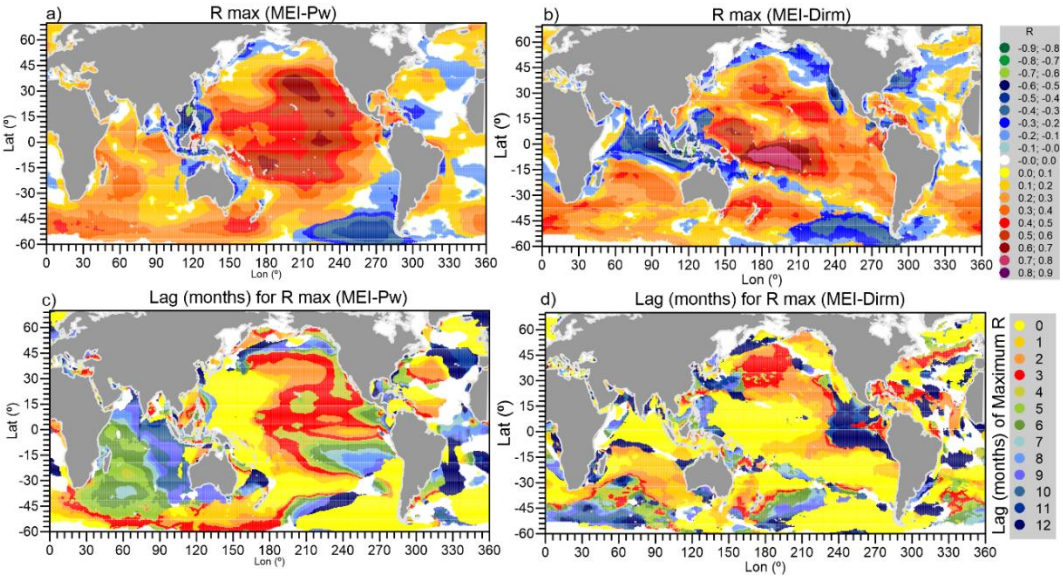


Figure A 1.13. Worldwide maximum cross-correlation coefficients of the MEI that are statistical significant. a) Wave power, b) mean wave direction. Lag-time when the maximum cross-correlated is presented c) wave power, d) mean wave direction.

| Cross-Correlation for each lag (*MEI-$P_w$*) | Cross-Correlation for each lag (*MEI-$Dir_m$*) |
|---|---|
| 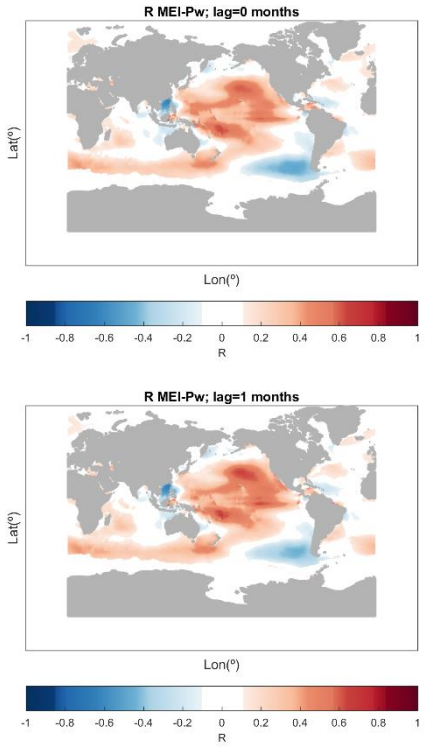 | 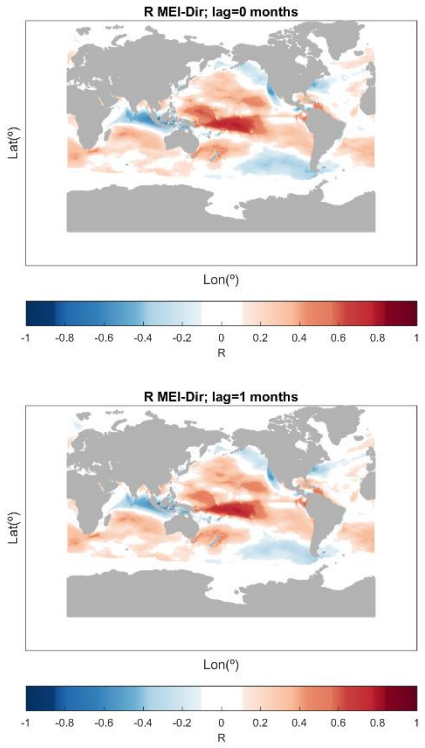 |

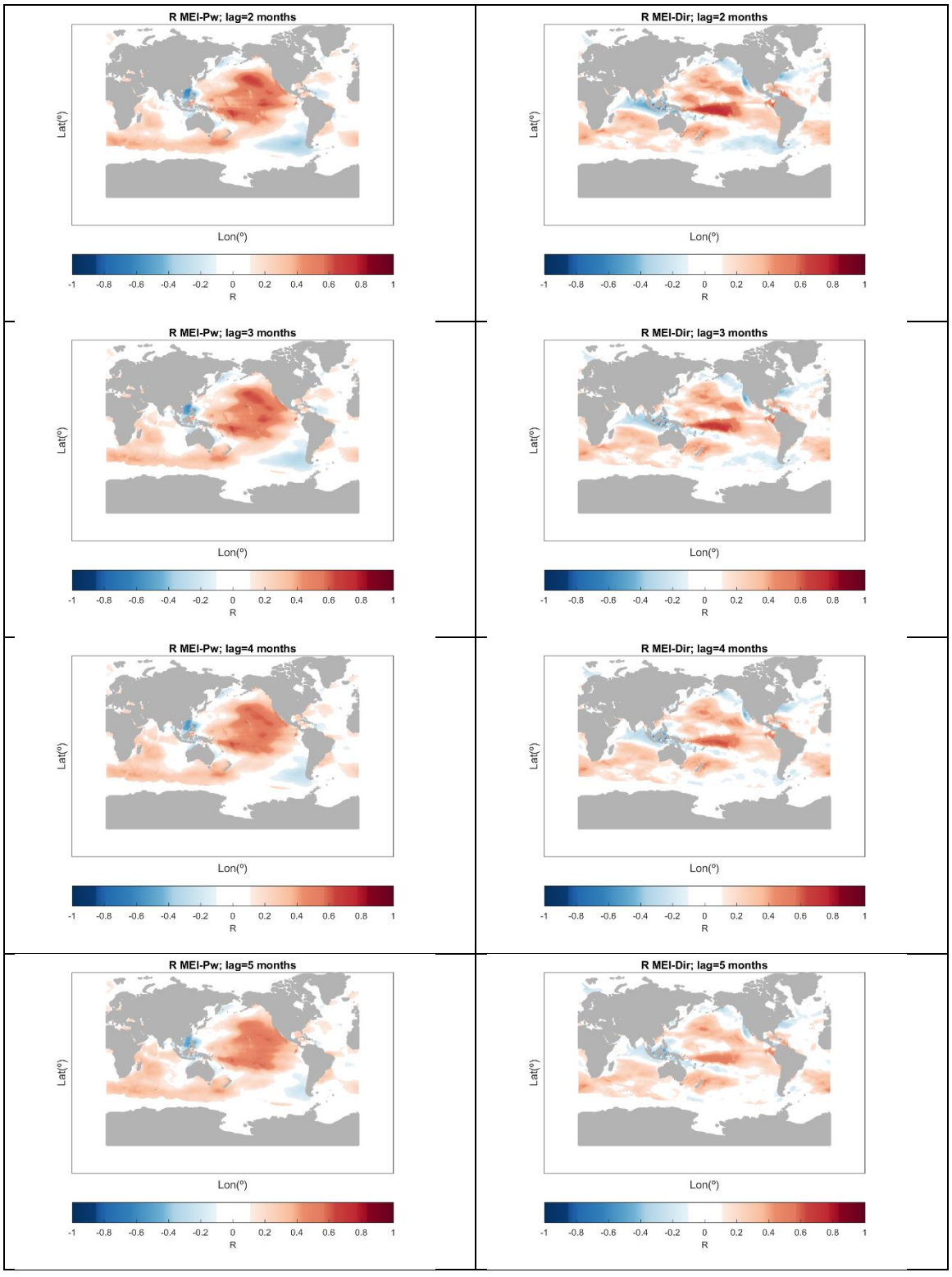
R MEI-Pw; lag=2 months
R MEI-Dir; lag=2 months
R MEI-Pw; lag=3 months
R MEI-Dir; lag=3 months
R MEI-Pw; lag=4 months
R MEI-Dir; lag=4 months
R MEI-Pw; lag=5 months
R MEI-Dir; lag=5 months
Lat(º)
Lon(º)
R
-1 -0.8 -0.6 -0.4 -0.2 0 0.2 0.4 0.6 0.8 1

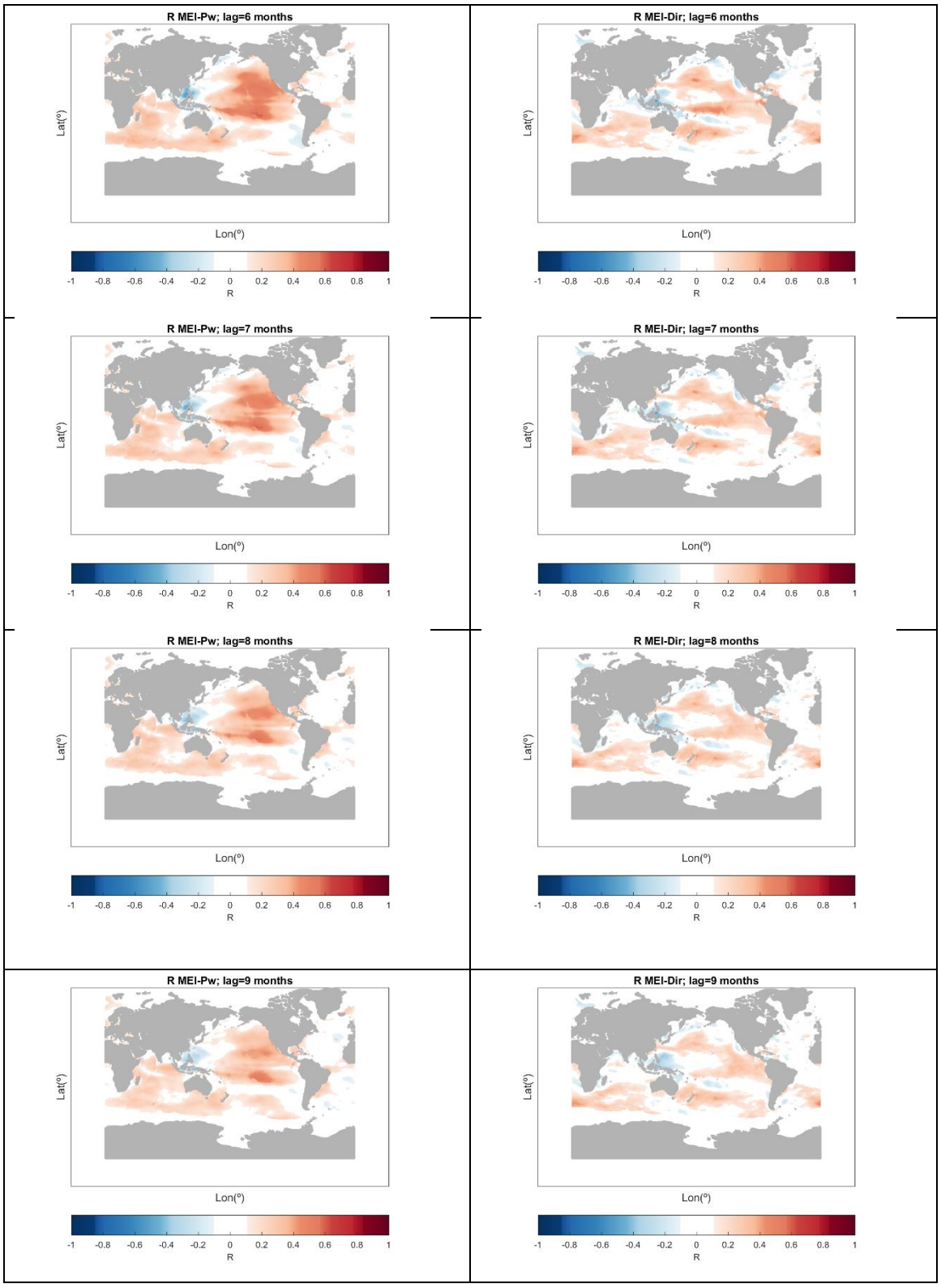
R MEI-Pw; lag=6 months
R MEI-Dir; lag=6 months
R MEI-Pw; lag=7 months
R MEI-Dir; lag=7 months
R MEI-Pw; lag=8 months
R MEI-Dir; lag=8 months
R MEI-Pw; lag=9 months
R MEI-Dir; lag=9 months
Lat(º)
Lon(º)
R
-1 -0.8 -0.6 -0.4 -0.2 0 0.2 0.4 0.6 0.8 1

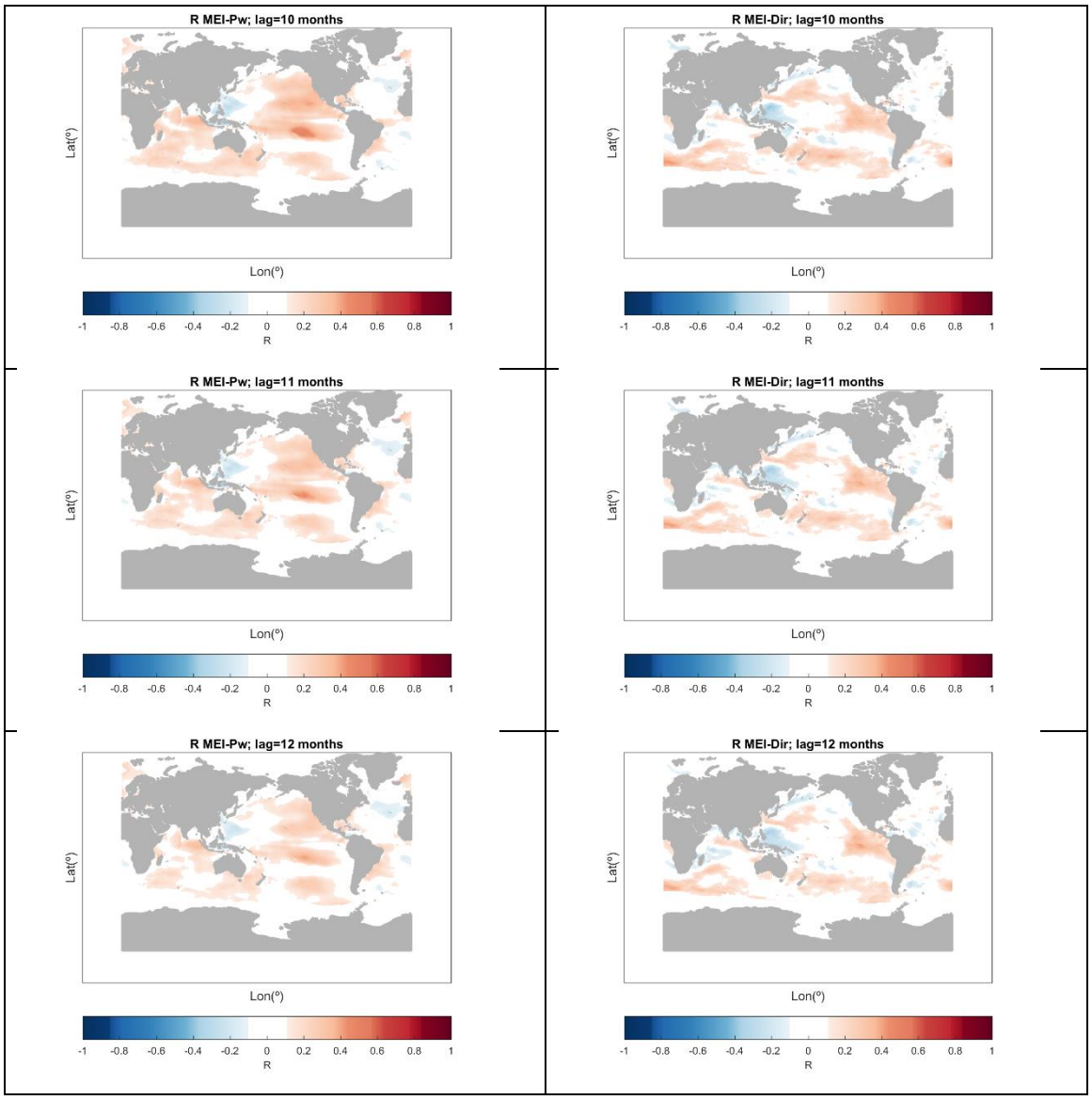


Figure A 1.14. Cross-correlation for lags 0-12 months for MEI-$P_w$ (first column) and MEI-$Dir_m$ (second column). All values are statistically significant.

# APPENDIX A2

This appendix is the supporting information for Chapter 4

List of figures



List of tables

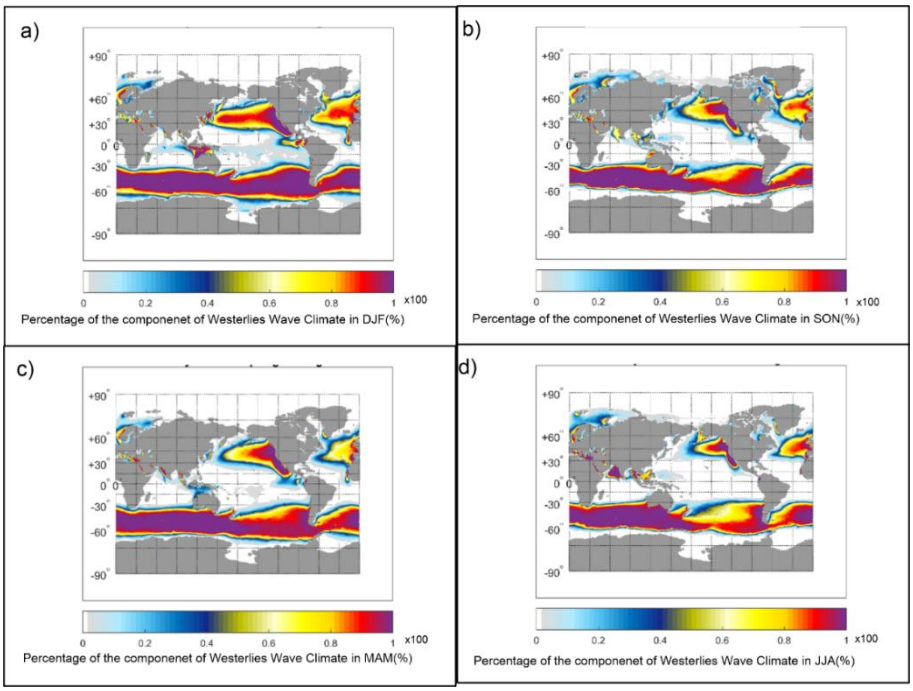


Figure A 2.1 Westerly wave climates component percentage in a) DJF, b) SON, c) MAM, and d) JJA.

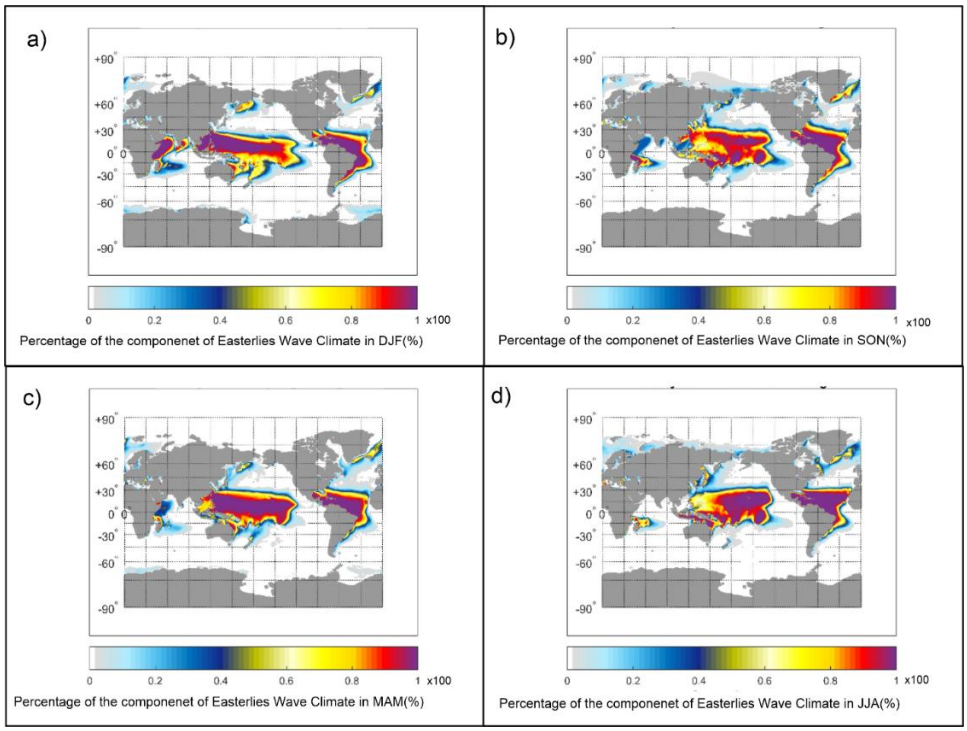


Figure A 2.2 Easterly wave climates component percentage in a) DJF, b) SON, c) MAM, and d) JJA.

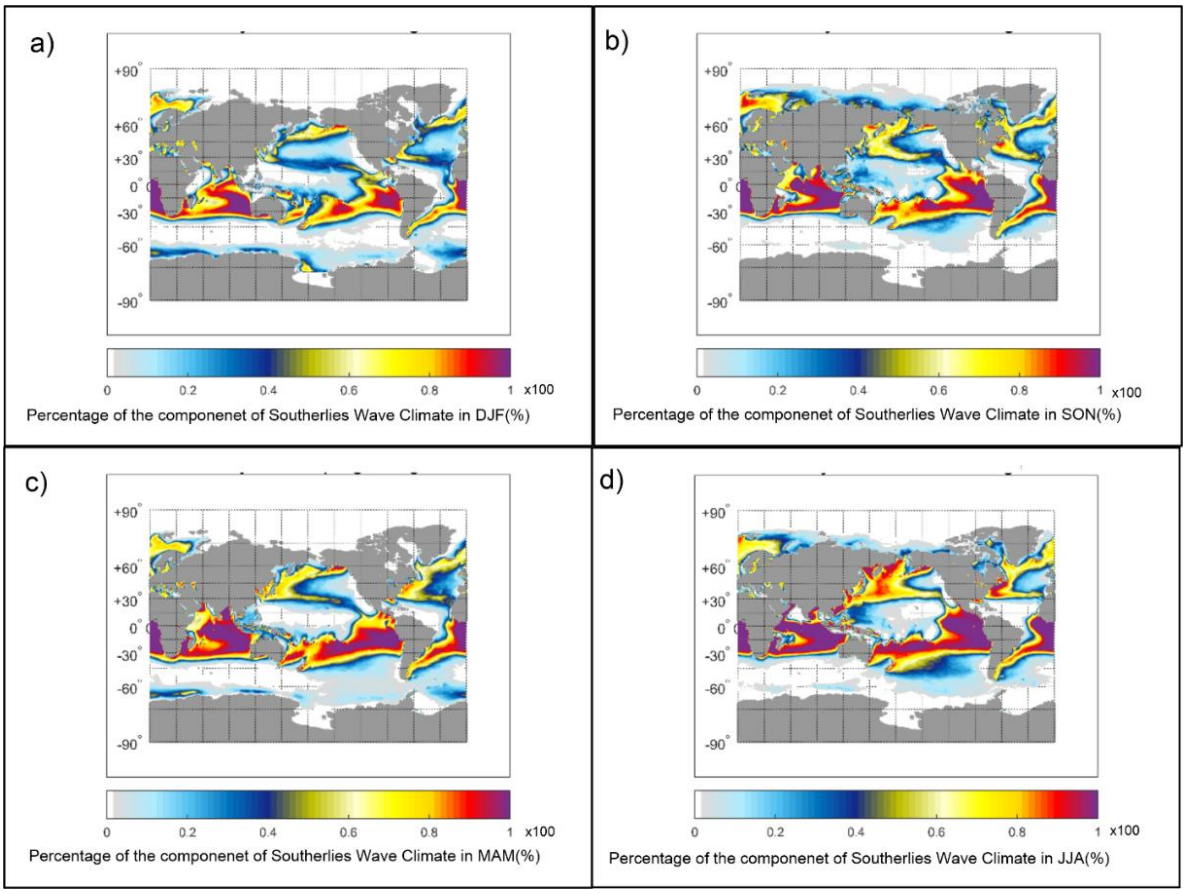


Figure A 2.3 Southerly wave climates component percentage in a) DJF, b) SON, c) MAM, and d) JJA.

Table A 2.1 Seasonal variability of mean wave power.

| | | $P_w$ (kW/m) | | | | |
|---|---|---|---|---|---|---|
| ID | Name | Total | DJF | MAM | JJA | SON |
| STS-IOSH | Subtropical Southerlies Indian Ocean SH | 24.95 | 21.42 | 23.03 | 32.63 | 22.71 |
| STS-SP | Subtropical Southerlies South Pacific | 26.94 | 25.29 | 29.14 | 27.39 | 25.92 |
| STS-NP | Subtropical Southerlies North Pacific | 6.70 | 14.08 | 4.48 | 2.62 | 5.62 |
| SPS-NP | Subpolar Southerlies North Pacific | 25.34 | 56.98 | 16.57 | 5.11 | 22.70 |
| STS-SA | Subtropical Southerlies South Atlantic | 19.58 | 16.40 | 18.34 | 23.35 | 20.21 |
| STS-NA | Subtropical Southerlies North Atlantic | 5.44 | 9.51 | 8.11 | 0.47 | 3.65 |
| SPS-NA | Subpolar Southerlies North Atlantic | 34.66 | 62.25 | 31.02 | 12.51 | 32.85 |
| EW-IOSH | Extratropical Westerlies Indian Ocean SH | 76.11 | 54.03 | 77.69 | 96.09 | 76.63 |
| WPW | Warm Pool Westerlies | 3.34 | 7.21 | 2.27 | - | 3.90 |
| MW | Monsson Westerlies | 7.24 | 0.74 | 4.39 | 18.78 | 5.03 |
| EW-SP | Extratropical Westerlies South Pacific | 67.38 | 48.64 | 73.64 | 78.51 | 68.74 |
| EW-MP | Extratropical Westerlies North Pacific | 41.29 | 64.82 | 40.29 | 17.35 | 42.70 |
| EW-SA | Extratropical Westerlies South Atlantic | 52.98 | 39.56 | 54.68 | 65.05 | 52.63 |
| EW-NA | Extratropical Westerlies North Atlantic | 44.92 | 76.13 | 41.30 | 16.37 | 45.88 |
| TE-IO | Tropical Easterlies Indian Ocean | 15.48 | 9.40 | 12.14 | 23.72 | 16.67 |
| TE-P | Tropical Easterlies Pacific | 18.35 | 22.42 | 18.04 | 14.84 | 18.08 |
| PE-NP | Polar Easterlies North Pacific | 21.08 | 48.54 | 17.76 | 4.92 | 13.10 |
| TE-A | Tropical Easterlies Atlantic | 14.20 | 17.18 | 14.06 | 11.38 | 14.17 |
| PE-NA | Polar Easterlies North Atlantic | 30.98 | 51.50 | 27.47 | 10.26 | 34.68 |

Table A 2.2 Seasonal variability of mean wave direction.

| ID | Name | Mean Wave Direction (º) | | | | |
|---|---|---|---|---|---|---|
| | | Total | DJF | MAM | JJA | SON |
| STS-IOSH | Subtropical Southerlies Indian Ocean SH | 177.51 | 177.47 | 177.01 | 177.42 | 178.12 |
| STS-SP | Subtropical Southerlies South Pacific | 177.32 | 178.34 | 177.96 | 176.12 | 176.85 |
| STS-NP | Subtropical Southerlies North Pacific | 176.19 | 181.75 | 177.31 | 170.46 | 172.37 |
| STS-SA | Subpolar Southerlies North Pacific | 177.08 | 179.64 | 177.68 | 175.20 | 175.98 |
| STS-NA | Subpolar Southerlies South Atlantic | 169.68 | 170.68 | 170.47 | 168.42 | 167.66 |
| SPS-NA | Subtropical Southerlies South Atlantic | 179.42 | 180.78 | 177.73 | 178.88 | 180.29 |
| EW-IOSH | Subtropical Southerlies North Atlantic | 256.42 | 258.16 | 254.76 | 255.80 | 256.94 |
| WPW | Subpolar Southerlies North Atlantic | 245.71 | 253.96 | 244.01 | - | 233.25 |
| MW | Extratropical Westerlies Indian Ocean SH | 239.26 | 258.39 | 240.37 | 235.57 | 235.64 |
| EW-SP | Warm Pool Westerlies | 251.12 | 254.64 | 250.73 | 246.70 | 252.41 |
| EW-MP | Monsson Westerlies | 254.21 | 259.39 | 256.35 | 249.24 | 251.84 |
| EW-SA | Extratropical Westerlies South Pacific | 249.77 | 253.69 | 247.05 | 247.75 | 250.59 |
| EW-NA | Extratropical Westerlies North Pacific | 252.53 | 252.81 | 251.34 | 253.01 | 252.97 |
| PE-IOSH | Extratropical Westerlies South Atlantic | 113.35 | 109.12 | 115.47 | - | - |
| TE-IO | Extratropical Westerlies North Atlantic | 117.79 | 95.59 | 124.56 | 129.96 | 123.71 |
| TE-P | Polar Easterlies Indian Ocean SH | 94.18 | 80.57 | 87.01 | 108.55 | 100.61 |
| PE-NP | Tropical Easterlies Indian Ocean | 115.89 | 108.20 | 117.82 | 122.75 | 118.39 |
| TE-A | Tropical Easterlies Pacific | 89.92 | 85.42 | 86.17 | 93.59 | 94.52 |
| PE-NA | Polar Easterlies North Pacific | 111.81 | 110.63 | 112.68 | 115.31 | 108.64 |

Table A 2.3 Seasonal variability of the total number of months in which each wave climate occurs.

| | | Number of Months in 40 yrs. | | | | |
|---|---|---|---|---|---|---|
| ID | Name | Total | DJF | MAM | JJA | SON |
| STS-IOSH | Subtropical Southerlies Indian Ocean SH | 480 | 120 | 120 | 120 | 120 |
| STS-SP | Subtropical Southerlies South Pacific | 467 | 119 | 116 | 119 | 113 |
| STS-NP | Subtropical Southerlies North Pacific | 182 | 60 | 40 | 34 | 48 |
| SPS-NP | Subpolar Southerlies North Pacific | 360 | 109 | 80 | 70 | 101 |
| SPS-SA | Subpolar Southerlies South Atlantic | 178 | 78 | 83 | 13 | 4 |
| STS-SA | Subtropical Southerlies South Atlantic | 441 | 112 | 98 | 119 | 112 |
| STS-NA | Subtropical Southerlies North Atlantic | 189 | 61 | 60 | 38 | 30 |
| SPS-NA | Subpolar Southerlies North Atlantic | 479 | 120 | 119 | 120 | 120 |
| EW-IOSH | Extratropical Westerlies Indian Ocean SH | 480 | 120 | 120 | 120 | 120 |
| WPW | Warm Pool Westerlies | 240 | 119 | 49 | - | 72 |
| MW | Monsson Westerlies | 355 | 33 | 115 | 120 | 87 |
| EW-SP | Extratropical Westerlies South Pacific | 480 | 120 | 120 | 120 | 120 |
| EW-MP | Extratropical Westerlies North Pacific | 480 | 120 | 120 | 120 | 120 |
| EW-SA | Extratropical Westerlies South Atlantic | 480 | 120 | 120 | 120 | 120 |
| EW-NA | Extratropical Westerlies North Atlantic | 480 | 120 | 120 | 120 | 120 |
| PE-IOSH | Polar Easterlies Indian Ocean SH | 12 | 4 | 8 | - | - |
| TE-IO | Tropical Easterlies Indian Ocean | 448 | 120 | 107 | 101 | 120 |
| TE-P | Tropical Easterlies Pacific | 480 | 120 | 120 | 120 | 120 |
| PE-NP | Polar Easterlies North Pacific | 286 | 96 | 67 | 69 | 54 |
| TE-A | Tropical Easterlies Atlantic | 480 | 120 | 120 | 120 | 120 |
| PE-NA | Polar Easterlies North Atlantic | 357 | 87 | 90 | 89 | 91 |

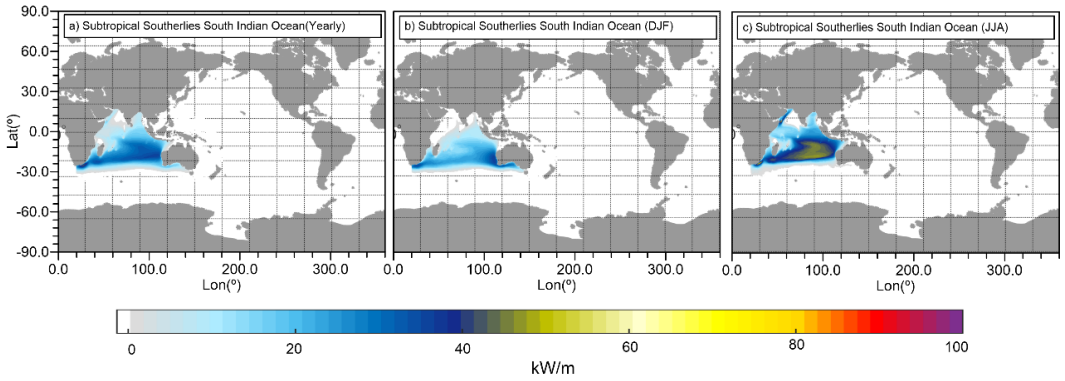


Figure A 2.4. Subtropical wave climate type in Indian Ocean a) yearly, b) DJF, and c) JJA.

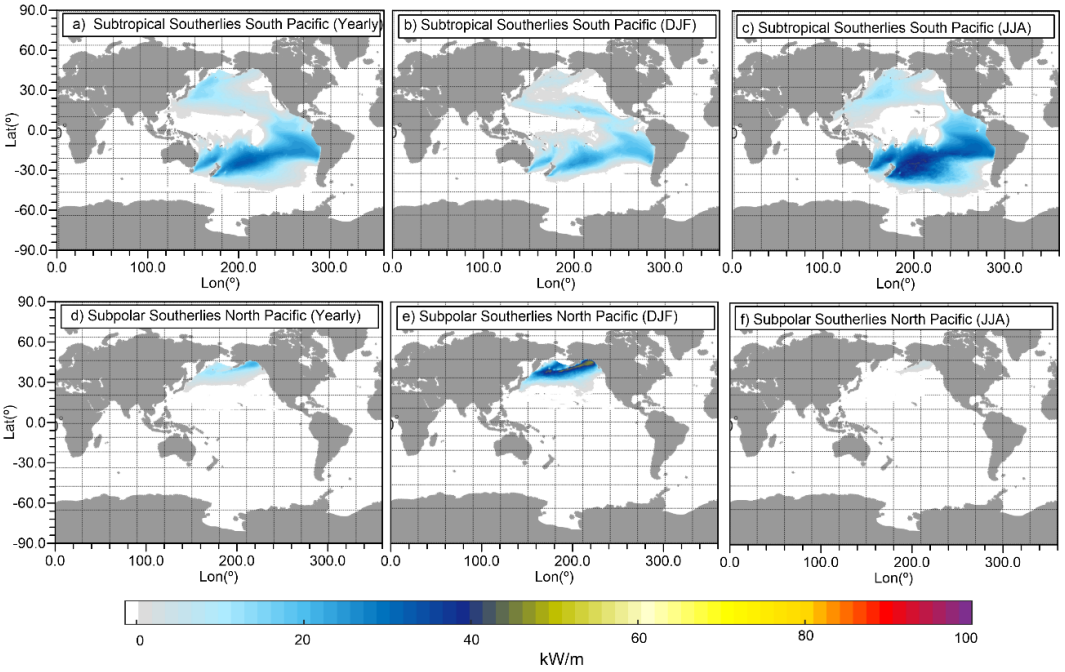


Figure A 2.5 Subtropical wave climate type South Pacific a) yearly, b) DJF, and c) JJA; and subpolar wave climate type North Pacific d) yearly, e) DJF, and f) JJA.

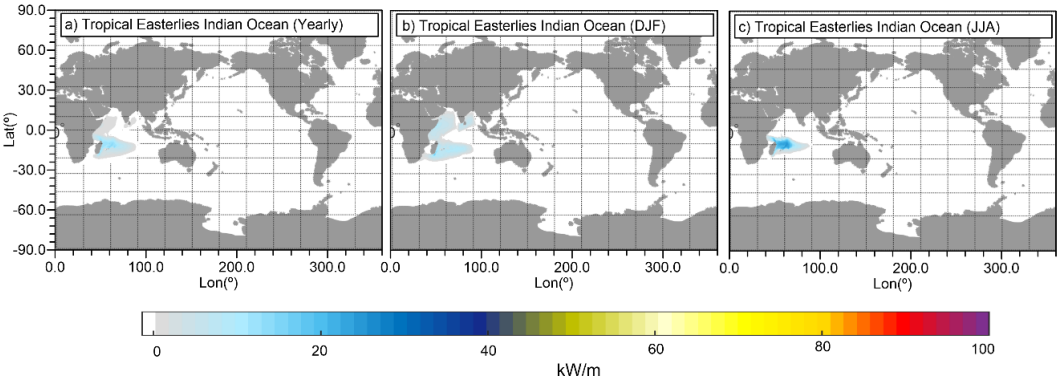


Figure A 2.6. Tropical wave climate type in the Indian Ocean a) yearly, b) DJF, and c) JJA.

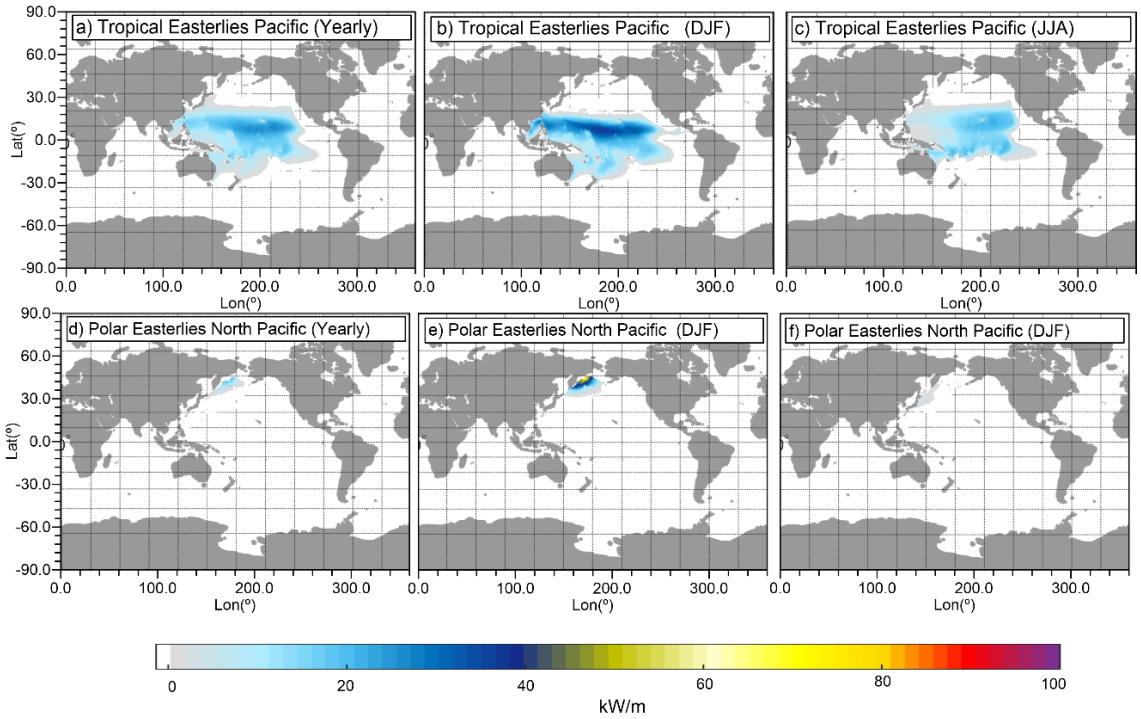


Figure A 2.7 Tropical wave climate type in the Pacific a) yearly, b) DJF, and c) JJA; and polar wave climate type in the North Pacific d) yearly, e) DJF, and f) JJA.

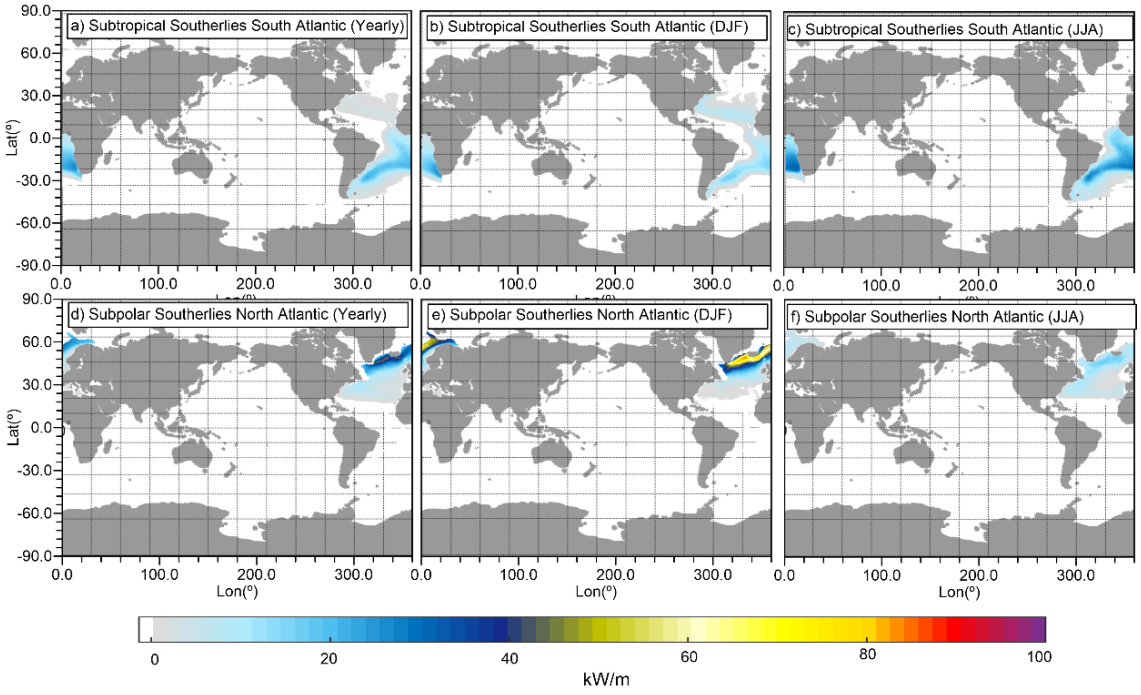


Figure A 2.8 Subtropical wave climate type in the South Atlantic a) yearly, b) DJF, and c) JJA; and subpolar wave climate type in the North Atlantic d) yearly, e) DJF, and f) JJA.

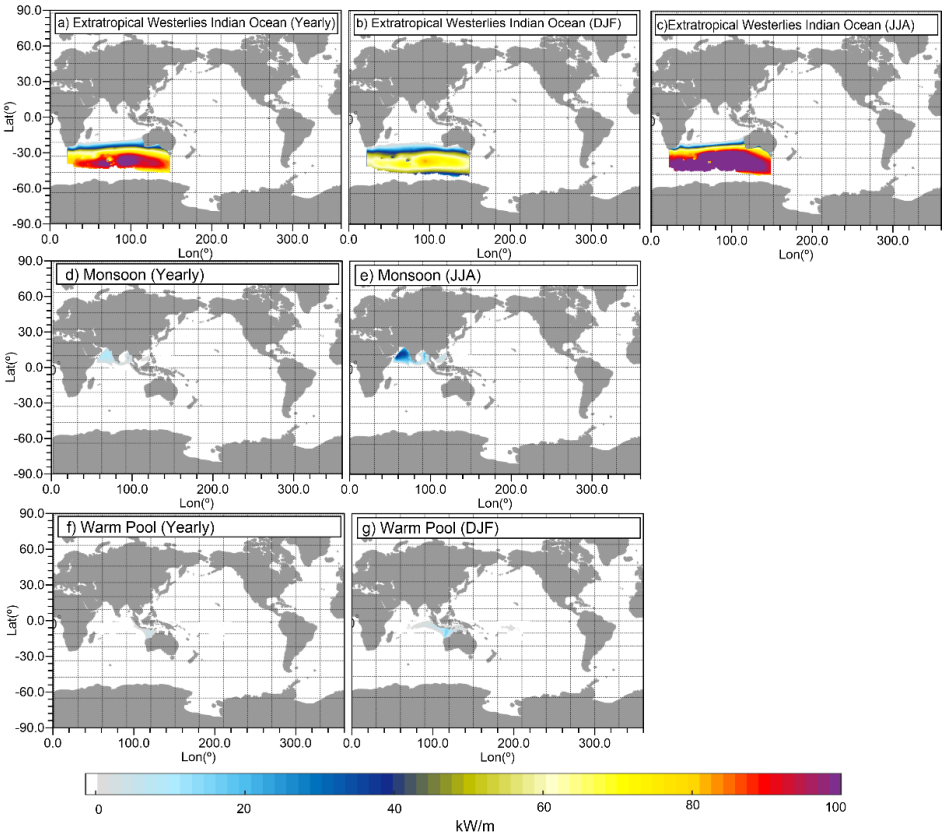


Figure A 2.9 Westerlies wave climate types in the Indian Ocean. Extratropical IO (a, b, c), monsoon wave climate type (d, e), warm pool wave climate type (f, g).

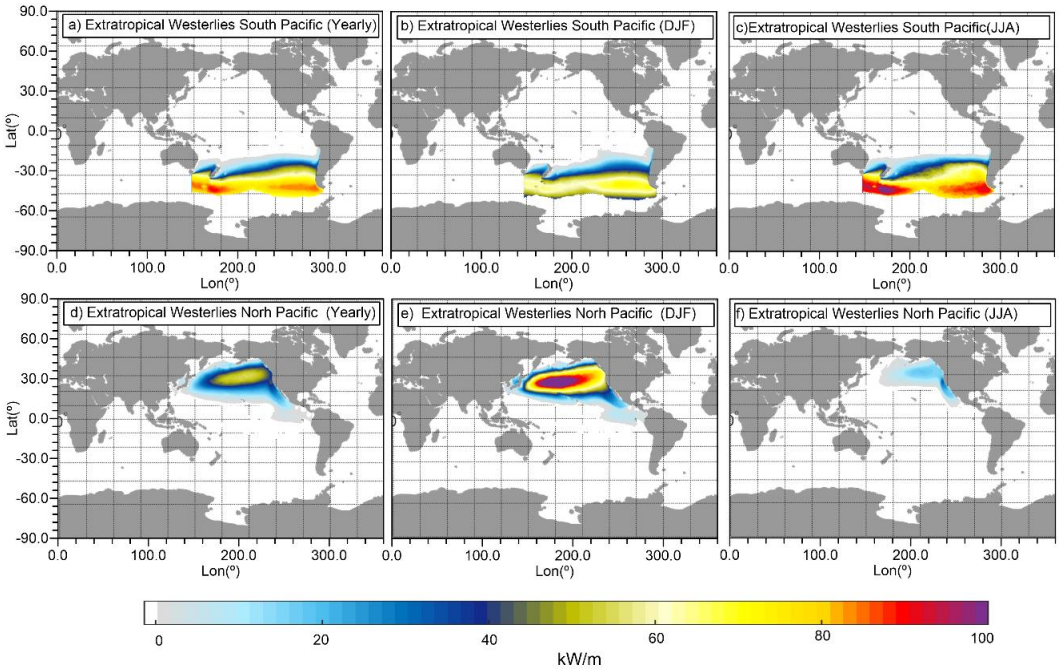


Figure A 2.10 Extratropical wave climate type in the South Pacific a) yearly, b) DJF, and c) JJA.; and extratropical wave climate type in the North Pacific d) yearly, e) DJF, and f) JJA.

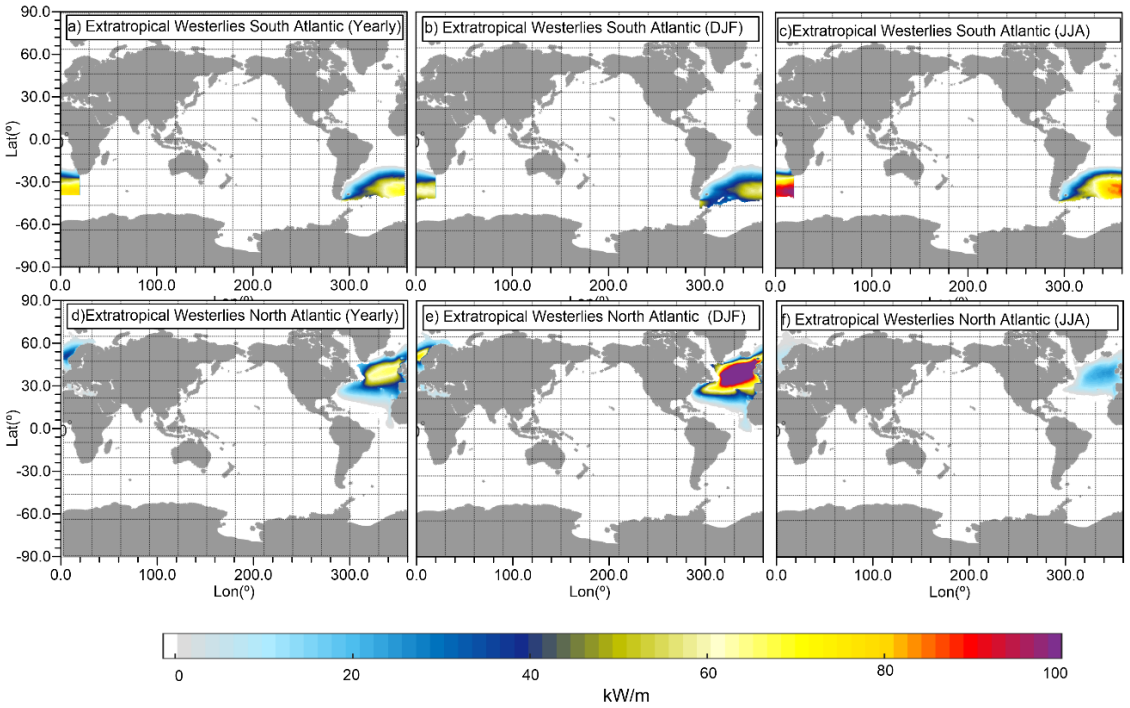


Figure A 2.11 Extratropical wave climate type in the South Atlantic a) yearly, b) DJF, and c) JJA; and extratropical wave climate type in the North Atlantic d) yearly, e) DJF, and f) JJA.

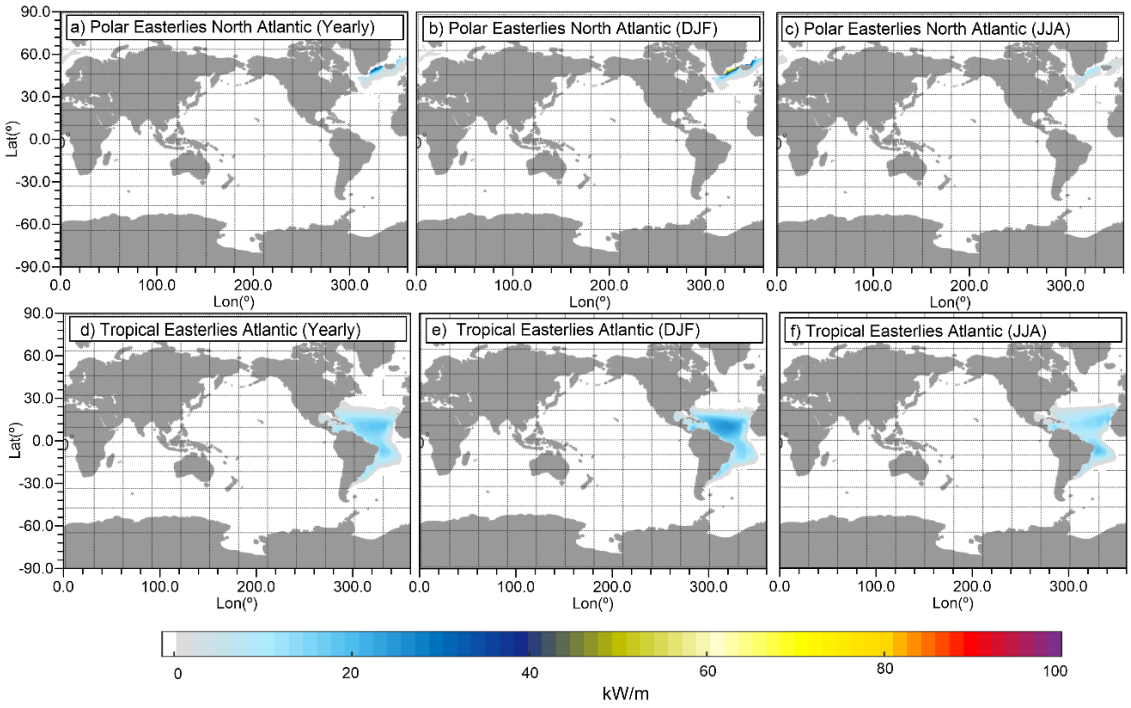


Figure A 2.12 Tropical wave climate type in the Atlantic a) yearly, b) DJF, and c) JJA; and polar wave climate type in the North Atlantic d) yearly, e) DJF, and f) JJA.

The number of the first column and row of the matrixes of Table S7, S8 and S9 follows the next nomenclature.

| | | | | | |
|---|---|---|---|---|---|
| 2= | Subtropical Indian Ocean SH | 12= | Extratropical Indian Ocean | 22= | Tropical Indian Ocean |
| 5= | Subtropical South Pacific | 13= | Warm Pool | 23= | Tropical Pacific |
| 6= | Subtropical North Pacific | 14= | Monsson | 24= | Polar North Pacific |
| 7= | Subpolar North Pacific | 15= | Extratropical South Pacific | 26= | Tropical Atlantic |
| 9= | Subtropical South Atlantic | 17= | Extratropical North Pacific | 27= | Polar North Atlantic |
| 10= | Subtropical North Atlantic | 18= | Extratropical South Atlantic | | |
| 11= | Subpolar North Atlantic | 20= | Extratropical North Atlantic | | |

Table A 2.4 Correlation coefficients between the wave power between wave climate types. Values statistically significant at the level of 95 %.

| | R-2 | R-5 | R-6 | R-7 | R-9 | R-10 | R-11 | R-12 | R-13 | R-14 | R-15 | R-17 | R-18 | R-20 | R-22 | R-23 | R-24 | R-26 | R-27 |
|---|---|---|---|---|---|---|---|---|---|---|---|---|---|---|---|---|---|---|---|
| R-2 | 1.00 | 0.11 | - | - | 0.12 | - | -0.53 | 0.80 | - | - | 0.55 | -0.68 | 0.70 | -0.61 | - | -0.43 | - | -0.42 | - |
| R-5 | 0.11 | 1.00 | - | - | 0.18 | - | - | 0.10 | - | - | 0.11 | - | 0.11 | - | - | - | - | - | - |
| R-6 | - | - | 1.00 | - | 0.23 | - | - | - | - | - | 0.00 | - | - | - | - | - | - | - | - |
| R-7 | - | - | - | 1.00 | - | - | - | - | - | - | 0.00 | - | - | - | - | - | 0.26 | - | - |
| R-9 | 0.12 | 0.18 | 0.23 | - | 1.00 | - | - | - | - | - | 0.10 | - | - | - | - | 0.15 | - | 0.13 | - |
| R-10 | - | - | - | - | - | 1.00 | - | - | - | - | 0.00 | - | - | 0.00 | - | - | - | - | 0.20 |
| R-11 | -0.53 | - | - | - | - | - | 1.00 | -0.68 | - | - | -0.63 | 0.71 | -0.63 | 0.75 | - | 0.57 | - | 0.61 | - |
| R-12 | 0.80 | 0.10 | - | - | - | - | -0.68 | 1.00 | - | - | 0.76 | -0.81 | 0.81 | -0.78 | - | -0.59 | - | -0.59 | - |
| R-13 | - | - | - | - | - | - | - | - | 1.00 | - | - | - | - | - | - | - | 0.17 | - | - |
| R-14 | - | - | - | - | - | - | - | - | - | 1.00 | - | - | - | - | - | - | - | - | - |
| R-15 | 0.55 | 0.11 | - | - | 0.10 | - | -0.63 | 0.76 | - | - | 1.00 | -0.70 | 0.66 | -0.69 | - | -0.48 | - | -0.52 | - |
| R-17 | -0.68 | - | - | - | - | - | 0.71 | -0.81 | - | - | -0.70 | 1.00 | -0.76 | 0.83 | - | 0.81 | - | 0.70 | - |
| R-18 | 0.70 | 0.11 | - | - | - | - | -0.63 | 0.81 | - | - | 0.66 | -0.76 | 1.00 | -0.72 | - | -0.53 | - | -0.53 | - |
| R-20 | -0.61 | - | - | - | - | - | 0.75 | -0.78 | - | - | -0.69 | 0.83 | -0.72 | 1.00 | 0.10 | 0.70 | - | 0.81 | - |
| R-22 | - | - | - | - | - | - | - | - | - | - | - | - | - | 0.10 | 1.00 | - | -0.13 | 0.11 | - |
| R-23 | -0.43 | - | - | - | 0.15 | - | 0.57 | -0.59 | - | - | -0.48 | 0.81 | -0.53 | 0.70 | - | 1.00 | - | 0.70 | - |
| R-24 | - | - | - | 0.26 | - | - | - | - | 0.17 | - | - | - | - | - | -0.13 | - | 1.00 | - | - |
| R-26 | -0.42 | - | - | - | 0.13 | - | 0.61 | -0.59 | - | - | -0.52 | 0.70 | -0.53 | 0.81 | 0.11 | 0.70 | - | 1.00 | - |
| R-27 | - | - | - | - | - | 0.20 | - | - | - | - | - | - | - | - | - | - | - | - | 1.00 |

Table A 2.5 Correlation coefficients between the wave mean direction between wave climate types. Values statistically significant at the level of 95 %.

| | R-2 | R-5 | R-6 | R-7 | R-9 | R-10 | R-11 | R-12 | R-13 | R-14 | R-15 | R-17 | R-18 | R-20 | R-22 | R-23 | R-24 | R-26 | R-27 |
|---|---|---|---|---|---|---|---|---|---|---|---|---|---|---|---|---|---|---|---|
| R-2 | 1 | - | - | - | - | - | - | -0.2 | - | - | -0.1 | -0.1 | - | - | - | - | - | - | - |
| R-5 | - | 1 | - | - | 0.13 | - | - | - | - | - | - | - | - | - | 0.11 | - | - | - | - |
| R-6 | - | - | 1 | - | - | - | - | - | - | - | - | - | - | - | - | - | - | - | - |
| R-7 | - | - | - | 1 | - | - | - | - | - | - | -0.1 | - | - | - | - | - | -0.2 | - | - |
| R-9 | - | 0.13 | - | - | 1 | - | - | - | - | - | - | 0.12 | - | - | 0.18 | -0.1 | - | -0.2 | - |
| R-10 | - | - | - | - | - | 1 | - | - | - | - | - | - | - | - | - | - | - | - | - |
| R-11 | - | - | - | - | - | - | 1 | - | - | - | - | - | - | -0.1 | - | - | - | - | - |
| R-12 | -0.2 | - | - | - | - | - | - | 1 | - | - | 0.34 | 0.11 | 0.37 | - | - | -0.2 | - | - | - |
| R-13 | - | - | - | - | - | - | - | - | 1 | - | - | - | - | - | - | - | - | - | - |
| R-14 | - | - | - | - | - | - | - | - | - | 1 | - | - | - | - | - | - | - | - | - |
| R-15 | -0.1 | - | - | -0.1 | - | - | - | 0.34 | - | - | 1 | 0.26 | 0.36 | -0.1 | - | -0.4 | - | -0.2 | - |
| R-17 | -0.1 | - | - | - | 0.12 | - | - | 0.11 | - | - | 0.26 | 1 | 0.21 | -0.1 | - | -0.6 | - | -0.4 | - |
| R-18 | - | - | - | - | - | - | - | 0.37 | - | - | 0.36 | 0.21 | 1 | - | - | -0.3 | - | - | - |
| R-20 | - | - | - | - | - | - | -0.1 | - | - | - | -0.1 | -0.1 | - | 1 | - | - | - | - | - |
| R-22 | - | 0.11 | - | - | 0.18 | - | - | - | - | - | - | - | - | - | 1 | - | - | - | 0.18 |
| R-23 | - | - | - | - | -0.1 | - | - | -0.2 | - | - | -0.4 | -0.6 | -0.3 | - | - | 1 | - | 0.65 | -0.1 |
| R-24 | - | - | - | -0.2 | - | - | - | - | - | - | - | - | - | - | - | - | 1 | - | 0.15 |
| R-26 | - | - | - | - | -0.2 | - | - | - | - | - | -0.2 | -0.4 | - | - | - | 0.65 | - | 1 | - |
| R-27 | - | - | - | - | - | - | - | - | - | - | - | - | - | - | 0.18 | -0.1 | 0.15 | - | 1 |

Table A 2.6 Correlation coefficients between the total area between wave climate types. Values statistically significant at the level of 95 %.

| | R-2 | R-5 | R-6 | R-7 | R-9 | R-10 | R-11 | R-12 | R-13 | R-14 | R-15 | R-17 | R-18 | R-20 | R-22 | R-23 | R-24 | R-26 | R-27 |
|---|---|---|---|---|---|---|---|---|---|---|---|---|---|---|---|---|---|---|---|
| R-2 | 1.00 | - | - | - | - | - | 0.19 | -0.19 | -0.22 | - | -0.09 | -0.20 | - | -0.34 | - | - | - | -0.13 | - |
| R-5 | - | 1.00 | 0.15 | - | - | - | - | -0.09 | - | - | - | - | - | - | 0.36 | - | - | - | - |
| R-6 | - | 0.15 | 1.00 | - | - | - | - | - | - | - | - | - | 0.17 | 0.17 | - | - | - | -0.20 | - |
| R-7 | - | - | - | 1.00 | - | - | - | - | - | - | - | - | - | - | - | - | - | - | - |
| R-9 | - | - | - | - | 1.00 | - | - | - | - | - | - | 0.10 | - | - | - | - | - | - | - |
| R-10 | - | - | - | - | - | 1.00 | - | - | - | - | - | - | - | - | - | - | - | - | - |
| R-11 | 0.19 | - | - | - | - | - | 1.00 | 0.35 | - | - | -0.27 | -0.40 | - | -0.45 | - | - | 0.14 | - | - |
| R-12 | -0.19 | -0.09 | - | - | - | - | 0.35 | 1.00 | - | - | -0.21 | -0.45 | - | -0.33 | - | - | - | - | - |
| R-13 | -0.22 | - | - | - | - | - | - | - | 1.00 | - | - | - | - | - | - | - | - | - | - |
| R-14 | - | - | - | - | - | - | - | - | - | 1.00 | - | - | - | - | - | - | - | - | - |
| R-15 | -0.09 | - | - | - | - | - | -0.27 | -0.21 | - | - | 1.00 | 0.45 | 0.10 | 0.30 | - | - | - | -0.17 | - |
| R-17 | -0.20 | - | - | - | 0.10 | - | -0.40 | -0.45 | - | - | 0.45 | 1.00 | 0.16 | 0.54 | - | -0.15 | - | -0.19 | - |
| R-18 | - | - | 0.17 | - | - | - | - | - | - | - | 0.10 | 0.16 | 1.00 | 0.22 | - | - | - | -0.19 | - |
| R-20 | -0.34 | - | 0.17 | - | - | - | -0.45 | -0.33 | - | - | 0.30 | 0.54 | 0.22 | 1.00 | - | - | - | -0.26 | - |
| R-22 | - | 0.36 | - | - | - | - | - | - | - | - | - | - | - | - | 1.00 | - | - | - | - |
| R-23 | - | - | - | - | - | - | - | - | - | - | - | -0.15 | - | - | - | 1.00 | - | 0.12 | - |
| R-24 | - | - | - | - | - | - | 0.14 | - | - | - | - | - | - | - | - | - | 1.00 | - | - |
| R-26 | -0.13 | - | -0.20 | - | - | - | - | - | - | - | -0.17 | -0.19 | -0.19 | -0.26 | - | 0.12 | - | 1.00 | - |
| R-27 | - | - | - | - | - | - | - | - | - | - | - | - | - | - | - | - | - | - | 1.00 |

# APPENDIX A3

This appendix is the supporting information for the Chapter 6

List of Figures

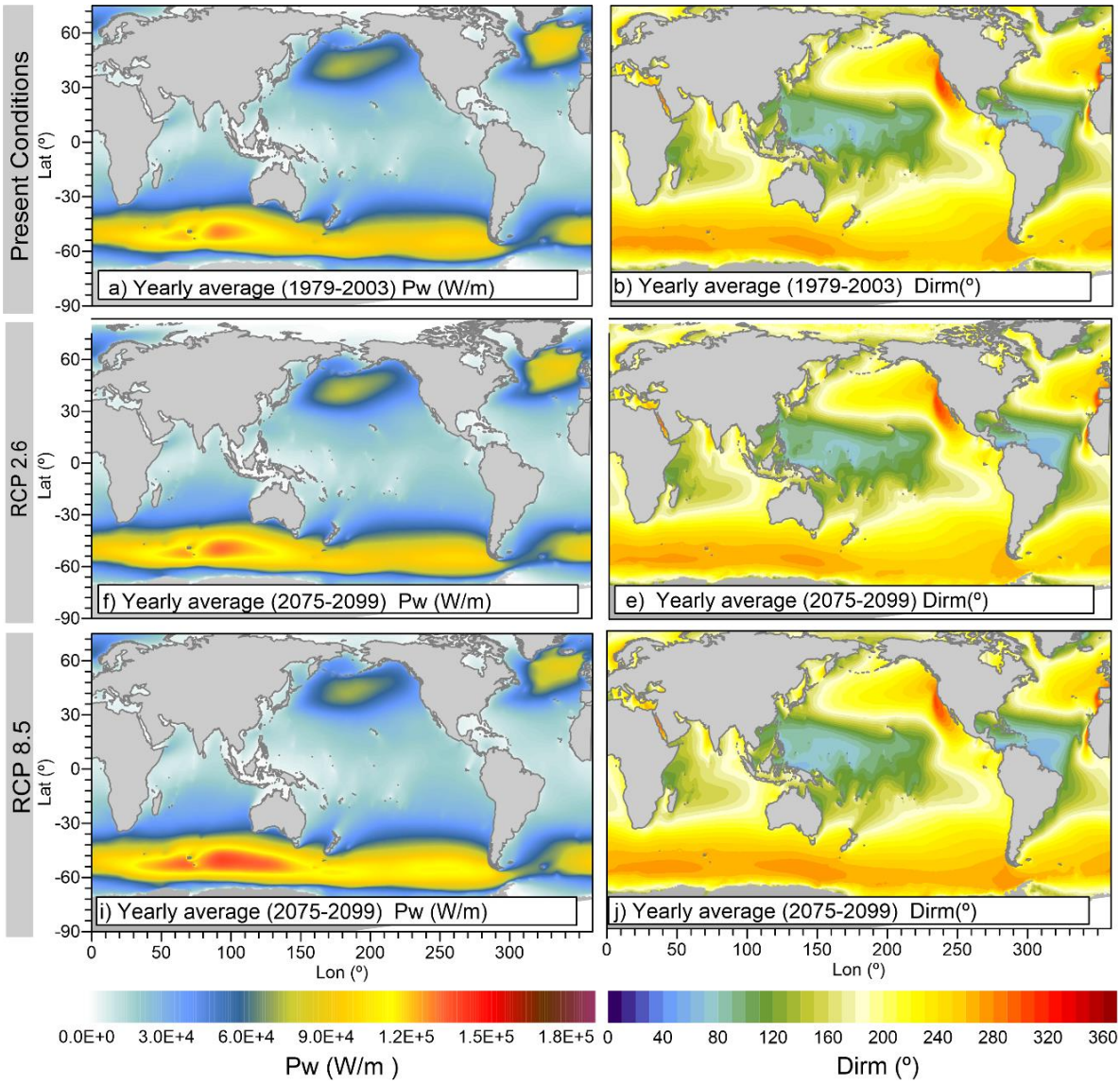


Figure A3. 1 Annual average for present conditions (a, b), RCP 2.6 (c, d), and RCP 8.5 (i, j) of wave power (a, c, i) and mean wave direction (b, d, j).

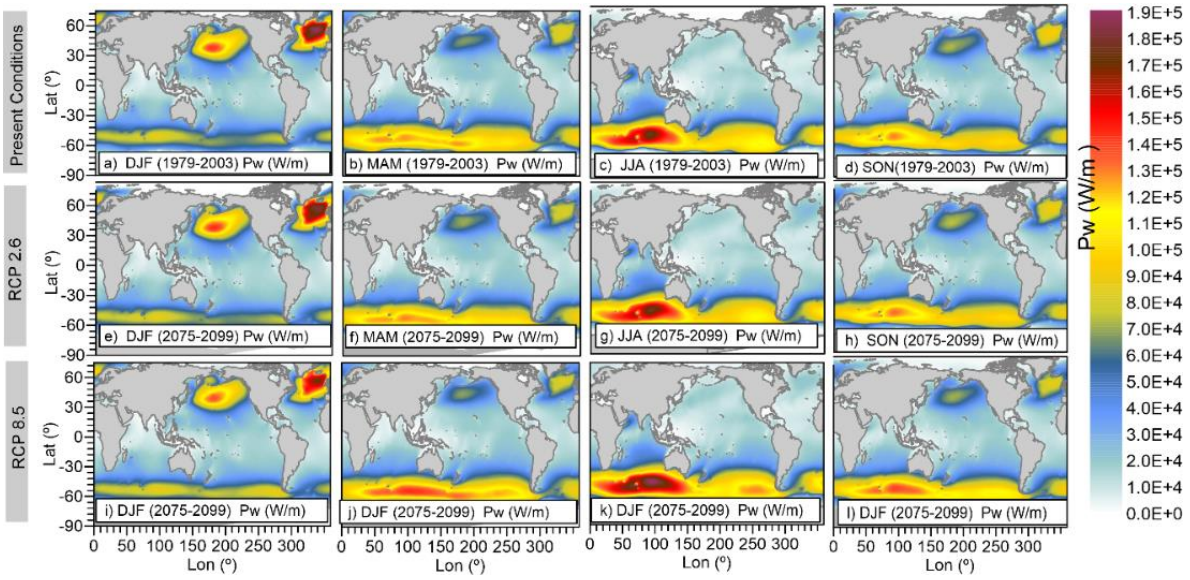


Figure A3. 2Wave power average for present conditions (a, b, c, d), RCP 2.6 (e, f, g, h), and RCP 8.5 (I, j, k, l) of wave during a) DJF (a, e, i), MAM (b, f, j), JJA (c, g, k) and SON (d, h, l).

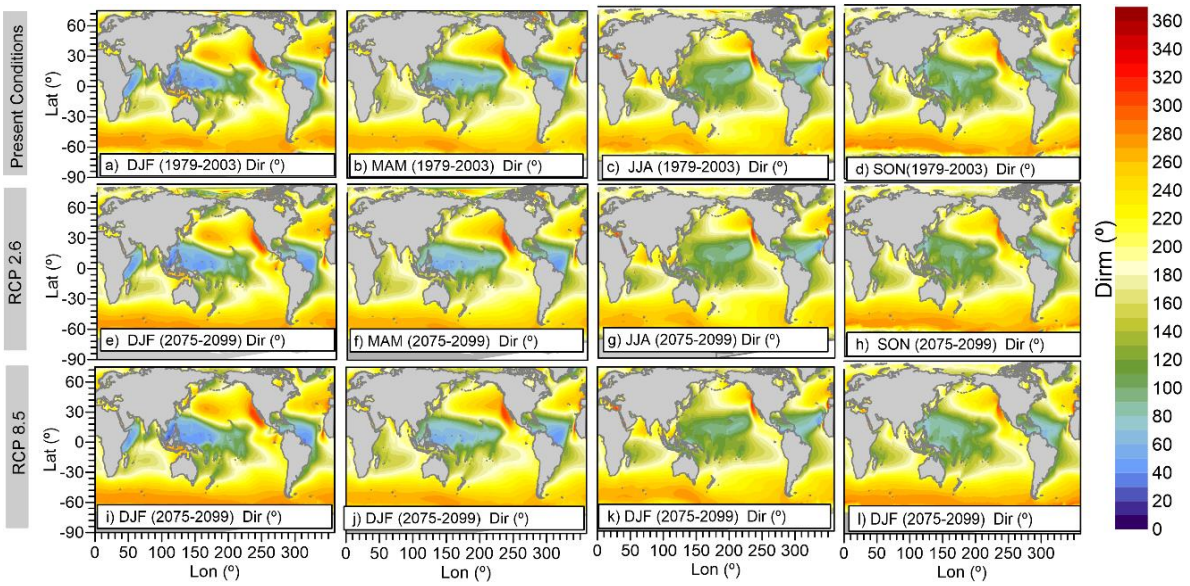


Figure A3. 3 Mean wave direction average for present conditions (a, b, c, d), RCP 2.6 (e, f, g, h), and RCP 8.5 (I, j, k, l) of wave during a) DJF (a, e, i), MAM (b, f, j), JJA (c, g, k) and SON (d, h, l).

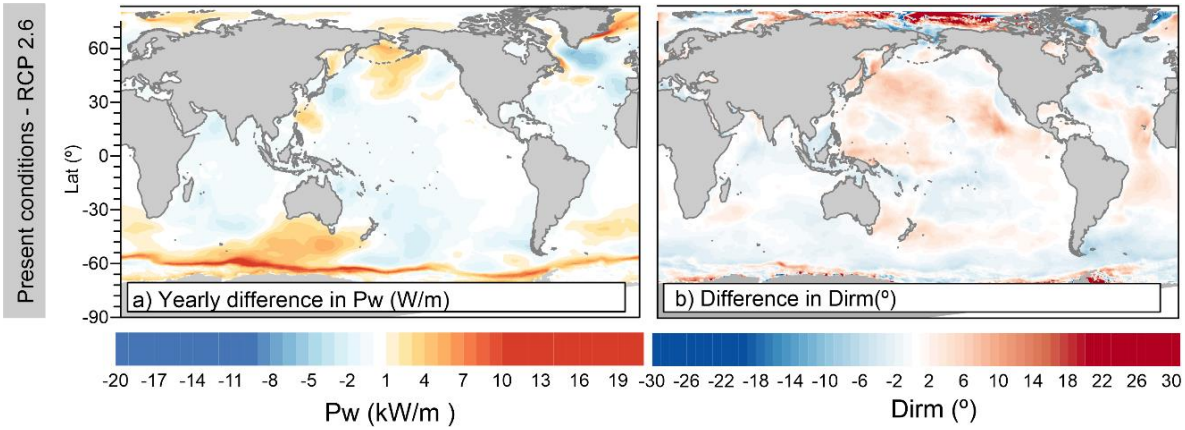


Figure A3. 4. Yearly difference between RCP2.6 and present conditions of wave power (a) and mean wave direction (b).

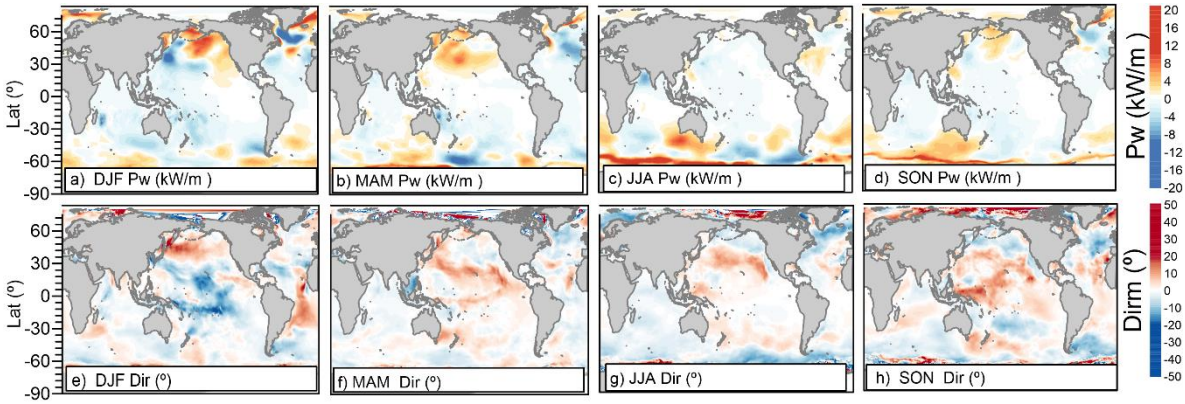


Figure A3. 5 Seasonal difference between RCP2.6 and present conditions of wave power (a, b, c, d) and mean wave direction (e, f, g, h) in DJF ( a, e), MAM(b, f), JJA(c, g), and SON(d, h).

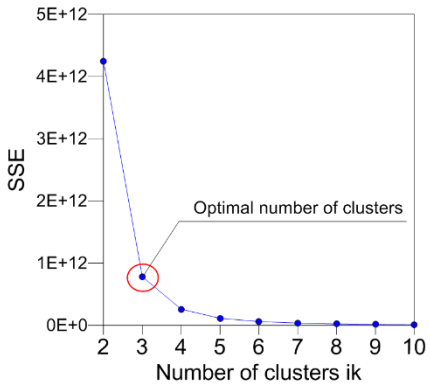


Figure A3. 6 Optimal number of cluster for present conditions (1979-2003).

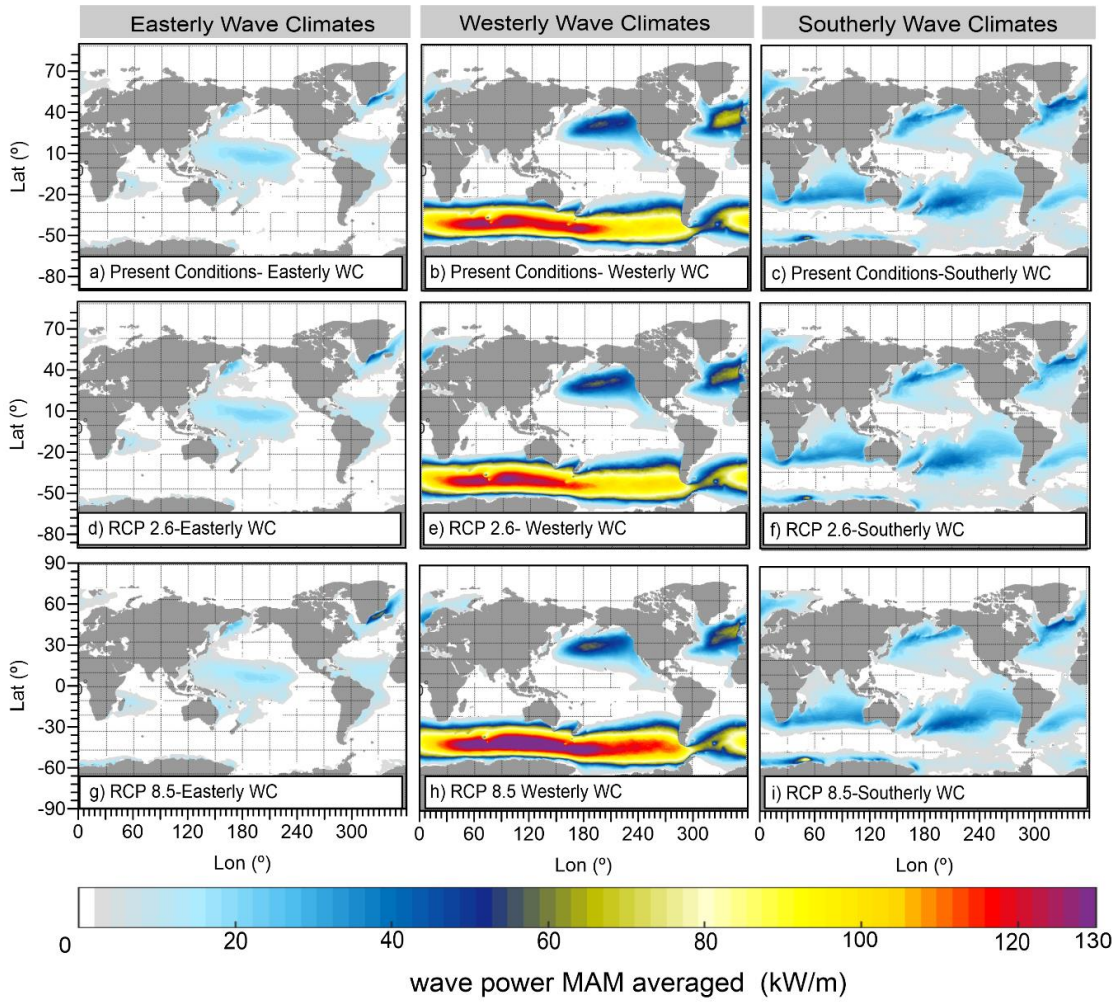


Figure A3. 7 MAM averaged of wave power for the (a, b, c) present scenario, (d, e, f) RCP2.6, and (h, I, j) RCP 8.5 scenarios for the (a, d, g,) easterly, (b, e, h) westerly, and (c, f, i) southerly wave climates.

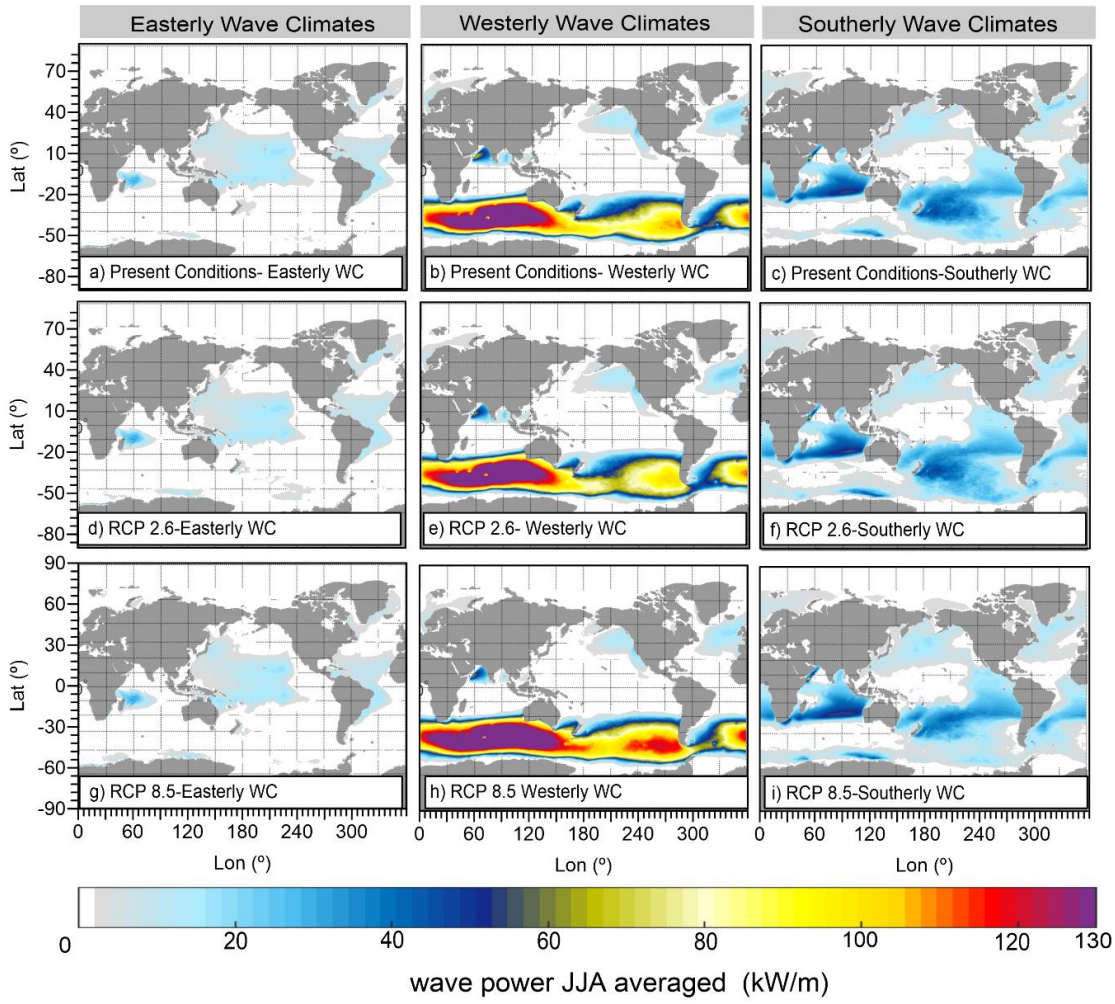


Figure A3. 8 JJA averaged of wave power for the (a, b, c) present scenario, (d, e, f) RCP2.6, and (h, I, j) RCP 8.5 scenarios for the (a, d, g,) easterly, (b, e, h) westerly, and (c, f, i) southerly wave climates.

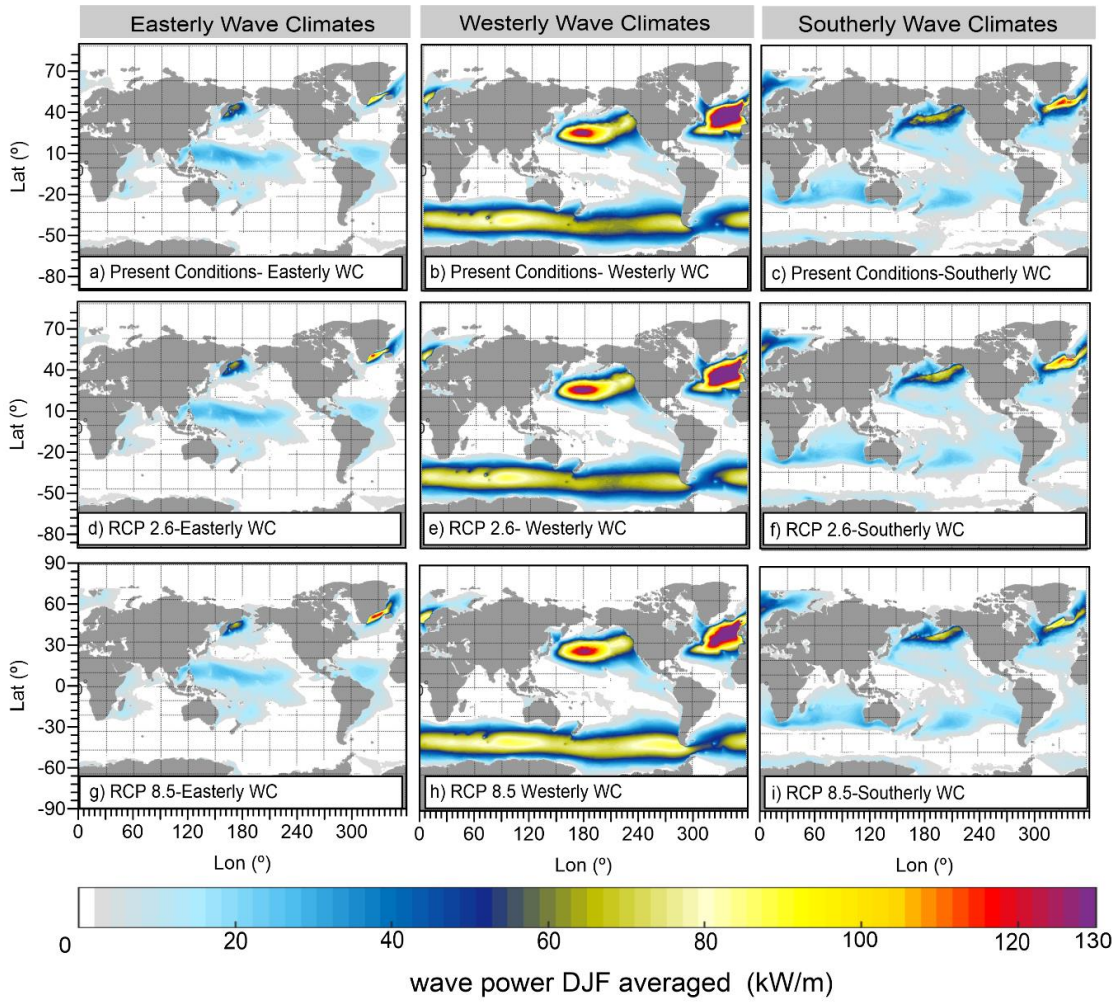


Figure A3. 9. DJF averaged of wave power for the (a, b, c) present scenario, (d, e, f) RCP2.6, and (h, I, j) RCP 8.5 scenarios for the (a, d, g,) easterly, (b, e, h) westerly, and (c, f, i) southerly wave climates.

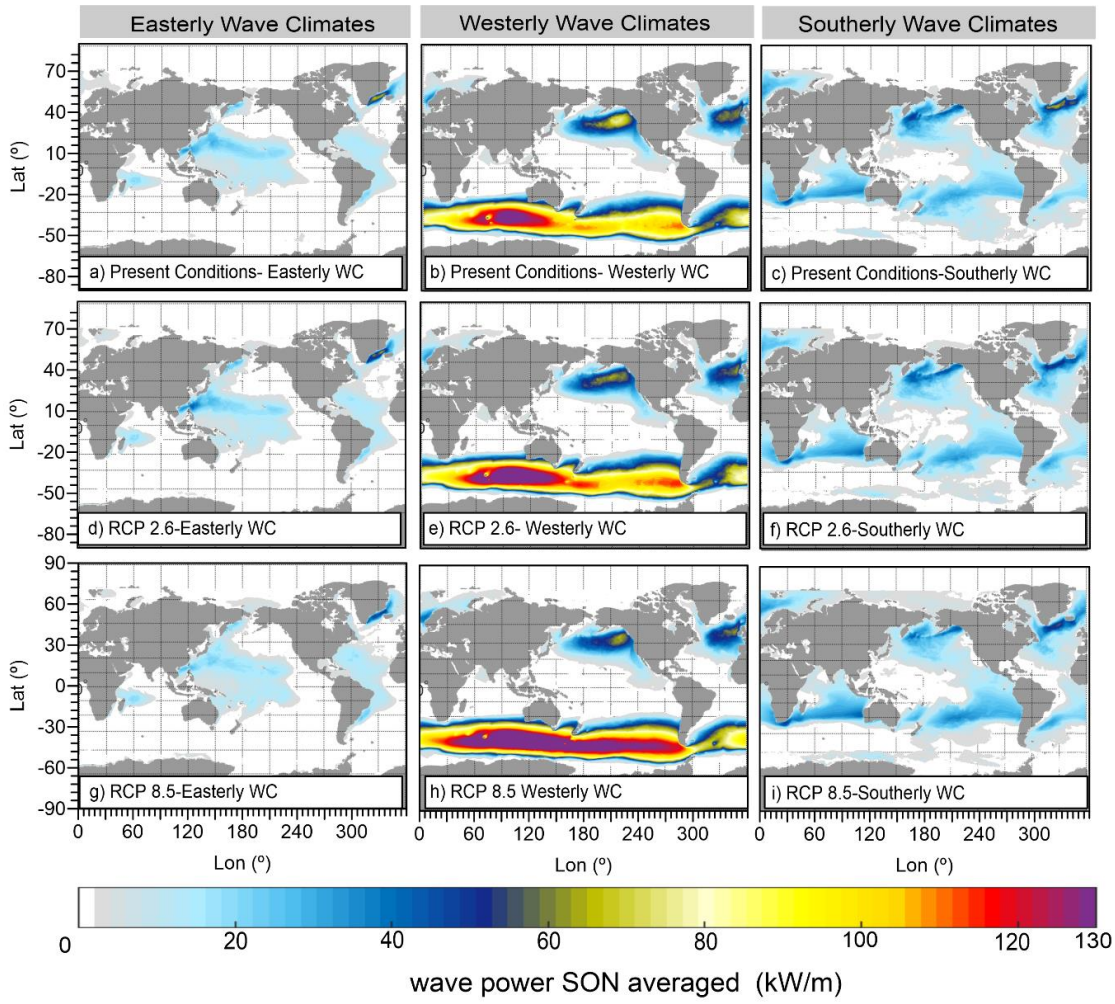


Figure A3. 10 SON averaged of wave power for the (a, b, c) present scenario, (d, e, f) RCP2.6, and (h, I, j) RCP 8.5 scenarios for the (a, d, g,) easterly, (b, e, h) westerly, and (c, f, i) southerly wave climates.

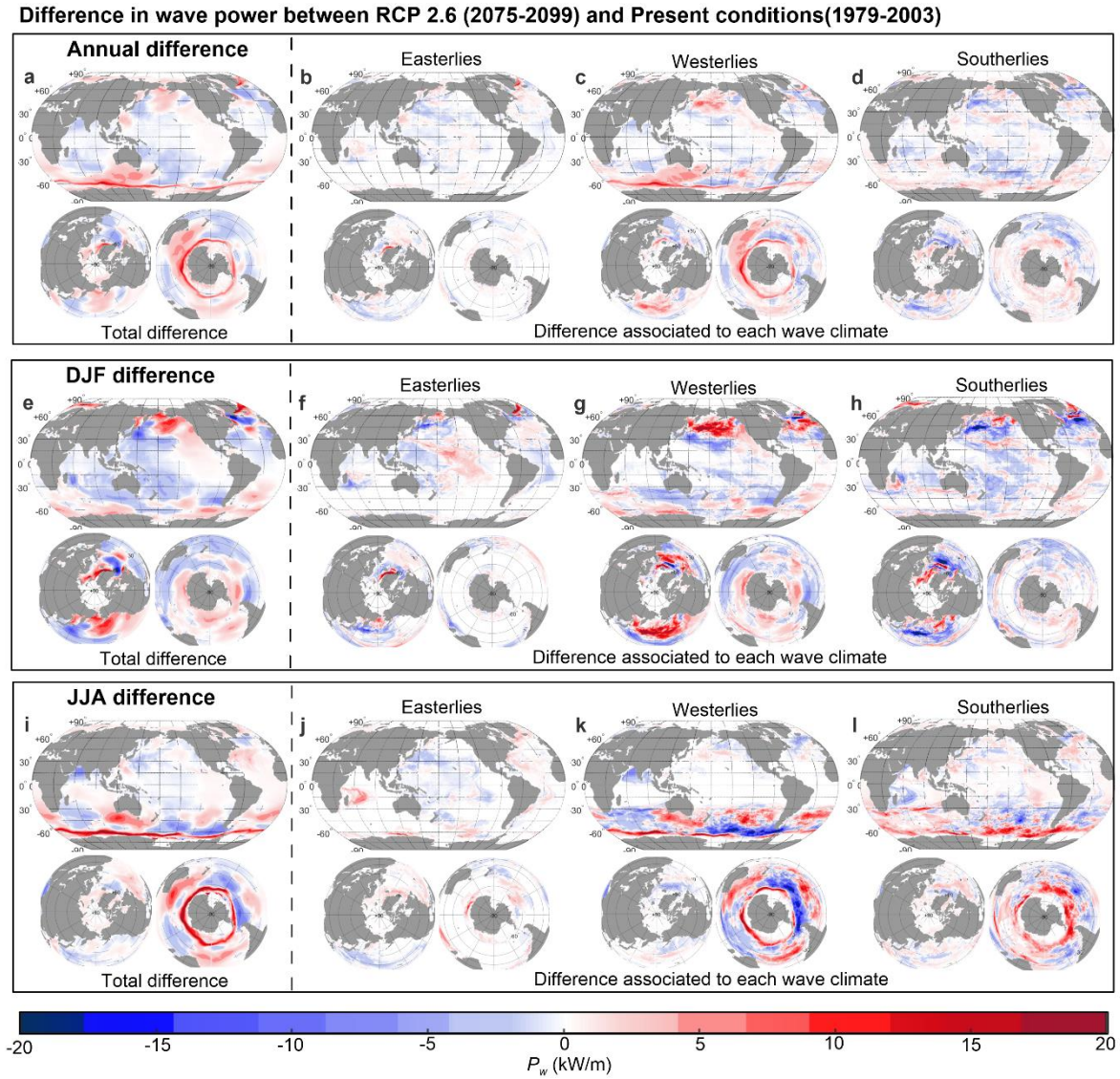


Figure A3. 11 Difference between RCP2.6 and present conditions in yearly averaged wave power for the (a, b, c) easterly, (d, e, f) westerly, and (g, h, i) and southerly wave climates. The results are shown in a (a, d, g,) global, (b, e, h) the Antarctic, and (c, f, i) the Arctic view.

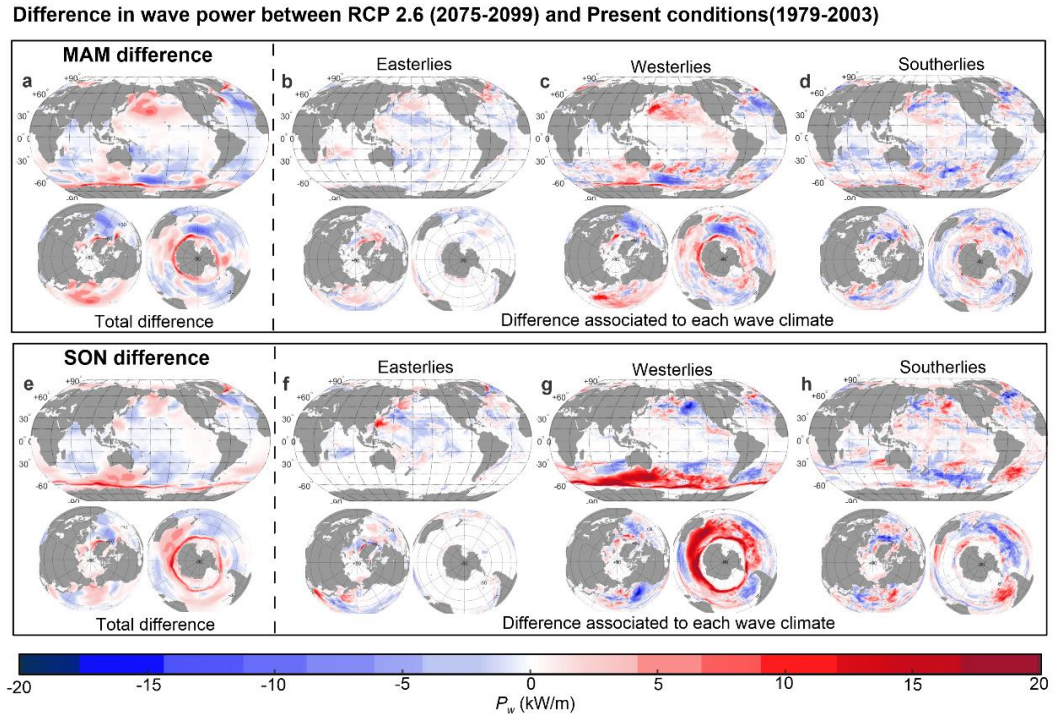


Figure A3. 12 Difference between RCP2.6 and present conditions in SON averaged wave power for the (a, b, c) easterly, (d, e, f) westerly, and (g, h, i) and southerly wave climates. The results are shown in a (a, d, g,) global, (b, e, h) the Antarctic, and (c, f, i) the Arctic view.

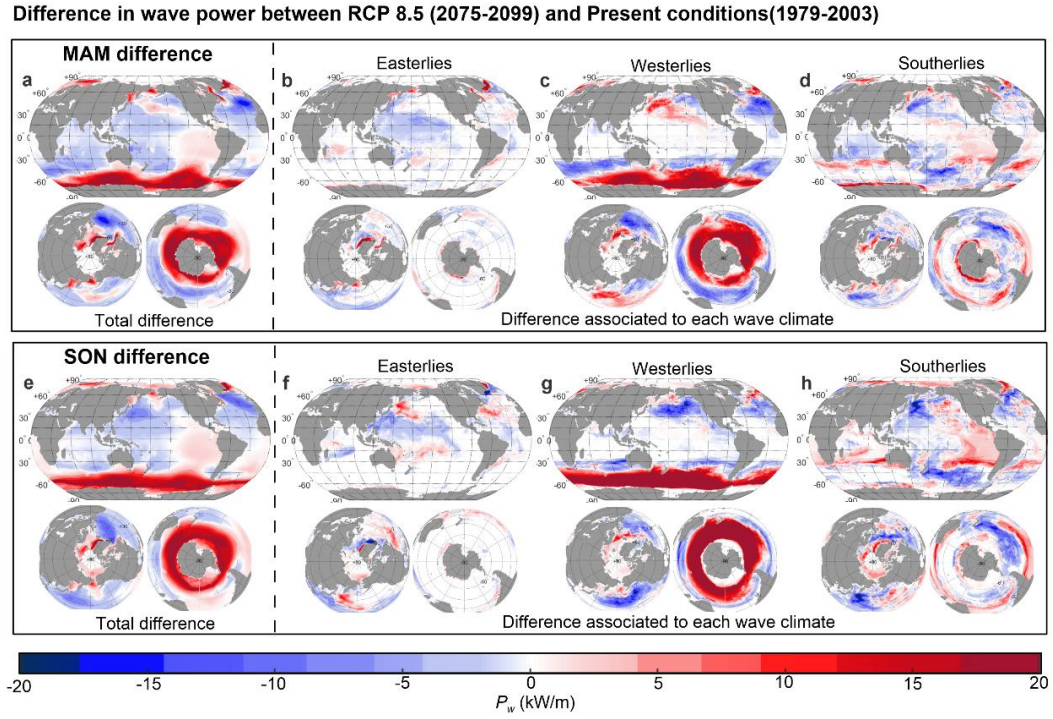


Figure A3. 13 Difference between RCP2.6 and present conditions in MAM averaged wave power for the (a, b, c) easterly, (d, e, f) westerly, and (g, h, i) and southerly wave climates. The results are shown in a (a, d, g,) global, (b, e, h) the Antarctic, and (c, f, i) the Arctic view.

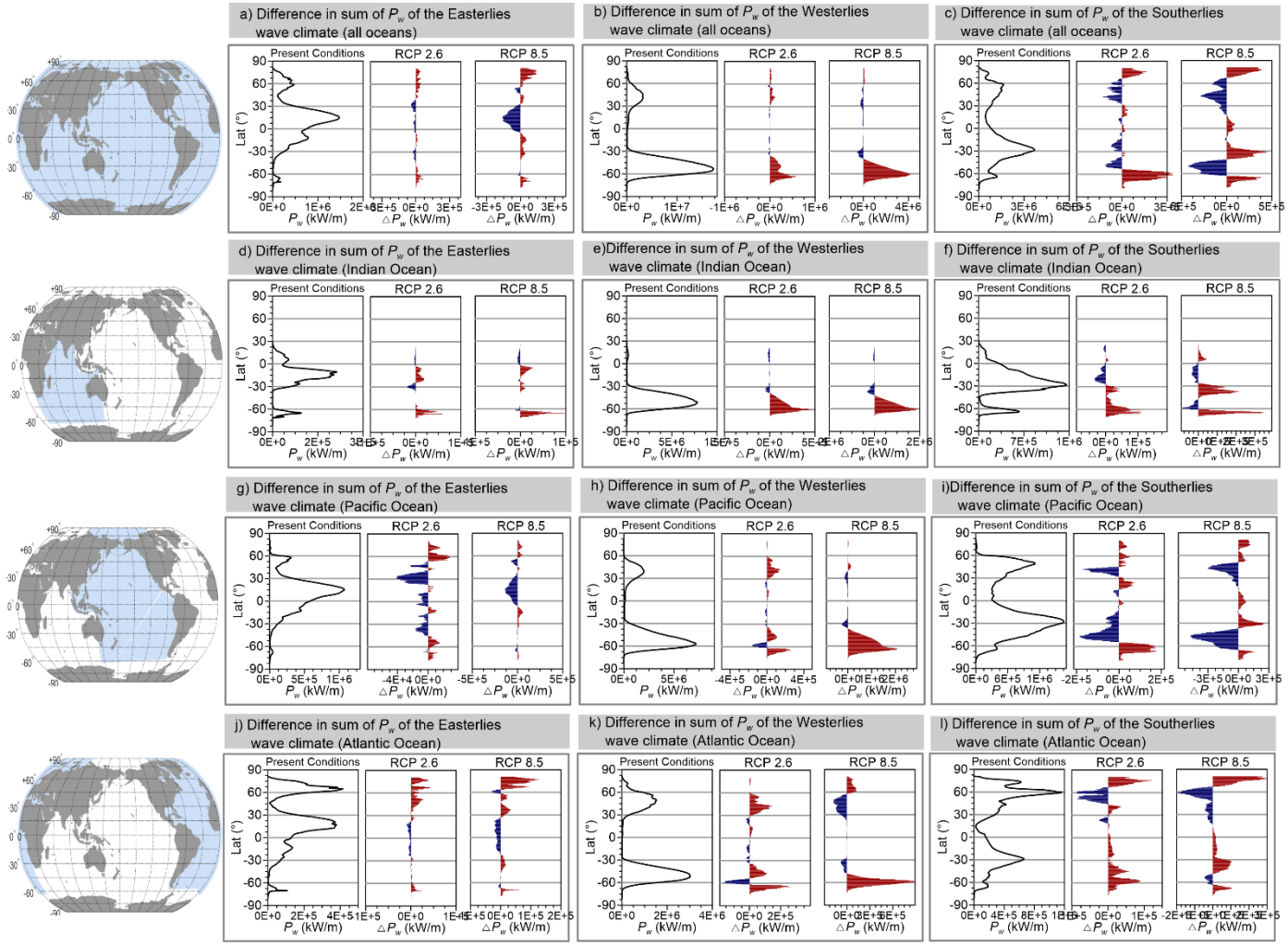


Figure A3. 14 Difference between RCP8.5, RCP 2.6 and present conditions in total wave power for (a-c) all the oceans, (d-f) Indian Ocean, (f-i) Pacific Ocean, and (j-l) Atlantic Ocean for the (a, d, g, j) easterly, (b, e, h, k) westerly, and (c, f, I, l) southerly wave climates.

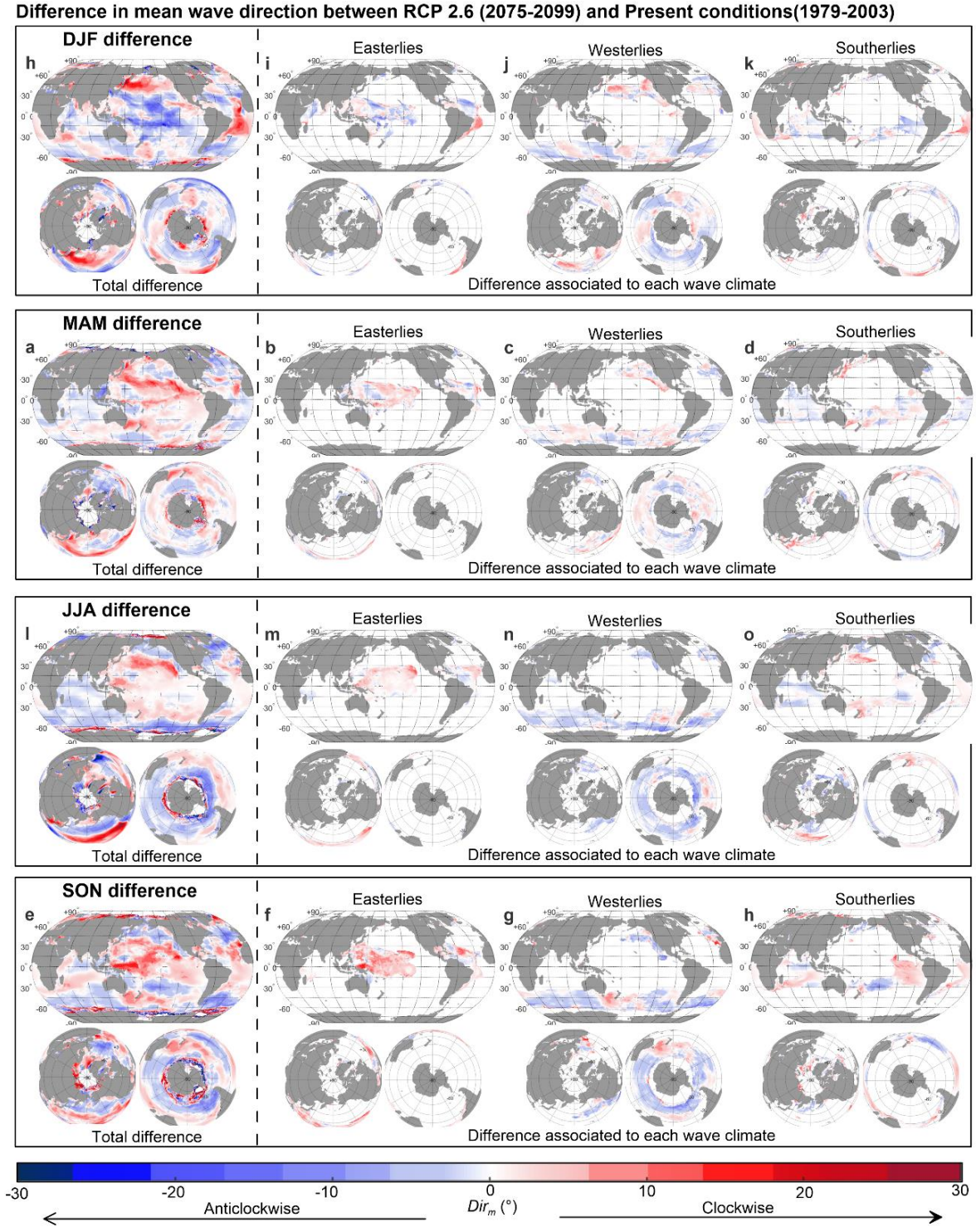


Figure A3. 15 Difference between RCP2.6 and present conditions in mean wave direction for the (a, d, g, j) easterly, (b, e, h, k) westerly, and (c, f, I, l) southerly wave climate. For (a, b, c) DJF, (d, e, f) MAM, (g, h, i) JJA, and (j, k, l) SON.

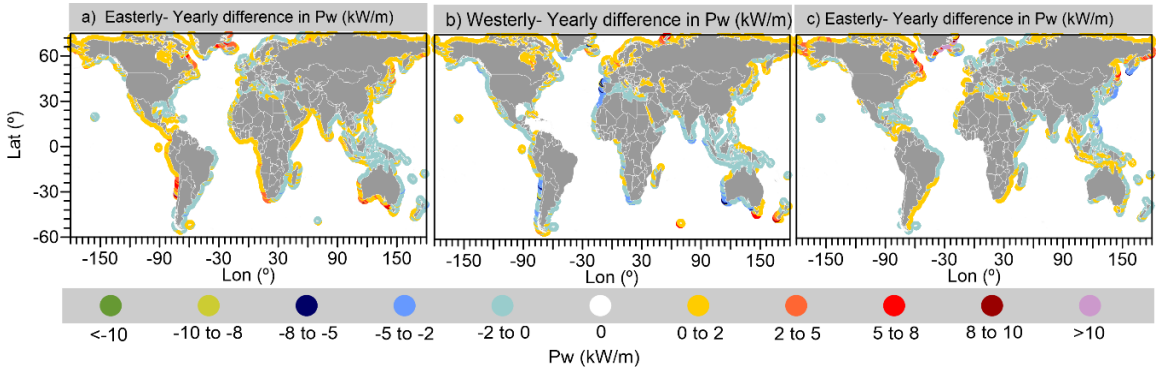


Figure A3. 16 Annual differences in wave power between RCP 8.5 scenario and present conditions for a) southerly, b) westerly, and C) easterly wave climates.

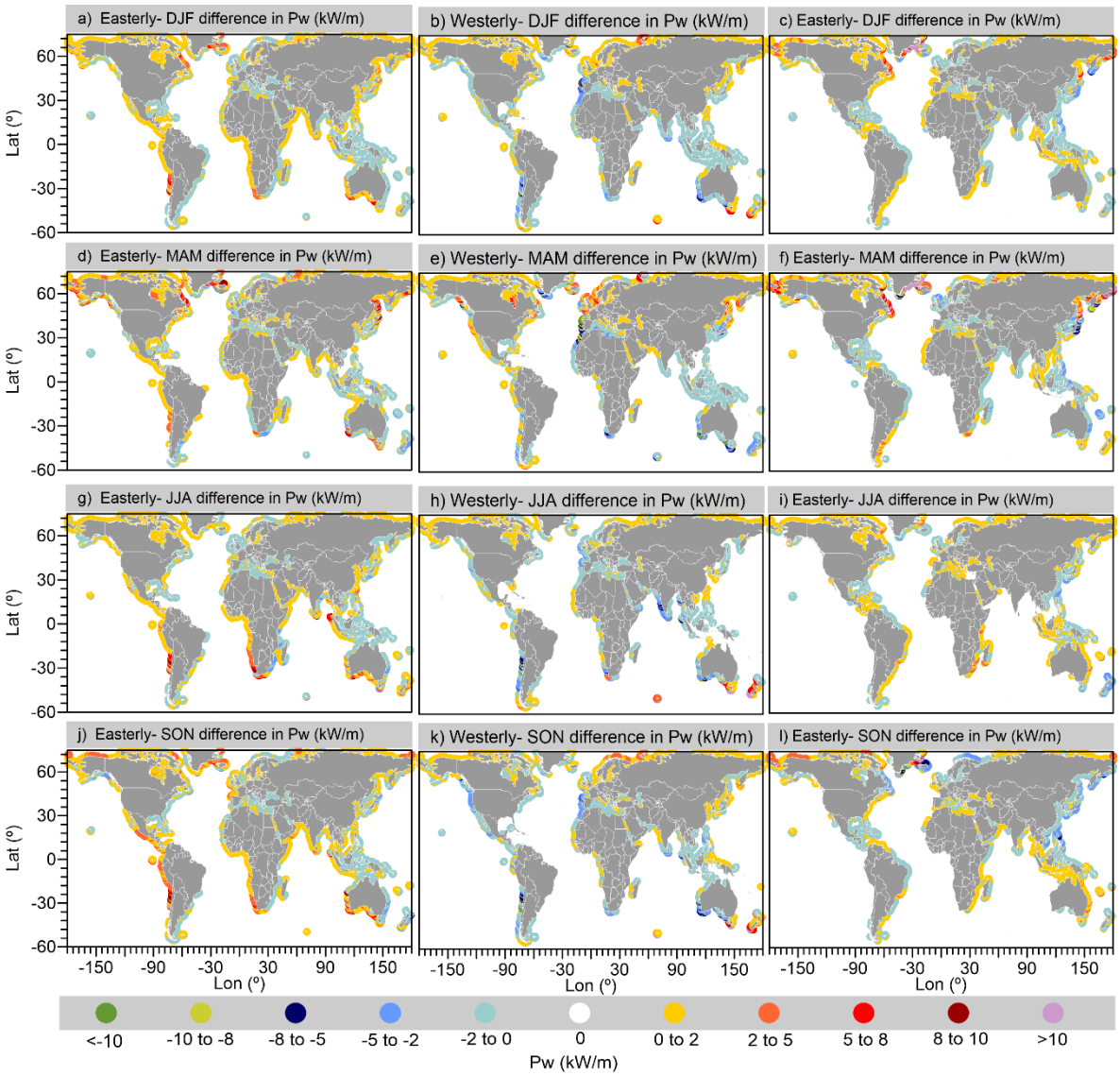


Figure A3. 17 Seasonal differences in wave power between RCP 8.5 and present conditions for the wave climates in DJF, MAM, JJA, and SON.

The percentage of ice was calculate as the total number of months minus the number of moths with wind waved $n_W$ data divided by the total number of months.

$$C_{ice}(\%) = 100 \cdot \frac{n_T - n_W}{n_T} \quad (3)$$

Where:

$C_{ice}(\%)$= Presence of ice cover [%]
$n_T$= Total number of months [months]
$n_W$= Months with wave data [months]

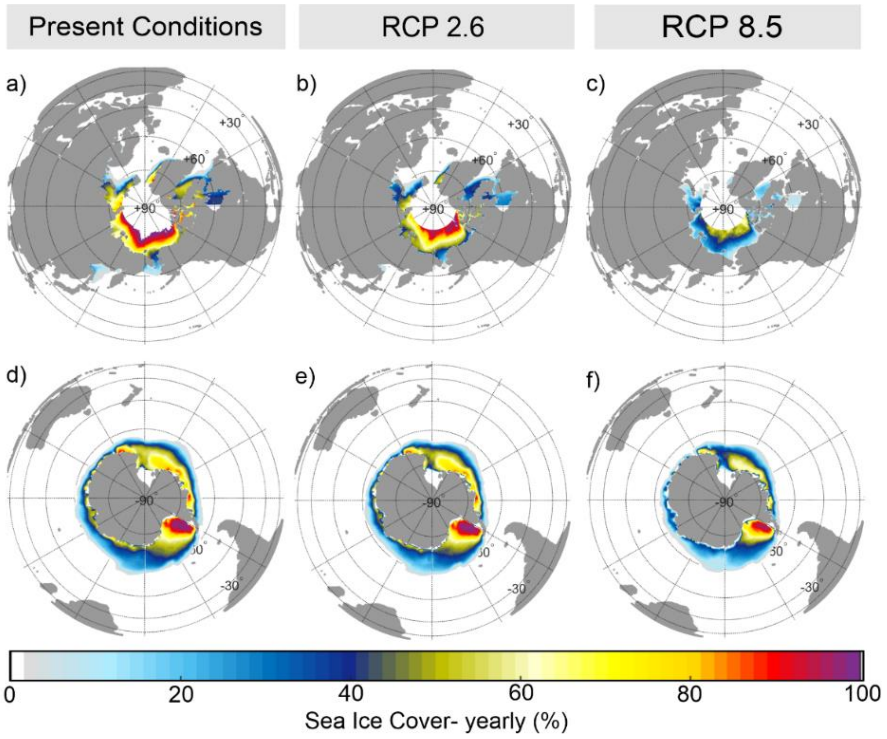


Figure A3. 18 Annual percentage of Ice Cover for (a, b) present (1979-2003), (b, e) RCP2.6 (2075-2099), and (c, f) RCP8.5 (2075-2099) scenarios.

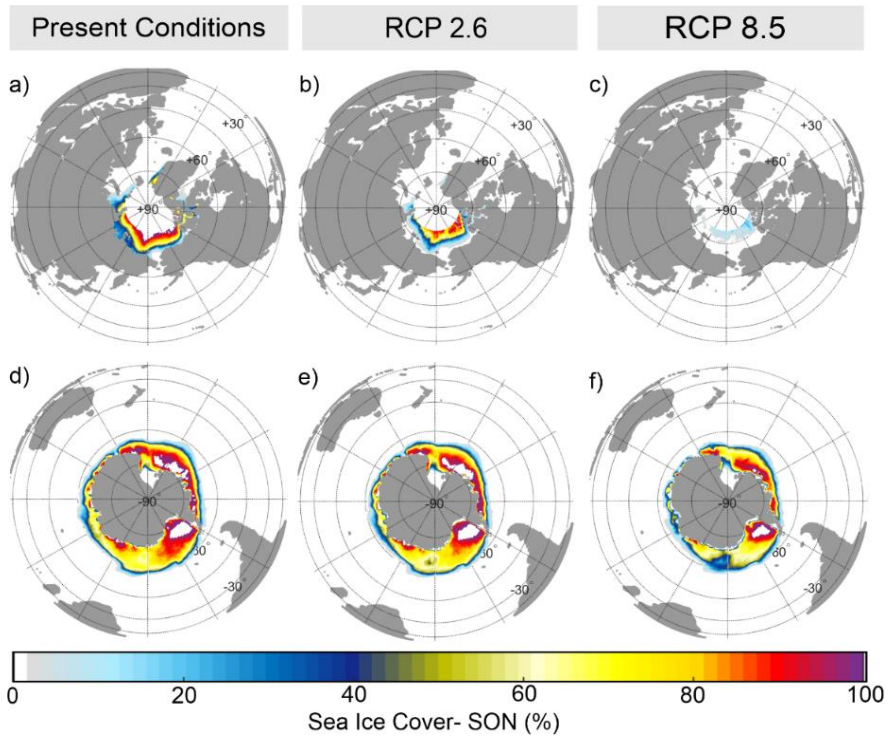


Figure A3. 19 SON percentage of Ice Cover for (a, b) present (1979-2003), (b, e) RCP2.6 (2075-2099), and (c, f) RCP8.5 (2075-2099) scenarios.

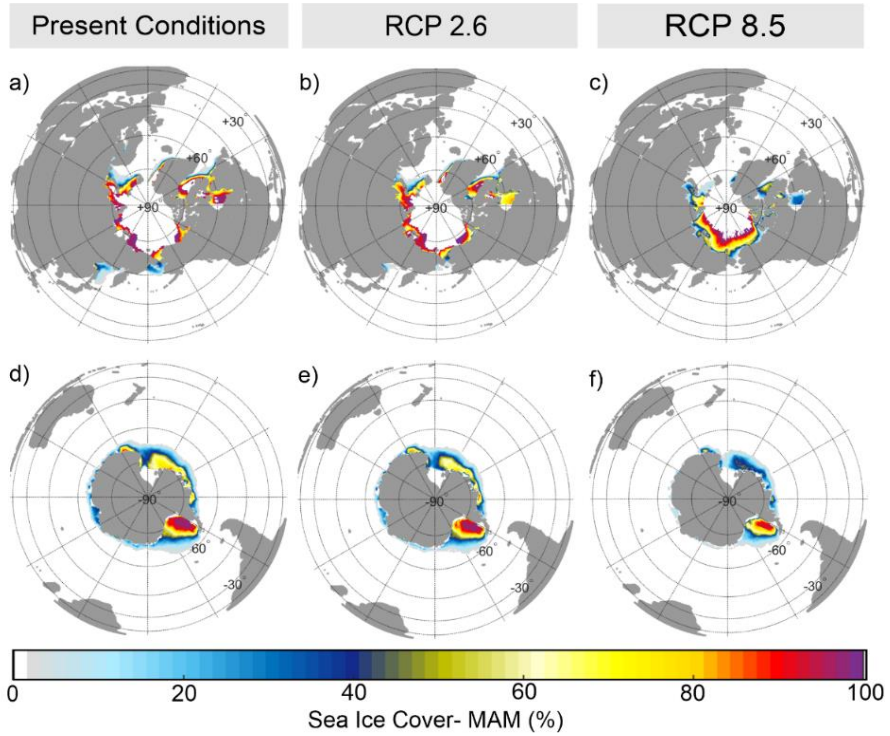


Figure A3. 20MAM percentage of Ice Cover for (a, b) present (1979-2003), (b, e) RCP2.6 (2075-2099), and (c, f) RCP8.5 (2075-2099) scenarios.

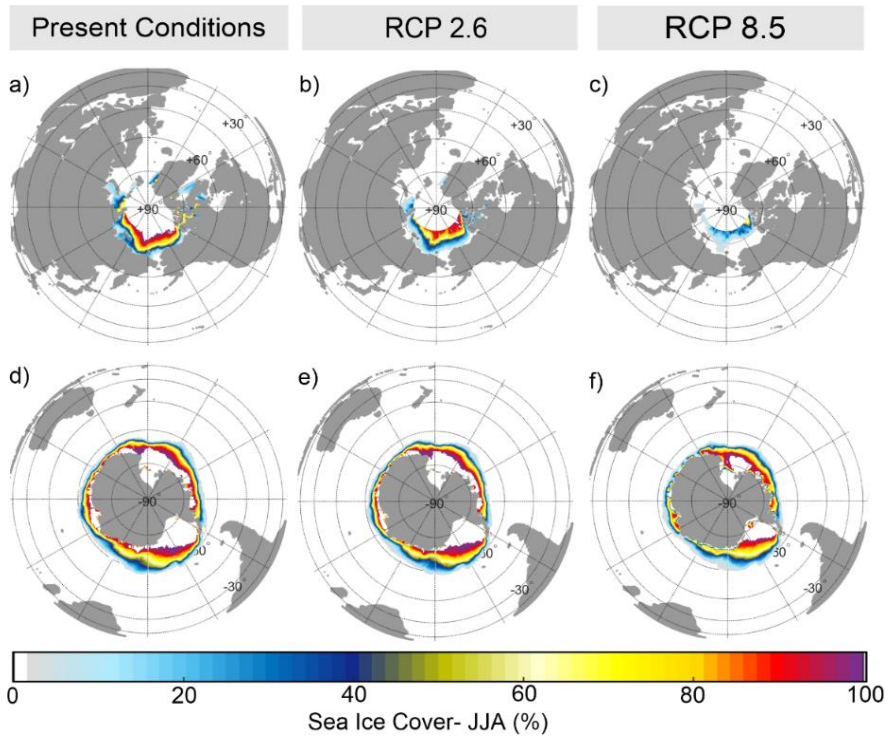


Figure A3. 21 JJA percentage of Ice Cover for (a, b) present (1979-2003), (b, e) RCP2.6 (2075-2099), and (c, f) RCP8.5 (2075-2099) scenarios.

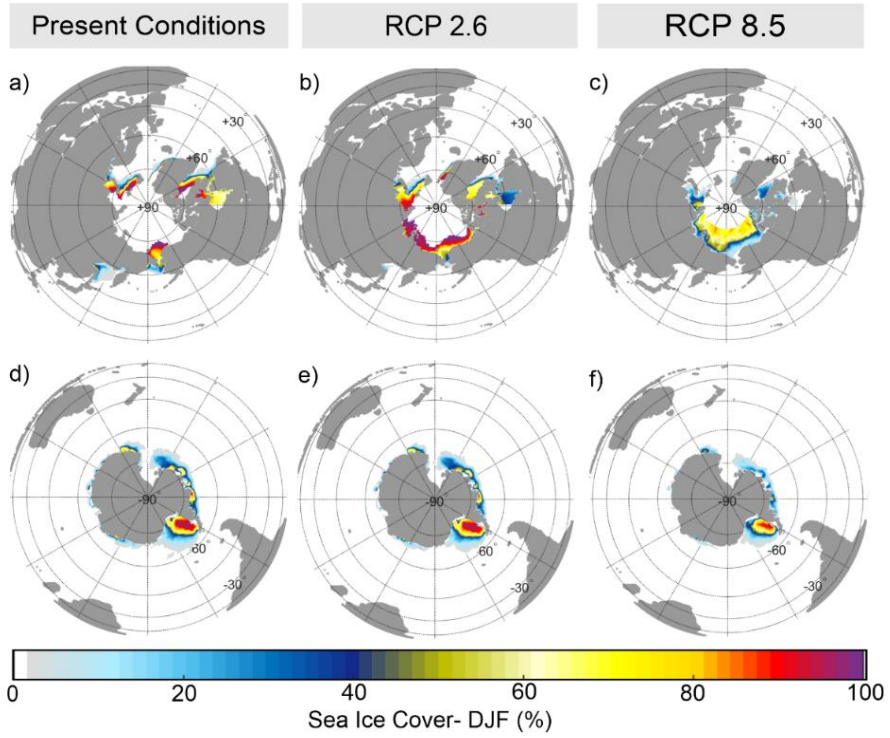


Figure A3. 22 DJF percentage of Ice Cover for (a, b) present (1979-2003), (b, e) RCP2.6 (2075-2099), and (c, f) RCP8.5 (2075-2099) scenarios

# APPENDIX A4

This appendix is the supporting information for the Chapter 8

List of Figures

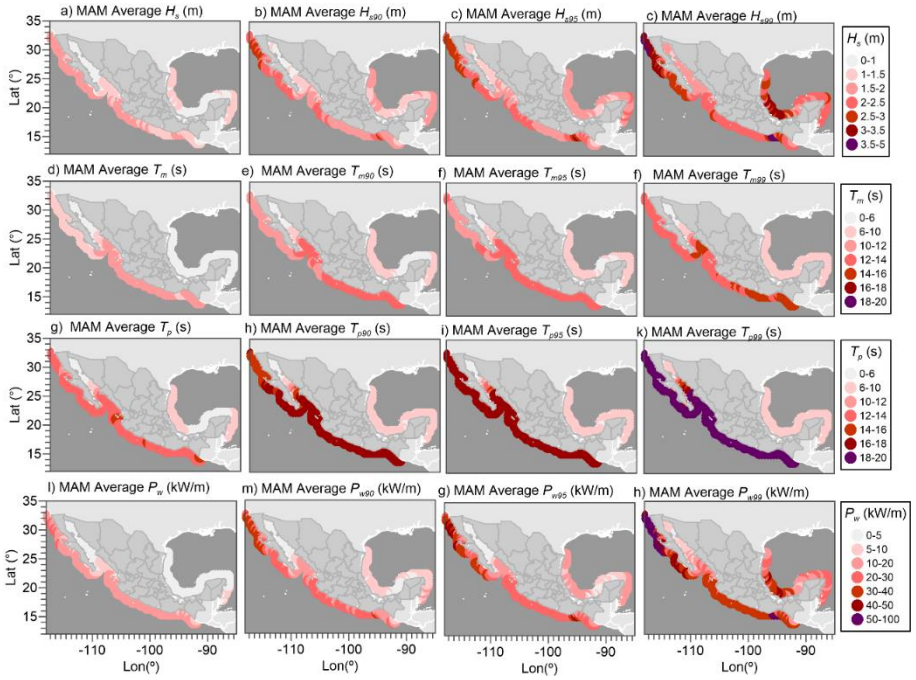


Figure A4. 1 MAM seasonal average of a) $H_s$ (m), b) $H_{s90}$ (m), c) $H_{s95}$ (m), d) $T_m$ (s) , e) $T_{m90}$ (s) , f) $T_{m95}$ (s), g) $T_{m99}$ (s),h) $T_p$ (s) , i) $T_{p90}$ (s) , j) $T_{p95}$ (s), k) $T_{p99}$ (s), l) $P_w$ (kW/m) , m) $P_{w\,90}$(kW/m) , o) $P_{w95}$ (kW/m) , and q) $P_{w99}$ (kW/m).

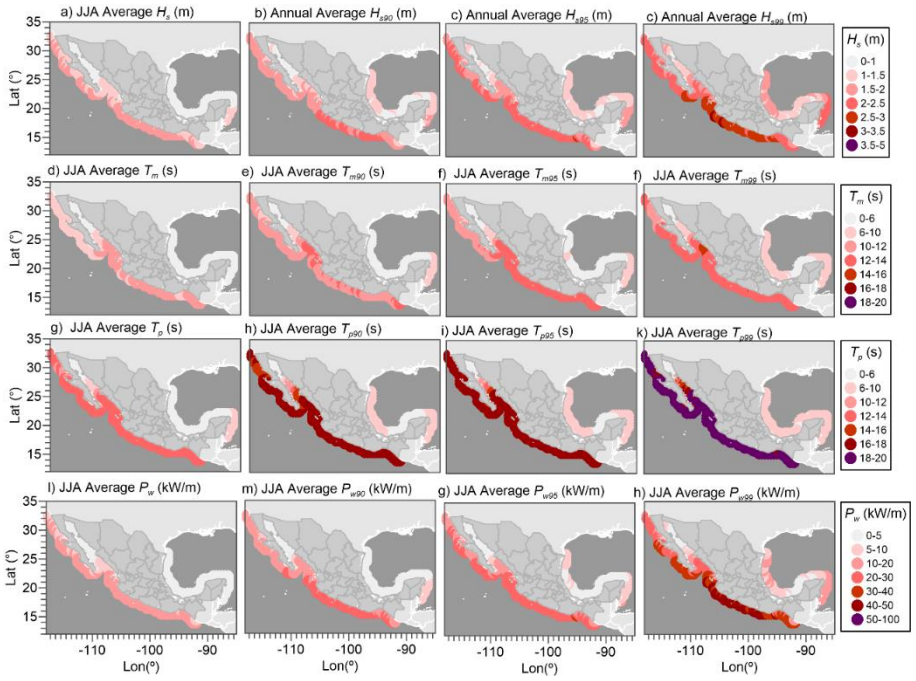


Figure A4. 2 JJA seasonal average of a) $H_s$ (m), b) $H_{s90}$ (m), c) $H_{s95}$ (m), d) $T_m$ (s) , e) $T_{m90}$ (s) , f) $T_{m95}$ (s), g) $T_{m99}$ (s),h) $T_p$ (s) , i) $T_{p90}$ (s) , j) $T_{p95}$ (s), k) $T_{p99}$ (s), l) $P_w$ (kW/m) , m) $P_{w\,90}$(kW/m) , o) $P_{w95}$ (kW/m) , and q) $P_{w99}$ (kW/m).

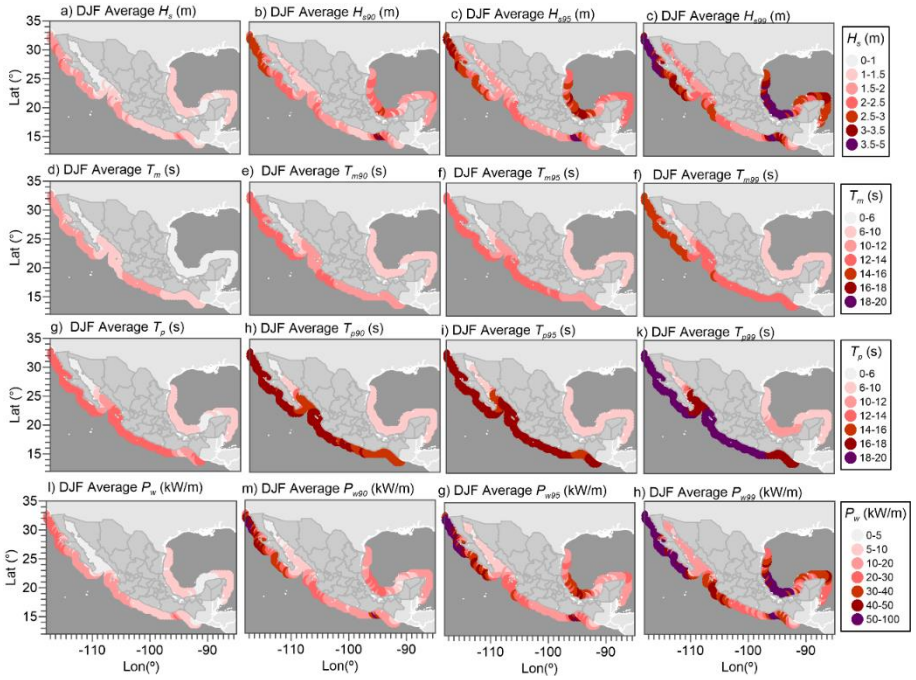


Figure A4. 3 DJF seasonal average of a) $H_s$ (m), b) $H_{s90}$ (m), c) $H_{s95}$ (m), d) $T_m$ (s) , e) $T_{m90}$ (s) , f) $T_{m95}$ (s), g) $T_{m99}$ (s),h) $T_p$ (s) , i) $T_{p90}$ (s) , j) $T_{p95}$ (s), k) $T_{p99}$ (s), l) $P_w$ (kW/m) , m) $P_{w\,90}$(kW/m) , o) $P_{w95}$ (kW/m) , and q) $P_{w99}$ (kW/m).

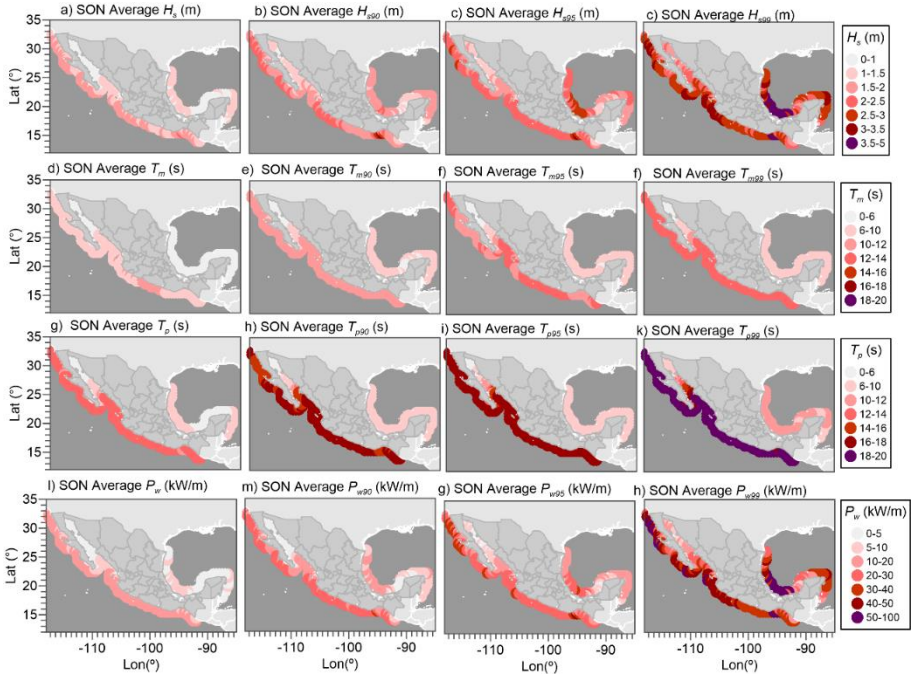


Figure A4. 4 SON seasonal average of a) $H_s$ (m), b) $H_{s90}$ (m), c) $H_{s95}$ (m), d) $T_m$ (s) , e) $T_{m90}$ (s) , f) $T_{m95}$ (s), g) $T_{m99}$ (s),h) $T_p$ (s) , i) $T_{p90}$ (s) , j) $T_{p95}$ (s), k) $T_{p99}$ (s), l) $P_w$ (kW/m) , m) $P_{w\,90}$(kW/m) , o) $P_{w95}$ (kW/m) , and q) $P_{w99}$ (kW/m).

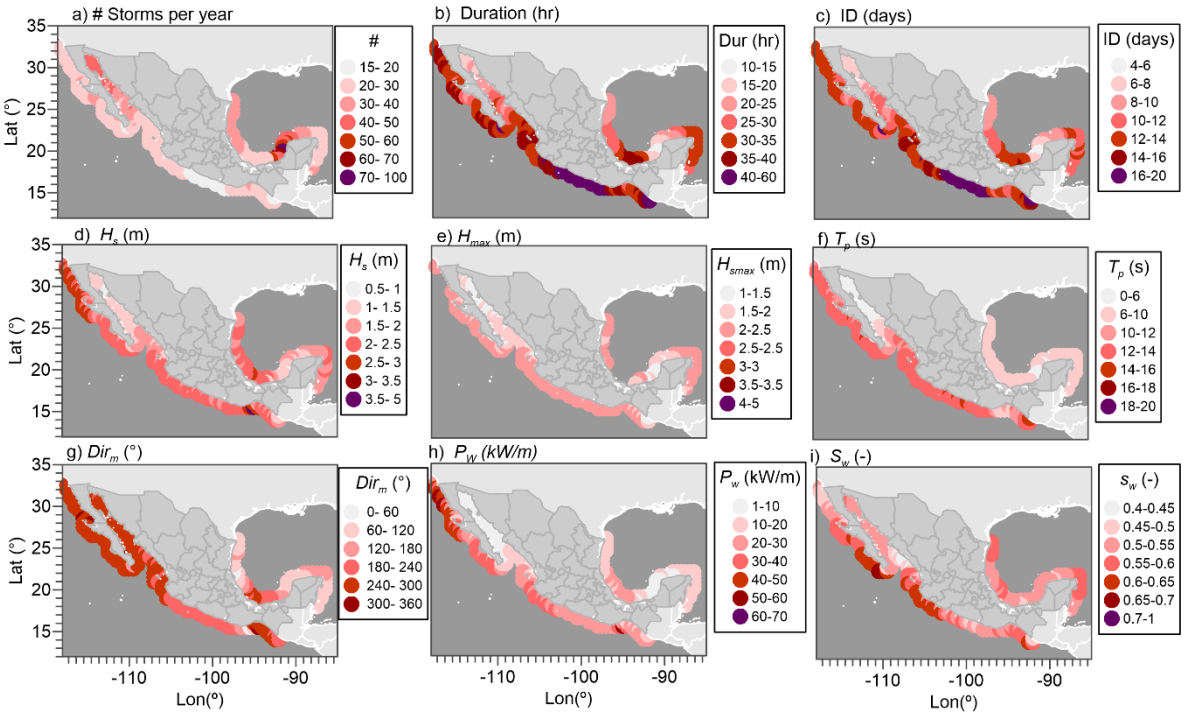


Figure A4. 5 Extreme events that exceed the 90% of the significant wave height in a year, a) number of events, b) duration (hr), c) ID (days, d) $H_s$ (m), e) $H_{smax}$ (m) , f) $T_p$ (s) , g) $Dir_m$ (s), h) $P_{w95}$ (kW/m) , and i) $s_w$ (-).

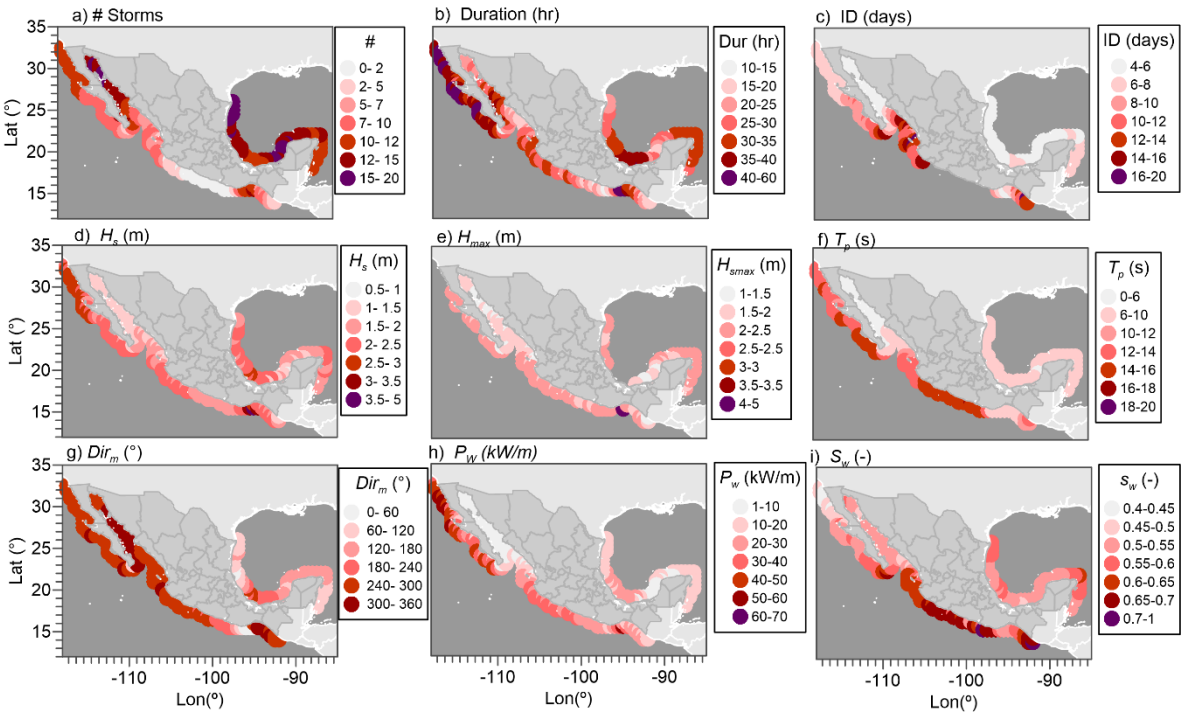


Figure A4. 6 Extreme events that exceed the 90% of the significant wave height in a DJF, a) number of events, b) duration (hr), c) ID (days, d) $H_s$ (m), e) $H_{smax}$ (m) , f) $T_p$ (s) , g) $Dir_m$ (s), h) $P_{w95}$ (kW/m) , and i) $s_w$ (-).

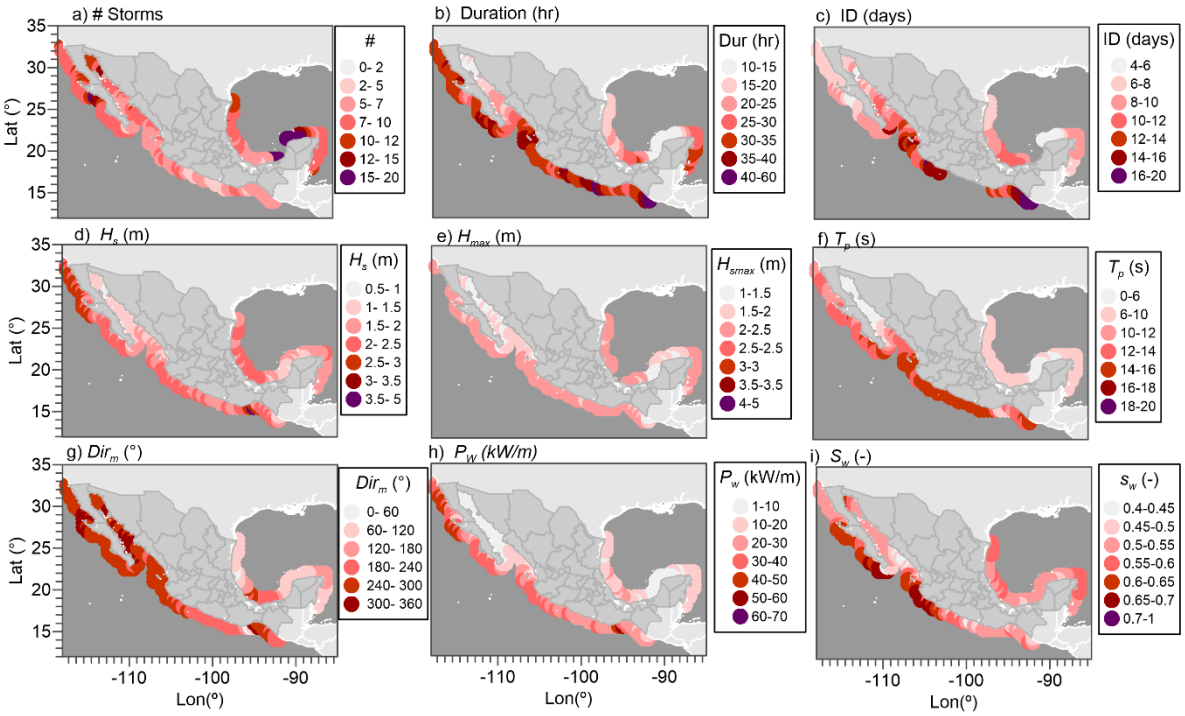


Figure A4. 7 Extreme events that exceed the 90% of the significant wave height in a MAM, a) number of events, b) duration (hr), c) ID (days, d) $H_s$ (m), e) $H_{smax}$ (m) , f) $T_p$ (s) , g) $Dir_m$ (s), h) $P_{w95}$ (kW/m) , and i) $s_w$ (-).

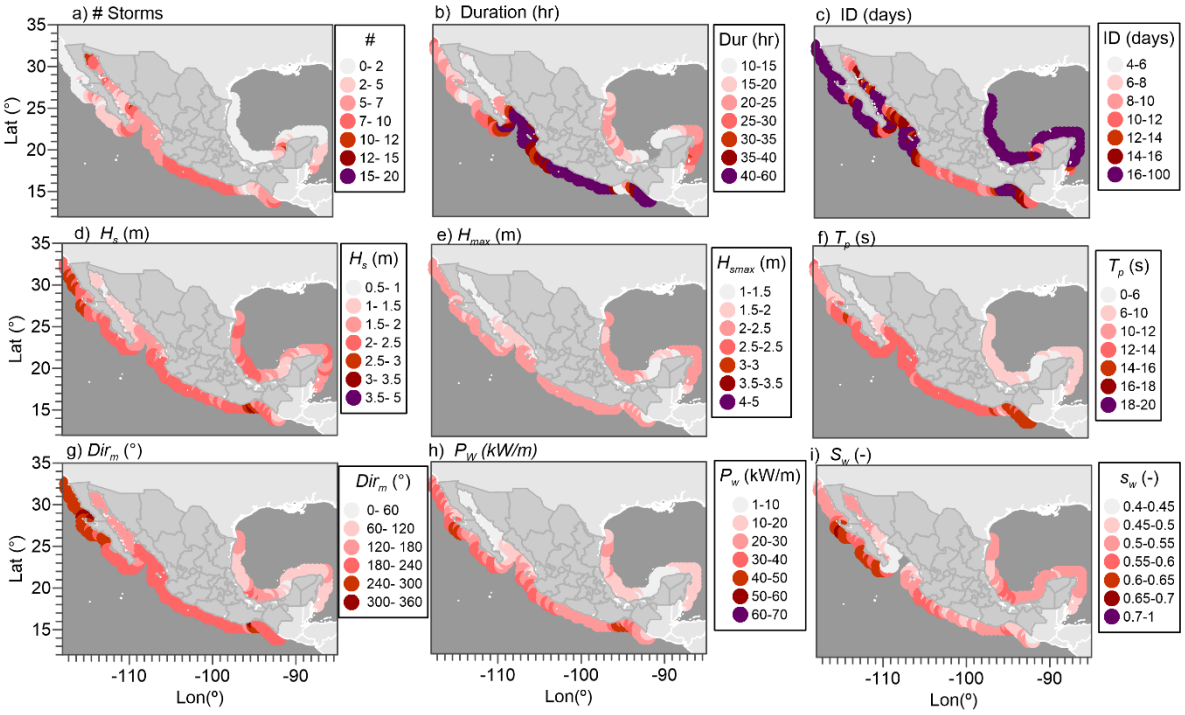


Figure A4. 8 Extreme events that exceed the 90% of the significant wave height in a JJA, a) number of events, b) duration (hr), c) ID (days, d) $H_s$ (m), e) $H_{smax}$ (m) , f) $T_p$ (s) , g) $Dir_m$ (s), h) $P_{w95}$ (kW/m) , and i) $s_w$ (-).

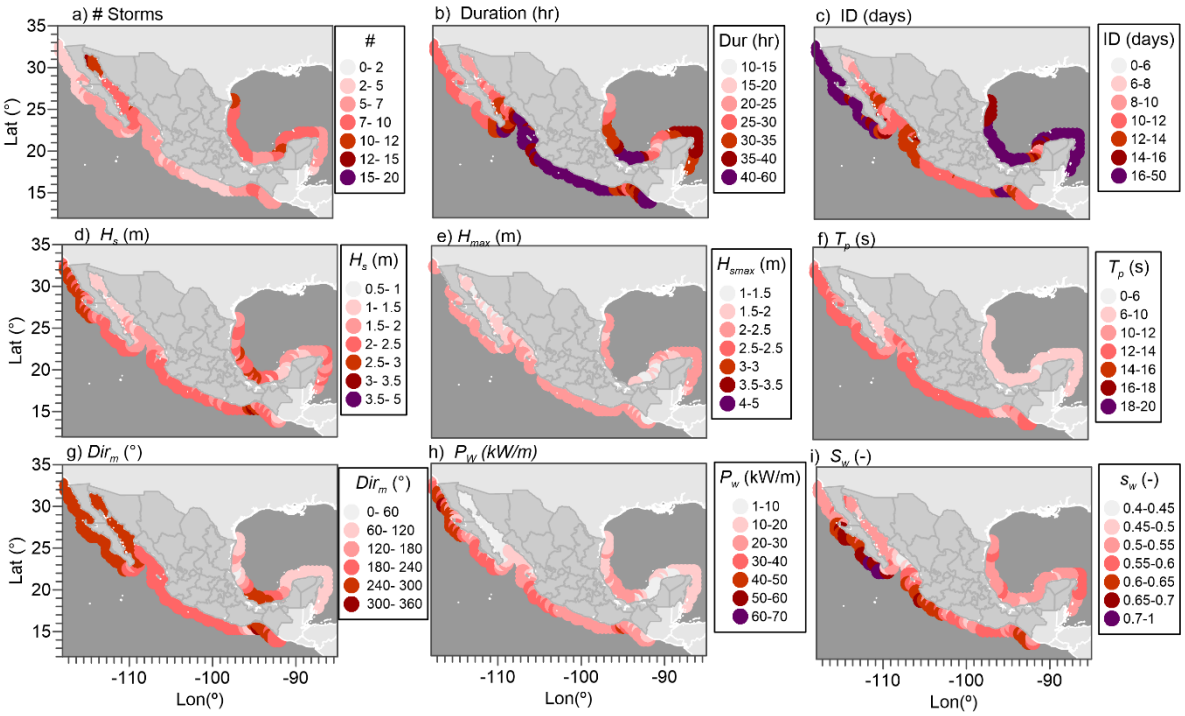


Figure A4. 9 Extreme events that exceed the 90% of the significant wave height in a SON, a) number of events, b) duration (hr), c) ID (days, d) Hs (m), e) Hsmax (m) , f) Tp (s) , g) Dirm (s), h) Pw95 (kW/m) , and i) sw (-).

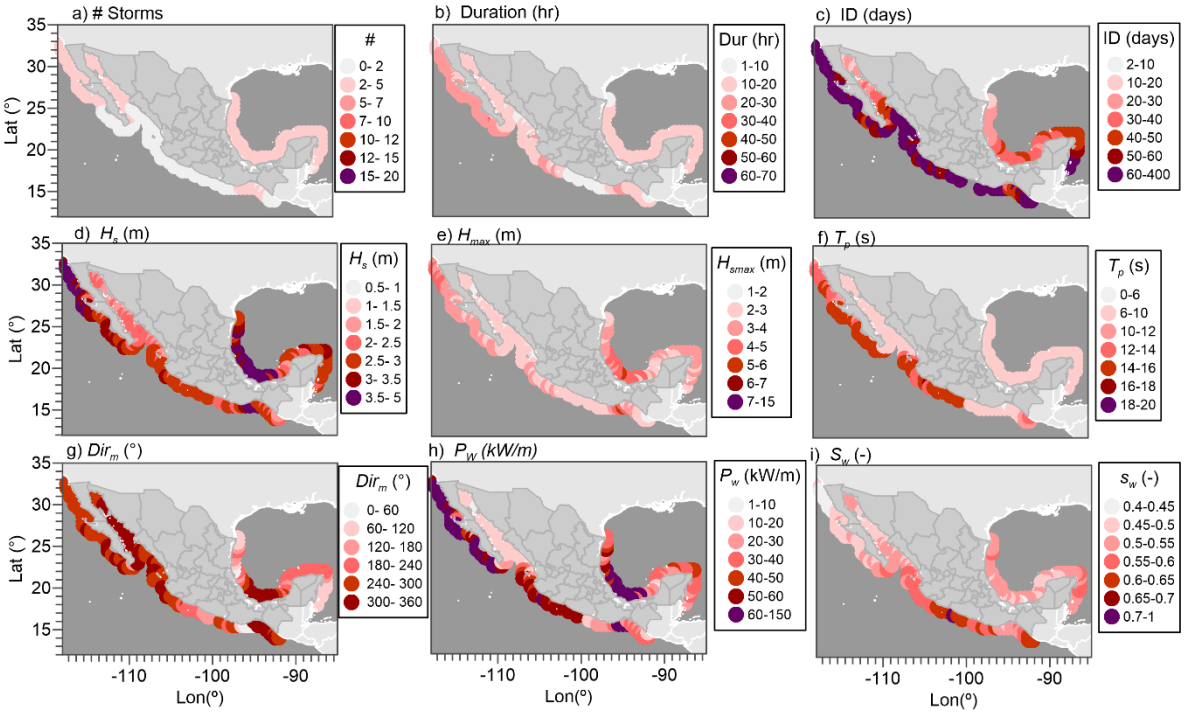


Figure A4. 10 Extreme events that exceed the 99% of the significant wave height in a DJF, a) number of events, b) duration (hr), c) ID (days, d) $H_s$ (m), e) $H_{smax}$ (m) , f) $T_p$ (s) , g) $Dir_m$ (s), h) $P_{w95}$ (kW/m) , and i) $s_w$ (-).

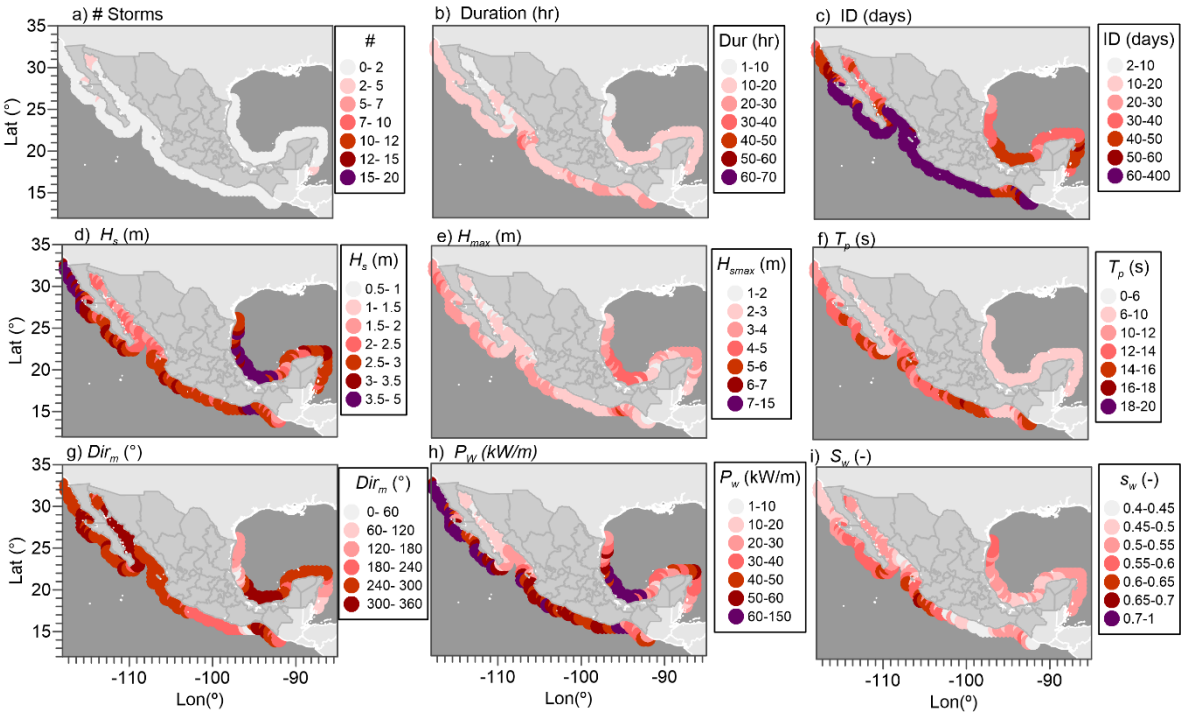


Figure A4. 11 Extreme events that exceed the 99% of the significant wave height in a MAM, a) number of events, b) duration (hr), c) ID (days, d) $H_s$ (m), e) $H_{smax}$ (m) , f) $T_p$ (s) , g) $Dir_m$ (s), h) $P_{w95}$ (kW/m) , and i) $s_w$ (-).

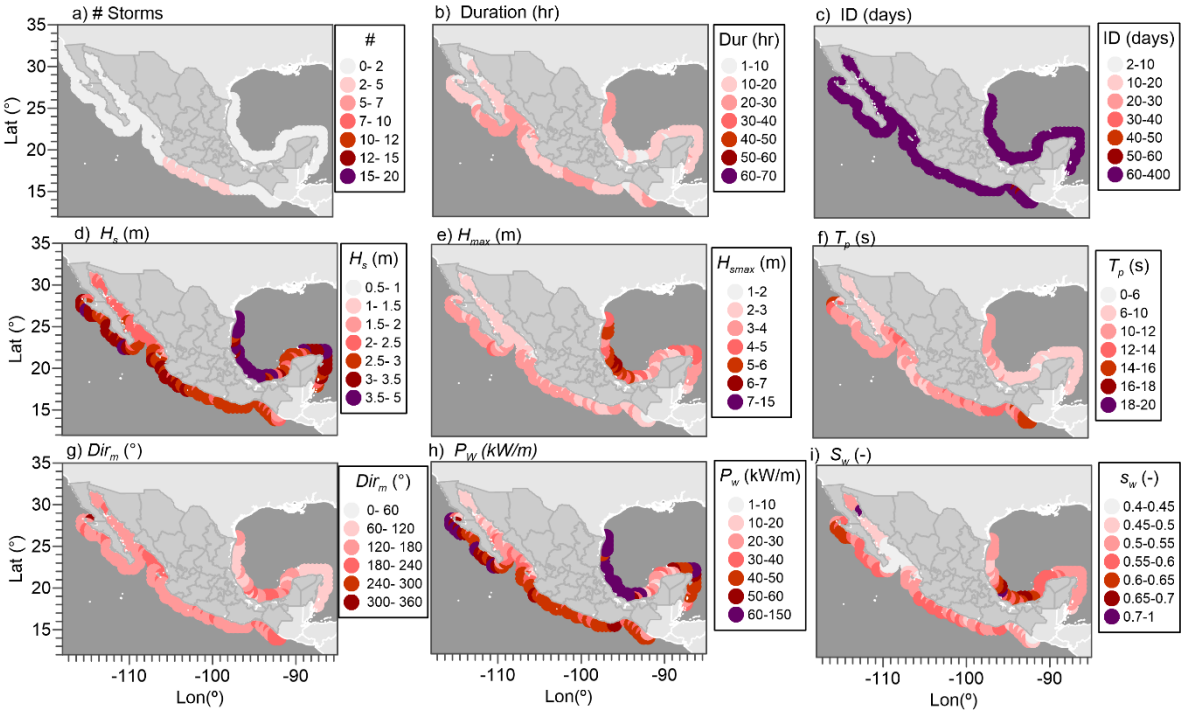


Figure A4. 12 Extreme events that exceed the 99% of the significant wave height in a JJA, a) number of events, b) duration (hr), c) ID (days, d) Hs (m), e) Hsmax (m) , f) Tp (s) , g) Dirm (s), h) Pw95 (kW/m) , and i) sw (-).

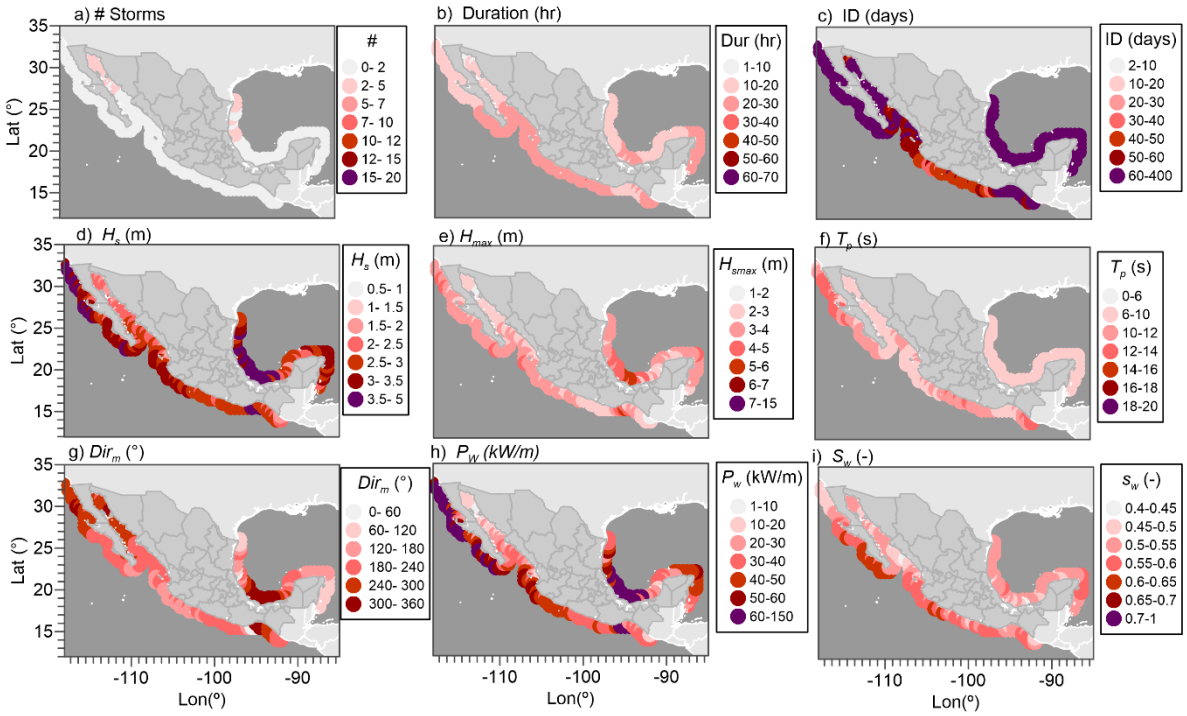


Figure A4. 13 Extreme events that exceed the 99% of the significant wave height in a SON, a) number of events, b) duration (hr), c) ID (days, d) $H_s$ (m), e) $H_{smax}$ (m) , f) $T_p$ (s) , g) $Dir_m$ (s), h) $P_{w95}$ (kW/m) , and i) $s_w$ (-).

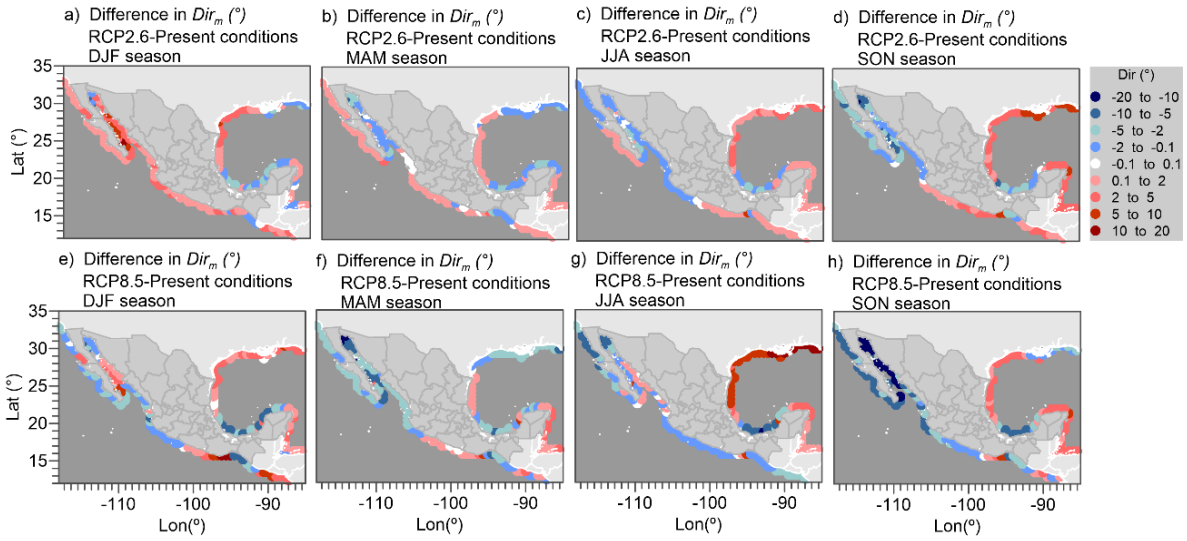


Figure A4. 14 Seasonal differences in wave direction between (a, b, c, d) RCP 2.6 and present conditions, (e, f, g, h) RCP 8.5 and present conditions in (a, e) DJF, (b, f) MAM, (c, g) JJA, and (d, h) SON seasons.

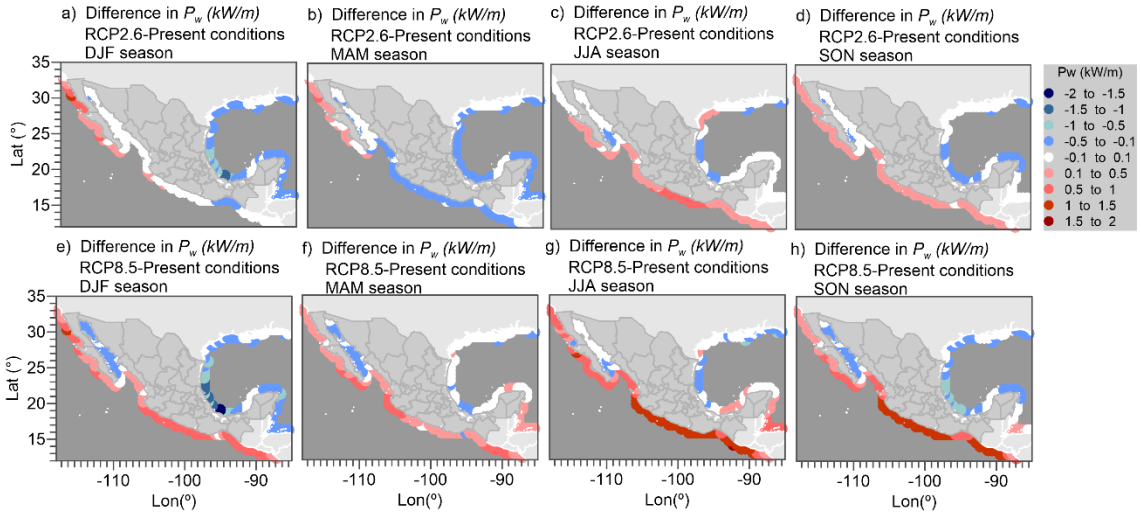


Figure A4. 15 Seasonal differences in wave power between (a, b, c, d) RCP 2.6 and present conditions, (e, f, g, h) RCP 8.5 and present conditions in (a, e) DJF, (b, f) MAM, (c, g) JJA, and (d, h) SON.

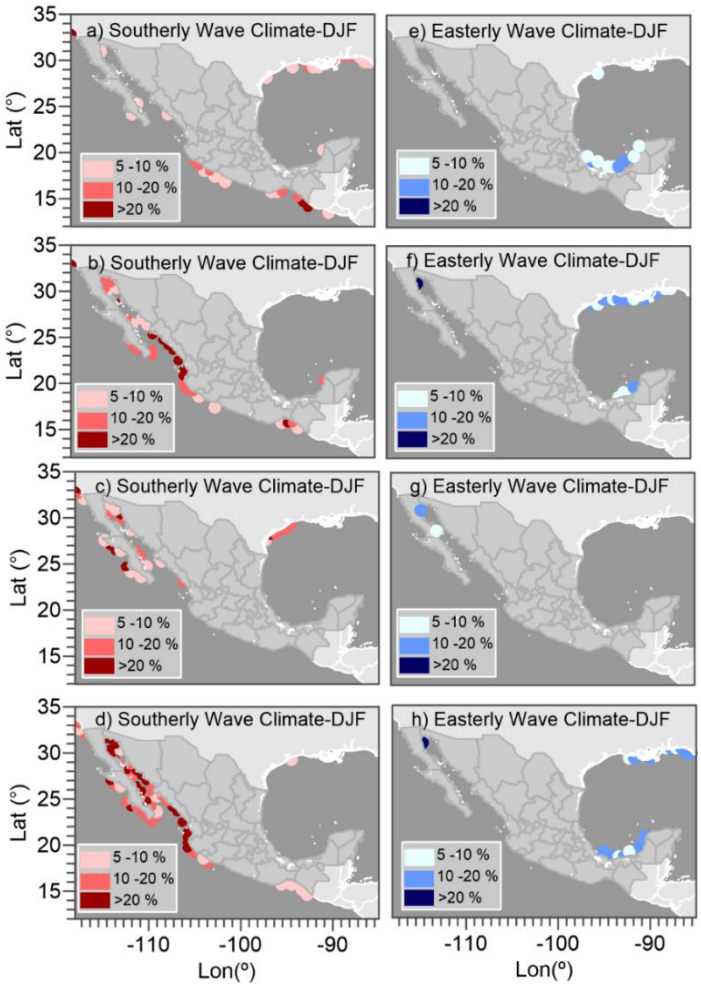


Figure A4. 16 Transitional regions of wave climates in DJF, MAM, JJA, and SON for southerly wave climate (a-d) and easterly wave climate (e-h).